UNIVERSITY OF SOUTHAMPTON

OSCILLATIONS AND STABILITY OF ROTATING SUPERFLUIDS

By
Kirsty Grosart

A thesis submitted for the degree of
Doctor of Philosophy

School of Mathematics,
University of Southampton,
Southampton, SO17 1BJ
United Kingdom.

November 2005

UNIVERSITY OF SOUTHAMPTON

ABSTRACT

FACULTY OF ENGINEERING, SCIENCE AND MATHEMATICS

MATHEMATICS

Doctor of Philosophy

Oscillations and Stability of Rotating Superfluids

by Kirsty Grosart

It is predicted that neutron stars contain a liquid interior of superfluid neutrons and superconducting protons. The effect of these superfluid components on the various oscillation modes and stability of a rotating neutron star is investigated. We model our superfluid using a simple non-relativistic, two-fluid model, where one fluid consists of the superfluid neutrons and the second fluid contains all the remaining constituents (protons, electrons). The two fluids are coupled through the equation of state, in particular by entrainment, and are free to rotate at different rotation rates around the same axis. The initial approach involves Eulerian perturbation theory and subsequently a Lagrangian perturbation framework is developed. The advantage of the Lagrangian framework is that we can construct a canonical energy for the system allowing us to develop stability criteria for superfluid stars analogous to the single fluid results by Friedman and Shutz [39]. At present our stability analysis neglects the entrainment effect, and its inclusion is the focus of future work. However, we do include entrainment in our normal mode investigations. We consider a self-gravitating, Newtonian, superfluid cylinder. Numerically, we investigate the normal mode solutions and investigate their dependence on the relative rotation rate and on entrainment. We observe avoided crossings of modes and the onset of a *two-stream instability* at a critical relative background rotation rate.

Our investigations are complicated by the presence of various singularities. As a result there exists situations for which we are unable to obtain a numerical solution. To check our numerics we limit our investigations to situations where these numerical problems are not encountered. We discover this corresponds to negative values of the entrainment function, α. Although it is predicted that in the neutron star core the entrainment will be positive, negative entrainment is not physically

unrealistic. In fact it has been shown [28] that it is what is predicted for neutron star crusts.

Acknowledgements

Thank you,

James Vickers, Reinhard Prix, Mel, Kay, Disco Duck and Muff the hamster, PPARC, Ross Collins, Carolyn Brinkworth, and all the general relativity students in particular Ian Hinder.

Anna - who told me *"Singularities are cool!"* and who more importantly taught me everything I know about cheese.

The ever wonderful **Aimee** - who despite a serious physical disability (no hands) never stopped me questioning if I'd ever given my cat flying lessons. I would not have survived *the thesis* without you!

And finally **Nils Andersson** without whom I would still be trying to find the mistakes in my Maple code.

For Mum, Dad, Fiona and Sally who love me despite all the stupid things I do.

"Because we're so trained to do life the right way. To not make mistakes. I figure, the bigger the mistake looks, the better chance I'll have to break out and live a real life. Like Christoper Columbus sailing toward disaster at the edge of the world. Our real discoveries come from chaos .. from going to the place that looks wrong and stupid and foolish"

INVISIBLE MONSTERS by Chuck Palahniuk

Contents

Chapter 1

Introduction

A new generation of extremely sensitive detectors, with the mission of observing the theoretically predicted gravitational waves are now operational. Despite no positive detection thus far it seems inevitable that after decades of controversy over its existence, this gravitational radiation will finally be observed. Gravitational waves are produced when matter is accelerated in an asymmetrical way. The challenge in detection lies in the fact that a detectable level of radiation is only generated by the acceleration of very large masses in very strong gravitational fields. It has been suggested [7] that instabilities in neutron stars could result in oscillations growing such that the resulting gravitational waves reach a detectable level. Building a *realistic* model of a neutron star to investigate these oscillations requires a detailed understanding of the physics behind them. This work focuses on the idea that neutron stars contain various superfluid components. Our purpose is to explore the effects that this superfluidity has on the dynamics of the star, in particular investigating the effect on the oscillations and stability.

1.1 An introduction to neutron stars

In 1934, only two years after the discovery of the neutron, the existence of neutron stars was proposed by astrophysicists Baade and Zwicky [17]. They suggested that neutron stars would be about 10km in diameter and would be formed during supernova explosions as massive old stars collapse. For many decades after the first prediction however, neutron stars were just hypothetical phenomena. It was over thirty years later that PhD student Jocelyn Bell and her supervisor Antony Hewish confirmed the theories when they detected these stars in the form of a pulsar [46]. They noticed rapid radio pulses from a specific direction of the sky. Due to the frequency of pulses it was concluded that the object producing these pulses was very small and the connection was made with the already theoretically predicted neutron stars. In reality pulsars do not pulse but emit two beams of radio waves in opposite directions along their magnetic axis. These beams sweep around the

sky once per stellar rotation, much like the beacon of a lighthouse. Therefore an observer receives a short pulse each time one of the radio beams points toward the Earth.

The life of a neutron star begins where that of an ordinary star ends. Throughout its life a chain of thermonuclear reactions take place within a star generating enough pressure to keep it from collapsing due to gravity. Initially hydrogen is burnt into helium followed by helium to carbon. If a star is massive enough heavier and heavier atoms will be fused until the star is composed of several concentric shells, each dominated by a particular fusion reaction, the hottest shell at the centre containing iron. Fusing iron to form heavier elements actually requires energy so at this point all the fuel is used up and the core collapses under its own weight. During this collapse, the outer layers of the star are blown off in a supernova explosion. What remains at the centre becomes either a black hole or if the initial weight is low enough a neutron star [41]. Stars with an initial mass of roughly 15 to 30 times the mass of our sun are believed to eventually form neutron stars, however, as supernova simulations become more precise these limits should become more absolute.

Neutron stars are predicted to have a radius of only 10km yet a mass 1.4 times that of our sun resulting in core densities which are well beyond what is accessible to laboratory experiment, [62], [63]. Therefore despite considerable theoretical analysis much of the physics of these compact objects is not well understood. The present model of a neutron star [75] consists of a solid outer crust, with various layers, enclosing a much hotter fluid core. We illustrate this model in Figure 1.1. Following a rather thin ocean, we find an outer crust consisting of nuclei, ranging from ^{56}Fe to ^{118}Kr, held together by Coulomb forces. The inner crust is made up of a lattice of nuclei, and of superfluid neutrons. It is believed that the unconfined neutrons condense by forming Cooper pairs. The neutrons therefore become endowed with the property of superfluidity enabling them to flow freely past the metallic lattice. At the base of the inner crust the nuclei dissolve and we find a uniform fluid composed mainly of superfluid neutron but also with a smaller number of superconducting protons and electrons. In addition to neutrons and protons the super-nuclear densities present within neutron stars give rise to various other hadronic possibilities, [42]. Hyperons, a class of sub-atomic particle, are predicted to appear in neutron star matter at a density of $0.38fm^{-3}$, about twice the nuclear saturation density [60]. Under terrestrial conditions hyperons are unstable and decay into nucleons through the weak interaction. The conditions in neutron stars, however, can make the conversion of nucleons into hyperons energetically favourable. Since Ambartsumyan and Saakyan [4] first suggested the appearance of hyperons in neutron stars in 1960 substantial theoretical analysis has been carried

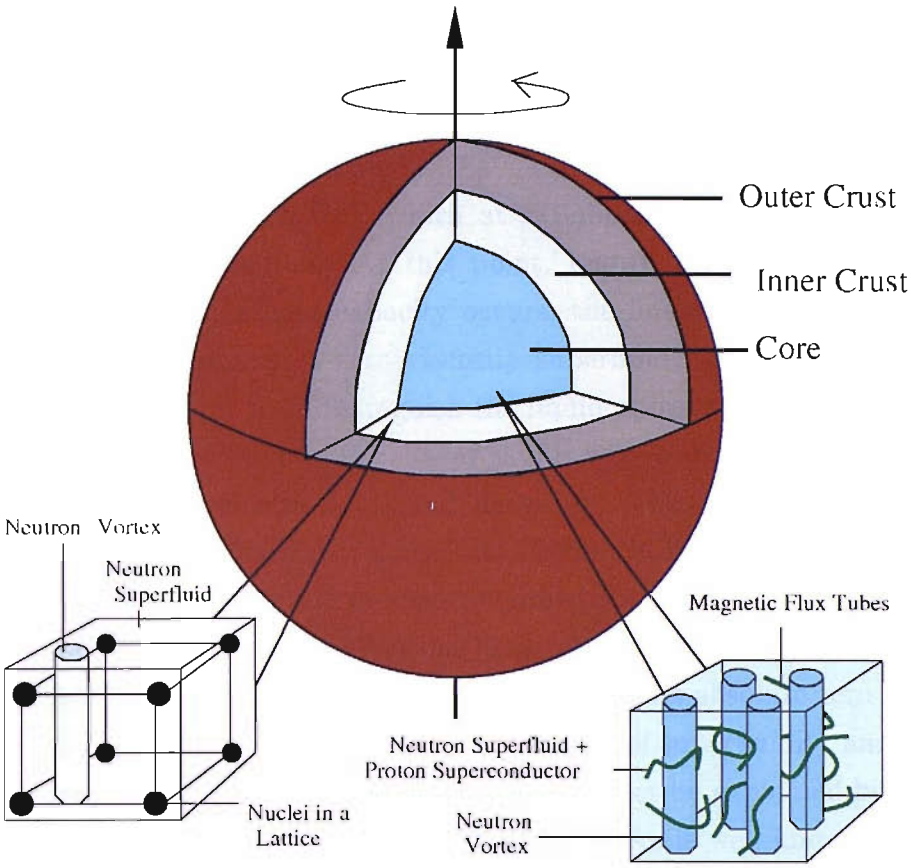

Figure 1.1: *Model of a Neutron Star: In the atmosphere and outer crust we find nuclei ranging from ^{56}Fe to ^{118}Kr, held together by Coulomb forces. The inner crust consists of superfluid neutrons and a lattice of proton clusters. The unconfined neutrons condense by forming Cooper pairs thus becoming superfluid. This superfluidity allows them to flow freely past the metallic lattice. At the base of the inner crust the nuclei dissolve and we find a uniform fluid composed mainly of superfluid neutron but also with a smaller number of superconducting protons and electrons.*

out on the consequences for neutron star physics. The principal effect caused by hyperon formation is a softening of the equation of state [91]. Other more exotic possibilities that have been suggested for the neutron star core include meson condensation and a deconfined quark phase. We focus our attention in this thesis on the effect of superfluidity in neutron stars and thus neglect the presence of these other more exotic particles. However, since these additional particles may also be superfluid, [84], one could conceivably adapt this analysis in some way to include their presence.

1.2 Superfluidity

Traditionally in physics one learns that the world is divided into two. There is the microscopic world of quantum mechanics and there is the macroscopic world where classical physics still reigns. Superfluids are astonishing in that they shatter this barrier between worlds. Quantum effects are essential for the existence of these

systems yet they can exist on length scale of a μm, a cm, or even $10^4 km$. Consider a liquid which can freely flow through a narrow capillary without transferring any of its momentum to the wall. This fluid would be moving without friction and this is what is known as a superfluid, [48]. The property of superfluidity was first observed in liquid helium He^4, which at a temperature of 2.18K undergoes a second-order phase transition. At this point, known as the lambda point, a remarkable discontinuity in heat capacity occurs, the liquid density drops, and a fraction of the liquid becomes a zero viscosity superfluid. Keesom [47] used the terms helium I and helium II to distinguish the liquid above and below the lambda temperature respectively. Helium II behaves as if it were a mixture of two different liquids with their own velocity fields and densities. There is a normal, viscous fluid component which is basically a classical Navier-Stokes fluid and an inviscid superfluid component. Energy and momentum are exchanged between the two fluids by an interaction known as mutual friction. The relative proportion of normal and superfluid is determined by the absolute temperature T. At absolute zero helium II is still a liquid and is entirely superfluid. The property of superfluidity and the fact that helium remains liquid down to absolute zero can not be explained by classical theory and are connected with quantum phenomena. As is well known, there are two stable isotopes of helium, He^3 and He^4. The liquid which exhibits superfluidity is the one formed from atoms of He^4 that is, from particles obeying Bose statistics. He^3 atoms also form a quantum liquid, known as a Fermi liquid, but do not exhibit superfluidity at temperatures of the order 1 or 2 K. This is because superfluidity arises from the fraction of helium atoms which have condensed to the lowest possible energy. Bosons can condense in unlimited numbers into a single ground state since they are governed by Bose-Einstein statistics where as fermions, such as He^3 atoms, are constrained by the Pauli exclusion principle. At low enough temperatures, however, pairing can occur in Fermi liquids, forming Bose type particles and hence instigating the occurrence of superfluidity. This is known as Cooper pairing and is essential for the formation of superfluids in neutron stars.

In a standard superconductor a Cooper pair consists of two electrons which are attracted to each other sufficiently strongly that they form a bound state. The force between the two negatively charged electrons becomes attractive as a result of their interactions with the crystalline lattice through which they are travelling. As one electron passes through a given region of the lattice it attracts the positive ions toward itself. The electron moves on, but the heavier ions take a longer time to return to their original position, and during this time they attract the second electron. The interaction with the lattice is shown schematically in Figure 1.2. These two electrons are known as a Cooper pair. If the energy required to bind

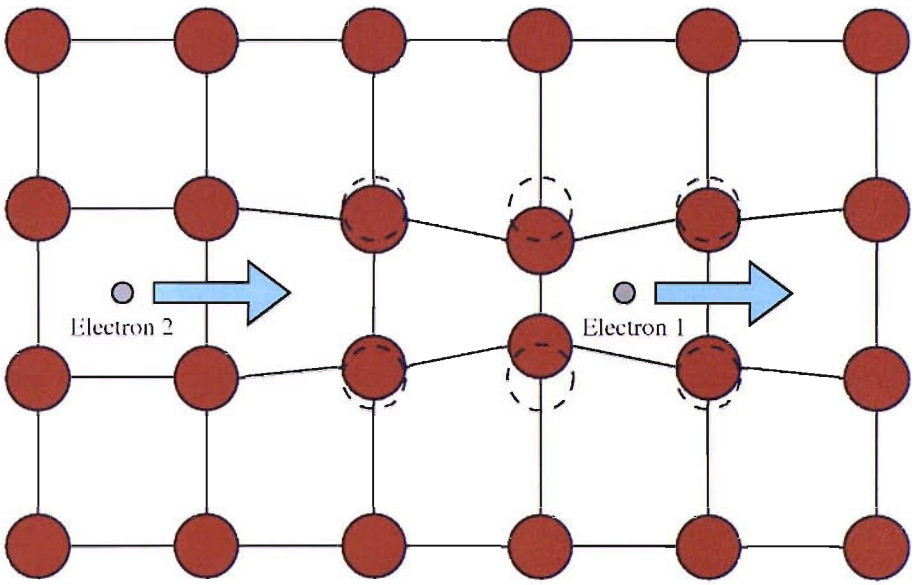

Figure 1.2: *A schematic representation of the basis for the attraction interaction between two electrons via lattice deformation. As one electron passes through a given region of the lattice it attracts the positive ions toward itself. The electron moves on, but the heavier ions take a longer time to return to their original position, and during this time they attract the second electron. The electron pair remain bound provided the energy required to bind them together is less than the energy from the thermal vibrations of the lattice attempting to break them apart. [43].*

these electrons together is less than the energy from the thermal vibrations of the lattice attempting to break them apart, the pair will remain bound [43].

In neutron stars superfluidity occurs through the creation of pairs of neutrons and protons. The Cooper pairs which are formed are bound systems of two fermions and must therefore be described by wave functions which are anti-symmetric under exchange of the coordinates and spins of the pairs. This results in the existence of two types of states, the spin-singlet state, $^1S_0$, with spin zero and the spin-triplet state, $^3P_2$, with spin 1. Figure 1.3 is a plot of temperature against density illustrating the transition from normal matter to superfluid matter. The regions below the curve represent the existence of the corresponding superfluid state. At the lower densities, typical for the neutron star crust we can expect to find superfluid neutrons in the $^1S_0$ state. At roughly $2 \times 10^{14} g/cm^3$ which indicates the crust-core interface, we observe, not only the emergence of $^1S_0$ protons but the dominant attraction for the neutrons now occurs in the $^3P_2$ channel. Hence in the neutron star core we expect to find both superfluid protons in the $^1S_0$ state and superfluid neutrons in the $^3P_2$ state [75]. It is now believed that the $^3P_2$ curve is lower than shown in the Figure, although maximum values of the transition temperature can vary considerably for different macroscopic models [87].

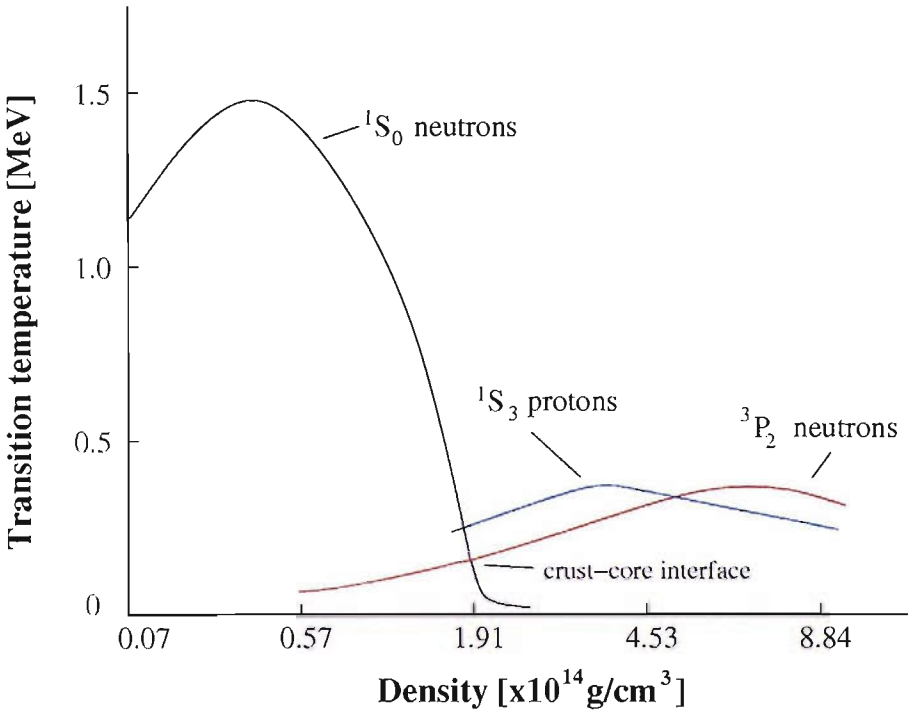

Figure 1.3: *Plot of transition temperature against density illustrating the transition from normal matter to superfluid matter. The regions below the curve represent the existence of the corresponding superfluid state. At the lower densities, typical for the neutron star crust, we can expect to find superfluid neutrons in the* $^1S_0$ *state but an absence of superfluid protons. At roughly* $2 \times 10^{14} g/cm^3$ *which indicates the crust-core interface, we observe, not only the emergence of* $^1S_0$ *protons but the dominant attraction for the neutrons now occurs in the* $^3P_2$ *channel. Hence in the neutron star core we expect to find both superfluid protons in the* $^1S_0$ *state and superfluid neutrons in the* $^3P_2$ *state [75]. It is now believed that the* $^3P_2$ *curve is lower than shown in the Figure.*

One of the most distinct features of superfluidity is its response to rotation. If we consider a normal fluid in a rotating cylinder, such as water in a rotating glass, after some initial slowness the fluid will begin to rotate uniformly with the cylinder. In the case of a superfluid we might assume that since the superfluid does not interact with the walls of the cylinder it would remain stationary. However, this conclusion is not observed experimentally. What happens is that the superfluid mimics rigid body rotation very closely by forming an array of vortices, see Figure 1.4 [64], [38]. A cylindrical non-superfluid region surrounded by stable currents spontaneously appears in the superfluid as shown in Figure 1.5. These tornado like tubes have non-zero curl and thus lead to a non-zero global circulation. It should be noted that the presence of a single vortex in a superfluid leads to an extremely non-rigid body flow. In this case, the flow is rapid near the centre of the vortex and falls off as $1/r$ where r is the distance from the vortex centre. However, with increased rotation more vortices can be added to the superfluid and a smooth average over a

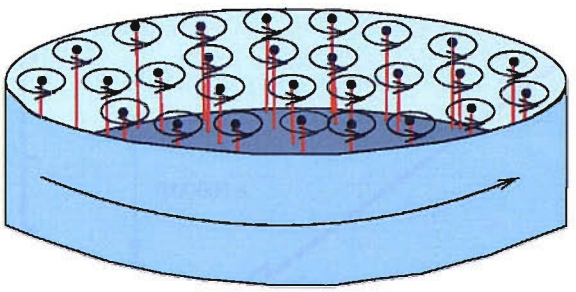

Figure 1.4: *A schematic representation of the vortex state in the interior neutron superfluid. The superfluid mimics rigid body rotation very closely by forming an array of vortices. If the superfluid is rotated at a constant angular velocity the vortices form an ordered array with the vortex lines being aligned with the axis of rotation. The number of vortices present is directly proportional to the angular speed of the superfluid.*

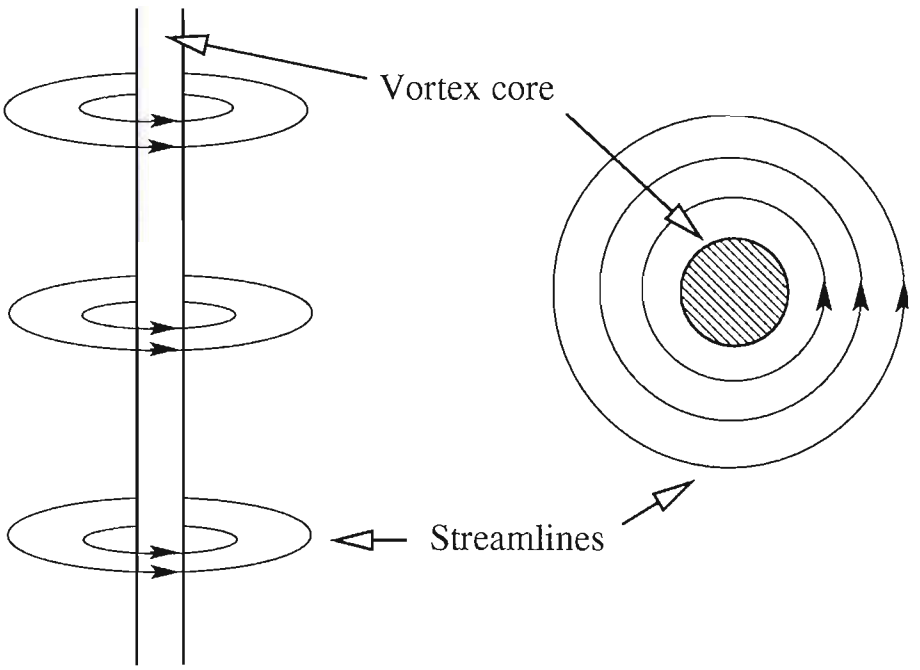

Figure 1.5: *A schematic representation of a vortex line, a cylindrical non-superfluid region surrounded by stable currents. These tornado like tubes which allow the superfluid to mimic rigid body rotation have non-zero curl and thus lead to a non-zero global circulation.*

large number of vortices causes the system to rotate in an increasingly rigid-body like manner [48].

The key property of a superfluid vortex line is that the circulation is quantised,

$$\kappa = \oint_C \vec{v_s} \cdot \vec{dl} = \frac{h}{2M} N \tag{1.1}$$

Where N is an integer and M is the bare neutron mass [43], [79]. The factor of two in equation (1.1) arises because we are considering neutron pairs. The energy

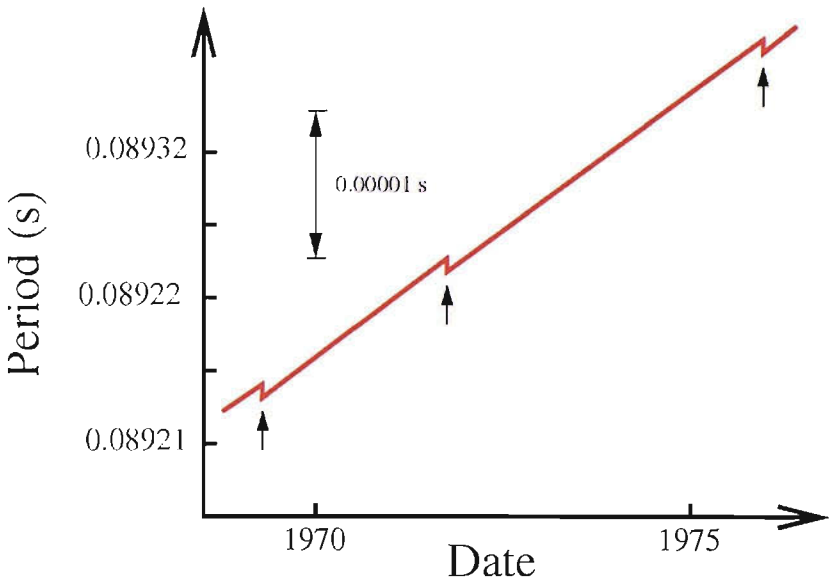

Figure 1.6: *A schematic sketch of an observational plot of pulsar period against time for the Vela pulsar. Glitches, indicated by the arrows, occur when the pulsar suddenly speeds up by a very small amount. The largest glitches have relative amplitudes ($\Delta\nu/\nu$) of several parts per million, but the range of amplitudes covers many orders of magnitude. The recovery back to the pre-glitch rotation rate ranges from days to years [44].*

associated with a vortex line depends on κ^2. Therefore it is energetically favourable to have two vortices each with one quantum of circulation, rather than one vortex with two quanta [25]. If the superfluid is rotated at a constant angular velocity the vortices form an ordered array with the vortex lines being aligned with the axis of rotation. The number of vortices present is directly proportional to the angular speed of the superfluid. As the speed of rotation decreases a new equilibrium state can only be achieved by the destruction of vortices. This process proceeds by the outward flow of vortices, and annihilation of vorticity at the interface between the superfluid and the boundary.

Strong observational evidence for the existence of superfluid components in neutron stars is provided by the well-known glitch phenomenon [29]. Signals received from pulsars arrive at a remarkably constant frequency which is considered to be the rotation frequency of the star. A startling observation was made, however, in 1969 when the Vela pulsar suddenly seemed to speed up [19]. This phenomenon has been called a glitch. Following this glitch event is a slow recovery of the angular deceleration back to the pre-glitch spin-down rate, see Figure 1.6. The timescale for this return is macroscopic, ranging from days to years.

The origin of glitches is poorly understood. However, since the interior of a neutron star is superfluid, it is useful to see if the observed speed-ups can in some way

be attributed to the properties of a rotating superfluid. A possible explanation for the glitches, suggested by Packard [67], is the metastability of superflow. A system can be described as metastable if it is above its minimum energy state, but requires an energy input before it can reach a lower energy state. Experiments on rotating vessels of liquid helium reveal that the vortices tend to pin themselves to imperfections on the walls of the vessel. If the vessel is decelerated the vortices may remain attached to the vessel and a metastable flow is created in which the superfluid is flowing faster than the vessel. The superfluid will spin down only if the vortices are destroyed on the vessel walls. In the case of a neutron star, to achieve equilibrium between the superfluid and the neutron star crust the superfluid must expel vortices as the star slows down. Pinning of this vorticity in the crust is thus a mechanism for storing superfluid kinetic energy, see Figure 1.7. As the relative velocity between the superfluid and crust builds up, the force tending to expel the vorticity increases, [34]. Eventually this will overcome the pinning forces. At a critical value of the relative angular speed of the superfluid and crust the vortices will unpin. A problem with this model is that to account for the observed change in angular acceleration roughly 10^{13} vortices must simultaneously depin during a glitch. We observe this in the following way; by considering equation (1.1) in the form,

$$\oint_C \vec{v_s} \cdot \vec{dl} = (\Omega R) \times (2\pi R) = \frac{h}{2M} N \tag{1.2}$$

we can see that the change in the number of vortices, i.e the number of vortices that must depin, δN can be written as,

$$\delta N = \frac{4\pi M R^2}{h} \delta\Omega_c \tag{1.3}$$

Where $\delta\Omega_c$ is the change in angular velocity of the crust during a glitch. To look at this quantitatively we note that typically

$$\delta\Omega_c \approx 10^{-2} s^{-1} \tag{1.4}$$

giving

$$\delta N \approx 3.16 \times 10^{13} \tag{1.5}$$

As can be seen in Figure 1.6 after a glitch event comes a long period of relaxation. The source of this long recovery has been the focus of much theoretical analysis [33], [73], [74], [85], [2] & [3]. Alpar et al [2] & [3] have, over many years, developed a model of the post-glitch relaxation in terms of the rotational dynamics of a superfluid with vortex pinning inside the neutron star crust, known as *vortex*

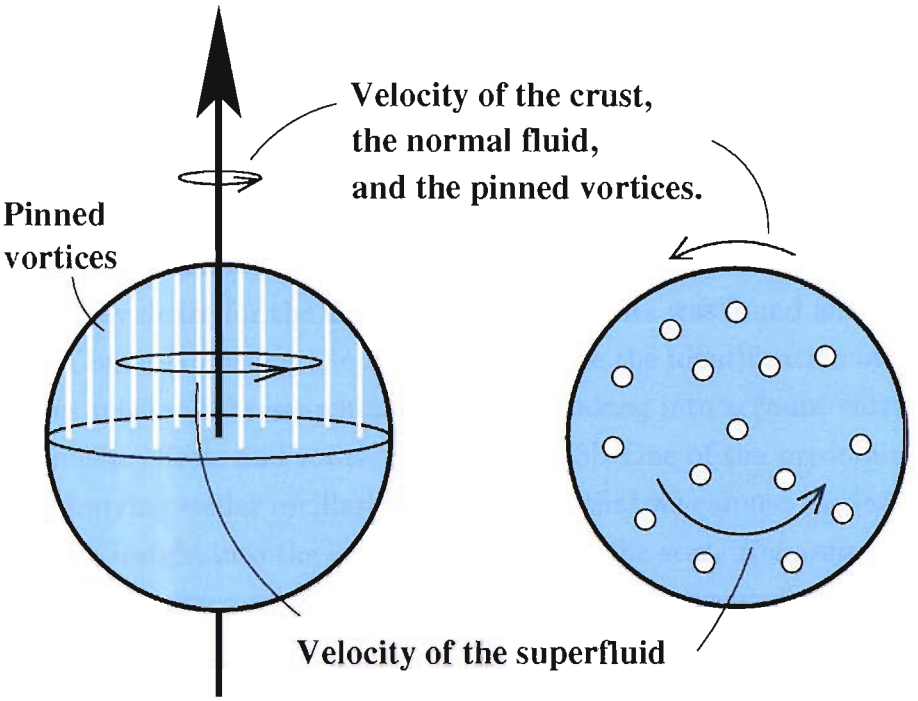

Figure 1.7: *An illustration of vortex pinning in a neutron star leading to a metastable flow in which the superfluid is flowing faster than the normal fluid. The velocity of the normal fluid, v_n, decreases due to magnetic breaking but since the vortices are pinned to the crust the number of vortices remains unchanged and thus the superfluid velocity, v_s, cannot change. Observationally deduced rotation rates are believed to correspond to v_n since the magnetic field is locked to the crust.*

creep theory. An alternate theory suggests the crustal lattice itself drifts while the vortices remain pinned [73], [74] & [85]. At present there is no firm consensus on the theory connected with neutron star glitches, however, the evidence is strong that both the glitch event and the subsequent relaxation reflect changes in the angular momentum distribution inside the star. This gives great confidence to the predictions of superfluidity in neutron stars.

1.3 Non-radial oscillations of neutron stars

It is well known that stars, being essentially large fluid balls, will tend to oscillate both radially and non-radially. Radial oscillations are simple contractions and expansions of the star whereas non-radial oscillations result in deformations whereby the star loses its symmetrical shape. Neutron stars are capable of experiencing a wide range of oscillatory modes which can be excited by various different astrophysical processes. Each restoring force which acts on a star will result in a family of pulsation modes and the modes are categorised accordingly. p modes are generated by acoustic waves for which pressure is the restoring force. The lowest acoustic mode is normally considered the fundamental mode, or f mode, of oscillation. The g modes are generated by gravity waves for which buoyancy is the restoring force.

Finally the r modes are from rotational waves where the Coriolis force is responsible for restoration. For a more in depth explanation of this extensive subject see [80] or review articles such as [14]. In 1988 Epstein [35] proposed that superfluidity in neutron stars should introduce additional modes to the oscillation spectrum. The first numerical observation of these mode was by Lee [51] who not only discovered the existence of modes not present in single fluid models but also the absence of g modes. Further evidence for the absence of these g modes was found analytically by Andersson & Comer [11] using a local analysis. Since the identification of these *superfluid* modes substantial research has been done taking into account entrainment, general relativistic effects and rotation [68], [26], [13]. One of the predominant motivations for studying stellar oscillations is the hope that we can use the information acquired to gain insight into the interior structure of the star. *Helioseismology*, the study of the Sun's interior using the solar oscillations, has revealed vast amounts of information on the internal structure of the Sun [78]. By investigating how waves propagate through the Sun scientists can infer the temperature, density, and composition of the material they pass through. An interesting proposition for neutron stars is the idea of *gravitational wave asteroseismology*, using gravitational wave data to probe neutron star interiors [15], [20]. Any non-axisymmetric pulsations will generate gravitational radiation. If these waves were to reach a detectable level they could allow us to put constraints on the interior structure of the star. Unfortunately the field of gravitational wave astronomy is highly challenging. The strongest astrophysical signals are predicted to produce signal amplitudes that are so small they could easily remain unnoticed amongst detector noise. To have any hope of detection we require not only a large signal but also an accurate model of the signal we are hoping to detect. Unstable oscillations of neutron stars could grow until the resulting gravitational waves reach a detectable level. Therefore investigating the instabilities of neutron star modes is of great astrophysical importance.

The instabilities discussed in this thesis can be identified as either dynamic or secular. Consider a star in hydrostatic equilibrium. Any small disturbance, which will inevitably be present in a real system, will create an imbalance of pressure and gravity resulting in oscillations. For a dynamically stable state these oscillations will be short-lived. However, if the system is dynamically unstable the fluctuations will grow on a timescale similar to that of the oscillation. Secular instabilities on the other hand are driven by some dissipative mechanism and act on a much longer time-scale. Of particular importance for superfluid neutron stars is the idea of the superfluid *two-stream instability* discovered by Andersson, Prix & Comer [9] which they suggested was a possible trigger mechanism for neutron star glitches [8]. It is well known that when two inter-penetrating streams in a plasma have a relative motion an instability can be produced, in which a perturbation in one

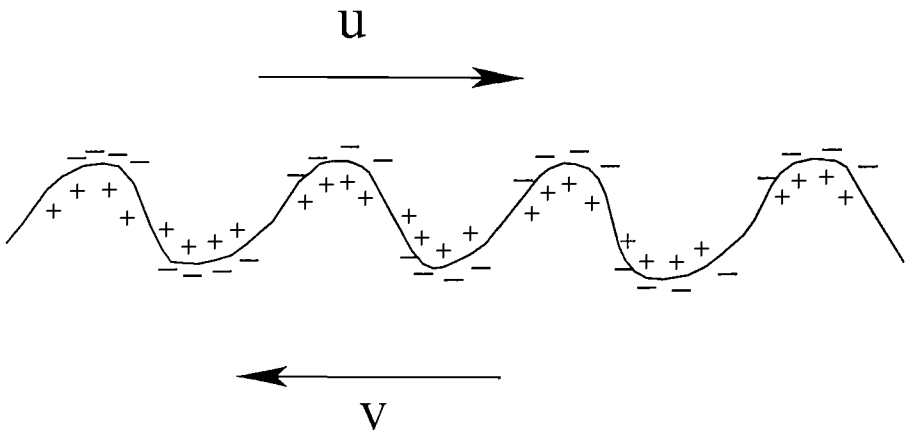

Figure 1.8: *An illustration of the mechanism behind the Kelvin-Helmholtz instability which arises as a result of relative motion of two surface waves [36]. The sinusoidal disturbance on the interface of the two fluids gives rise to pressure perturbations. At the peaks we observe an increase in fluid velocity and hence a decrease in pressure compared to the undisturbed value. In contrast at the dips a decrease in velocity and hence increase in pressure is observed. This pressure imbalance leads to an increase in the amplitude of the disturbance which in turn creates even larger variations in the pressure. As this proceeds we observe a self amplifying perturbation.*

stream produces a spatial bunching of the second [37], [5]. More recently it was shown that a similar *two-stream instability* can be induced in superfluids by the relative motion of the normal and superfluid components of the same liquid [9]. This instability is analogous to the Kelvin-Helmholtz instability which arises as a result of relative motion of two surface waves [36]. If we introduce a sinusoidal disturbance on the interface of the two fluids, as shown in Figure 1.8, we notice that the dips and peaks will give rise to pressure perturbations. At the peaks we observe an increase in fluid velocity and hence a decrease in pressure compared to the undisturbed value. In contrast at the dips a decrease in velocity and hence increase in pressure is observed. These perturbations result in an increase in the amplitude of the disturbance which in turn creates an even larger pressure imbalance. As this proceeds we observe a *self amplifying* perturbation which is the main mechanism behind the Kelvin-Helmholtz instability. The difference in the case of the *two-stream instability* is that the two fluids are inter-penetrating. It was shown that the instability sets in once the relative flow between the two fluids reaches a critical value. This result has also been confirmed in a mode calculation on inertial modes of non-stratified superfluid stars [68]. These results highlight the importance of further investigations into superfluid systems. In particular they provide motivation for developing stability criteria for superfluid stars analogous to the single fluid results derived by Friedman and Schutz [39], [40]. This derivation is the focus of much of the work in this thesis.

Since the effect of these *two-stream instabilities* has been investigated only for the case of inertial modes of non-stratified stars, we investigate general modes in the stratified case by limiting our considerations to a rotating superfluid cylinder, using cylindrical coordinates (r, ϕ, z). The advantage over the spherical case lies with the fact that in a cylindrical system the problem of linear oscillations can be reduced to the solving of a one dimensional system of ordinary differential equations. By considering infinite self-gravitating cylinders we can not only ignore variations in the z-direction we can also assume that the unperturbed quantities depend solely on r. Furthermore if we assume that the azimuthal dependence of the perturbations is given by $\exp(im\phi)$ we arrive at a system of ordinary differential equations which depend only on r. It is expected that many of the features that are valid for rotating superfluid cylinders will also hold for rotating superfluid stars [81]. More specifically, the study of rotating superfluid cylinders may contribute to the understanding of oscillations in the equatorial regions of these stars.

An exciting possibility is experimental tests of these superfluid oscillations and in particular the superfluid *two-stream instability* in, for example, superfluid ^4He. The equations used to describe our superfluid neutron stars are analogous to the standard Landau model for superfluid helium. Modifications to our equation of state and boundary conditions should in principle allow us to investigate the oscillations and stability of superfluid ^4He. Since the experimental setup for rotating fluid experiments usually consists of a rotating bucket, i.e. a cylindrical problem, our analysis of superfluid neutron stars in terms of superfluid cylinders should be relevant for this alternate situation.

This thesis begins in Chapter 2 where we define a general Newtonian model for a rotating, self-gravitating single fluid star and subsequently extend the results to describe a two-fluid system. One fluid is composed of the superfluid neutrons while the other comprises of the remaining constituents, such as the crust nuclei, core protons and crust and core electrons. In Chapter 3 we find solutions to these systems for the case of uniformly rotating fluids in cylinders.

In Chapter 4 both Eulerian and Lagrangian perturbation theory are used to investigate superfluid neutron stars. Initially the problem of a normal fluid in a rotating cylinder was studied using Eulerian perturbation theory. In the same framework we develop a system of equations for the superfluid case. In order to investigate the stability properties of the two-fluid system a Lagrangian perturbation framework is constructed, analogous to the single fluid results developed by Friedman and Schutz [39]. Initially we ignore the entrainment effect which is a coupling between the two fluids in which the movement of one of the fluids induces a momentum in the other. This is a serious omission and hence we make a preliminary step in

developing stability criteria for this more complicated system by deriving the Lagrangian perturbation equations. Constructing the corresponding canonical energy equation and the associated stability criteria is left for future work.

In Chapters 5 and 6 we apply the results obtained to investigate the modes of oscillation of a rotating cylinder of superfluid, where the two fluids are allowed to rotate at different velocities. Initially we consider the entrainment free problem where we find numerous different modes of oscillation and show that the r modes are secularly unstable, in agreement with previous work on spherical systems. The final consideration is that of a system with constant entrainment. We find this inclusion drastically complicates the corresponding system.

Our final Chapter brings together all the key results from this thesis and discusses the astrophysical relevance of our investigations. We conclude by considering extensions and improvements which must be made in order for this superfluid neutron star research to proceed.

Chapter 2

Newtonian hydrodynamics

We investigate the oscillations and stability of superfluid systems by solving the relevant ordinary differential equations. In Appendix A we introduce the numerical techniques required to solve these equations. In this Chapter we introduce the relevant Newtonian hydrodynamic equations we hope to solve. To understand how a fluid in a rotating cylinder or in a neutron star behaves we must consider the equations which govern fluid flow. Fluid dynamics is a macroscopic science, concerned with properties that can be observed and measured on the laboratory scale. To describe a fluid completely requires a function which gives the distribution of the fluid velocity $\vec{v} = \vec{v}(x, y, z, t)$ and any two of the fluid's thermodynamic quantities such as density and pressure. There are four equations which when combined give a complete mathematical description of the fluid. These are the Euler equation, the equation of continuity, Poisson's equation and an equation of state. The relevant equations for a single fluid and a two-fluid system are discussed in this chapter, however, for a detailed description of fluid dynamics and a variational description of multi-fluid hydrodynamics see Landau and Lifshitz [49] and Prix [70] respectively.

2.1 Single fluid equations

Throughout this thesis an analysis of the single, perfect fluid case is used as a prelude to the superfluid problem. This allows a straightforward introduction to the relevant formalism which can subsequently be extended to the two-fluid case. The Euler equations are the equations of motion of the fluid which, for a single-fluid, can be written as,

$$(\partial_t + v^j \nabla_j) v_i + \frac{1}{\rho} \nabla_i p + \nabla_i \Phi = 0 \tag{2.1}$$

Where v_i is the fluid velocity, ρ the fluid density, p the fluid pressure and Φ the gravitational potential. In some circumstances it is more constructive to work in terms of the chemical potential, μ, rather than the pressure. The reason for this is that in the two-fluid case we have a separate velocity and density for each of the two

fluid components but the pressure is a variable that depends on contributions from both the normal and superfluid parts. Thus by working with the chemical potentials we have terms which describe the individual fluid components but which if needed can be combined to tell us the pressure. The chemical potential of a thermodynamic system is the change in the energy of the system when an additional constituent particle is introduced, with the entropy and volume held fixed. If a system contains more than one species of particle, there is a separate chemical potential associated with each species, defined as the change in energy when the number of particles of that species is increased by one. The precise definition is,

$$\mu = \left(\frac{\partial E}{\partial N}\right)_{s,V} \tag{2.2}$$

Where μ is the chemical potential, E is the energy, N is the number of particles and s and V are the entropy and volume respectively. The chemical potential can be related to the pressure as follows,

$$\nabla p = n \nabla \mu \tag{2.3}$$

where n is the number density. We make use of equation (2.3) and introduce the notation $\tilde{\mu} = \mu / m_{\mathrm{B}}$, where m_{B} is the particle mass, to write the Euler equation in terms of the chemical potential,

$$(\partial_t + v^j \nabla_j) v_i + \nabla_i \tilde{\mu} + \nabla_i \Phi = 0 \tag{2.4}$$

The equation of continuity is the equation which expresses the conservation of matter. It can be written as,

$$\partial_t \rho + \nabla_i (\rho v^i) = 0 \tag{2.5}$$

which in terms of the number density, $n = \rho / m_{\mathrm{B}}$, becomes

$$\partial_t n + \nabla_i (n v^i) = 0 \tag{2.6}$$

Poisson's equations is a mathematical description of the gravitational field,

$$\nabla^2 \Phi = 4\pi G \rho = 4\pi G m_{\mathrm{B}} n \tag{2.7}$$

The final equation necessary to describe the single-fluid system is an equation of state relating the pressure to the density. For the interior of a neutron star the true equation of state is far from indisputable. The many so-called realistic models which have been proposed vary considerably, largely due to nuclear physics uncertainties

in the interactions of matter at the extreme densities which occur within these compact objects. Consequently we chose to describe our system using a simple polytropic equation on state.

$$p = K\rho^{\Gamma} \tag{2.8}$$

Where K is a constant and Γ is the polytropic exponent, such that $\Gamma = 1 + 1/n$. It is important to note that here n refers to the polytropic index and should not be confused with the number density. For a neutron star we expect a value of n between 1 and 1.5, [16].

2.2 Two-fluid hydrodynamics

An accurate description of the crust and outer core of a neutron star consists of three main constituents; neutrons, protons and electrons. However we describe our system using a simple two-fluid model which describes a superfluid as a mixture of two fluid components, the *normal fluid* and the *superfluid* [13], [50], [61], [10], [70]. Each fluid has its own velocity v_X^i, and number density n_X. $X = \mathrm{n}, \mathrm{p}$ are the constituent indices with n representing the superfluid neutrons and p representing the remaining constituents (protons, electrons, etc). The justification for this simplified picture is as follows. The electrons in a neutron star behave as a normal fluid, however, the protons will exist either in nuclei in the crust or as superconducting protons in the core. Due to the magnetic field on a very short timescale it has been shown that these protons are coupled to the normal electron fluid [1]. We therefore consider the electrons and protons to be locked together and we label this constituent the *protons*. The superfluid neutron component on the other hand is able to move independently due to a lack of viscosity.

In Section 1.2 the creation of a lattice of microscopic vortices to allow for rotation of superfluids was discussed. Locally the superfluid is constrained to be in a state of irrotational flow, however, in order to describe the dynamics of our superfluid neutron star we need only consider macroscopic properties. In a typical pulsar it is predicted that the density of neutron vortices is $10^2 - 10^5 cm^{-2}$ [70]. Therefore on a macroscopic scale we can average over many vortices and find that the superfluid behaves almost as if it were an ordinary fluid. Our model treats the *superfluid* and *normal* fluid identically as two ordinary fluids which are able to move relative to each other, due to the absence of local superfluid viscosity. A further complication is the presence of an interaction which exists between the vortex lattice and the *normal* fluid [61], [1], [31]. In general this dissipative effect, known as mutual friction acts to bring the two fluids into co-rotation. However, if this interaction is either very weak or very strong a stationary description of the star with the two fluids rotating at different rates around the same axis is appropriate [69]. In this investigation we

assume that on the timescales we are considering the vortex friction is negligible, such that the two fluids are *free*. This assumption allows us to avoid unnecessary complications resulting from the inclusion of vortex friction and focus our attention on the effect of coupling by entrainment.

We also assume that the electron and proton charge densities are balanced ($n_{\rm p} = n_e$) allowing us to neglect electrodynamic effects. Furthermore we neglect the presence of exotic matter, which is expected to exist within the neutron star inner core, and the presence of an elastic crust.

We define the relative velocity of the two fluids as, $w_i^{YX} \equiv v_i^Y - v_i^X$ ($w_{YX}^i \equiv v_Y^i - v_X^i$) where $Y \neq X$. In order to avoid confusion we should stress that repeated constituent indices never imply summation, while repeated vector component indices always do.

Following an identical approach as Prix [70] we introduce a Lagrangian density, Λ_H, to describe the Newtonian hydrodynamics of our two fluid system. Λ_H depends on the number densities n_X and currents $n_X^i = n_X v_X^i$ such that,

$$\Lambda_H = \Lambda_H(n_X, n_X^i) \tag{2.9}$$

The dynamical quantities of our system such as the 'energy', p_0^X, and 'momentum', p_X^i, are defined by the differential of Λ_H,

$$d\Lambda_H = \sum_{X=\rm n,p} \left(p_0^X dn_X + p_i^X dn_X^i\right) \tag{2.10}$$

giving,

$$p_0^X = \frac{\partial \Lambda_H}{\partial n_X} \qquad\qquad p_X^i = \frac{\partial \Lambda_H}{\partial n_X^i} \tag{2.11}$$

In this work we consider a hydrodynamic Lagrangian density of the form,

$$\Lambda_H(n_x, n_X^i) = \frac{1}{2} \sum_{X=\rm n,p} m_X \frac{{n_X^i}^2}{n_X} - E \tag{2.12}$$

where E is the internal action. Prix [70] showed that E must satisfy Galilean invariance which implies the velocity dependence of E must be,

$$E = E(n_X, w_{YX}^i)$$

Since we restrict our investigations to isotropic fluids this internal action can only be of the form,

$$E = E(n_X, w_{YX}^2) \tag{2.13}$$

The first law of thermodynamics can be represented by the total differential of $E(n_X, w_{YX}^2)$,

$$dE = \sum_{X=\mathrm{n,p}} \mu_X dn_X + \alpha d(w_{YX}^2) \tag{2.14}$$

This leads to the definition of the two chemical potentials

$$\mu_X = \left(\frac{\partial E}{\partial n_X}\right)_{n_Y, w^2} \tag{2.15}$$

as well as the entrainment α. The entrainment function describes how the internal energy of the system depends on the relative velocity of the two fluids.

$$\alpha = \left(\frac{\partial E}{\partial (w_{YX}^2)}\right)_{n_X, n_Y} \tag{2.16}$$

We therefore find the momentum of our system can be written as,

$$p_i^X = m_B(v_i^X + \varepsilon_X w_i^{YX}) \tag{2.17}$$

where

$$\varepsilon_X = 2\alpha/n_X \tag{2.18}$$

is introduced as a dimensionless entrainment parameter. A flow in one of the fluid components will induce a momentum in the other constituent. A fundamental consequence of entrainment is that in general the momenta are not aligned with the respective fluid velocities. It is only in the case where there is either no entrainment or no relative velocity between the two fluids that the familiar result that $p_i^X = m_B v_i^X$ is observed.

In our superfluid model we ignore β-reactions ($n \rightleftharpoons p + e + \bar{\nu}$) between the two fluids, as has been done in many previous investigations of oscillations in superfluid systems [53] & [68], such that strict conservation of neutrons and protons applies and we have the following two continuity equations

$$\partial_t n_X + \nabla_i(n_X v_X^i) = 0 \tag{2.19}$$

We also find two coupled Euler equations

$$\left(\partial_t + v_X^j \nabla_j\right)\left(v_i^X + \varepsilon_X w_i^{YX}\right) + \nabla_i\left(\Phi + \tilde{\mu}_X\right) + \varepsilon_X w_j^{YX} \nabla_i v_X^j = 0 \tag{2.20}$$

Where $\tilde{\mu}_X = \mu_X/m_B$. These can be derived from the Lagrangian density using a *convective* variational principle, as was done by Prix [70]. We emphasise that equation (2.20) is expressed in terms of the chemical potential rather than the pressure.

As discussed earlier we find this constructive in the two fluid case since the pressure is a variable that depends on contributions from both the normal fluid and the superfluid where as there exists an individual chemical potential for each constituent. The final equation is the standard Poisson equation for the gravitational potential Φ,

$$\nabla^2\Phi = 4\pi m_{\rm B} G\left(n_{\rm n} + n_{\rm p}\right) \tag{2.21}$$

In this study we assume a stationary and axisymmetric background, with the *normal fluid* and the *superfluid* rotating around the z-axis at different angular velocities $\Omega_{\rm n}$ and $\Omega_{\rm p}$. Hence we have

$$v_X^i = \Omega_X \varphi^i \quad \text{and} \quad w_{YX}^i = (\Omega_Y - \Omega_X)\varphi^i \tag{2.22}$$

with φ^i given by

$$\varphi^i \partial_i = \partial_\varphi \ . \tag{2.23}$$

The system of equations we have constructed to describe our superfluid neutron star could equally describe any rotating two-fluid system, e.g. rotating superfluid helium. However, in the field of condensed matter physics an alternative formalism where the interaction between the two fluids is described in terms of an effective mass, rather than entrainment, is often used [92]. A detailed discussion of this alternative formalism can be found in Prix et al 2002, [69]. It is important to understand the connection between entrainment and effective mass if we are to have any hope of applying our work to this alternative scenario. The effective mass of a particle is the mass that it *seems* to carry. For example consider electrons and holes in a crystal. Under most circumstances the particles respond to electric and magnetic fields almost as if they were free particles in a vacuum, but with a different mass. The entrainment and effective mass can be related through the following equation,

$$2\alpha = \rho_{\rm p}\left(1 - \frac{m_{\rm p}^*}{m_B}\right) \tag{2.24}$$

Where $m_{\rm p}^*$ is the proton effective mass. Prix et al [69] discuss the proton effective mass at neutron star densities and conclude that it can range over values $0.3 \leq m_{\rm p}^*/m_B \leq 0.7$.

Chapter 3

Equilibrium models of rotating, polytropic cylinders

Having introduced, in Chapter 2, the equations describing the behaviour of single and two fluid systems we now consider equilibrium models for uniform rotation in self gravitating, polytropic cylinders. Since much of the work intended to be done in this project is in a cylindrically symmetric system it is necessary to obtain these background solutions. The model we will consider is uniform rotation about the z-axis, allowing the possibility that in the two-fluid case the fluids can rotate at different speeds. The edge of the cylinder is defined as the point at which the fluid densities vanishes. This would be similar to what one would expect for a star. We begin by considering the single fluid case.

3.1 A single fluid in a cylinder

In an infinitely long cylinder in hydrostatic equilibrium, rotating uniformly about its axis of symmetry, equation (2.1) becomes,

$$\frac{1}{\rho}\nabla_i p = -\nabla_i\left(\Phi - \frac{\Omega^2}{2}r^2\right) \tag{3.1}$$

Combining this with the polytropic equation of state, equation (2.8),

$$\nabla_i\left[K(n+1)\rho^{1/n}\right] = -\nabla_i\left(\Phi - \frac{\Omega^2}{2}r^2\right) \tag{3.2}$$

Integrating this equation directly gives,

$$K(n+1)(\rho_0^{1/n} - \rho^{1/n}) + \frac{\Omega^2}{2}r^2 = \Phi - \Phi_0 \tag{3.3}$$

Where ρ_0 and Φ_0 are the values of the density and gravitational potential along the

axis of symmetry. Substituting this expression for Φ into Poisson's equation (2.7) gives,

$$-K(n+1)\nabla^2(\rho^{1/n}) + \nabla^2\left(\frac{\Omega^2}{2}r^2\right) = 4\pi G\rho \tag{3.4}$$

In cylindrical coordinates we can express this as,

$$-K(n+1)\frac{1}{r}\frac{d}{dr}\left[r\frac{d}{dr}(\rho^{1/n})\right] + 2\Omega^2 = 4\pi G\rho \tag{3.5}$$

Where we have used the fact that the density has only a radial dependence, i.e. $\rho = \rho(r)$. Finally we scale the variables as follows,

$$\begin{aligned} \rho &= \rho_0\theta^n, \quad \Omega^2 = \pi G\rho_0\omega^2 \\ r &= \alpha\zeta, \quad \alpha = \left[\frac{K(n+1)\rho_0^{1/n}}{4\pi G\rho_0}\right]^{\frac{1}{2}} \end{aligned} \tag{3.6}$$

to obtain the Lane-Emden equation for a rotating cylinder, [66],

$$\frac{1}{\zeta}\frac{d}{d\zeta}\left(\zeta\frac{d\theta}{d\zeta}\right) = -\theta^n + \frac{\omega^2}{2} \tag{3.7}$$

The boundary conditions on the axis of symmetry are,

$$\theta(0) = 1 \qquad \text{and} \qquad \frac{d\theta(0)}{d\zeta} = 0 \tag{3.8}$$

and the boundary condition at the free surface, $p(\zeta = \zeta_s) = 0$, requires that,

$$\theta(\zeta_s) = 0 \qquad \text{where} \qquad \zeta_s = R/\alpha \tag{3.9}$$

In the two special cases when $n = 0$ and $n = 1$ the cylindrical Lane-Emden equation is linear and the solutions can be easily obtained, [65].

$$\begin{aligned} n = 0, &\quad \theta = 1 + \frac{\omega^2 - 2}{8}\zeta^2 \\ n = 1, &\quad \theta = \left(1 - \frac{\omega^2}{2}\right)J_0(\zeta) + \frac{\omega^2}{2} \end{aligned} \tag{3.10}$$

Where $J_0(\zeta)$ is the zeroth order Bessel function. For all other values of n the equation must be solved numerically. By reducing the second order Lane-Emden equation to two first-order differential equations the Runge-Kutta integration method, outlined in Appendix A.2, can be used to obtain a numerical solution to our problem. The two first order equations that need to be integrated are,

$$y = \frac{d\theta}{d\zeta} \tag{3.11}$$

$$\frac{dy}{d\zeta} = -\frac{y}{\zeta} - \theta^n + \frac{\omega^2}{2} \tag{3.12}$$

Since the point $\zeta = 0$ is a singular point of equation (3.12), we derive a series expansion for θ around $\zeta = 0$ and use this expansion to start the numerical integration at a small distance from the centre. We find,

$$\theta = 1 + a_2\zeta^2 + a_4\zeta^4 + a_6\zeta^6 + ... \tag{3.13}$$

$$\frac{d\theta}{d\zeta} = 2a_2\zeta + 4a_4\zeta^3 + 6a_6\zeta^5 + ... \tag{3.14}$$

with

$$a_2 = -\frac{1}{4}\left(1 - \frac{\omega^2}{2}\right) \tag{3.15}$$

$$a_4 = \frac{n}{64}\left(1 - \frac{\omega^2}{2}\right) \tag{3.16}$$

$$a_6 = -\frac{n}{1152}\left(1 - \frac{\omega^2}{2}\right)\left[\frac{n}{2} + (n-1)\left(1 - \frac{\omega^2}{2}\right)\right] \tag{3.17}$$

The value of ζ for which θ equals zero for the first time determines the value of ζ_s.

3.1.1 Physical parameters and the condition for maximum rotation

A solution to equation (3.7) exists provided the density remains positive ($\theta \geq 0$) and its derivative remains negative ($d\theta/d\zeta \leq 0$). Therefore at the surface,

$$\left.\frac{d\theta}{d\zeta}\right|_{\zeta_s} \leq 0 \tag{3.18}$$

The configuration where this derivative is equal to zero determines the maximum value of the rotation of the system. At this point the centrifugal force is balanced perfectly by the gravitational force and increasing the rotation rate further would result in mass shedding. By trial and error we can determine the value of this maximum rotation for different values of the polytropic index, n, using our numerical integration scheme, see Table 3.1.

The mass per unit length of our system is given by,

$$M = \int_0^{2\pi} d\phi \int_0^R \rho r dr = 2\pi\alpha^2\rho_0 \int_0^{\zeta_s} \theta^n \zeta d\zeta \tag{3.19}$$

If we substitute for θ^n from the Lane-Emden equation we find,

$$M = 2\pi\alpha^2\rho_0 \left[\zeta_s^2 \frac{\omega^2}{4} - \zeta_s \left. \frac{d\theta}{\delta\zeta} \right|_{\zeta_s} \right] \tag{3.20}$$

which is related to the mean density, $\bar{\rho}$ by,

$$M = \pi R^2 \bar{\rho} = \pi\alpha^2\zeta_s^2\bar{\rho} \tag{3.21}$$

Equating equations (3.20) and (3.21) we obtain an expression for the ratio $\rho_0/\bar{\rho}$, which is a measure of the mass concentration,

$$\frac{\rho_0}{\bar{\rho}} = \left[\frac{\omega^2}{2} - \frac{2}{\zeta_s} \left. \frac{d\theta}{d\zeta} \right|_{\zeta_s} \right]^{-1} \tag{3.22}$$

This equation shows that maximum rotation is characterised by,

$$\left(\frac{\Omega^2}{\pi G\bar{\rho}} \right)_{max} = 2 \tag{3.23}$$

This limit is independent of the polytropic index n.

If we assign the parameters in a non-rotating cylinder with an index $*$ the mass per unit length of a non-rotating system can be written as,

$$M_* = \pi\alpha_*^2\zeta_{s,*}^2\bar{\rho}_* \tag{3.24}$$

Therefore we can relate the mass of a cylinder in rotation to that of a non-rotating cylinder such that,

$$\frac{M}{M_*} = \left(\frac{\alpha}{\alpha_*} \right)^2 \left(\frac{\zeta_s}{\zeta_{s,*}} \right)^2 \frac{\bar{\rho}}{\bar{\rho}_*} \tag{3.25}$$

If we substitute for α from equation (3.6) we find,

$$\frac{M}{M_*} = f \left(\frac{K}{K_*} \right) \left(\frac{\rho_0}{\rho_{0,*}} \right)^{1/n} \tag{3.26}$$

where,

$$f = \left(\frac{\zeta_s}{\zeta_{s,*}} \right)^2 \left(\frac{\bar{\rho}/\rho_0}{\bar{\rho}_*/\rho_{0,*}} \right) \tag{3.27}$$

The factor f is always greater than one and we can obtain it from the numerical calculation. Supposing K is kept constant as the rotation varies, such that the equation of state does not change, we observe that we can insist the mass of our cylinder remains constant as we change the rotation rate provided the value of the

central density is altered. This is the conventional approach taken when investigating stars. An alternative to considering spinning up a cylinder of fixed mass, is to consider various cylinders with an identical central density such that as the rotation rate is increased the mass of the system must be increased accordingly. In the two fluid case, we consider a system such that the two fluids share a common surface. In this problem keeping both the proton mass and the neutron mass fixed whilst simultaneously insisting both densities vanish at a common surface is non trivial. Hence in this more complicated problem we take the approach of insisting the neutron central density is constant and allow the other parameters to change accordingly. It makes sense therefore to proceed in a similar fashion in the single fluid case by insisting the central density is fixed. We stress that consequently as we vary the rotation rate, ω, we are not considering the same cylinder.

3.1.2 Numerical results and discussion

We integrated equations (3.11) and (3.12) numerically for various values of n and ω. Figures 3.1 and 3.2 show how the density varies with radius for different configurations. Increasing the polytropic index results in a considerable increase in mass concentration. This can also be observed in Table 3.1 where we show ζ_s, $\rho_0/\bar{\rho}$ and $d\theta(\zeta_s)/d\zeta$ for various values of ω and n. We also highlight the values of maximum rotation obtained through the method of trial and error. In agreement with results by Robe [72] and Veugelen [83] we discover that increasing the rotation, ω, leads to an increase in both ζ_s and mass concentration. This is due to the centrifugal force, which has a larger effect on the outer layers of the cylinder. This gives rise to a stronger expansion of the outer layers and thus to an increase in the concentration of mass. These results are illustrated clearly in Table 3.1.

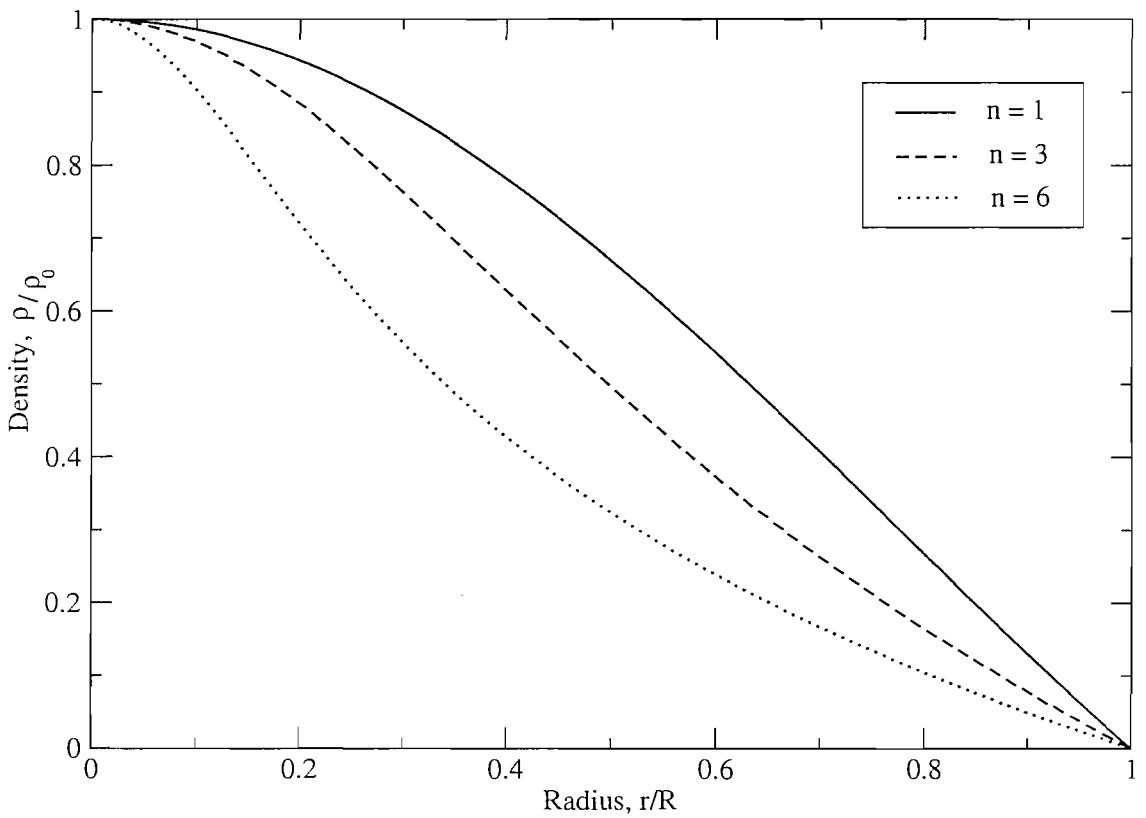

Figure 3.1: *The density of a single fluid in a rotating cylinder against radius for various values of the polytropic index, n. Increasing the polytropic index results in a considerable increase in mass concentration.*

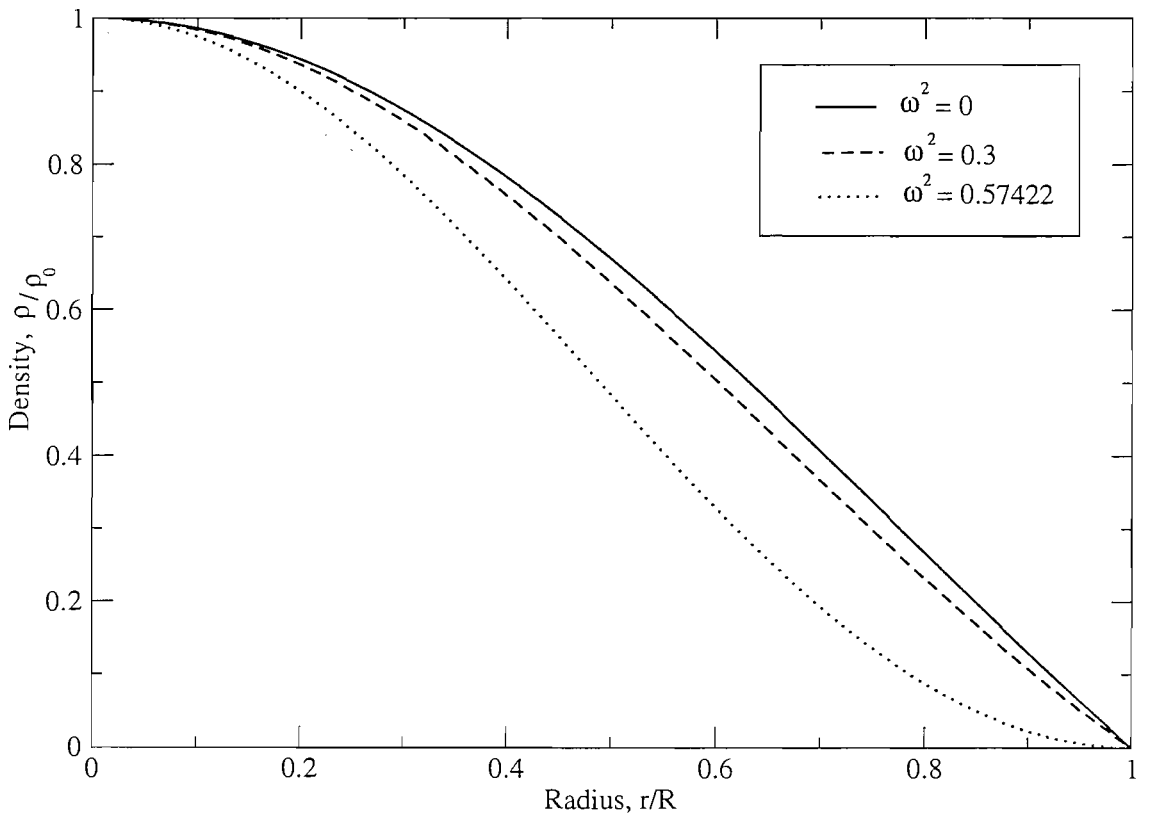

Figure 3.2: *The density of a single fluid in a rotating cylinder against radius for various values of ω. We can see that increasing the rotation leads to an increase of the mass concentration. When $w^2 = 0.57422$ the gravitational force at the surface is roughly equal to the centrifugal force and we see that for this case $d\rho/dr \sim 0$ at the surface.*

Rotation, ω^2	Surface, ζ_s	Mass concentration, $\rho_0/\bar{\rho}$	$d\theta(\zeta_s)/\delta\zeta$
Cylinder with $n = 1$			
0	2.41	2.32	-0.52
0.1	2.51	2.35	-0.47
0.3	2.78	2.47	-0.35
0.57422	3.82	3.47	-0.0025
Cylinder with $n = 3$			
0	3.57	8.63	-0.21
0.02	3.69	9.03	-0.19
0.06	4.01	10.26	-0.14
0.10947	5.49	18.18	-0.00076
Cylinder with $n = 6$			
0	6.73	48.35	-0.07
0.004	7.04	52.76	-0.06
0.01	7.75	63.39	-0.04
0.016422	10.75	121.02	-0.0003

Table 3.1: *Properties of uniformly rotating, self gravitating cylinders for various values of the polytropic index, n. The results highlight the effect of increasing the rotation of the system on the mass concentration and radius, ζ_s. As ω is increased the centrifugal force increases. Since it has a larger effect on the outer layers of the cylinder it gives rise to a stronger expansion of the outer layers and thus to an increase of the mass concentration. It is also clear from the results that increasing n significantly increases the mass concentration. A key result highlighted in the Table is the maximum rotation rate at which point the centrifugal force is balanced by the gravitational force. These values are emphasised with a grey box. In this Figure ω is the scaled, dimensionless, rotation rate such that $\omega^2 = \Omega^2/\pi G\rho_0$.*

3.2 Two fluids in a cylinder

The problem of a fluid in a rotating cylinder can be extended to the superfluid case by adding another fluid. We consider two cases; the situation where the entrainment function, α, is a constant and the situation where the dimensionless entrainment parameter, ε_X, is a constant. We find that in both cases the background solutions are identical and independent of the entrainment. The two fluids are coupled only through the gravitational potential. We begin our analysis by introducing an energy functional of the form,

$$E = \gamma_{\rm n} n_{\rm n}^2 + \gamma_{\rm p} n_{\rm p}^2 + \alpha w_{YX}^2 \tag{3.28}$$

which is simply a sum of two ordinary polytropes and an entrainment term. This *equation of state* is similar to that used by Prix & Rieutord [71] and Andersson & Comer [10] and is effective for investigating the characteristics of a two-fluid system.

The chemical potentials are defined by equation (2.15). We notice that the chemical potentials will be different for each of our two cases. When we assume α to be constant we find,

$$\mu_X = \frac{\partial E}{\partial n_X} = 2\gamma_X n_X \tag{3.29}$$

whereas when we consider ε_X to be a constant we find,

$$\mu_X = \frac{\partial E}{\partial n_X} = 2\gamma_X n_X + \frac{\varepsilon_X}{2} w_{YX}^2 \tag{3.30}$$

and

$$\mu_Y = \frac{\partial E}{\partial n_Y} = 2\gamma_Y n_Y \tag{3.31}$$

In this equilibrium state both the fluids are uniformly rotating around the z-axis such that

$$v_X^i = \Omega_X \phi^i \tag{3.32}$$

and since the velocities are stationary,

$$\frac{\partial v_X^i}{\partial t} = 0 \tag{3.33}$$

The Euler equations (2.20) therefore become,

$$-r\Omega_X^2 + \frac{d}{dr}(\Phi + \tilde{\mu}_X) = 0 \tag{3.34}$$

Integrating gives the Bernoulli equation,

$$-\frac{1}{2} r^2 \Omega_X^2 + \Phi + \tilde{\mu}_X = C_X \tag{3.35}$$

Equation (3.35) gives us 2 equations, one with index n and one with index p. By eliminating Φ we can combine these two equations to give,

$$\frac{1}{2}(\Omega_Y^2 - \Omega_X^2)r^2 + \tilde{\mu}_X - \tilde{\mu}_Y + C = 0 \tag{3.36}$$

To obtain an equation for the densities we must substitute for $\tilde{\mu}_X$. We initially consider the first case, where α is assumed constant. In this situation we find,

$$\rho_Y = \frac{m_B^2}{2\gamma_Y}\left[\frac{2\gamma_X}{m_B^2}\rho_X + \frac{1}{2}(\Omega_Y^2 - \Omega_X^2)r^2 + C\right] \tag{3.37}$$

The constant of integration C is found by insisting that both the densities vanish at a common surface, $r = R$. Thus

$$\rho_Y = \frac{m_B^2}{2\gamma_Y}\left[\frac{2\gamma_X}{m_B^2}\rho_X + \frac{1}{2}(\Omega_Y^2 - \Omega_X^2)(r^2 - R^2)\right] \tag{3.38}$$

In the $\varepsilon_{\rm n}$ constant case equation (3.36) gives us

$$\rho_Y = \frac{m_B^2}{2\gamma_Y}\left[\frac{2\gamma_X}{m_B^2}\rho_X + \frac{\varepsilon_X}{2}w^2 + \frac{1}{2}(\Omega_Y^2 - \Omega_X^2)r^2 + C\right] \tag{3.39}$$

Implementing the boundary condition leads once again to equation (3.38), giving an identical relationship between the two densities in both cases.

To obtain a differential equation for ρ_X we also require Poisson's equation which for this equilibrium state can be written as,

$$\frac{1}{r}\frac{d}{dr}\left[r\frac{d\Phi}{dr}\right] = 4\pi G(\rho_X + \rho_Y) \tag{3.40}$$

By eliminating Φ and ρ_Y we find for both the α constant and ε_X constant cases,

$$2\Omega_X^2 - \frac{2\gamma_X}{rm_B^2}\frac{d}{dr}\left[r\frac{d\rho_X}{dr}\right] = 4\pi G\left(\rho_X + \frac{m_B^2}{2\gamma_Y}\left[\frac{2\gamma_X}{m_B^2}\rho_X + \frac{1}{2}(\Omega_Y^2 - \Omega_X^2)(r^2 - R^2)\right]\right) \tag{3.41}$$

To simplify the equations we introduce the scaled variables given in Table 3.2 which will be used throughout this thesis. In the Table ρ_{n0} represents the central density of the neutrons and r_0 is defined such that,

$$\gamma_{\rm n} = 2\pi G m_B^2 r_0^2 \tag{3.42}$$

We stress that this definition, which has been made in order to eliminate $\gamma_{\rm n}$ from equation (3.41), indicates that $\bar{r}$, $\bar{\mu}_X$ and $\bar{\Phi}$ are not dimensionless variables as one might expect. We also introduce the following,

Physical variable	Corresponding scaled variable
Density, ρ_X	$\bar{\rho}_X = \theta_X = \rho_X/\rho_{n0}$
Angular velocity, Ω_X	$\bar{\Omega}_X = \Omega_X/\sqrt{4\pi G\rho_{n0}}$
Radius, r	$\bar{r} = r/r_0$
Chemical potential, μ_X	$\bar{\mu}_X = \mu_X/(4\pi G\rho_{n0}r_0^2)$
Gravitational potential, Φ	$\bar{\Phi} = \Phi/(4\pi G\rho_{n0}r_0^2)$
Entrainment function, α	$\bar{\alpha} = m_B\alpha/\rho_{n0}r_0^2$
Entrainment parameter, ε_X	$\bar{\varepsilon}_X = m_B\varepsilon_X/r_0^2$

Table 3.2: *Scaled variables*

$$K_X = \frac{\gamma_X}{\gamma_Y}$$

and

$$N_X = \frac{\gamma_X}{\gamma_{\rm n}}$$

Dropping the bars we arrive at the generalised Lane-Emden equation,

$$\theta_X'' + \frac{1}{r}\theta_X' + \frac{(1+K_X)}{N_X}\theta_X = \frac{2}{N_X}\Omega_X^2 - \frac{K_X}{2N_X^2}(\Omega_Y^2 - \Omega_X^2)(r^2 - R^2) \tag{3.43}$$

Which we can simplify to

$$\theta_X'' + \frac{1}{r}\theta_X' + (1+K_{\rm n})\theta_X = \frac{2}{N_X}\Omega_X^2 - \frac{K_{\rm n}}{2}(\Omega_Y^2 - \Omega_X^2)(r^2 - R^2) \tag{3.44}$$

Before finding a solution to equation (3.44) it is important to look at the boundary conditions that apply to the problem. We define a common surface for our system as the point at which both densities vanish, i.e $\rho_X(R) = 0$. The other conditions apply at the origin. At this point $\theta_{\rm n}(0) = 1$ and $\theta_{\rm n}'(0) = 0$. If we solve equation (3.44) for $\theta_{\rm n}$ we can straightforwardly obtain $\theta_{\rm p}$ using a scaled version of equation (3.38),

$$\theta_{\rm p} = K_{\rm n}\left[\theta_{\rm n} + \frac{1}{2}(\Omega_{\rm p}^2 - \Omega_{\rm n}^2)(r^2 - R^2)\right] \tag{3.45}$$

Initially this problem was solved in FORTRAN by integrating the equations numerically, obtaining solutions for θ_X and Φ. Subsequently Green's functions were used to attain an analytic solution. The analytical results are summarised in Appendix C. The first step in solving the equations numerically is to write equation (3.44) as two coupled first order equations,

$$S = \theta_{\rm n}' \tag{3.46}$$

$$S' + \frac{1}{r}S + (1 + K_{\rm n})\theta_{\rm n} = 2\Omega_{\rm n}^2 - Q_{\rm n}(r^2 - R^2) \tag{3.47}$$

Where,

$$Q_{\rm n} = \frac{K_{\rm n}}{2}(\Omega_{\rm p}^2 - \Omega_{\rm n}^2) \tag{3.48}$$

As in the single fluid case we find that $r = 0$ is a singular point of our equations. Once again we expand $\theta_{\rm n}$ as a power series around this point, to obtain an appropriate starting point for integration,

$$\theta_{\rm n} = 1 + \frac{1}{4}(2\Omega_{\rm n}^2 + Q_{\rm n}R^2 - 1 - K_{\rm n})r^2 - \frac{1}{16}(2\Omega_{\rm n}^2 + Q_{\rm n}R^2 - 1 - K_{\rm n} + Q_{\rm n})r^4 + ... \tag{3.49}$$

$$S = \theta_{\rm n}' = \frac{1}{2}(2\Omega_{\rm n}^2 + Q_{\rm n}R^2 - 1 - K_{\rm n})r - \frac{1}{4}(2\Omega_{\rm n}^2 + Q_{\rm n}R^2 - 1 - K_{\rm n} + Q_{\rm n})r^3 + ... \tag{3.50}$$

3.2.1 Physical parameters and the condition for maximum rotation

A solution to equation (3.44) exists provided both densities remains positive ($\theta_X \geq 0$) and their derivatives remain negative ($d\theta_X/dr \leq 0$). Therefore at the surface,

$$\left.\frac{d\theta_X}{dr}\right|_R \leq 0 \tag{3.51}$$

In the single fluid case the maximum rotation of the system occurred for a value of ω such that $d\theta/d\zeta$ vanished at the surface. In the superfluid case we are allowing the two fluids to rotate at different velocities. Therefore the maximum rotation of a particular constituent corresponds to a value of Ω_X such that $d\theta_X/dr$ vanishes at the surface. At this point the centrifugal force is balanced perfectly by the gravitational force and increasing the rotation rate further would result in mass shedding.

We define the mass per unit length of the neutrons as $M_{\rm n}$,

$$\begin{aligned} M_{\rm n} &= 2\pi r_0^2 \rho_{n0} \int_0^R r\theta_{\rm n} dr \\ &= 2\pi r_0^2 \rho_{n0} \frac{1}{1 + K_{\rm n}} \left[R^2\Omega_{\rm n}^2 + \frac{K_{\rm n}}{8}(\Omega_{\rm p}^2 - \Omega_{\rm n}^2)R^4 - R \left.\frac{d\theta_{\rm n}}{dr}\right|_R \right] \end{aligned} \tag{3.52}$$

and the mass per unit length of the protons as,

$$\begin{aligned} M_{\rm p} &= 2\pi r_0^2 \rho_{n0} \int_0^R r\theta_{\rm p} dr \\ &= K_{\rm n} M_{\rm n} - \frac{K_{\rm n}}{4}\pi r_0^2 \rho_{n0}(\Omega_{\rm p}^2 - \Omega_{\rm n}^2)R^4 \end{aligned} \tag{3.53}$$

The conventional approach when investigating rotating stars is to vary the rotation rate whilst keeping the mass fixed. In this way we are considering the same system at a variety of different rotation rates. In the superfluid problem we have the mass of the neutrons and the mass of the protons to consider. In equations (3.52) and (3.53) for a certain choice of $\Omega_{\rm n}$ and $\Omega_{\rm p}$ we are free to specify the parameters r_0, ρ_{n0} and $K_{\rm n}$. Therefore as we alter the rotation rates we can in principle keep the masses fixed by an appropriate choice of values for these quantities. In the single fluid case we found that we could straightforwardly assign the central density at each value of Ω to ensure that the mass of the system stayed the same. In this more complicated problem we must firstly insist that the ratio of neutrons to protons remains constant at which point we can specify ρ_{n0} to keep the masses fixed. The total proton fraction, $M_{\rm p}/M_{\rm n}$, can be written as,

$$\frac{M_{\rm p}}{M_{\rm n}} = K_{\rm n} - \frac{K_{\rm n}}{8(1+K_{\rm n})}\left\{\frac{(\Omega_{\rm p}^2-\Omega_{\rm n}^2)R^4}{\left[R^2\Omega_{\rm n}^2+\frac{K_{\rm n}}{8}(\Omega_{\rm p}^2-\Omega_{\rm n}^2)R^4 - R\,\frac{d\theta_{\rm n}}{dr}\Big|_R\right]}\right\} \tag{3.54}$$

Ensuring this remains fixed as we vary the rotation rates is in principle possible. Since the radius R is determined numerically through integration of the Lane-Emden equation, preserving the total proton fraction requires numerically solving equation (3.54) as an eigenvalue problem for $K_{\rm n}$. Due to the non-trivial nature of this procedure we choose instead to investigate the effect of rotation whilst keeping $K_{\rm n}$ constant. As a consequence we find that the total proton fraction changes with $\Omega_{\rm n}$ and $\Omega_{\rm p}$. If we increase $\Omega_{\rm n}$ whilst keeping $\Omega_{\rm p}$ constant we observe that the neutrons will tend to spread out due to the increased centrifugal force. To ensure that the protons and neutrons continue to share a common surface an increase in the total proton fraction is inevitable. It is important to stress therefore that in our analysis we are not considering the same system at different rates of rotation.

In the single fluid case we used the ratio $\rho_0/\bar{\rho}$, as a measure of the mass concentration. In this two fluid case it is interesting to look at the mass concentration of each individual constituent, i.e. $\rho_{n0}/\bar{\rho}_{\rm n}$ and $\rho_{p0}/\bar{\rho}_{\rm p}$.

$$\frac{\rho_{n0}}{\bar{\rho}_{\rm n}} = \frac{1+K_{\rm n}}{2}\left[\Omega_{\rm n}^2 + \frac{Q_{\rm n}R^2}{4} - \frac{1}{R}\,\frac{d\theta_{\rm n}}{dr}\Big|_R\right]^{-1} \tag{3.55}$$

Similarly for the protons

$$\frac{\rho_{p0}}{\bar{\rho}_{\rm p}} = (K_{\rm n}-Q_{\rm n})\left[K_{\rm n}\left(\frac{\bar{\rho}_{\rm n}}{\rho_{n0}}\right) - \frac{Q_{\rm n}R^2}{2}\right]^{-1} \tag{3.56}$$

In analogy with equation (3.19) the total mass per unit length in this two fluid system can be written as,

$$\begin{aligned} M &= 2\pi r_0^2 \rho_{n0} \int_0^R r(\theta_\mathrm{b} + \theta_\mathrm{p}) dr \\ &= 2\pi r_0^2 \rho_{n0} \left[R^2 \Omega_\mathrm{n}^2 - R \left. \frac{d\theta_\mathrm{n}}{dr} \right|_R \right] \end{aligned} \tag{3.57}$$

We can relate this to the mean density using equation (3.21) giving,

$$\bar{\theta} = 2 \left[\frac{1}{R} \left. \frac{d\theta_\mathrm{n}}{dr} \right|_R + \Omega_\mathrm{n}^2 \right] \tag{3.58}$$

Therefore maximum rotation of the neutrons occurs at a point such that,

$$\left(\frac{\Omega_\mathrm{n}^2}{\bar{\theta}} \right)_{max} = \frac{1}{2} \tag{3.59}$$

If we take into account the scaling used we observe that this is identical to equation (3.23), the limit for maximum rotation in the single fluid problem. This makes sense since we are balancing the gravitational force, which depends on the total mass of the system, to the centrifugal force, which depends on the rotation rate at the surface. However, in our analysis we are not considering the same system at different rates of rotation and it is not therefore constructive to investigate these values numerically.

3.2.2 Results and discussion

Equations (3.46) and (3.47) were integrated numerically to calculate $\rho_X(r)$ for specified values of Ω_X and K_X. We look initially at the co-rotating case, shown in Figures 3.3 and 3.4. We observe that the proton fraction remains constant for all r, i.e. the cylinder is non-stratified. As we increase the rate of rotation the radius is enlarged and the mass concentration intensified. This is a result of the increase in the centrifugal force as the rotation rate increases. Since the effect is greatest on the outer layers a larger expansion near the surface and hence an increase in the mass concentration is observed. These results are emphasised in Table 3.3. Figure 3.4 demonstrates the effect of varying K_n which we can recall is $\gamma_\mathrm{n}/\gamma_\mathrm{p}$ from the two fluid equation of state. As K_n is decreased the proton fraction is also decreased. In the co-rotating case we can see that the proton fraction, $x_\mathrm{p} = \rho_\mathrm{p}/\rho_\mathrm{n} = K_\mathrm{n}$. As one would expect the total density distribution, $\rho(r) = \rho_\mathrm{n}(r) + \rho_\mathrm{p}(r)$, in this co-rotating case is identical to the density distribution in the single fluid case.

Introducing a relative rotation between the two fluids leads to stratification, see Figure 3.5. The proton fraction no longer remains constant throughout the cylinder.

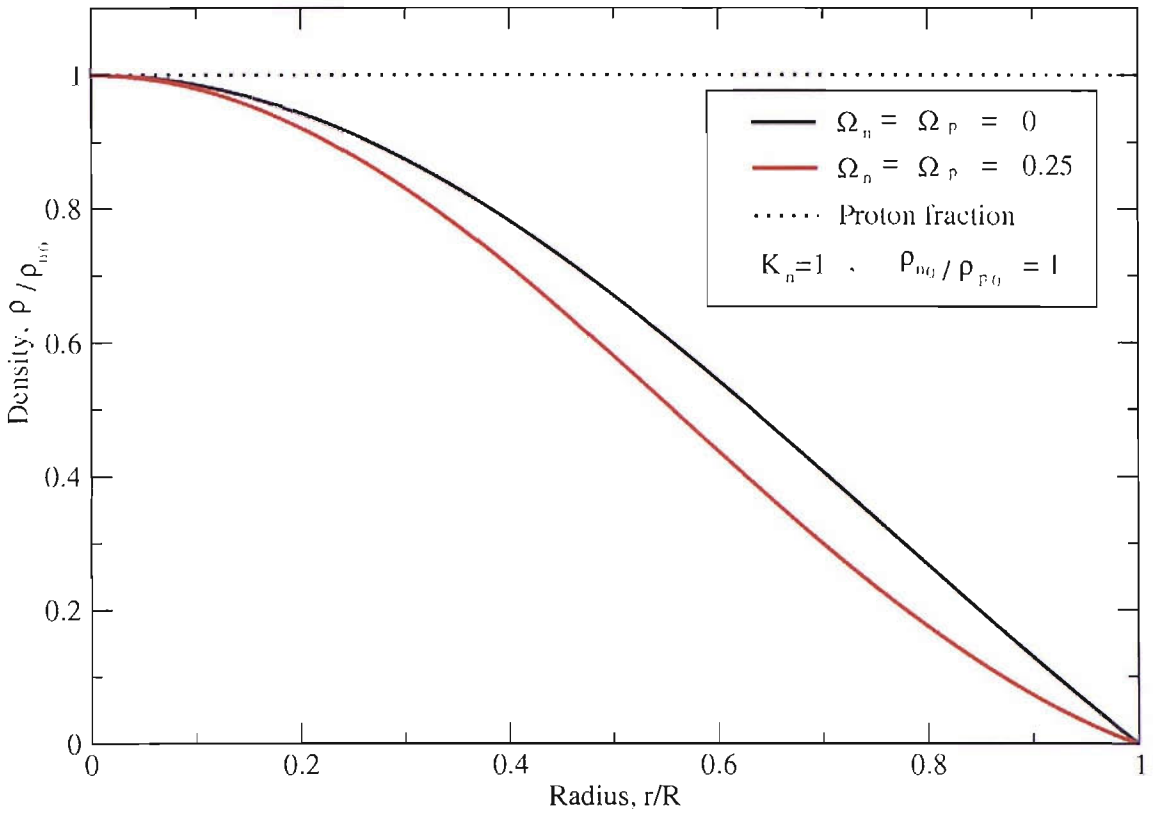

Figure 3.3: *Graph of density against radius for two co-rotating fluids in a cylinder illustrating the effect of varying the rotation rates, Ω_n and Ω_p. The neutron and proton densities in this configuration are identical since $K_n = 1$. As we increase the rate of rotation the radius is enlarged and the mass concentration intensified. This is a result of the increase in the centrifugal force as the rotation rate increases. These results are emphasised in Table 3.3.*

We take a similar approach as Prix, Comer and Andersson [68] and choose to use the proton angular velocity Ω_p as the *reference* rotation rate. The motivation for this choice is that observationally deduced rotation rates obtained from pulsars are believed to correlate with the proton rotation rate. The rotation rate of the neutrons on the other hand is unfortunately not directly observable. We thus define the relative rotation rate $\mathcal{R}$ as

$$\mathcal{R} \equiv \frac{\Omega_n - \Omega_p}{\Omega_p} \tag{3.60}$$

From Figure 3.5 we confirm that increasing the rotation rate of the neutrons, whilst keeping Ω_p and K_n fixed results in an increase in the total proton fraction. Table 3.3 reveals that at co-rotation, with $K_n = 0.5$, $M_p/M_n = 0.5$, but as we increase the neutron rotation rate this value increases to 0.57. Similarly if we decrease the neutron rotation rate the proton fraction is observed to decrease accordingly. This is a consequence of our decision to keep K_n constant as we alter the rotation rates

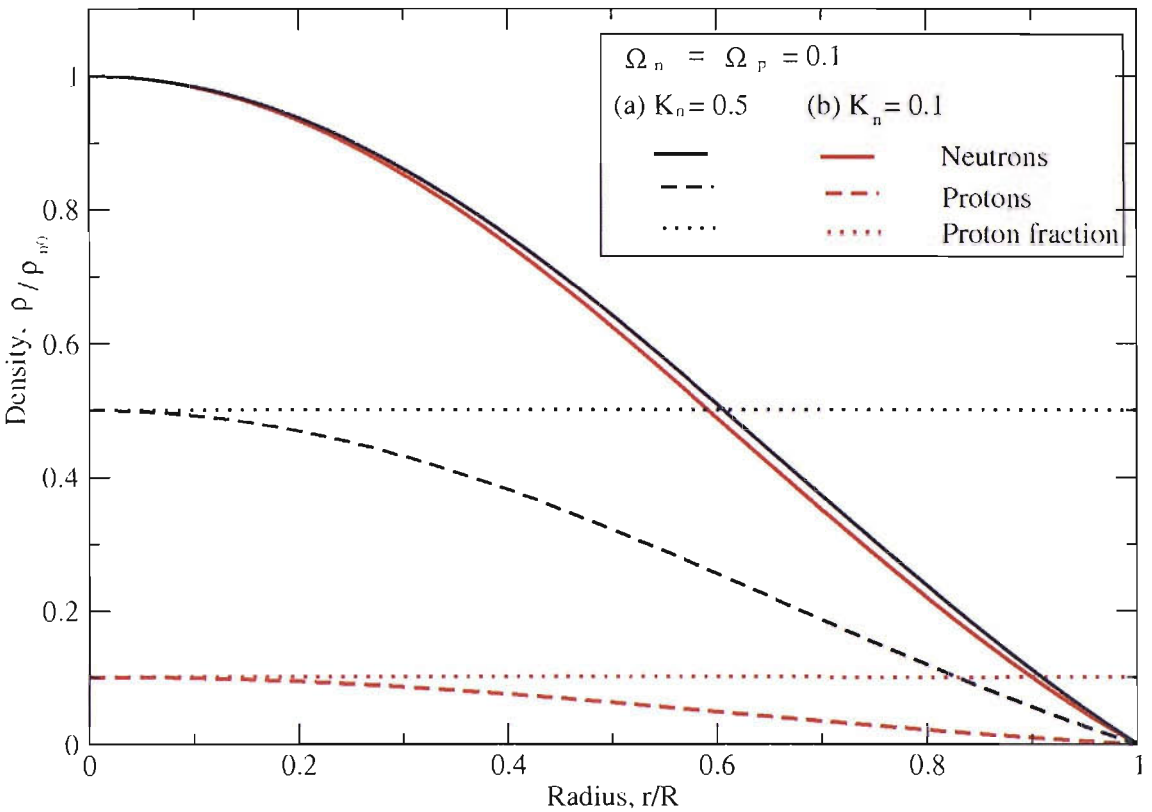

Figure 3.4: *Graph of density against radius for two co-rotating fluids in a cylinder illustrating the effect of varying K_n. In this co-rotating case the proton fraction, $x_p = \rho_p/\rho_n = K_n$, remains constant throughout the cylinder.*

yet still insist that the neutrons and protons share a common surface. Another effect of introducing a relative rotation, apparent from Table 3.3, is that the mass concentration of the fluid which is moving faster increases while that of the slower moving fluid decreases. If we increase Ω_n the centrifugal force on the neutrons increases. Since it has a larger effect on the outer layers it gives rise to a stronger expansion near the surface and hence an increase in mass concentration. However, the reverse is true for the protons which continue to rotate at the same velocity. The increase in neutron rotation rate leads to an increased radius R, see Table 3.3. Therefore at the surface the centrifugal force on the protons is decreased and a corresponding decrease in proton mass concentration is observed. These results highlight the fact that we are not considering the same system at different rotation rates and it is important to keep this in mind during our mode analysis in Sections 5 and 6.

In neutron stars it is estimated that about 10% of the mass is found in the protons and the remaining 90% results from the superfluid neutrons. It is also predicted, from observations of large Vela glitches, that the maximum relative rotation of the neutrons and protons is roughly $\mathcal{R} \sim 10^{-4}$ [59]. We can reproduce this situation by selecting appropriate values of K_n, Ω_n and Ω_p, this can be seen in Figure 3.7. It

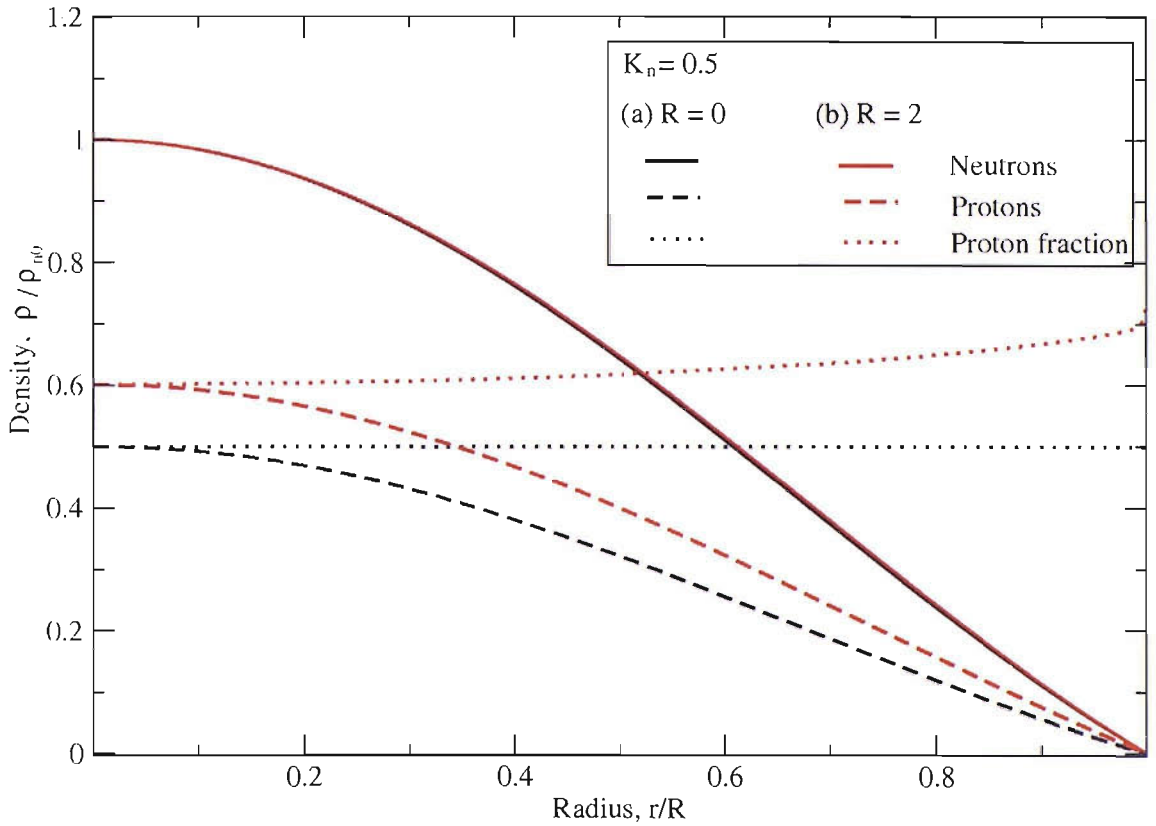

Figure 3.5: *Graph of density against radius for two fluids in a cylinder, illustrating the effect of introducing a neutron and proton relative rotation. We observe that relative rotation leads to a stratification of the two fluids and a change in the total proton fraction (this is emphasised in Table 3.3). This is a consequence of our decision to keep K_n constant as we alter the rotation rates yet still insist that the neutrons and protons share a common surface. Another effect of introducing a relative rotation, is that the mass concentration of the fluid which is moving faster increases while that of the slower moving fluid decreases. This is due to the increase in centrifugal force on the faster fluid and a corresponding decrease on the slower fluid.*

should be pointed out that although we are trying to make the data as similar as possible to actual neutron stars there are still many approximations being made and thus we do not expect to achieve any results that we could compare to any observable physical quantities. For instance we are considering cylinders and assuming that the density of both constituents drops to zero at the same point. In a real neutron star one would expect an approximately spherical configuration and a neutron and proton composition more similar to that shown in Figure 3.6, where the protons and electrons extend further than the neutrons mimicking the configuration in the neutron star crust. Nonetheless our model should provide a sufficiently complex background configuration to allow us to meaningfully investigate the oscillations of a superfluid system.

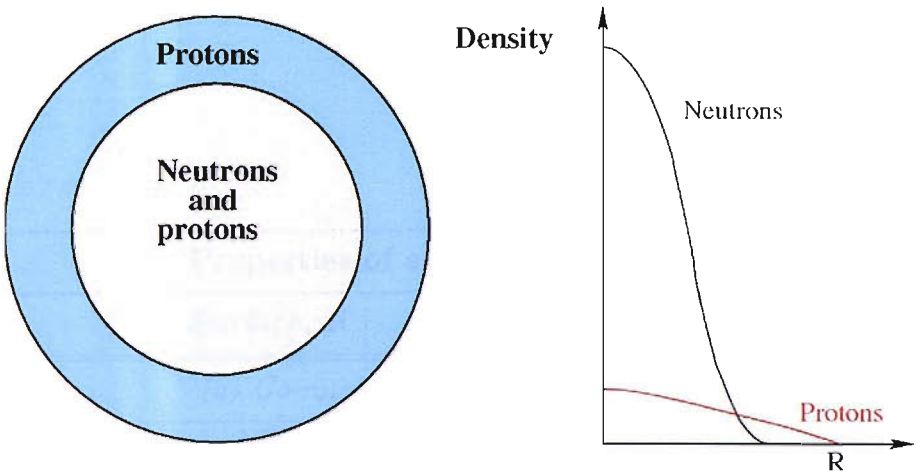

Figure 3.6: *A schematic illustration of a more realistic neutron star configuration, where the protons and electrons extend further than the neutrons.*

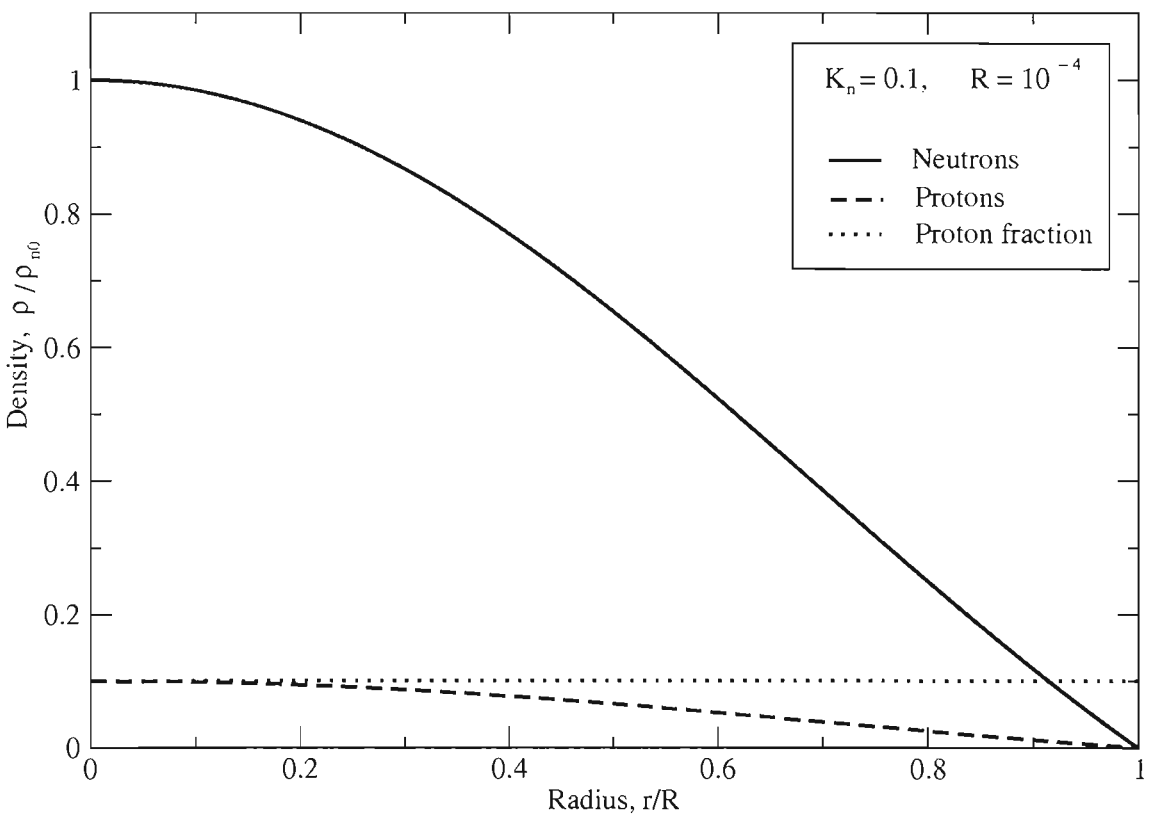

Figure 3.7: *A graph of density against radius for a typical neutron star mass ratio and relative rotation. The relative rotation leads to stratification of the fluids. However, since $\mathcal{R}$ is small the effect is minimal.*

Properties of superfluid cylinders				
	Surface, R	$\rho_{n0}/\bar{\rho}_{\rm n}$	$\rho_{p0}/\bar{\rho}_{\rm p}$	$M_{\rm p}/M_{\rm n}$
(a) Co-rotating cylinder with $K_{\rm n} = 1$				
$\Omega = 0$	1.71	2.32	2.32	1
$\Omega = 0.25$	2.30	2.77	2.77	1
(b) Co-rotating cylinder with $\Omega_{\rm n} = \Omega_{\rm p} = 0.1$				
$K_{\rm n} = 0.3$	2.45	2.48	2.48	0.3
$K_{\rm n} = 0.1$	2.76	2.53	2.53	0.1
(c) Cylinder with $K_{\rm n} = 0.5$, $\Omega_{\rm p} = 0.05$				
$\mathcal{R} = 0$	2.08	2.37	2.37	0.5
$\mathcal{R} = 2$	2.26	2.52	2.00	0.57
$\mathcal{R} = -1$	2.00	2.33	2.57	0.47
(d) Cylinder with typical neutron star configuration, $\mathcal{R} \sim 10^{-4}$				
	2.76	2.5310	2.5312	0.1

Table 3.3: *Properties of uniformly rotating, self gravitating two fluid cylinders for various values of* $\Omega_{\rm n}$, $\Omega_{\rm p}$ *and* $K_{\rm n}$. *For the co-rotating cylinders in (a) and (b) increasing the rotation rate results in an increase in the radius* R *and the mass concentration. This is due to an increase in the centrifugal force which has a larger effect on the outer layers of the cylinder giving rise to a stronger expansion of the outer layers and thus to an increase in the mass concentration. We also observe from (b) that varying* $K_{\rm n}$ *results in a corresponding change in the total proton fraction. The results in (c) highlight the effects of introducing a relative rotation. We confirm that increasing the rotation rate of the neutrons, whilst keeping* $\Omega_{\rm p}$ *and* $K_{\rm n}$ *fixed results in an increase in the total proton fraction. Another effect of introducing a relative rotation is that the mass concentration of the fluid which is moving faster increases while that of the slower moving fluid decreases. In (d) we illustrate the results for a cylinder with a typical neutron star proton fraction and relative rotation.*

Chapter 4

Linearised perturbation theory

In Chapter 3 we obtained solutions for single and two fluid uniformly rotating, polytropic cylinders. We now hope to investigate what happens as we move away from this equilibrium configuration. Superimposing small perturbations, representing weak disturbances, upon an otherwise *unperturbed* system is the basis of perturbation theory. By assuming the disturbances are sufficiently small we can neglect any terms which are non-linear in the perturbation resulting in equations describing the linear oscillations of our system. Solving these equations as an eigenvalue problem gives us the normal mode solutions.

4.1 Eulerian and Lagrangian perturbations

Two types of description can be used to analyse the oscillations of a system about a known state of equilibrium. Either we specify disturbances noted by an external observer who, at every instant t, views a given volume element at a fixed location in space, or we describe the fluctuations within a given mass element which is followed along its path. These are named Eulerian and Lagrangian perturbations respectively. These descriptions can be written mathematically in the following way. We define $Q(\vec{x},t)$ and $Q_0(\vec{x},t)$ to be the values of a physical quantity in the perturbed and unperturbed flow. If $\vec{\xi}(\vec{x},t)$ represents the perturbation the Eulerian (δ) and Lagrangian (Δ) change in the physical quantity Q can be written,

$$\delta Q = Q(\vec{x},t) - Q_0(\vec{x},t) \tag{4.1}$$

$$\Delta Q = Q(\vec{x}+\vec{\xi}(\vec{x},t),t) - Q_0(\vec{x},t) \tag{4.2}$$

These two different types of perturbation are related through the following relation.

$$\Delta Q = \delta Q + \pounds_\xi Q \tag{4.3}$$

Where $\pounds_\xi$ represents the Lie derivative. Lie differentiation involves comparing a tensor, $T^{ab}(x')$ which is already at a point Q with the tensor $T'^{ab}(x')$ which has been dragged along the curve from point P to point Q. This is shown in Figure 4.1,

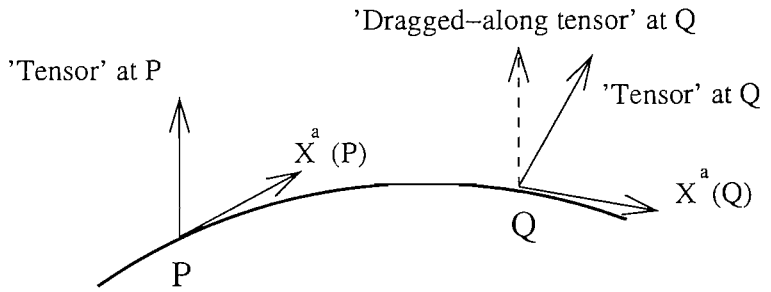

Figure 4.1: *A schematic diagram illustrating how the Lie derivative compares two tensors at the point Q.*

For a scalar f the Lie derivative is defined as,

$$\pounds_\xi f = \xi^i \nabla_i f \tag{4.4}$$

For contravariant vector fields v^i,

$$\pounds_\xi v^i = \xi^j \nabla_j v^i - v^j \nabla_j \xi^i \tag{4.5}$$

For covariant vector fields v_i,

$$\pounds_\xi v_i = \xi^j \nabla_j v_i + v_j \nabla_i \xi^j \tag{4.6}$$

In this section the general Eulerian perturbation equations for a single and a two fluid entrainment free system are derived. To study the oscillations and stability of the infinite, self gravitating, uniformly rotating cylinder introduced in Section 2 we subsequently express these equations in cylindrical co-ordinates and for the single fluid case investigate the normal modes.

4.2 Eulerian perturbation equations for a single fluid

We begin by deriving the Eulerian perturbation equations for a single fluid. It is convenient in this case to work in terms of perturbations to the density, $\delta\rho$, and the radial part of the displacement vector ξ_r. This is the conventional approach which has been used in a vast range of studies of single fluid systems [14],[71], and allows for a straightforward comparison to previous work on linear oscillations in cylinders, [81], [82].

A displacement vector, ξ_i, can be defined to describe how the perturbation affects the fluid. This correspond to a change in fluid velocity,

$$\Delta v_i = \partial_t \xi_i \tag{4.7}$$

Since the background configuration is stationary and axisymmetric we can separate the displacement vector into a radial part and an azimuthal part. The azimuthal function should be proportional to $e^{im\phi}$, with m an integer. If we also assume a harmonic time dependence we can write the displacement vector as,

$$\xi_i(r, \phi, t) = \xi_i(r) e^{i(m\phi + \omega t)} \tag{4.8}$$

We have also made the assumption that there is no variation in the z-direction and hence the displacement vector has r and ϕ components only. Equations which govern how the perturbed fluid behaves can be obtained by substituting $v_i \rightarrow v_i + \delta v_i$, $p \rightarrow p + \delta p$, $\rho \rightarrow \rho + \delta\rho$ and $\Phi \rightarrow \Phi + \delta\Phi$ in the equations which describe the fluid flow. Where δp , $\delta\rho$ and $\delta\Phi$ represent the Eulerian perturbations in the density, pressure and gravitational potential. It is convenient in this cylindrically symmetric case to work in a rotating frame of reference, such that the background velocity of the fluid is zero. We define, $\vec{\Omega}$, as the rotation rate of this frame such that in cylindrical coordinates,

$$\vec{\Omega} = \Omega_0 \vec{e}_z \tag{4.9}$$

In this frame the Euler equations can be written as:

$$\partial_t \vec{v} + \vec{v} \cdot \nabla \vec{v} + 2\vec{\Omega} \times \vec{v} + \vec{\Omega} \times (\vec{\Omega} \times \vec{r}) = -\frac{1}{\rho} \nabla p - \nabla \Phi \tag{4.10}$$

Where the centrifugal term can be rewritten as,

$$\vec{\Omega} \times (\vec{\Omega} \times \vec{r}) = -\frac{1}{2} \nabla (\vec{\Omega} \times \vec{r})^2 \tag{4.11}$$

By perturbing and linearising equation (4.10) we obtain the following differential equation,

$$\partial_t \delta\vec{v} + 2\vec{\Omega} \times \delta\vec{v} = \frac{\delta\rho}{\rho^2} \nabla p - \frac{1}{\rho} \nabla \delta p - \nabla \delta\Phi \tag{4.12}$$

Where we have made use of the fact that the background velocity in the rotating frame is zero. Assuming condition (4.8) leads to,

$$i\omega\delta\vec{v} + 2\vec{\Omega} \times \delta\vec{v} = \frac{\delta\rho}{\rho^2} \nabla p - \frac{1}{\rho} \nabla \delta p - \nabla \delta\Phi \tag{4.13}$$

or using indicial notation,

$$i\omega\delta v_i + 2\epsilon_{ijk}\Omega^j \delta v^k - \frac{\delta\rho}{\rho^2} g_i^j \nabla_j p + \frac{1}{\rho} g_i^j \nabla_j \delta p + g_i^j \nabla_j \delta\Phi = 0 \tag{4.14}$$

We must also represent the conservation of mass of our system. Introducing a perturbation to equation (2.5) we obtain the following linearised continuity equation,

$$\partial_t \delta\rho + \nabla_i(\rho\delta v^i) + \nabla_i(\delta\rho v^i) = 0 \tag{4.15}$$

Since the background velocity is zero in the rotating frame and the density variation can be written as $\delta\rho = \delta\rho e^{i(m\phi+\omega t)}$ the continuity equation becomes,

$$i\omega\delta\rho + i\omega\nabla_i(\rho\xi^i) = 0 \tag{4.16}$$

Which can be simplified to,

$$\delta\rho + \nabla_i(\rho\xi^i) = 0 \tag{4.17}$$

By considering perturbations to equation (2.7), the equation for the gravitational field, we arrive at the following perturbed Poisson equation,

$$\partial_i\partial^i\delta\Phi = 4\pi G\delta\rho \tag{4.18}$$

The final consideration required is to prescribe an equation of state for the perturbation. Since, on the short timescale associated with the perturbation, different physical processes may dominate we can not automatically assume that this equation of state is identical to that of our background configuration. The Lagrangian perturbations of pressure and density can be related by,

$$\frac{\Delta p}{p} = \Gamma_1 \frac{\Delta\rho}{\rho} \tag{4.19}$$

Where Γ_1 is the adiabatic index. Which gives the following equation for the Eulerian density and pressure,

$$\frac{1}{p}\delta p + \frac{1}{p}\xi^i\nabla_i p = \frac{\Gamma_1}{\rho}\delta\rho + \frac{\Gamma_1}{\rho}\xi^i\nabla_i\rho \tag{4.20}$$

Since the background density and pressure vary only in r this equation becomes,

$$\begin{aligned}
\delta\rho &= \frac{\rho}{p\Gamma_1}\left(\delta p + \xi_r\frac{dp}{dr}\right) - \xi_r\frac{d\rho}{dr} \\
&= \frac{\delta p}{c_s^2} + \left(\frac{1}{c_s^2}\frac{dp}{dr} - \frac{d\rho}{dr}\right)\xi_r \\
&= \frac{\delta p}{c_s^2} - \rho\left(\frac{g}{c_s^2} + \frac{1}{\rho}\frac{d\rho}{dr}\right)\xi_r
\end{aligned} \tag{4.21}$$

$$\delta\rho = \frac{\delta p}{c_s^2} + \frac{\rho N^2}{g}\xi_r \tag{4.22}$$

Where g is the effective gravity,

$$g = \frac{d\Phi}{dr} - r\Omega_0^2 = -\frac{1}{\rho}\frac{dp}{dr} \tag{4.23}$$

c_s is the adiabatic sound speed, and N^2 is the square of the Brunt-Vaisala frequency, given by

$$N^2 = -g\left(\frac{1}{\rho}\frac{d\rho}{dr} + \frac{g}{c_s^2}\right) \tag{4.24}$$

If this frequency is zero we can say that the system is isentropic and the perturbation obeys the same equation of state as the background fluid. We now have a set of equations describing the Eulerian perturbations for a general single fluid system. To investigate the oscillations and stability of a rotating cylinder we express the perturbed equations in cylindrical coordinates.

4.3 Eulerian perturbations in a cylinder

Appendix B summarises the basic properties of a cylindrical coordinate system and introduces the various operators using this framework. The linearised Euler equation gives us the following two equations,

$$-\omega^2\xi_r - 2i\omega\Omega_0\xi_\phi = \frac{\delta\rho}{\rho^2}\frac{dp}{dr} - \frac{1}{\rho}\frac{d\delta p}{dr} - \frac{d\delta\Phi}{dr} \tag{4.25}$$

and

$$-\omega^2\xi_\phi + 2i\omega\Omega_0\xi_r = -\frac{im\delta p}{\rho r} - \frac{im\delta\Phi}{r} \tag{4.26}$$

In cylindrical coordinates the divergence and Laplacian are given by equations (B.11) and (B.14) respectively. Thus the continuity equation becomes,

$$\delta\rho + \xi_r\frac{\partial\rho}{\partial r} + \frac{\rho}{r}\frac{\partial}{\partial r}(r\xi_r) + \frac{im\rho}{r}\xi_\phi = 0 \tag{4.27}$$

and the perturbed Poisson equation becomes

$$\frac{\partial^2\delta\Phi}{\partial r^2} + \frac{1}{r}\frac{\partial\delta\Phi}{\partial r} - \frac{m^2}{r^2}\delta\Phi = 4\pi G\left[\frac{\delta p}{c_s^2} + \frac{\rho N^2}{g}\xi_r\right] \tag{4.28}$$

The Euler equations, the continuity equation and the equation of state can now be combined to give the following equations for the normal modes.

$$\omega^2 \frac{d}{dr}(r\xi_r) = \omega \left[\frac{2m\Omega_0}{r} + \omega\frac{g}{c_s^2}\right] r\xi_r + \left[\frac{m^2}{r} - \omega^2\frac{r}{c_s^2}\right]\frac{\delta p}{\rho} + \frac{m^2}{r}\delta\Phi \tag{4.29}$$

$$\frac{d}{dr}\left(\frac{\delta p}{\rho}\right) = \omega\left[\omega - 4\Omega_0^2 - N^2\right]\xi_r + \left[\omega\frac{N^2}{g} - \frac{2\Omega_0 m}{r}\right]\frac{\delta p}{\rho} - \frac{2\Omega_0 m}{r}\delta\Phi - \frac{d\delta\Phi}{dr} \tag{4.30}$$

Combined with equation (4.28) these two equations fully describe the perturbed system.

It is appropriate to use the Cowling approximation, which constitutes ignoring the perturbation to the gravitational potential, to greatly simplify our investigations, [32]. It has been shown that for perfect fluid cylinders making this approximation introduces only a very small error for low frequency modes, [81]. This can be understood in the following way. Consider the integral of the Poisson equation,

$$\delta\Phi = -G\int \frac{\delta\rho(r')}{|r - r'|}dr' \tag{4.31}$$

For some modes the contributions $\delta\rho(r')$ from different places within the cylinder tend to cancel each other out leaving a negligible net effect. Thus it is reasonable to drop the perturbation to the gravitational potential from our analysis.

The normal mode solutions for a rotating self-gravitating cylinder were found using a spectral linear eigenvalue solver package, called LSB, developed by L. Valdettaro and M. Rieutord. The LSB program is a FORTRAN code which evaluates approximate eigenvalues and eigenvectors for boundary value problems using spectral methods. The program takes an equation or a system of equations, which must be written in a specific data file and then calculates the eigenvalues subject to the specified boundary conditions.

Before looking at the eigenfunctions of the normal modes it is of interest to know the regions in which the different waves can propagate. This is done by local analysis with the aid of propagation diagrams. Since we are neglecting perturbations to the gravitational potential we can ignore the Poisson equation and the problem reduces to that of two equations,

$$\omega^2 \frac{d}{dr}(r\xi_r) = \omega \left[\frac{2m\Omega_0}{r} + \omega\frac{g}{c_s^2}\right] r\xi_r + \left[\frac{m^2}{r} - \omega^2\frac{r}{c_s^2}\right]\frac{\delta p}{\rho} \tag{4.32}$$

$$\frac{d}{dr}\left(\frac{\delta p}{\rho}\right) = \omega\left[\omega^2 - 4\Omega_0^2 - N^2\right]\xi_r + \left[\omega\frac{N^2}{g} - \frac{2\Omega_0 m}{r}\right]\frac{\delta p}{\rho} \tag{4.33}$$

The method of local analysis is performed by assuming that the perturbed displacement and pressure can be written as plane waves,

$$\xi_r = \frac{1}{r}\xi_{rk}e^{ikr} \tag{4.34}$$

$$\delta p = \delta p_k e^{ikr} \tag{4.35}$$

Where k is the wavenumber and ξ_{rk} and δp_k are constants. Substituting these into equation (4.32) gives,

$$ik\omega^2\xi_{rk}e^{ikr} = \omega\left[\frac{2m\Omega_0}{r} + \omega\frac{g}{c_s^2}\right]\xi_{rk}e^{ikr} + \left[\frac{m^2}{r} - \omega^2\frac{r}{c_S^2}\right]\frac{\delta p_k}{\rho}e^{ikr} \tag{4.36}$$

A similar substitution into equation (4.33) leads to,

$$\left[ik + \omega\frac{N^2}{g} - \frac{2\Omega_0 m}{r}\right]\frac{\delta p_k}{\rho}e^{ikr} = \omega\left[\omega^2 - 4\Omega_0^2 - N^2\right]\frac{1}{r}\xi_{rk}e^{ikr} \tag{4.37}$$

Equation (4.37) can then be used to eliminate δp_k from equation (4.36) giving the following dispersion relation for $\omega(k)$,

$$\begin{aligned}\omega^3 k^2 - i\omega^3\left(\frac{1}{\rho}\frac{d\rho}{dr}\right)k + \omega\left[\left(\frac{2m\Omega_0}{r} + \omega\frac{g}{c_s^2}\right)\left(\frac{2m\Omega_0}{r} - \omega\frac{N^2}{g}\right)\right. \\ + \left.\left(\omega^2 - 4\Omega_0^2 - N^2\right)\left(\frac{m^2}{r^2} - \omega^2\frac{1}{c_S^2}\right)\right] = 0\end{aligned} \tag{4.38}$$

Using the quadratic formula,

$$k = \frac{1}{2\omega^6}i\omega^3\left(\frac{1}{\rho}\frac{d\rho}{dr}\right) \pm \frac{1}{2\omega^6}\sqrt{-\omega^6(\frac{1}{\rho}\frac{d\rho}{dr})^2 - 4\omega^3 C} \tag{4.39}$$

where,

$$C = \left[\left(\frac{2m\Omega_0}{r} + \omega\frac{g}{c_s^2}\right)\left(\frac{2m\Omega_0}{r} - \omega\frac{N^2}{g}\right) + \left(\omega^2 - 4\Omega_0^2 - N^2\right)\left(\frac{m^2}{r^2} - \omega^2\frac{1}{c_S^2}\right)\right] \tag{4.40}$$

The condition for propagation is that k has a real part for real ω. Therefore we require the term in the square root to be greater than zero. This gives the following criterion for propagation,

$$\omega^4 \frac{1}{c_s^2} - \omega^2 \left[\frac{m^2}{r^2} + \frac{1}{4} \left(\frac{1}{\rho} \frac{d\rho}{dr} \right)^2 + \frac{1}{c_s^2} 4\Omega_0^2 \right] + \omega \frac{2m\Omega_0}{r} \left(\frac{N^2}{g} - \frac{g}{c_s^2} \right) + \frac{m^2}{r^2} N^2 > 0 \quad (4.41)$$

Solving this inequality for every value of r determines the regions of propagation in an (r, ω) diagram. The propagation diagram of a non-rotating ($\Omega_0 = 0$), isentropic ($N^2 = 0$) cylinder is shown in Figure 4.2. In the non-rotating case the regions of propagation are symmetric with respect to the line $\omega = 0$. There are two regions of propagation observed in this case known as A-regions. They are both regions of acoustic wave propagation where pressure is the main restoring force. The regions where $\omega > 0$ are given the index (b) since the waves propagate in the backward direction with respect to the pattern speed of the mode. Similarly the regions where $\omega < 0$ are labelled (f) since these waves propagate in the forward direction. In this non-rotating, isentropic case we can write equation (4.41) as

$$\omega^2 \left\{ \omega^2 \frac{1}{c_s^2} - \left[\frac{m^2}{r^2} + \frac{1}{4} \left(\frac{1}{\rho} \frac{d\rho}{dr} \right)^2 \right] \right\} > 0 \quad (4.42)$$

and it is obvious why we observe two distinct regions.

Figure 4.3 shows the regions of propagation for a uniformly rotating but still isentropic cylinder. The rotation has given rise to an additional region of propagation known as the R-region which is defined as a region of propagation of rotational waves. It is clear from equation (4.41) why this occurs. Non-zero Ω_0 results in the inclusion of an additional term involving ω in the inequality. We can therefore factor out ω and the three regions result from solving the remaining cubic,

$$\omega \left\{ \omega^3 \frac{1}{c_s^2} - \omega \left[\frac{m^2}{r^2} + \frac{1}{4} \left(\frac{1}{\rho} \frac{d\rho}{dr} \right)^2 + \frac{1}{c_s^2} 4\Omega_0^2 \right] - \frac{2m\Omega_0 g}{r c_s^2} \right\} > 0 \quad (4.43)$$

As well as showing the regions of propagation Figures 4.2 and 4.3 show some of the mode eigenfrequencies and the zeros of the associated radial displacement. The eigenfunctions are oscillatory in the propagation regions. All zeros of the p modes lie within the A region and all zeros of the r modes lie within the R-region. The f modes are surface modes, which do not originate from propagating body waves

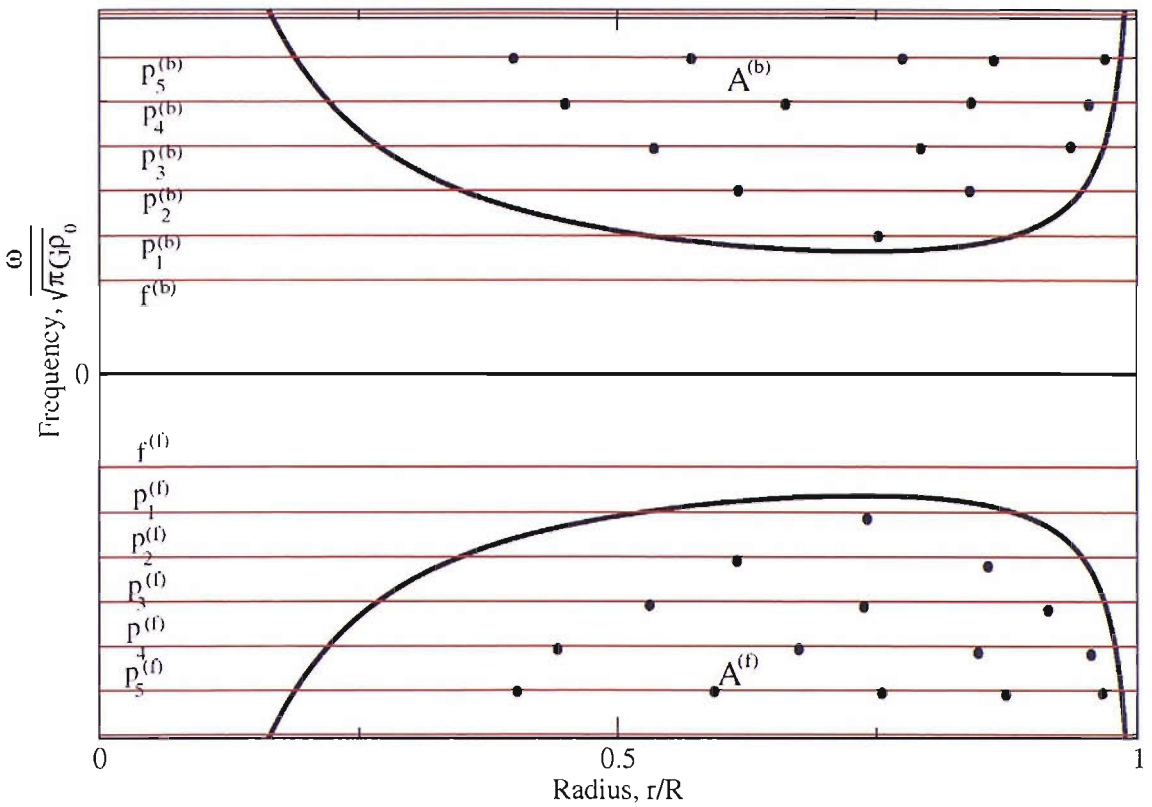

Figure 4.2: *The propagation diagram of a non-rotating isentropic cylinder. There are two regions of propagation observed in this case which are symmetric with respect to the line* $\omega = 0$. *These are known as A-regions. The regions where* $\omega > 0$ *are given the index (b) since the waves propagate in the backward direction. Similarly the regions where* $\omega < 0$ *are labelled (f) since these waves propagate in the forward direction. Also shown are the mode eigenfrequencies and the zeros of the associated radial displacement (•). All zeros of the p modes lie within the A region. The f modes are surface modes, which do not originate from propagating body waves and thus lie outside the regions of propagation. In this example we consider* $n = 3$, $\gamma = 4/3$, $m = 2$, $\Omega_0 = 0$.

and thus lie outside the regions of propagation.

In the non-isentropic, non-rotating case when $N \neq 0$ and $\Omega_0 = 0$ condition (4.41) reduces to

$$\omega^4 \frac{1}{c_s^2} - \omega^2 \left[\frac{m^2}{r^2} + \frac{1}{4} \left(\frac{1}{\rho} \frac{d\rho}{dr} \right)^2 \right] + \frac{m^2}{r^2} N^2 > 0 \tag{4.44}$$

and we observe four distinct regions of propagation. These are the two A-regions and additional regions called G-regions, which are regions of low-frequency gravity waves. For non-isentropic uniformly rotating cylinders we once again observe four regions of propagation. No distinct r modes or g modes exist in this case [81]. We can consider the non-acoustic regions as either a region of g modes modified by rotation or a region of r modes modified by non-isentropy.

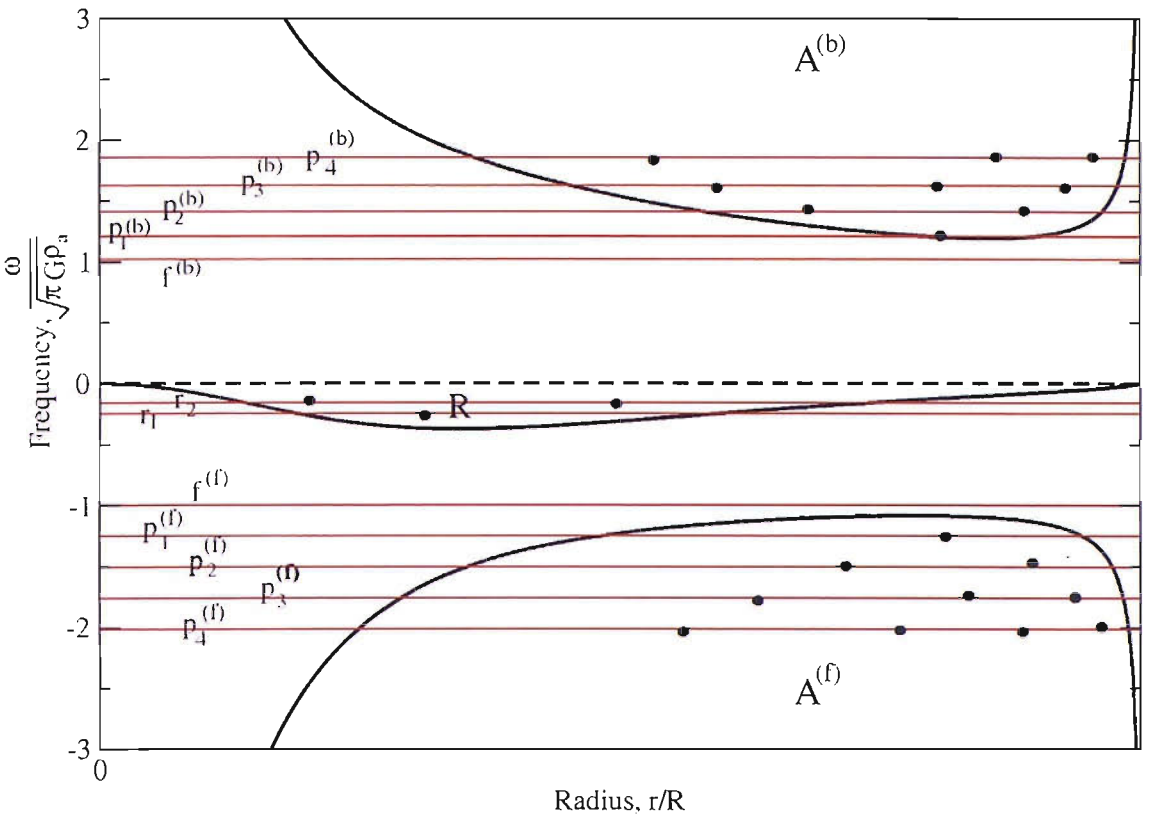

Figure 4.3: *The propagation diagram for a uniformly rotating but still isentropic cylinder. The rotation has given rise to an additional region of propagation known as the R-region which is defined as a region of propagation of rotational waves. We also observe that the acoustic regions are no longer symmetric with respect to* $\omega = 0$. *The Figure illustrates the mode eigenfrequencies and the zeros of the associated radial displacement (•). In this example we consider* $n = 3$, $\gamma = 4/3$, $m = 2$, $\Omega_0 = 0.1$.

As well as calculating the eigenfrequencies LSB can also find eigenfunctions. Figure 4.4 shows the influence of rotation on the f modes. We can see that as the angular velocity of the cylinder is increased the modes become less important in the central regions and relatively more important near the surface. The graphs are normalised such that $r\delta u_r$ is unity at $r/R = 1$, where R is the radius of the cylinder. Figure 4.5 shows the first three modes for a uniformly rotating cylinder. The f mode has no nodes, the p_1 mode has one and the p_2 mode has two.

The results from this single fluid analysis are confirmed by previous research by Veugelen [81] where an identical approach was taken to investigate the effect of differential rotation on self-gravitating cylinders. The focus of this work is the effect of introducing an additional fluid. We now look at the Eulerian perturbation equations for this situation.

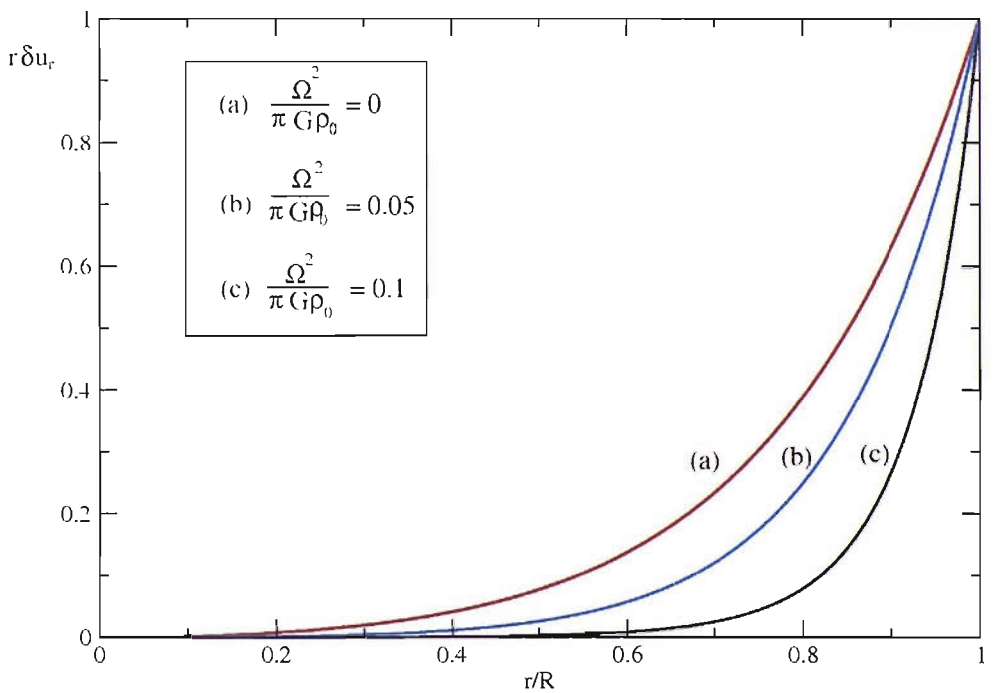

Figure 4.4: *The fundamental mode for a single fluid in a uniformly rotating cylinder, considering various values of the angular velocity, Ω_0. As the rotation rate is increased the modes become less significant in the central regions and more significant in the outer layers. The eigenfunctions are normalised such that $r\delta u_r$ is unity at $r/R = 1$. In this example $n = 3$, $\gamma = 4/3$ and $m = 2$.*

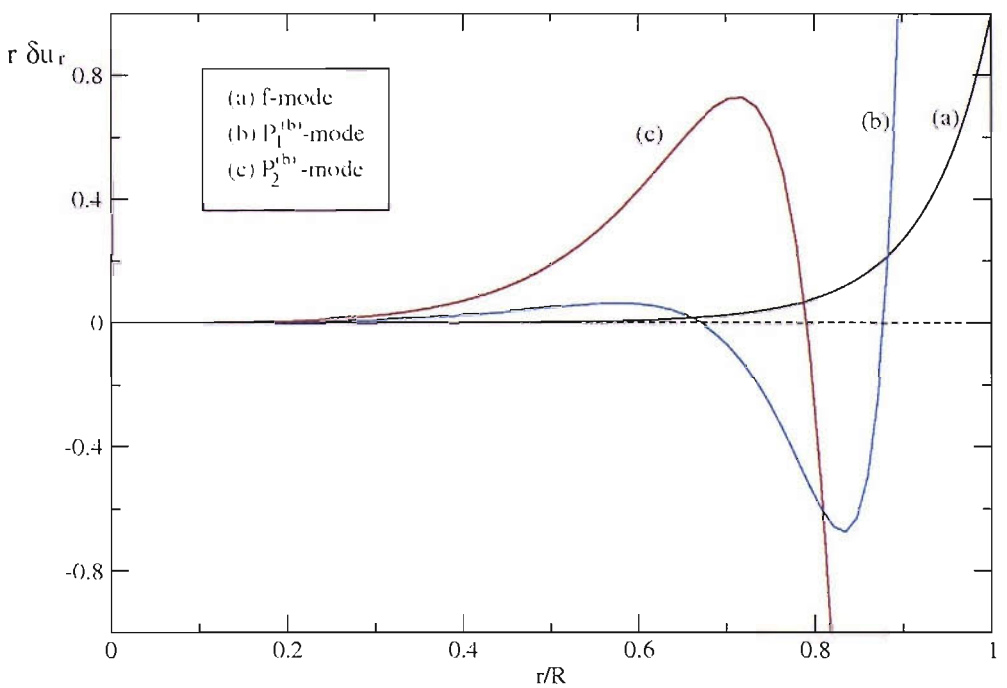

Figure 4.5: *The lowest 3 modes of oscillation for a single fluid in a uniformly rotating cylinder. The f mode has no nodes, the p_1 mode has one and the p_2 mode has three. The eigenfunctions are normalised such that $r\delta u_r$ is unity at $r/R = 1$. In this example $n = 3$, $\gamma = 4/3$, $m = 2$ and $\Omega_0 = 0.1$.*

4.4 Eulerian perturbation equations for a two fluid system

We now look at Eulerian perturbations in the two-fluid case. Since we now have the possibility of two distinct rotation rates, that of the protons and that of the superfluid neutrons, we no longer find it constructive to work in a rotating frame. The system is described by equations (2.19), (2.20) and (2.21). We begin our analysis with the case of vanishing entrainment, i.e. $\alpha = 0$. A perturbation can be applied to this system such that, $v_X^i \to v_X^i + \delta v_X^i$, $\Phi \to \Phi + \delta\Phi$, $\mu_X \to \mu_X + \delta\mu_X$, and $n_X \to n_X + \delta n_X$ giving the following linearised Euler equations,

$$\frac{\partial \delta v_X^i}{\partial t} + v_X^j \nabla_j \delta v_X^i + \delta v_X^j \nabla_j v_X^i + g^{ij} \nabla_j (\delta\Phi + \delta\tilde{\mu}_X) = 0 \tag{4.45}$$

the following perturbed continuity equations,

$$\frac{\partial \delta n_X}{\partial t} + \nabla_i (n_X \delta v_X^i) + \nabla_i (\delta n_X v_X^i) = 0 \tag{4.46}$$

and the perturbed Poisson equation,

$$\partial_i \partial^i \delta\Phi = 4\pi G m_{\mathrm{B}} (\delta n_X + \delta n_Y) \tag{4.47}$$

Since we have assumed $\alpha = 0$ the perturbed equations are only coupled gravitationally through $\delta\Phi$ and chemically through the equation of state. We can investigate this chemical coupling by looking at $\delta\tilde{\mu}_X$. In terms of δn_X and δn_Y,

$$\delta\tilde{\mu}_X = \left(\frac{\partial \tilde{\mu}_X}{\partial n_X}\right)_{n_Y, w^2} \delta n_X + \left(\frac{\partial \tilde{\mu}_X}{\partial n_Y}\right)_{n_X, w^2} \delta n_Y \tag{4.48}$$

If we assume the perturbation obeys the same equation of state as the background configuration described in Section 3.2, where we use a simple sum of two ordinary polytropes, we observe that $\left(\frac{\partial \tilde{\mu}_X}{\partial n_Y}\right)_{n_X, w^2} = 0$ giving,

$$\delta\tilde{\mu}_X = \left(\frac{\partial \tilde{\mu}_X}{\partial n_X}\right)_{n_Y, w^2} \delta n_X \tag{4.49}$$

If we also assume the Cowling approximation, i.e. ignore variations to the gravitational potential, we find the perturbation equations are no longer coupled. In this case there will be completely independent oscillation modes for each fluid, which will be identical to those in the single fluid case.

Using results from Appendix B we express the two fluid perturbation equations in cylindrical coordinates. Equation (4.45), the linearised perturbed Euler equations, lead to,

$$i(\omega + m\Omega_X)\delta v_r^X - \frac{2\Omega_X}{r}\delta v_\phi^X + \frac{\partial}{\partial r}(\delta\tilde{\mu}_X) = 0 \tag{4.50}$$

and

$$i(\omega + m\Omega_X)\delta v_\phi^X + 2\frac{\Omega_X}{r}\delta v_r^X + \frac{im}{r}(\delta\tilde{\mu}_X) = 0 \tag{4.51}$$

Equation (6.87), the continuity equation in the perturbed system, becomes

$$i(\omega + m\Omega_X)\delta n_X + \frac{n_X}{r}\frac{\partial}{\partial r}(r\delta v_r^X) + \frac{\partial n_X}{\partial r}\delta v_r^X + \frac{imn_X}{r}(\delta v_\phi)_X = 0 \tag{4.52}$$

Combining these equations to eliminate δn_X gives us the following four first order differential equations in δv_r^X and δv_ϕ^X.

$$\begin{aligned} &\frac{\partial \delta v_r^X}{\partial r}\left[m\left(\frac{\partial\tilde{\mu}_X}{\partial n_X}\right)n_X r^2\right] + \delta v_r^X\left[m\left(\frac{\partial\tilde{\mu}_X}{\partial n_X}\right)r(n_X + n_X' r) - 2\Omega_X\sigma_X r^3\right] \\ +\ &\delta v_\phi^X\left[m^2\left(\frac{\partial\tilde{\mu}_X}{\partial n_X}\right)n_X - \sigma_X^2 r^2\right] i = 0 \end{aligned} \tag{4.53}$$

$$\begin{aligned} &\frac{\partial \delta v_\phi^X}{\partial r}\left[m\left(\frac{\partial\tilde{\mu}_X}{\partial n_X}\right)\sigma_X n_X\right] + \delta v_\phi^X\left[2\Omega_X\sigma_X^2\right] \\ +\ &\delta v_r^X\left[m\left(\frac{\partial\tilde{\mu}_X}{\partial n_X}\right)(2\Omega_X n_X' r - m\sigma_X n_X) - 4\Omega_X^2\sigma_X r^2\right] i = 0 \end{aligned} \tag{4.54}$$

It would be possible to investigate the two-fluid equations using numerical integration in the same way the single fluid equations were analysed. However, we instead chose to investigate the two-fluid equations in a Lagrangian perturbation framework, allowing us to investigate the stability of the system. The equations describing the two fluid system with non-vanishing entrainment can be derived in an identical way. This is discussed further in Section 6.8 to highlight the differences between an Eulerian and a Lagrangian approach in this more complicated case.

4.5 Lagrangian perturbation theory

The strong advantage that Lagrangian perturbation theory offers over the corresponding Eulerian description lies in its capability to determine whether or not a system is stable. Friedman and Schutz [39], [40], developed a Lagrangian perturbation framework describing rotating Newtonian stars. In doing so they were able to construct appropriate stability criteria and show that all rotating, self-gravitating perfect fluids are unstable or marginally unstable to gravitational radiation. The aim of this section is to extend the work of Friedman and Schutz to create a system of equations describing a superfluid neutron star in terms of Lagrangian perturbations. Before investigating the problem of a rotating superfluid it is useful to look at the case of a single fluid. This allows us to develop a formalism in the simplest case which can subsequently be extended to the more advanced two-fluid system. Although the single fluid problem has been investigated previously we will redo the calculation as we prefer to work with the number density n, the fluid velocity v_i, and the chemical potential μ rather than the pressure p.

This system can be described by the single fluid Euler equations (2.4), a continuity equation (2.6) and an equation for the gravitational potential (2.7). The Lagrangian change in the fluid velocity follows from

$$\Delta v^i = \partial_t \xi^i \tag{4.55}$$

where ξ^i is the Lagrangian displacement. Given this, and

$$\Delta g_{ij} = \nabla_i \xi_j + \nabla_j \xi_i \tag{4.56}$$

we have

$$\Delta v_i = \partial_t \xi_i + v^j \nabla_i \xi_j + v^j \nabla_j \xi_i \ . \tag{4.57}$$

It is also useful to note that the Eulerian variations are given by

$$\delta v^i = \partial_t \xi^i + v^j \nabla_j \xi^i - \xi^j \nabla_j v^i \tag{4.58}$$

and

$$\delta v_i = \partial_t \xi_i + v^j \nabla_j \xi_i - \xi^j \nabla_j v_i \tag{4.59}$$

(since $v_i = g_{ij} v^j$ and $\nabla_k g_{ij} = 0$).

Applying a perturbation to this system the continuity equation becomes,

$$\Delta n = -n \nabla_i \xi^i \longrightarrow \delta n = -\nabla_i (n \xi^i) \ . \tag{4.60}$$

and consequently the gravitational potential equation becomes,

$$\nabla^2\delta\Phi = 4\pi G m_B \delta n = -4\pi G m_B \nabla_i(n\xi^i) \tag{4.61}$$

Perturbing the Euler equations gives,

$$\Delta[(\partial_t + v^j\nabla_j)v_i + \nabla_i\tilde{\mu} + \nabla_i\Phi] = 0 \tag{4.62}$$

Since the Lagrangian variation commutes with the Lie derivative such that $\Delta(\partial_t + \pounds_v)v_i = (\partial_t + \pounds_v)\Delta v_i$ it is convenient to write,

$$v^j\nabla_j v_i = \pounds_v v_i - v_j\nabla_i v^j \tag{4.63}$$

$$\nabla_i v^2 = \nabla_i(v_j v^j) = v_j\nabla_i v^j + v^j\nabla_i v_j = 2v_j\nabla_i v^j \tag{4.64}$$

$$\Rightarrow v^j\nabla_j v_i = \pounds_v v_i - \frac{1}{2}\nabla_i v^2 \tag{4.65}$$

Thus the perturbed equation of motion becomes,

$$(\partial_t + \pounds_v)\Delta v_i + \nabla_i\left(\Delta\tilde{\mu} + \Delta\Phi - \frac{1}{2}\Delta(v^2)\right) = 0\ . \tag{4.66}$$

Each term in this equation can be investigated individually enabling us to write this equation in terms of the displacement vector ξ_i. For the first term we obtain,

$$\begin{aligned}
(\partial_t + \pounds_v)\Delta v_i &= \partial_t[\partial_t\xi_i + v^j\nabla_i\xi_j + v^j\nabla_j\xi_i] + v^j\nabla_j\Delta v_i + \Delta v_j\nabla_i v^j \\
&= \partial_t^2\xi_i + \partial_t v^j\nabla_i\xi_j + v^j\nabla_i\partial_t\xi_j + \partial_t v^j\nabla_j\xi_i + v^j\nabla_j\partial_t\xi_i \\
&+ v^j\nabla_j[\partial_t\xi_i + v^k\nabla_i\xi_k + v^k\nabla_k\xi_i] + \Delta v_j\nabla_i v^j \\
&= \partial_t^2\xi_i + 2v^j\nabla_j\partial_t\xi_i + v^j\nabla_i\partial_t\xi_j + v^j\nabla_j(v^k\nabla_i\xi_k) \\
&+ (v^j\nabla_j)^2\xi_i + \Delta v_j\nabla_i v^j + \partial_t v^j\nabla_i\xi_j + \partial_t v^j\nabla_j\xi_i
\end{aligned} \tag{4.67}$$

Since $\partial_t v^j = 0$ this becomes,

$$\begin{aligned}
(\partial_t + \pounds_v)\Delta v_i &= \partial_t^2\xi_i + 2v^j\nabla_j\partial_t\xi_i + v^j\nabla_i\partial_t\xi_j + v^j\nabla_j(v^k\nabla_i\xi_k) + (v^j\nabla_j)^2\xi_i \\
&+ \Delta v_j\nabla_i v^j
\end{aligned} \tag{4.68}$$

We now need to look at the perturbations of the gravitational and chemical potentials.

$$\Delta\Phi = \delta\Phi + \pounds_\xi \Phi = \delta\Phi + \xi^i \nabla_i \Phi \tag{4.69}$$

Therefore

$$\begin{aligned} \nabla_i \Delta\Phi &= \nabla_i \delta\Phi + \nabla_i(\xi^j \nabla_j \Phi) \\ &= \nabla_i \delta\Phi + (\nabla_i \xi^j)(\nabla_j \Phi) + \xi^j \nabla_i \nabla_j \Phi \end{aligned} \tag{4.70}$$

The equilibrium equation gives,

$$\nabla_j \Phi = -v^k \nabla_k v_j - \nabla_j \tilde{\mu} \tag{4.71}$$

Consequently

$$\nabla_i \Delta\Phi = \nabla_i \delta\Phi + \xi^j \nabla_i \nabla_j \Phi - (\nabla_i \xi^j)(v^k \nabla_k v_j + \nabla_j \tilde{\mu}) \tag{4.72}$$

Finally the Lagrangian perturbation of the chemical potential can be written as,

$$\begin{aligned} \Delta\tilde{\mu} &= \delta\tilde{\mu} + \xi^j \nabla_j \tilde{\mu} \\ &= \frac{\partial \tilde{\mu}}{\partial n} \delta n + \xi^j \nabla_j \tilde{\mu} \\ &= -\frac{\partial \tilde{\mu}}{\partial n} \nabla_j (n \xi^j) + \xi^j \nabla_j \tilde{\mu} \end{aligned} \tag{4.73}$$

Therefore

$$\begin{aligned} \nabla_i \Delta\tilde{\mu} &= -\nabla_i \left[\frac{\partial \tilde{\mu}}{\partial n} \nabla_j (n \xi^j) \right] + \nabla_i \left[\xi^j \nabla_j \tilde{\mu} \right] \\ &= -\nabla_i \left[\frac{\partial \tilde{\mu}}{\partial n} \nabla_j (n \xi^j) \right] + \nabla_i \xi^j \nabla_j \tilde{\mu} + \xi^j \nabla_i \nabla_j \tilde{\mu} \end{aligned} \tag{4.74}$$

Finally the last term in the perturbed Euler equation can be written as,

$$\Delta v^2 = \Delta(v^j v_i) = v^j \Delta v_j + v_j \Delta v^j \tag{4.75}$$

$$\begin{aligned} -\frac{\rho}{2} \nabla_i (\Delta v^2) &= -\frac{\rho}{2} \nabla_i (v^j \Delta v_j) - \frac{\rho}{2} \nabla_i (v_j \Delta v^j) \\ &= -\frac{\rho}{2} v^j [\nabla_i (\Delta v_j)] - \frac{\rho}{2} \Delta v_j [\nabla_i (v^j)] - \frac{\rho}{2} v_j [\nabla_i (\Delta v^j)] - \frac{\rho}{2} \Delta v^j [\nabla_i (v_j)] \\ &= -\rho v^j [\nabla_i (\Delta v_j)] - \rho \Delta v_j [\nabla_i (v^j)] \\ &= -\rho v^j [\nabla_i \partial_t \xi_j] - \rho \Delta v_j [\nabla_i (v^j)] \end{aligned} \tag{4.76}$$

Substituting these results into the perturbed Euler equations,

$$\begin{aligned} & \partial_t^2\xi_i + 2v^j\nabla_j\partial_t\xi_i + v^j\nabla_i\partial_t\xi_j + v^j\nabla_j(v^k\nabla_i\xi_k) + (v^j\nabla_j)^2\xi_i + \Delta v_j\nabla_i v^j \\ - \; & v^j[\nabla_i\partial_t\xi_j] - \Delta v_j[\nabla_i(v^j)] + \nabla_i\delta\Phi + \xi^j\nabla_i\nabla_j\Phi - (\nabla_i\xi^j)(v^k\nabla_k v_j + \nabla_j\tilde{\mu}) \\ - \; & \nabla_i\left[\frac{\partial\tilde{\mu}}{\partial n}\nabla_j(n\xi^j)\right] + \nabla_i\xi^j\nabla_j\tilde{\mu} + \xi^j\nabla_i\nabla_j\tilde{\mu} = 0 \end{aligned} \tag{4.77}$$

Upon cancellation we obtain,

$$\begin{aligned} & n\partial_t^2\xi_i + 2nv^j\nabla_j\partial_t\xi_i + n(v^j\nabla_j)^2\xi_i + n\nabla_i\delta\Phi + n\xi^j\nabla_i\nabla_j\Phi + n\xi^j\nabla_i\nabla_j\tilde{\mu} \\ - \; & n\nabla_i\left[\frac{\partial\tilde{\mu}}{\partial n}\nabla_j(n\xi^j)\right] = 0 \end{aligned} \tag{4.78}$$

This equation can be written in the following, simplified form,

$$A\partial_t^2\xi + B\partial_t\xi + C\xi = 0 \tag{4.79}$$

Where

$$A\partial_t^2\xi = n\partial_t^2\xi_i \tag{4.80}$$

$$B\partial_t\xi = 2nv^j\nabla_j\partial_t\xi_i \tag{4.81}$$

$$C\xi = n(v^j\nabla_j)^2\xi_i + n\nabla_i\delta\Phi + n\xi^j\nabla_i\nabla_j\Phi - n\nabla_i\left[\frac{\partial\tilde{\mu}}{\partial n}\nabla_j(n\xi^j)\right] + n\xi^j\nabla_i\nabla_j\tilde{\mu} \tag{4.82}$$

The equation for the perturbed gravitational potential, equation (4.61), can be solved using Green's functions. The equation is of the form,

$$\mathbf{L}\phi(\vec{x}) = f(\vec{x}) \tag{4.83}$$

where $\mathbf{L}$ is, in our case, the Laplacian operator, and $\phi(\vec{x})$ is the solution. The solution to this problem is,

$$\phi(\vec{x}) = \int G(\vec{x},\vec{x}')f(\vec{x}')d^3\vec{x}' \tag{4.84}$$

When the operator is ∇^2 the Green's function is,

$$G(x,x') = \frac{1}{4\pi}\frac{1}{|\vec{x}-\vec{x}'|} \tag{4.85}$$

Applying this to the perturbed equation for the gravitational potential gives,

$$\begin{aligned}
\delta\Phi &= \int \frac{1}{4\pi}\frac{1}{|\vec{x}-\vec{x}'|}4\pi mG\nabla_i'\left[n'(\xi^i)'\right]dV' \\
&= mG\int \frac{1}{|\vec{x}-\vec{x}'|}\nabla_i'\left[n'(\xi^i)'\right]dV' \\
&= mG\int\left\{\nabla_i'\left[\frac{1}{|\vec{x}-\vec{x}'|}n'(\xi^i)'\right] - n'(\xi^i)'\nabla_i'\left[\frac{1}{|\vec{x}-\vec{x}'|}\right]\right\}dV' \\
&= -mG\int n'(\xi^i)'\nabla_i'\left[\frac{1}{|\vec{x}-\vec{x}'|}\right]dV' \qquad (4.86)
\end{aligned}$$

4.5.1 Trivial displacements

In Friedman and Schutz [39] the idea of *trivial displacements* was introduced revealing that a physical perturbation does not uniquely determines a displacement ξ^i. We can describe the Eulerian perturbations in terms of ξ^i such that,

$$\delta\rho = -\nabla_i(\rho\xi^i) \qquad (4.87)$$

$$\delta s = -\xi^i\nabla_i s \qquad (4.88)$$

$$\delta v^i = \partial_t\xi^i + v^j\nabla_j\xi^i - \xi^j\nabla_j v^i \qquad (4.89)$$

$$\delta p = -\gamma p\nabla_i\xi^i - \xi^i\nabla_i p \qquad (4.90)$$

where equation (4.88) describes the entropy for an adiabatic perturbation. If we look closely at these four equations we can see that there are values of ξ^i for which the corresponding Eulerian changes in p, ρ, v^i and s all vanish. If we call this *trivial displacement* η^i then when η^i satisfies the following three equations,

$$\nabla_i(\rho\eta^i) = 0 \qquad (4.91)$$

$$\eta^i\nabla_i s = 0 \qquad (4.92)$$

$$[\partial_t + \pounds_v]\eta^i = \partial_t\eta^i + v^j\nabla_j\eta^i - \eta^j\nabla_j v^i = 0 \qquad (4.93)$$

ξ^i and $\hat{\xi}^i$ correspond to the same physical perturbation, where we have defined $\hat{\xi}^i$ as,

$$\hat{\xi}^i = \xi^i + \eta^i \tag{4.94}$$

The general solution, taken from Friedman and Schutz [39] is,

$$\rho\eta^i = \epsilon^{ijk}\nabla_j s \nabla_k f \tag{4.95}$$

Where f is a scalar which must be constant along fluid trajectories,

$$(\partial_t + \pounds_v) f = 0 \tag{4.96}$$

These *trivial displacements* are problematic in the sense that they affect the value of the canonical energy, E_c, which we introduce in Section 4.5.4. Since we intend to use E_c to test the stability of our system it is important to ensure the data is not contaminated by these *trivial displacements*. In Section 4.6.7 we consider the implications for the constructed stability criteria and discuss how to overcome this unfortunate complication.

4.5.2 Formal properties of the equations and of the conserved quantities

To analyse the stability of our system we construct certain conserved quantities known as the canonical energy and the canonical angular momentum. The reasons why and how these assess whether or not a system is stable will be discussed later for now we will simply calculate their form. Using the conventional definition for the inner product,

$$\langle \eta^i, \xi_i \rangle = \int (\eta^i)^* \xi_i dV \tag{4.97}$$

we can prove that the following symmetries hold,

$$\langle y, A\xi \rangle = \langle \xi, Ay \rangle^* \tag{4.98}$$

$$\langle y, B\xi \rangle = -\langle \xi, By \rangle^* \tag{4.99}$$

$$\langle y, C\xi \rangle = \langle \xi, Cy \rangle^* \tag{4.100}$$

We prove these symmetries as follows,

$$\begin{aligned}
\langle y, A\xi \rangle &= \int (y^i)^* n \xi_i dV \\
&= \left\{ \int (y^i) n (\xi_i)^* dV \right\}^* \\
&= \left\{ \int (\xi_i)^* n (y^i) dV \right\}^* \\
&= \langle \xi, Ay \rangle^* \qquad (4.101)
\end{aligned}$$

$$\begin{aligned}
\langle y, B\xi \rangle &= \int y^* 2 n v^j \nabla_j \xi_i dV \\
&= \left\{ \int (y^i) 2 n v^j \nabla_j (\xi_i)^* dV \right\}^* \\
&= \left\{ \int \left\{ \nabla_j \left[2n (y^i) v^j (\xi_i)^* \right] - 2n (\xi_i)^* v^j \nabla_j y - 2 (y^i) (\xi_i)^* \nabla_j (n v^j) \right\} dV \right\}^* \\
&= - \left\{ \int 2n (\xi_i)^* v^j \nabla_j (y^i) dV \right\}^* \\
&= - \langle \xi, By \rangle^* \qquad (4.102)
\end{aligned}$$

Where we have used the fact that $\nabla_j (n v^j) = 0$. The final task is to prove the symmetry of C. Expanding the inner product $\langle y, C\xi \rangle$ gives us the following 5 terms which we can then analyse individually.

$$\begin{aligned}
\langle y, C\xi \rangle &= \int (y^i)^* \left\{ n \left(v^j \nabla_j \right)^2 \xi_i + n \nabla_i \delta_\xi \Phi - n \nabla_i \left[\frac{\partial \tilde{\mu}}{\partial n} \nabla_j (n \xi^j) \right] \right. \\
&+ \left. n \xi^j \nabla_i \nabla_j \Phi + n \xi^j \nabla_i \nabla_j \tilde{\mu} \right\} dV \qquad (4.103)
\end{aligned}$$

The first term is,

$$\begin{aligned}
\int n (y^i)^* (v^j \nabla_j)^2 \xi_i dV &= \int \left\{ \nabla_j \left[n v^j v^k (y_i)^* \nabla_k \xi^i \right] - n v^j v^k \left[\nabla_j (y_i)^* \right] (\nabla_k \xi^i) \right. \\
&- \left. \left[\nabla_j (n v^j) \right] v^k (y_i)^* (\nabla_k \xi^i) \right\} dV \\
&= - \int n v^j v^k \left[\nabla_j (y_i)^* \right] (\nabla_k \xi^i) dV \\
&= \int n \xi_i (v^j \nabla_j)^2 (y^i)^* dV \qquad (4.104)
\end{aligned}$$

By substituting for $\delta\Phi$ in the second term we see that,

$$\begin{aligned}
\int \left\{n(y^i)^*\nabla_i\delta\Phi\right\} dV &= \int \left\{n(y^i)^*\nabla_i\left[-m_{\rm B}G\int n'(\xi^j)'\nabla'_j\left(\frac{1}{|\vec{x}-\vec{x}'|}\right)dV'\right]\right\} dV \\
&= -m_{\rm B}G\int\int \left\{n'(\xi^j)'n(y^i)^*\nabla_i\nabla'_j\left(\frac{1}{|\vec{x}-\vec{x}'|}\right)\right\} dV'dV \\
&= -m_{\rm B}G\int \left\{n'(\xi^j)'\nabla'_j\int\left[n(y^i)^*\nabla_i\left(\frac{1}{|\vec{x}-\vec{x}'|}\right)\right]\right\} dVdV' \\
&= \int \left\{n(\xi^j)\nabla_j(\delta_y\Phi)^*\right\} dV \qquad (4.105)
\end{aligned}$$

Finally by rearranging the third term we get,

$$\begin{aligned}
\int \left\{n(y^i)^*\nabla_i\left[\frac{\partial\tilde{\mu}}{\partial n}\nabla_j(n\xi^j)\right]\right\} dV &= \int \left\{\nabla_i\left[n(y^i)^*\frac{\partial\tilde{\mu}}{\partial n}\nabla_j(n\xi^j)\right]\right\} dV \\
&- \int \left\{\frac{\partial\tilde{\mu}}{\partial n}\nabla_j(n\xi^j)\nabla_i\left[n(y^i)^*\right]\right\} dV \\
&= -\int \left\{\frac{\partial\tilde{\mu}}{\partial n}\nabla_j(n\xi^j)\nabla_i\left[n(y^i)^*\right]\right\} dV \\
&= -\int \left\{\nabla_j\left(n\xi^j\frac{\partial\tilde{\mu}}{\partial n}\nabla_i\left[n(y^i)^*\right)\right\} dV \\
&+ \int \left\{n\xi^j\nabla_j\left(\frac{\partial\tilde{\mu}}{\partial n}\nabla_i\left[n(y^i)^*\right]\right)\right\} dV \\
&= \int \left\{n\xi^j\nabla_j\left(\frac{\partial\tilde{\mu}}{\partial n}\nabla_i\left[n(y^i)^*\right]\right)\right\} dV \qquad (4.106)
\end{aligned}$$

Therefore

$$\begin{aligned}
\langle y, C\xi\rangle &= \int \Big\{n\xi_i(v^j\nabla_j)^2(y^i)^* + n(\xi^j)\nabla_j(\delta\Phi)^* \\
&+ n(y^i)^*\xi^j\nabla_i\nabla_j(\Phi+\tilde{\mu}) - n\xi^j\nabla_j\left(\frac{\partial\tilde{\mu}}{\partial n}\nabla_i\left[n(y^i)^*\right]\right)\Big\} dV \\
&= \langle \xi, Cy\rangle^* \qquad (4.107)
\end{aligned}$$

4.5.3 Symplectic structure

A symplectic structure is a dynamically conserved antisymmetric product involving the configuration space variables and their conjugate momenta. The symplectic structure is written as,

$$W(y,\xi) = \left\langle y, A\partial_t\xi + \frac{1}{2}B\xi\right\rangle - \left\langle A\partial_t y + \frac{1}{2}By, \xi\right\rangle \qquad (4.108)$$

where y and ξ both solve the perturbed Euler equation. It is easily shown that this inner product is conserved,

$$\begin{aligned}\partial_t W(y,\xi) &= \left\langle \partial_t y, A\partial_t\xi + \frac{1}{2}B\xi \right\rangle + \left\langle y, A\partial_t^2\xi + \frac{1}{2}B\partial_t\xi \right\rangle \\ &- \left\langle A\partial_t^2 y + \frac{1}{2}B\partial_t y, \xi \right\rangle - \left\langle A\partial_t y + \frac{1}{2}By, \partial_t\xi \right\rangle \end{aligned} \tag{4.109}$$

Using the fact that $A\partial_t^2\xi + B\partial_t\xi + C\xi = 0$

$$\begin{aligned}\partial_t W(y,\xi) &= \left\langle \partial_t y, A\partial_t\xi + \frac{1}{2}B\xi \right\rangle + \left\langle y, -\frac{1}{2}B\partial_t\xi - C\xi \right\rangle \\ &- \left\langle -\frac{1}{2}B\partial_t y - Cy, \xi \right\rangle - \left\langle A\partial_t y + \frac{1}{2}By, \partial_t\xi \right\rangle \\ &= (\langle \partial_t y, A\partial_t\xi\rangle - \langle A\partial_t y, \partial_t\xi\rangle) \\ &+ \frac{1}{2}(\langle \partial_t y, B\xi\rangle + \langle B\partial_t y, \xi\rangle) \\ &- \frac{1}{2}(\langle y, B\partial_t\xi\rangle + \langle By, \partial_t\xi\rangle) \\ &- (\langle y, C\xi\rangle - \langle Cy, \xi\rangle) \\ &= 0 \end{aligned} \tag{4.110}$$

4.5.4 Canonical energy

The canonical energy is the conserved energy of the perturbation. It is defined as,

$$E_c = \frac{m_{\mathrm{B}}}{2} W(\dot{\xi}, \xi) \tag{4.111}$$

Expanding this out gives,

$$\begin{aligned} E_c &= \frac{m_{\mathrm{B}}}{2}\left\{ \left\langle \partial_t\xi, A\partial_t\xi + \frac{1}{2}B\xi \right\rangle - \left\langle A\partial_t^2\xi + \frac{1}{2}B\partial_t\xi, \xi \right\rangle \right\} \\ &= \frac{m_{\mathrm{B}}}{2}\left\{ \langle \partial_t\xi, A\partial_t\xi\rangle + \left\langle \partial_t\xi, \frac{1}{2}B\xi \right\rangle + \left\langle \frac{1}{2}B\partial_t\xi + C\xi, \xi \right\rangle \right\} \\ &= \frac{m_{\mathrm{B}}}{2}\left\{ \langle \partial_t\xi, A\partial_t\xi\rangle + \langle C\xi, \xi\rangle \right\} \\ &= \frac{m_{\mathrm{B}}}{2}\left\{ \langle \partial_t\xi, A\partial_t\xi\rangle + \langle \xi, C\xi\rangle \right\} \end{aligned} \tag{4.112}$$

Substituting for the operators A and C,

$$\frac{m_{\mathrm{B}}}{2}\langle \partial_t\xi, A\partial_t\xi\rangle = \frac{m_{\mathrm{B}}}{2}\int n|\partial_t\xi|^2 dV = \frac{1}{2}\int \rho|\partial_t\xi|^2 dV \tag{4.113}$$

$$\begin{aligned}\frac{m_{\rm B}}{2}\langle\xi, C\xi\rangle &= \frac{m_{\rm B}}{2}\int\left\{(\xi^i)^*\left(n(v^j\nabla_j)^2\xi_i + n\nabla_i\delta\Phi - n\nabla_i\left[\frac{\partial\tilde{\mu}}{\partial n}\nabla_j(n\xi^j)\right]\right.\right.\\ &+ \left.\left. n\xi^j\nabla_i\nabla_j\Phi + n\xi^j\nabla_i\nabla_j\tilde{\mu}\ \right)\right\}dV \qquad (4.114)\end{aligned}$$

The terms in this equation can again be analysed individually. For the first term we write,

$$\begin{aligned}\frac{m_{\rm B}}{2}\int\left\{n(\xi^i)^*(v^j\nabla_j)^2\xi_i\right\}dV &= -\frac{1}{2}\int\left\{\rho v^j v^k(\nabla_j(\xi_i)^*)(\nabla_k\xi^i)\right\}dV\\ &= -\frac{1}{2}\int\left\{\rho|v^j\nabla_j\xi^i|^2\right\}dV \qquad (4.115)\end{aligned}$$

The second term can be written as,

$$\begin{aligned}\frac{m_{\rm B}}{2}\int\left\{(\xi^i)^*n\nabla_i(\delta_\xi\Phi)\right\}dV &= \frac{m_{\rm B}}{2}\int\left\{\nabla_i(n(\xi^i)^*\delta\Phi) - \delta\Phi\nabla_i\left[n(\xi^i)^*\right]\right\}dV\\ &= \frac{1}{2}\int\left\{\frac{1}{4\pi G}\delta\Phi\nabla_i\nabla^i(\delta\Phi)^*\right\}dV\\ &= \frac{1}{2}\int\left\{\frac{1}{4\pi G}\left(\nabla_i\left[\delta\Phi\nabla^i(\delta\Phi)^*\right] - \nabla_i\delta\Phi\nabla^i(\delta\Phi)^*\right)\right\}dV\\ &= -\frac{1}{2}\int\left\{\frac{1}{4\pi G}\nabla_i\delta\Phi\nabla^i(\delta\Phi)^*\right\}dV\\ &= -\frac{1}{2}\int\left\{\frac{1}{4\pi G}|\nabla_i\delta\Phi|^2\right\}dV \qquad (4.116)\end{aligned}$$

Finally

$$\begin{aligned}-\frac{m_{\rm B}}{2}\int\left\{n(\xi^i)^*\nabla_i\left[\frac{\partial\tilde{\mu}}{\partial n}\nabla_j(n\xi^j)\right]\right\}dV &= -\frac{1}{2}\int\left\{\nabla_i\left[n(\xi^i)^*\frac{\partial\mu}{\partial n}\nabla_j(n\xi^j)\right]\right\}dV\\ &+ \frac{1}{2}\int\left\{\frac{\partial\mu}{\partial n}\nabla_j(n\xi^j)\nabla_i\left[n(\xi^i)^*\right]\right\}dV\\ &= \frac{1}{2}\int\left\{\frac{\partial\mu}{\partial n}\delta n(\delta n)^*\right\}dV\\ &= \frac{1}{2}\int\left\{\frac{\partial\mu}{\partial n}|\delta n|^2\right\}dV \qquad (4.117)\end{aligned}$$

Substituting everything back gives the following expression for the canonical energy,

$$\Rightarrow E_c = \frac{1}{2}\int \Big\{\rho|\partial_t\xi|^2 - \rho|v^j\nabla_j\xi^i|^2 - \frac{1}{4\pi G}|\nabla_i\delta\Phi|^2 + \rho(\xi^i)^*\xi^j\nabla_i\nabla_j\Phi$$
$$+ \rho(\xi^i)^*\xi^j\nabla_i\nabla_j\mu + \frac{\partial\mu}{\partial n}|\delta n|^2 \Big\}dV \tag{4.118}$$

4.5.5 The canonical angular momentum

The canonical angular momentum is defined as,

$$J_c(\xi) = -\frac{1}{2}W(\partial_\phi\xi, \xi) \tag{4.119}$$

$$J_c(\xi) = -\frac{1}{2}\left[\left\langle \partial_\phi\xi, A\partial_t\xi + \frac{1}{2}B\xi\right\rangle - \left\langle A\partial_{t\phi}\xi + \frac{1}{2}B\partial_\phi\xi, \xi\right\rangle\right] \tag{4.120}$$

$$\left\langle A\partial_\phi\dot{\xi} + \frac{1}{2}B\partial_\phi\xi, \xi\right\rangle = \left\langle \partial_\phi\left(A\dot{\xi} + \frac{1}{2}B\xi\right), \xi\right\rangle = \int\left\{\left[\partial_\phi\left(A\dot{\xi} + \frac{1}{2}B\xi\right)\right]^*\xi\right\}dV \tag{4.121}$$

Using integration by parts

$$\left\langle A\partial_\phi\dot{\xi} + \frac{1}{2}B\partial_\phi\xi, \xi\right\rangle = \left[\left(A\dot{\xi} + \frac{1}{2}B\xi\right)^*\xi\right] - \int\left\{\left(A\dot{\xi} + \frac{1}{2}B\xi\right)^*\partial_\phi\xi\right\}dV \tag{4.122}$$

$$= \left\langle\left(A\dot{\xi} + \frac{1}{2}B\xi\right), \partial_\phi\xi\right\rangle = -\left\langle\partial_\phi\xi, \left(A\dot{\xi} + \frac{1}{2}B\xi\right)\right\rangle^* \tag{4.123}$$

$$\Rightarrow J_c(\xi) = -\frac{1}{2}\left[\left\langle\partial_\phi\xi, \left(A\partial_t\xi + \frac{1}{2}B\xi\right)\right\rangle + \left\langle\partial_\phi\xi, \left(A\dot{\xi} + \frac{1}{2}B\xi\right)\right\rangle^*\right] \tag{4.124}$$

$$\Rightarrow J_c(\xi) = -Re\left\langle\partial_\phi\xi, A\partial_t\xi + \frac{1}{2}B\xi\right\rangle \tag{4.125}$$

4.5.6 Normal modes

For normal mode solutions we have $\xi^i = \xi^i(x)e^{i\omega t}$

$$
\begin{aligned}
E_c(\xi) &= \frac{1}{2}\left\langle \dot{\xi}, A\dot{\xi} \right\rangle + \frac{1}{2}\langle \xi, C\xi \rangle \\
&= \frac{1}{2}\langle i\omega\xi, i\omega A\xi \rangle + \frac{1}{2}\left\langle \xi, -A\ddot{\xi} - B\dot{\xi} \right\rangle \\
&= \frac{1}{2}\int \left\{ (i\omega\xi)^* \, i\omega A\xi \right\} dV + \frac{1}{2}\omega^2 \langle \xi, A\xi \rangle - \frac{1}{2}\langle \xi, i\omega B\xi \rangle \\
&= \frac{1}{2}\int \left\{ \omega^*\xi^* i\omega A\xi \right\} dV + \frac{1}{2}\omega^2 \langle \xi, A\xi \rangle - \frac{\omega}{2}\langle \xi, iB\xi \rangle \\
&= \frac{1}{2}\omega\omega^* \langle \xi, A\xi \rangle + \frac{\omega^2}{2}\langle \xi, A\xi \rangle - \frac{\omega}{2}\langle \xi, iB\xi \rangle \\
&= \omega\left\{ \frac{1}{2}(\omega^* + \omega)\langle \xi, A\xi \rangle - \frac{1}{2}\langle \xi, iB\xi \rangle \right\} \\
&= \omega\left\{ Re(\omega)\langle \xi, A\xi \rangle - \frac{1}{2}\langle \xi, iB\xi \rangle \right\}
\end{aligned} \tag{4.126}
$$

To calculate to canonical angular momentum for the normal modes we write $\xi^i = \xi^i(r,\theta)e^{i(m\phi+\omega t)}$. Thus giving,

$$
\begin{aligned}
J_c(\xi) &= -Re\left\langle \partial_\phi\xi, A\partial_t\xi + \frac{1}{2}B\xi \right\rangle \\
&= -Re\left\{ \langle im\xi, i\omega A\xi \rangle + \frac{1}{2}\langle im\xi, B\xi \rangle \right\} \\
&= -Re\left\{ \omega m^* \langle \xi, A\xi \rangle - \frac{1}{2}m^* \langle \xi, iB\xi \rangle \right\} \\
&= -Re(\omega m^*)\langle \xi, A\xi \rangle + \frac{1}{2}Re(m^*)\langle \xi, iB\xi \rangle \\
&= -m\left\{ Re(\omega)\langle \xi, A\xi \rangle - \frac{1}{2}\langle \xi, iB\xi \rangle \right\}
\end{aligned} \tag{4.127}
$$

Where the final step assumes m is an integer. Therefore for normal modes,

$$
\frac{E_c}{J_c} = -\frac{\omega}{m} \equiv \sigma_p \tag{4.128}
$$

Which defines the pattern speed of the mode. Since $\langle \xi, A\xi \rangle$ and $\langle \xi, iB\xi \rangle$ are both real and we know E_c is real the canonical energy must vanish if ω is not real.

4.5.7 Stability of modes

The canonical energy provides the basis for our stability analysis. Dynamical instabilities correspond to a vanishing canonical energy. The amplitude of the mode can grow indefinitely while the canonical energy remains unchanged. Instabilities also arise if the system is coupled to radiation such as gravitational waves. If E_c is initially positive then, because of the time independence of the equilibrium, it must

always remain positive. Thus it can only radiate a finite amount of energy and will consequently return eventually to the equilibrium state. However, if the initial data is such that $E_c < 0$ then since the radiation can only carry away positive energy the perturbation is unable to die away in time. Thus the evolution is unstable. This gives us the following criterion for stability,

- If $E_c > 0$ initially the configuration is stable.
- If $E_c < 0$ initially the configuration is unstable or marginally unstable.

This situation is complicated slightly by the existence of the *trivial displacements* introduced in Section 4.5.1. These displacements leave the physical variables unchanged but do affect the canonical energy. This is unfortunate because we would like to be able to use the condition that E_c is positive definite as a stability test. To overcome this problem we must ensure that the displacement vector ξ^i is orthogonal to all trivials. Fortunately for normal modes one can prove that this is the case [39] and thus we can now use the above criteria to consider the stability of the normal modes.

If we consider a real frequency mode we can write,

$$\frac{J_c(\xi)}{\langle \xi, \rho\xi \rangle} = -m\omega + m\frac{\langle \xi, i\rho\vec{v}\cdot\nabla\xi \rangle}{\langle \xi, \rho\xi \rangle} \tag{4.129}$$

Using cylindrical coordinates and by writing $v^j = \Omega\phi^j$,

$$\begin{aligned}
-i\rho(\xi_i)^* v^j \nabla_j \xi^i &= -i\rho(\xi_i)^* v^j (\partial_j \xi^i + \Gamma^i_{kj}\xi^k) \\
&= -i\rho\Omega\left[im(\xi_i)^*\xi^i + (\xi_1)^*(-r\xi^2) + (\xi_2)^*(\frac{1}{r}\xi^1)\right] \\
&= -i\rho\Omega\left[im|\xi^i|^2 - r(\xi_1)^*\xi^2 + \frac{1}{r}(\xi_2)^*\xi^1\right] \\
&= -i\rho\Omega\left[im|\xi|^2 - r\left((\xi^1)^*\xi^2 - (\xi^2)^*\xi^1\right)\right] \\
&= \rho\Omega\left[m|\xi|^2 + i\left((\vec{\xi})^* \times \vec{\xi}\right)_z\right]
\end{aligned} \tag{4.130}$$

Where we have used the fact that in cylindrical coordinates $(\xi_1)^* = (\xi^1)^*$ and $(\xi_2)^* = r^2(\xi^2)^*$, Therefore,

$$\frac{\langle \xi, i\rho\vec{v}\cdot\nabla\xi \rangle}{\langle \xi, \rho\xi \rangle} = \Omega\left(m + \frac{i\int\left\{\left[(\vec{\xi})^* \times \vec{\xi}\right]_z\right\}dV}{\langle \xi, \xi \rangle}\right) \tag{4.131}$$

Since $|(\vec{\xi})^* \times \vec{\xi})_z| \leq |\xi|^2$ we find the following limits for the canonical angular momentum,

$$\sigma_p - \Omega\left(1+\frac{1}{m}\right) \leq \frac{J_c}{m^2\langle\xi,\rho\xi\rangle} \leq \sigma_p - \Omega\left(1-\frac{1}{m}\right) \tag{4.132}$$

We recall that for normal modes,

$$\sigma_p = \frac{E_c}{J_c}$$

If we consider the situation where the rotation is small ($\Omega \to 0$) then we find

Small Rotation Case ($\Omega \to 0$)		
	$\sigma_p < 0$	$\sigma_p > 0$
J_c	$-$	$+$
E_c	$+$	$+$

Table 4.1: *Regions of stability for a single fluid with small rotation. We observe that regardless of the sign of the mode pattern speed the canonical energy is positive. We conclude that as $\Omega \to 0$ the system is stable.*

Since for both co-rotating modes ($\sigma_p > 0$) and counter-rotating modes ($\sigma_p < 0$) the canonical energy is positive the system will be stable. However, in a system with finite Ω we find the results summarised in Table 4.2. When $\sigma_p < 0$, and the mode is counter-rotating, we observe that it is stable. However, as it begins co-rotating the canonical energy becomes negative and the mode unstable. In the non-rotating limit we found no such instability, and hence we deduce that this change of sign signifies the introduction of an instability at a critical rotation rate.

Finite Rotation Case ($\Omega \neq 0$)			
	$\sigma_p < 0$	$0 < \sigma_p < \Omega(1-\frac{1}{m})$	$\sigma_p > \Omega(1+\frac{1}{m})$
J_c	$-$	$-$	$+$
E_c	$+$	$-$	$+$

Table 4.2: *Regions of stability for a single fluid with finite rotation. When $\sigma_p < 0$, and the mode is counter-rotating, we observe that it is stable. However, as it begins co-rotating the canonical energy becomes negative and the mode unstable. In the non-rotating limit we found no such instability, and hence we deduce that this change of sign signifies the introduction of an instability at a critical rotation rate.*

4.5.8 The r mode instability

Inertial modes are those which have the Coriolis force as the main restoring force. In Newtonian stars inertial modes have velocity fields described by a mixture of both polar and axial parity components. The r modes are a class of inertial modes

which at order Ω have axial parity components only and a frequency given by

$$\omega = m\Omega\left[1 - \frac{2}{l(l+1)}\right] \tag{4.133}$$

Since the discovery by Andersson [6] that the r modes of rotating neutron stars are unstable, much work on the r mode instability has been done, [57], [21], [56], [52] & [88]. It is interesting to revisit this work in the framework developed to demonstrate how the canonical energy can be used to prove stability.

For the r modes we assume the perturbations obey the following ordering in Ω,

$$\vec{v} \sim \delta\vec{v} \sim \dot{\vec{\xi}} \sim O(\Omega), \quad \delta\Phi \sim \delta n \sim O(\Omega^2) \quad \text{and} \quad \delta v_r \sim O(\Omega^2) \tag{4.134}$$

which when combined with the continuity equation leads to

$$\nabla \cdot \delta\vec{v} \sim O(\Omega^3) \rightarrow \nabla \cdot \vec{\xi} \sim O(\Omega^2) \tag{4.135}$$

Thus to order Ω^2 equation (4.118) reduces to the following expression for the canonical energy,

$$E_c \approx \frac{1}{2}\int \rho\left\{|\partial_t \xi|^2 - |v \cdot \nabla\xi|^2 + \xi^{i*}\xi^j \nabla_i \nabla_j (\Phi + \tilde{\mu})\right\} dV \tag{4.136}$$

Using the equations that govern the axisymmetric equilibrium we can rewrite the last term in equation (4.136) as,

$$\begin{aligned} \xi^{i*}\xi^j \nabla_i \nabla_j (\Phi + \tilde{\mu}) &= \Omega^2 \xi^{i*}\xi^j \nabla_i \nabla_j (r^2 \sin^2\theta) \\ &= 2\Omega^2 r^2 \left[\cos^2\theta |\xi^\theta|^2 + \sin^2\theta |\xi^\varphi|^2\right] \end{aligned} \tag{4.137}$$

and

$$\begin{aligned} |v^i \nabla_i \xi_j|^2 &= \Omega^2 \Big\{ m^2 |\xi|^2 - 2imr^2 \sin\theta\cos\theta \left[\xi^\theta \xi^{\varphi *} - \xi^\varphi \xi^{\theta *}\right] \\ &+ r^2 \left[\cos^2\theta |\xi^\theta|^2 + \sin^2\theta |\xi^\varphi|^2\right] \Big\} \end{aligned} \tag{4.138}$$

which means that the canonical energy can be written in the form

$$E_c \approx -\frac{1}{2}\int \rho\left\{(m\Omega - \omega)(m\Omega + \omega)|\xi|^2 - 2im\Omega^2 r^2 \sin\theta\cos\theta \left[\xi^\theta \xi^{\varphi *} - \xi^\varphi \xi^{\theta *}\right] dV \right. \tag{4.139}$$

Introducing the axial stream function,

$$\xi^{\theta} = -\frac{iU}{r^2 \sin\theta}\partial_{\varphi} Y_l^m e^{i\omega t} , \tag{4.140}$$

$$\xi^{\varphi} = \frac{iU}{r^2 \sin\theta}\partial_{\theta} Y_l^m e^{i\omega t} , \tag{4.141}$$

we have

$$|\xi|^2 = \frac{|U|^2}{r^2}\left[\frac{1}{\sin^2\theta}|\partial_{\varphi} Y_l^m|^2 + |\partial_{\theta} Y_l^m|^2\right] \tag{4.142}$$

and

$$ir^2 \sin\theta\cos\theta\left[\xi^{\theta}\xi^{\varphi *} - \xi^{\varphi}\xi^{\theta *}\right] = \frac{1}{r^2}\frac{\cos\theta}{\sin\theta} m|U|^2\left[Y_l^m \partial_{\theta} Y_l^{m*} + Y_l^{m*}\partial_{\theta} Y_l^m\right] . \tag{4.143}$$

After performing the angular integrals, we find that

$$E_c = -\frac{l(l+1)}{2}\left\{(m\Omega - \omega)(m\Omega + \omega) - \frac{2m^2\Omega^2}{l(l+1)}\right\}\int \rho|U|^2 dr . \tag{4.144}$$

Therefore we see that for all $l > 1$ r modes the canonical energy is less than zero, and the $l = m = 1$ r mode results in $E_c = 0$. This agrees with previous work suggesting the r modes are unstable against the gravitational radiation reaction.

4.6 The superfluid problem

We now wish to extend the Lagrangian perturbation analysis to the superfluid case. For this system we use the two-fluid model outlined in Section 2. To recap, the essential equations are two continuity equations (2.19), two coupled Euler equations (2.20), and an equation for the gravitational potential (2.21). As a first step we will initially only be considering the case of vanishing entrainment for which we can write the Euler equations as,

$$\left(\partial_t + \pounds_{v_X}\right) v_i^X + \nabla_i \left(\Phi + \tilde{\mu}_X - \frac{1}{2} v_X^2\right) = 0 \tag{4.145}$$

we recall that $X = n$ or p.

To investigate the Lagrangian perturbations of this system we introduce two distinct Lagrangian displacement vectors ξ_X^i, one for the neutrons ξ_n^i, and one for the protons ξ_p^i. To distinguish between the two possibilities we use variations Δ_X such that

$$\Delta_X Q = \delta Q + \pounds_{\xi_X} Q \ . \tag{4.146}$$

The continuity equations therefore become,

$$\Delta_X n_X = -n_X \nabla_i \xi_X^i \longrightarrow \delta n_X = -\nabla_i (n_X \xi_X^i) \ . \tag{4.147}$$

The equation describing the perturbed gravitational potential is,

$$\nabla^2 \delta\Phi = 4\pi m_B G(\delta n_X + \delta n_Y) = -4\pi m_B G \nabla_i (n_X \xi_X^i + n_Y \xi_Y^i) \tag{4.148}$$

This equation is linear which means that we can write,

$$\delta\Phi = \delta\Phi_{\rm n} + \delta\Phi_{\rm p} \tag{4.149}$$

Where

$$\nabla^2 \delta\Phi_X = 4\pi m_B G \delta n_X = -4\pi m_B G \nabla_i (n_X \xi_X^i) \tag{4.150}$$

As in the single fluid case these equation can be solved using Green's functions to give,

$$\delta\Phi_X = -m_B G \int n_X' (\xi_X^i)' \nabla_i' \left[\frac{1}{|\vec{x} - \vec{x}'|}\right] dV' \tag{4.151}$$

Applying a perturbation to the Euler equations gives,

$$(\partial_t + \pounds_{v_X})\,\Delta_X v_i^X + \nabla_i\left(\Delta_X\Phi + \Delta_X\tilde{\mu}_X - \frac{1}{2}\Delta_X v_X^2\right) = 0 \tag{4.152}$$

We can see that this is almost identical to the single fluid perturbed Euler equations. Therefore we can immediately write,

$$\partial_t^2\xi_i^X + 2v_X^j\nabla_j\partial_t\xi_i^X + (v_X^j\nabla_j)^2\xi_i^X + \nabla_i\delta\Phi + \xi_X^j\nabla_i\nabla_j\Phi - (\nabla_i\xi_X^j)\nabla_j\tilde{\mu}_X + \nabla_i\Delta_X\tilde{\mu}_X = 0\,. \tag{4.153}$$

The Lagrangian perturbation of the chemical potential can be written as,

$$\begin{aligned}
\Delta_X\tilde{\mu}_X &= \delta\tilde{\mu}_X + \xi_X^j\nabla_j\tilde{\mu}_X \\
&= \left(\frac{\partial\tilde{\mu}_X}{\partial n_X}\right)_{n_Y}\delta n_X + \left(\frac{\partial\tilde{\mu}_X}{\partial n_Y}\right)_{n_X}\delta n_Y + \xi_X^j\nabla_j\tilde{\mu}_X \\
&= -\left(\frac{\partial\tilde{\mu}_X}{\partial n_X}\right)_{n_Y}\nabla_j(n_X\xi_X^j) - \left(\frac{\partial\tilde{\mu}_X}{\partial n_Y}\right)_{n_X}\nabla_j(n_Y\xi_Y^j) \\
&+ \xi_X^j\nabla_j\tilde{\mu}_X
\end{aligned} \tag{4.154}$$

Therefore

$$\begin{aligned}
\nabla_i\Delta_X\tilde{\mu}_X &= -\nabla_i\left[\left(\frac{\partial\tilde{\mu}_X}{\partial n_X}\right)_{n_Y}\nabla_j(n_X\xi_X^j)\right] - \nabla_i\left[\left(\frac{\partial\tilde{\mu}_X}{\partial n_Y}\right)_{n_X}\nabla_j(n_Y\xi_Y^j)\right] \\
&+ \nabla_i\left[\xi_X^j\nabla_j\tilde{\mu}_X\right] \\
&= -\nabla_i\left[\left(\frac{\partial\tilde{\mu}_X}{\partial n_X}\right)_{n_Y}\nabla_j(n_X\xi_X^j)\right] - \nabla_i\left[\left(\frac{\partial\tilde{\mu}_X}{\partial n_Y}\right)_{n_X}\nabla_j(n_Y\xi_Y^j)\right] \\
&+ \nabla_i\xi_X^j\nabla_j\tilde{\mu}_X + \xi_X^j\nabla_i\nabla_j\tilde{\mu}_X
\end{aligned} \tag{4.155}$$

and we arrive at the following form for the perturbed Euler equations

$$\begin{aligned}
\partial_t^2\xi_i^X &+ 2v_X^j\nabla_j\partial_t\xi_i^X + (v_X^j\nabla_j)^2\xi_i^X + \nabla_i\delta\Phi + \xi_X^j\nabla_i\nabla_j(\Phi + \tilde{\mu}_X) \\
&- \nabla_i\left[\left(\frac{\partial\tilde{\mu}_X}{\partial n_X}\right)_{n_Y}\nabla_j(n_X\xi_X^j) + \left(\frac{\partial\tilde{\mu}_X}{\partial n_Y}\right)_{n_X}\nabla_j(n_Y\xi_Y^j)\right] = 0
\end{aligned} \tag{4.156}$$

As in the single fluid case we can write these equations as

$$A_X\partial_t^2\xi_X + B_X\partial_t\xi_X + C_X\xi_X + D_X\xi_Y = 0 \tag{4.157}$$

Where

$$A_X \partial_t^2 \xi_i^X = n_X \partial_t^2 \xi_i^X \tag{4.158}$$

$$B_X \partial_t \xi_i^X = 2 n_X v^j \nabla_j \partial_t \xi_i^X \tag{4.159}$$

$$\begin{aligned} C_X \xi_i^X &= n_X (v^j \nabla_j)^2 \xi_i^X + n_X \nabla_i \delta\Phi_n + n_X \xi_X^j \nabla_i \nabla_j \Phi \\ &- n_X \nabla_i \left[\left(\frac{\partial \tilde{\mu}_X}{\partial n_X} \right)_{n_Y} \nabla_j (n_X \xi_X^j) \right] + n_X \xi_X^j \nabla_i \nabla_j \tilde{\mu_X} \end{aligned} \tag{4.160}$$

$$D_X \xi_i^Y = -n_x \nabla_i \left[\left(\frac{\partial \tilde{\mu}_X}{\partial n_Y} \right)_{n_X} \nabla_j (n_Y \xi_Y^j) \right] + n_X \nabla_i \delta\Phi_Y \tag{4.161}$$

4.6.1 Trivial displacements

In Section 4.5.1 we introduced the idea that for a particular physical perturbation there does not exist a corresponding unique displacement vector ξ^i. We identified certain *trivial displacements* that while not affecting the physical perturbation can alter the canonical energy. In the two-fluid case we need to introduce two such displacements, one for each fluid. The equations these displacements need to satisfy are identical to equations (4.91) - (2.19) except now we require two sets of equations. Once again it can be shown that for the normal modes the displacement vectors ξ_X^i are orthogonal to all the trivials and hence the canonical energy can be used to test for stability given a normal mode solution.

4.6.2 Symmetries of the operators

In analogy with the single case we want to derive conserved quantities for the system to enable us to assess stability. Given the single fluid results it can easily be shown that the following symmetries hold,

$$\begin{aligned} \langle \eta_X, A_X \xi_X \rangle &= \langle \eta_X, A_X \xi_X \rangle^* \\ \langle \eta_X, B_X \xi_X \rangle &= - \langle \eta_X, B_X \xi_X \rangle^* \\ \langle \eta_X, C_X \xi_X \rangle &= \langle \eta_X, C_X \xi_X \rangle^* \end{aligned} \tag{4.162}$$

4.6.3 Symplectic structures

We introduce the symplectic structures which are used to construct the canonical energy. To do this we consider two sets of solutions to our perturbation equations, $[\xi_\mathrm{n}, \xi_\mathrm{p}]$ and $[\eta_\mathrm{n}, \eta_\mathrm{p}]$, and define,

$$W_X(\eta_X, \xi_X) = \left\langle \eta_X, A_X \partial_t \xi_X + \frac{1}{2} B_X \xi_X \right\rangle - \left\langle A_X \partial_t \eta_X + \frac{1}{2} B_X \eta_X, \xi_X \right\rangle \quad (4.163)$$

Therefore,

$$\begin{aligned}
\partial_t W_X(\eta_X, \xi_X) &= \left\langle \partial_t \eta_X, A_X \partial_t \xi_X + \frac{1}{2} B_X \xi_X \right\rangle + \left\langle \eta_X, A_X \partial_t^2 \xi_X + \frac{1}{2} B_X \partial_t \xi_X \right\rangle \\
&- \left\langle A_X \partial_t^2 \eta_X + \frac{1}{2} B_X \partial_t \eta_X, \xi_X \right\rangle - \left\langle A_X \partial_t \eta_X + \frac{1}{2} B_X \eta_X, \partial_t \xi_X \right\rangle \\
&= \left\langle \partial_t \eta_X, A_X \partial_t \xi_X + \frac{1}{2} B_X \xi_X \right\rangle + \left\langle \eta_X, -\frac{1}{2} B_X \partial_t \xi_X - C_X \xi_X - D_X \xi_Y \right\rangle \\
&- \left\langle -\frac{1}{2} B_X \partial_t \eta_X - C_X \eta_X - D_X \eta_Y, \xi_X \right\rangle - \left\langle A_X \partial_t \eta_X + \frac{1}{2} B_X \eta_X, \partial_t \xi_X \right\rangle \\
&= \langle \partial_t \eta_X, A_X \partial_t \xi_X \rangle - \langle A_X \partial_t \eta_X, \partial_t \xi_X \rangle \\
&+ \left\langle \partial_t \eta_X, \frac{1}{2} B_X \xi_X \right\rangle + \left\langle \frac{1}{2} B_X \partial_t \eta_X, \xi_X \right\rangle \\
&- \left\langle \eta_X, \frac{1}{2} B_X \partial_t \xi_X \right\rangle - \left\langle \frac{1}{2} B_X \eta_X, \partial_t \xi_X \right\rangle \\
&- \langle \eta_X, C_X \xi_X \rangle + \langle C_X \eta_X, \xi_X \rangle \\
&- \langle \eta_X, D_X \xi_Y \rangle + \langle D_X \eta_Y, \xi_X \rangle \\
&= - \langle \eta_X, D_X \xi_Y \rangle + \langle D_X \eta_Y, \xi_X \rangle \\
&\neq 0
\end{aligned} \quad (4.164)$$

Explicitly,

$$\partial_t W_{\mathrm{n}} = - \langle \eta_{\mathrm{n}}, D_{\mathrm{n}} \xi_{\mathrm{p}} \rangle + \langle D_{\mathrm{n}} \eta_{\mathrm{p}}, \xi_{\mathrm{n}} \rangle \neq 0 \quad (4.165)$$

and

$$\partial_t W_{\mathrm{p}} = - \langle \eta_{\mathrm{p}}, D_{\mathrm{p}} \xi_{\mathrm{n}} \rangle + \langle D_{\mathrm{p}} \eta_{\mathrm{n}}, \xi_{\mathrm{p}} \rangle \neq 0 \quad (4.166)$$

We can see that individually W_{n} and W_{p} are not conserved, so we look to see if the sum of the two is conserved. Since,

$$D_X \eta_X = -n_X \nabla_i \left[\left(\frac{\partial \tilde{\mu}_X}{\partial n_Y} \right)_{n_X} \nabla_j (n_Y \eta_X^j) \right] + n_X \nabla_i \delta \Phi_Y \quad (4.167)$$

we can write,

$$\begin{aligned}
\partial_t W_{\rm n} &= \int n_{\rm n}\eta_{\rm n}^{i*}\nabla_i\left[\left(\frac{\partial\tilde{\mu}_{\rm n}}{\partial n_{\rm p}}\right)_{n_{\rm n}}\nabla_j(n_{\rm p}\xi_{\rm p}^j)\right]dV \\
&- \int n_{\rm n}\xi_{\rm n}^i\nabla_i\left[\left(\frac{\partial\tilde{\mu}_{\rm n}}{\partial n_{\rm p}}\right)_{n_{\rm n}}\nabla_j(n_{\rm p}\eta_{\rm p}^{j*})\right]dV \\
&- \int n_{\rm n}\eta_{\rm n}^{i*}\nabla_i\delta_{\xi_{\rm p}}\Phi_{\rm p}dV + \int n_{\rm n}\xi_{\rm n}^i\nabla_i(\delta_{\eta_{\rm p}}\Phi_{\rm p})^*dV \qquad (4.168)
\end{aligned}$$

and

$$\begin{aligned}
\partial_t W_{\rm p} &= \int n_{\rm p}\eta_{\rm p}^{i*}\nabla_i\left[\left(\frac{\partial\tilde{\mu}_{\rm p}}{\partial n_{\rm n}}\right)_{n_{\rm p}}\nabla_j(n_{\rm n}\xi_{\rm n}^j)\right]dV \\
&- \int n_{\rm p}\xi_{\rm p}^i\nabla_i\left[\left(\frac{\partial\tilde{\mu}_{\rm p}}{\partial n_{\rm n}}\right)_{n_{\rm p}}\nabla_j(n_{\rm n}\eta_{\rm p}^{j*})\right]dV \\
&- \int n_{\rm p}\eta_{\rm p}^{i*}\nabla_i\delta_{\xi_{\rm n}}\Phi_{\rm n}dV + \int n_{\rm p}\xi_{\rm p}^i\nabla_i(\delta_{\eta_{\rm n}}\Phi_{\rm n})^*dV \qquad (4.169)
\end{aligned}$$

Using the fact that,

$$\left(\frac{\partial\tilde{\mu}_{\rm p}}{\partial n_{\rm n}}\right)_{n_{\rm p}} = \left(\frac{\partial\tilde{\mu}_{\rm n}}{\partial n_{\rm p}}\right)_{n_{\rm n}} \qquad (4.170)$$

the first term in $\partial_t W_{\rm p}$ can therefore be written as

$$\begin{aligned}
\int n_{\rm p}\eta_{\rm p}^{i*}\nabla_i\left[\left(\frac{\partial\tilde{\mu}_{\rm p}}{\partial n_{\rm n}}\right)_{n_{\rm p}}\nabla_j(n_{\rm n}\xi_{\rm n}^j)\right]dV &= \int\nabla_i\left[n_{\rm p}\eta_{\rm p}^{i*}\left(\frac{\partial\tilde{\mu}_{\rm p}}{\partial n_{\rm n}}\right)_{n_{\rm p}}\nabla_j(n_{\rm n}\xi_{\rm n}^j)\right]dV \\
&- \int\left(\frac{\partial\tilde{\mu}_{\rm n}}{\partial n_{\rm p}}\right)_{n_{\rm n}}\nabla_j(n_{\rm n}\xi_{\rm n}^j)\nabla_i(n_{\rm p}\eta_{\rm p}^{i*})dV \\
&= -\int\nabla_j\left[n_{\rm n}\xi_{\rm n}^j\left(\frac{\partial\tilde{\mu}_{\rm n}}{\partial n_{\rm p}}\right)_{n_{\rm n}}\nabla_i(n_{\rm p}\eta_{\rm p}^{i*})\right]dV \\
&+ \int n_{\rm n}\xi_{\rm n}^j\nabla_j\left[\left(\frac{\partial\tilde{\mu}_{\rm n}}{\partial n_{\rm p}}\right)_{n_{\rm n}}\nabla_i(n_{\rm p}\eta_{\rm p}^{i*})\right]dV \\
&= \int n_{\rm n}\xi_{\rm n}^j\nabla_j\left[\left(\frac{\partial\tilde{\mu}_{\rm n}}{\partial n_{\rm p}}\right)_{n_{\rm n}}\nabla_i(n_{\rm p}\eta_{\rm p}^{i*})\right]dV \qquad (4.171)
\end{aligned}$$

Therefore when added to $\partial_t W_{\rm n}$ this term will cancel with the second term. Similarly,

$$\int n_{\rm p}\xi_{\rm p}^{i*}\nabla_i\left[\left(\frac{\partial\tilde{\mu}_{\rm p}}{\partial n_{\rm n}}\right)_{n_{\rm p}}\nabla_j(n_{\rm n}\eta_{\rm n}^j)\right]dV = \int n_{\rm n}\eta_{\rm n}^{j*}\nabla_j\left[\left(\frac{\partial\tilde{\mu}_{\rm n}}{\partial n_{\rm p}}\right)_{n_{\rm n}}\nabla_i(n_{\rm p}\xi_{\rm p}^i)\right]dV \tag{4.172}$$

Therefore the second term of $\partial_t W_{\rm p}$ will cancel with the first term of $\partial_t W_{\rm n}$. If we now look at the third term of $\partial_t W_{\rm p}$

$$\begin{aligned}\int n_{\rm p}(\eta_{\rm p}^i)^*\nabla_i\delta\Phi_{\rm n}dV &= \int n_{\rm p}(\eta_{\rm p}^i)^*\nabla_i\left[-m_{\rm B}G\int n'_{\rm n}(\xi_{\rm n}^i)'\nabla'_i\left[\frac{1}{|\vec{x}-\vec{x}'|}\right]dV'\right]dV\\ &= -m_{\rm B}G\int\int n'_{\rm n}(\xi_{\rm n}^i)'n_{\rm p}(\eta_{\rm p}^i)^*\nabla_i\nabla'_i\left[\frac{1}{|\vec{x}-\vec{x}'|}\right]dV'dV\\ &= -m_{\rm B}G\int n'_{\rm n}(\xi_{\rm n}^i)'\int\nabla'_i\left(n_{\rm p}(\eta_{\rm p}^i)^*\nabla_i\left[\frac{1}{|\vec{x}-\vec{x}'|}\right]\right)dVdV'\\ &= \int n_{\rm n}\xi_{\rm n}^i\nabla_i(\delta\Phi_{\rm p})\end{aligned} \tag{4.173}$$

Similarly

$$\int\left\{n_{\rm p}\xi_{\rm p}^i\nabla_i(\delta\Phi_{\rm n})^*\right\}dV = \int\left\{n_{\rm n}(\eta_{\rm n}^i)^*\nabla_i\delta\Phi_{\rm p}\right\}dV \tag{4.174}$$

Therefore it is clear that

$$\partial_t W_{\rm n} + \partial_t W_{\rm p} = 0 \tag{4.175}$$

and, $W_{\rm n}(\eta_{\rm n},\xi_{\rm n}) + W_{\rm p}(\eta_{\rm p},\xi_{\rm p})$ is a conserved quantity.

4.6.4 Canonical energy

The canonical energy of the system is defined as,

$$E_c = \frac{m_{\rm B}}{2}[W_{\rm n}(\partial_t\xi_{\rm n},\xi_{\rm n}) + W_p(\partial_t\xi_{\rm p},\xi_{\rm p})] \tag{4.176}$$

Expanding this out gives,

$$\begin{aligned}E_c &= \frac{m_{\rm B}}{2}\left[\left\langle\partial_t\xi_{\rm n}, A_{\rm n}\partial_t\xi_{\rm n}+\frac{1}{2}B_{\rm n}\xi_{\rm n}\right\rangle - \left\langle A_{\rm n}\partial_t^2\xi_{\rm n}+\frac{1}{2}B_{\rm n}\partial_t\xi_{\rm n},\xi_{\rm n}\right\rangle\right.\\ &+ \left.\left\langle\partial_t\xi_{\rm p}, A_{\rm p}\partial_t\xi_{\rm p}+\frac{1}{2}B_{\rm p}\xi-{\rm p}\right\rangle - \left\langle A_{\rm p}\partial_t^2\xi_{\rm p}+\frac{1}{2}B_{\rm p}\partial_t\xi_{\rm p},\xi_{\rm p}\right\rangle\right]\end{aligned} \tag{4.177}$$

Which easily leads to,

$$\begin{aligned}E_c &= \frac{m_{\rm B}}{2}[\langle\partial_t\xi_{\rm n}, A_{\rm n}\partial_t\xi_{\rm n}\rangle + \langle\partial_t\xi_{\rm p}, A_{\rm p}\partial_t\xi-{\rm p}\rangle + \langle\xi_{\rm n}, C_{\rm n}\xi_{\rm n}\rangle^* + \langle\xi_{\rm p}, C_{\rm p}\xi_{\rm p}\rangle^*\\ &+ \langle\xi_{\rm n}, D_{\rm n}\xi_{\rm p}\rangle^* + \langle\xi_{\rm p}, D_{\rm p}\xi_{\rm n}\rangle^*]\end{aligned} \tag{4.178}$$

The terms involving A and C are identical to those in the single fluid case, thus we need only consider the final two terms. We can see that,

$$\frac{m_{\rm B}}{2}\left\langle \xi_Y, D_X\xi_X\right\rangle^* = \int \left\{ \rho_X \xi_X^i \nabla_i(\delta\Phi_Y)^* - n_X \xi_X^i \nabla_i \left[\left(\frac{\partial \mu_X}{\partial n_Y} \right)_{n_X} \nabla_j (n_Y (\xi_Y^j)^*) \right] \right\} dV \tag{4.179}$$

By analogy with the results from the single fluid case it follows straightforwardly that the canonical energy can be written as,

$$\begin{aligned} E_c &= \frac{1}{2}\int \Big\{ \rho_{\rm n}|\partial_t \xi_{\rm n}|^2 + \rho_{\rm p}|\partial_t \xi_{\rm p}|^2 - \rho_{\rm n}|v_{\rm n}^j \nabla_j \xi_i^{\rm n}|^2 - \rho_{\rm p}|v_{\rm p}^j \nabla_j \xi_i^{\rm p}|^2 \\ &+ [\rho_{\rm n}\xi_{\rm n}^i \xi_{\rm n}^{j*} + \rho_{\rm p}\xi_{\rm p}^i \xi_{\rm p}^{j*}]\nabla_i\nabla_j\Phi + n_{\rm n}\xi_{\rm n}^i\xi_{\rm n}^{j*}\nabla_i\nabla_j\mu_{\rm n} + n_{\rm p}\xi_{\rm p}^i\xi_{\rm p}^{j*}\nabla_i\nabla_j\mu_{\rm p} \\ &+ \left(\frac{\partial\mu_{\rm n}}{\partial n_{\rm n}}\right)_{n_{\rm p}} |\delta n_{\rm n}|^2 + \left(\frac{\partial\mu_{\rm p}}{\partial n_{\rm p}}\right)_{n_{\rm n}} |\delta n_{\rm p}|^2 - \frac{1}{4\pi G}|\nabla_i\delta\Phi|^2 \\ &+ \left(\frac{\partial\mu_{\rm n}}{\partial n_{\rm p}}\right)_{n_{\rm n}} [\delta n_{\rm n}\delta n_{\rm p}^* + \delta n_{\rm n}^*\delta n_{\rm p}] \Big\} dV \end{aligned} \tag{4.180}$$

4.6.5 Canonical angular momentum

The canonical angular momentum is defined as,

$$J_c = -\frac{m_{\rm B}}{2}W_{\rm n}(\partial_\phi\xi_{\rm n}, \xi_{\rm n}) - \frac{m_{\rm B}}{2}W_{\rm p}(\partial_\phi\xi_{\rm p}, \xi_{\rm p}) \tag{4.181}$$

Using the result from the single fluid case,

$$J_c = -m_{\rm B} Re\left\{ \left\langle \partial_\phi\xi_{\rm n}, A_{\rm n}\partial_t\xi_{\rm n} + \frac{1}{2}B_{\rm n}\xi_{\rm n} \right\rangle + \left\langle \partial_\phi\xi_{\rm p}, A_{\rm p}\partial_t\xi_{\rm p} + \frac{1}{2}B_{\rm p}\xi_{\rm p} \right\rangle \right\} \tag{4.182}$$

4.6.6 Normal mode solutions

If we consider a normal mode of the form,

$$\xi_X^i = \hat{\xi}_X^i e^{i(m\phi+\omega t)} \tag{4.183}$$

and considering initially only the terms with index n we get,

$$
\begin{aligned}
E_{cn} &= \frac{m_B}{2}\left[\langle \partial_t \xi_{\rm n}, A_{\rm n}\partial_t \xi_{\rm n}\rangle + \langle \xi_{\rm n}, C_{\rm n}\xi_{\rm n} + D_{\rm n}\xi_{\rm p}\rangle^*\right] \\
&= \frac{m_B}{2}\left[\langle i\omega\xi_{\rm n}, i\omega A_{\rm n}\xi_{\rm n}\rangle + \left\langle \xi_{\rm n}, -A_{\rm n}\ddot{\xi}_{\rm n} - B_{\rm n}\dot{\xi}_{\rm n}\right\rangle^*\right] \\
&= \frac{m_B}{2}\left[\omega^*\omega\,\langle \xi_{\rm n}, A_{\rm n}\xi_{\rm n}\rangle + \omega^2\,\langle \xi_{\rm n}, A_{\rm n}\xi_{\rm n}\rangle^* - i\omega\,\langle \xi_{\rm n}, B_{\rm n}\xi_{\rm n}\rangle^*\right] \\
&= \frac{m_B}{2}\left[\omega(\omega^* + \omega)\,\langle \xi_{\rm n}, A_{\rm n}\xi_{\rm n}\rangle - \omega\,\langle \xi_{\rm n}, iB_{\rm n}\xi_{\rm n}\rangle^*\right] \qquad (4.184)
\end{aligned}
$$

Where $\dot{\xi}_{\rm n} = \partial_t \xi_{\rm n}$, $\ddot{\xi}_{\rm n} = \partial_t^2 \xi_{\rm n}$, and where we have used the symmetry of $A_{\rm n}$ to substitute $\langle \xi_{\rm n}, A_{\rm n}\xi_{\rm n}\rangle^* = \langle \xi_{\rm n}, A_{\rm n}\xi_{\rm n}\rangle$. Finally we obtain,

$$
E_{cn} = m_{\rm B}\omega[Re(\omega)\,\langle \xi_{\rm n}, A_{\rm n}\xi_{\rm n}\rangle - \frac{1}{2}\,\langle \xi_{\rm n}, iB_{\rm n}\xi_{\rm n}\rangle] \qquad (4.185)
$$

Including the proton terms the total canonical energy becomes,

$$
\begin{aligned}
E_c &= m_{\rm B}\omega\{Re(\omega)[\langle \xi_{\rm n}, A_{\rm n}\xi_{\rm n}\rangle + \langle \xi_{\rm p}, A_{\rm p}\xi_{\rm p}\rangle] \\
&- \frac{1}{2}[\langle \xi_{\rm n}, iB_{\rm n}\xi_{\rm n}\rangle + \langle \xi_{\rm p}, iB_{\rm p}\xi_{\rm p}\rangle]\} \qquad (4.186)
\end{aligned}
$$

By comparison with the single fluid results the canonical angular momentum for the case of normal modes is,

$$
\begin{aligned}
J_c &= -m_{\rm B}m\{Re(\omega)[\langle \xi_{\rm n}, A_{\rm n}\xi_{\rm n}\rangle + \langle \xi_{\rm p}, A_{\rm p}\xi_{\rm p}\rangle] \\
&- \frac{1}{2}[\langle \xi_{\rm n}, iB_{\rm n}\xi_{\rm n}\rangle + \langle \xi_{\rm p}, iB_{\rm p}\xi_{\rm p}\rangle]\} \qquad (4.187)
\end{aligned}
$$

$$
\Rightarrow \frac{E_c}{J_c} = -\frac{\omega}{m} \equiv \sigma_p \qquad (4.188)
$$

4.6.7 Stability

In the single fluid case when the pattern speed changes sign a counter-rotating mode becomes unstable. We can see if this remains valid in the two fluid case. We consider the canonical angular momentum for normal modes in cylindrical coordinates under uniform rotation. In this case equation (4.187) becomes,

$$
J_c = -m\left\{\omega[\langle \xi_{\rm n}, \rho_{\rm n}\xi_{\rm n}\rangle + \langle \xi_{\rm p}, \rho_{\rm p}\xi_{\rm p}\rangle] - [\langle \xi_{\rm n}, i\rho_{\rm n}\vec{v}_{\rm n}\cdot\nabla\xi_{\rm n}\rangle + \langle \xi_{\rm p}, i\rho_{\rm p}\vec{v}_{\rm p}\cdot\nabla\xi_{\rm p}\rangle]\right\} \qquad (4.189)
$$

Therefore

$$\frac{J_c}{\langle \xi_{\rm n}, \rho_{\rm n}\xi_{\rm n}\rangle + \langle \xi_{\rm p}, \rho_{\rm p}\xi_{\rm p}\rangle} = -m\omega + m\frac{\langle \xi_{\rm n}, i\rho_{\rm n}\vec{v}_{\rm n}\cdot\nabla\xi_{\rm n}\rangle + \langle \xi_{\rm p}, i\rho_{\rm p}\vec{v}_{\rm p}\cdot\nabla\xi_{\rm p}\rangle}{\langle \xi_{\rm n}, \rho_{\rm n}\xi_{\rm n}\rangle + \langle \xi_{\rm p}, \rho_{\rm p}\xi_{\rm p}\rangle} \tag{4.190}$$

As in the single fluid case we can use cylindrical coordinates, $v_X^j = \Omega_X \phi^j$ giving,

$$-i\rho_X(\xi_{Xi})^* v_X^j \nabla_j \xi_X^i = \rho_X \Omega_X \left[m|\xi_X|^2 + i(\vec{\xi_X}^* \times \vec{\xi_X})_z\right] \tag{4.191}$$

Since $|(\vec{\xi_X}^* \times \vec{\xi_X})_z| \leq |\xi_X|^2$

$$\rho_X\Omega_X|\xi_X|^2(m-1) \leq -i\rho_X(\xi_{Xi})^* v_X^j \nabla_j \xi_X^i \leq \rho_X\Omega_X|\xi_X|^2(m+1) \tag{4.192}$$

Therefore

$$\frac{\langle \xi_X, \rho_X i v_X^j \nabla_j \xi_X\rangle}{\langle \xi_X, \rho_X\xi_X\rangle + \langle \xi_Y, \rho_Y\xi_Y\rangle} \geq -\Omega_X(m+1) \tag{4.193}$$

and consequently

$$\langle \xi_X, \rho_X i v_X^j \nabla_j \xi_X\rangle \geq -\Omega_X(m+1)a_X \tag{4.194}$$

Where $a_X = \langle \xi_X, \rho_X\xi_X\rangle > 0$. The next challenge is to find an upper limit. From equation (4.192)

$$\frac{\langle \xi_X, \rho_X i v_X^j \nabla_j \xi_X\rangle}{\langle \xi_X, \rho_X\xi_X\rangle + \langle \xi_Y, \rho_Y\xi_Y\rangle} \leq -\frac{\Omega_X}{2}(m-1) \tag{4.195}$$

and hence

$$\langle \xi_X, \rho_X i v_X^j \nabla_j \xi_X\rangle \leq -\frac{\Omega_X}{2}(m-1)a_X \tag{4.196}$$

Combining the two cases we obtain the following condition for the canonical angular momentum,

$$\sigma_p(a_{\rm n}+a_{\rm p}) - \left(1+\frac{1}{m}\right)\tilde{\Omega} \leq J_c/m^2 \leq \sigma_p(a_{\rm n}+a_{\rm p}) - \frac{1}{2}\left(1-\frac{1}{m}\right)\tilde{\Omega} \tag{4.197}$$

Where $\tilde{\Omega} = [\Omega_{\rm n}a_{\rm n} + \Omega_{\rm p}a_{\rm p}]$. In the same way as in the single fluid case we can use this canonical angular momentum limit along with the relationship between the pattern speed, the canonical energy and the canonical angular momentum ($\sigma_p = E_c/J_c$) to investigate the stability of the normal modes. If both the fluids are rotating slowly ($\tilde{\Omega} \to 0$) we find the results summarised in Table 4.3.

Small Rotation Case ($\tilde{\Omega} \to 0$)		
	$\sigma_p < 0$	$\sigma_p > 0$
J_c	$-$	$+$
E_c	$+$	$+$

Table 4.3: *Regions of stability for a two fluids with small rotation.Since for both co-rotating modes ($\sigma_p > 0$) and counter-rotating modes ($\sigma_p < 0$) the canonical energy is positive the system will be stable.*

Since for both co-rotating modes ($\sigma_p > 0$) and counter-rotating modes ($\sigma_p < 0$) the canonical energy is positive the system will be stable. However, in a system with finite $\tilde{\Omega}$ we find the results summarised in Table 4.4. Therefore we can conclude that as in the case of a single fluid when $\sigma_p < 0$, and the mode is counter-rotating, we observe that it is stable. However, as it begins co-rotating the canonical energy becomes negative and the mode becomes unstable.

Finite Rotation Case ($\tilde{\Omega} \neq 0$)			
	$\sigma_p < 0$	$0 < \sigma_p(a_\mathrm{n} + a_\mathrm{p}) < \frac{1}{2}(1 - \frac{1}{m})\tilde{\Omega}$	$\sigma_p(a_\mathrm{n} + a_\mathrm{p}) > (1 + \frac{1}{m})\tilde{\Omega}$
J_c	$-$	$-$	$+$
E_c	$+$	$-$	$+$

Table 4.4: *Regions of stability for a two fluids with finite rotation. When $\sigma_p < 0$, and the mode is counter-rotating, we observe that it is stable. However, as it begins co-rotating the canonical energy becomes negative and the mode unstable. In the non-rotating limit we found no such instability, and hence we deduce that this change of sign signifies the introduction of an instability at a critical rotation rate.*

4.6.8 The superfluid r mode instability

We now extend the analysis of the r mode instability introduced in Section 4.5.8 to the superfluid case. Again a significant amount of previous work has been done on this topic and we will make use of their results in our investigation. Many studies have restricted their analysis to co-rotating backgrounds, $\Omega_\mathrm{n} = \Omega_\mathrm{p}$, [55], [76], [10] where it is found that provided the background model is not stratified, i.e. if $\nabla x_\mathrm{p} = 0$, the system can be separated into purely co- and counter-moving modes. However, in the general case with a background allowing the two fluids to rotate at different rates around the same axis, i.e. $\Omega_\mathrm{n} \neq \Omega_\mathrm{p}$, Prix et al [68] showed that purely co- or counter-moving modes are not observed. However, their investigations showed that in the absence of entrainment the r mode fluid motion must be such that only one of the fluids oscillates. We will consider this entrainment free case before turning our attention to the co-rotating case with entrainment.

The case with relative rotation

Since we have ignored entrainment the two fluid system is basically two uncoupled systems with identical solutions. Therefore when $\Omega_{\rm n} \neq \Omega_{\rm p}$ we cannot find a single mode solution. What we find is that only one fluid will oscillate giving,

$$\delta\vec{v}_X \neq 0 \ , \quad \delta\vec{v}_Y = 0 \ , \quad \omega = m\Omega_X \left[1 - \frac{2}{l(l+1)}\right] \ . \tag{4.198}$$

and by analogy with the single fluid case we immediately get,

$$E_c = \frac{1}{2}\int \left\{\rho_X|\partial_t\xi_X|^2 - \rho_X|v^j\nabla_j\xi_i^X|^2 + \rho_X\xi_X^i\xi_X^{j*}\nabla_i\nabla_j(\Phi+\tilde{\mu}_X)\right\} dV \tag{4.199}$$

Thus both these classes of modes will be unstable due to the emission of gravitational radiation.

The co-rotating case $\Omega_{\rm n} = \Omega_{\rm p} = \Omega$

If we write,

$$\xi_i^+ = \frac{n_n\xi_i^{\rm n} + n_{\rm p}\xi_i^{\rm p}}{n_{\rm n} + n_{\rm p}} \tag{4.200}$$

and

$$\xi_i^- = \xi_i^{\rm n} - \xi_i^{\rm p} \tag{4.201}$$

then when $\xi_i^{\rm n} = \xi_i^{\rm p}$ and the two fluids move together only ξ_i^+ is present. We can write the canonical energy in this situation as,

$$\begin{aligned} E_c \ &\approx \ \frac{1}{2}\int \left\{\rho|\partial_t\xi^+|^2 - \rho|v^j\nabla_j\xi_i^+|^2 + \rho\xi_+^i\xi_+^{j*}\nabla_i\nabla_j\Phi\right. \\ &+ \ \left.\xi_+^i\xi_+^{j*}[n_{\rm n}\nabla_i\nabla_j\mu_{\rm n} + n_{\rm p}\nabla_i\nabla_j\mu_{\rm p}]\right\} dV \end{aligned} \tag{4.202}$$

where we have neglected the higher order contributions from δn_X and $\delta\Phi$.

In this expression, the last term can be rewritten using the fact that we must have

$$\nabla_i\mu_{\rm n} = \nabla_i\mu_{\rm p} \equiv \nabla_i\mu \tag{4.203}$$

if the two fluids rotate at the same rate, cf equation (4.152). This immediately leads to

$$n_{\rm n}\nabla_i\nabla_j\mu_{\rm n} + n_{\rm p}\nabla_i\nabla_j\mu_{\rm p} = n\nabla_i\nabla_j\mu \tag{4.204}$$

(where $n = n_{\rm n} + n_{\rm p}$) and consequently

$$E_c \ = \ \frac{1}{2}\int \rho\left\{|\partial_t\xi^+|^2 - |v^j\nabla_j\xi_i^+|^2 + \xi_+^i\xi_+^{j*}\nabla_i\nabla_j(\Phi+\tilde{\mu})\right\} dV \tag{4.205}$$

This is identical to the single fluid problem, suggesting that pure $\vec{\xi}^{+}$ modes are unstable.

The next case we consider is the canonical energy for counter-rotating modes where,

$$n_{\rm n}\xi^i_{\rm n} + n_{\rm p}\xi^i_{\rm p} = 0 \ . \tag{4.206}$$

In this situation only ξ^-_i is present, and we have

$$\xi^{\rm n}_i = \frac{n_{\rm p}}{n}\xi^-_i \ , \tag{4.207}$$

$$\xi^{\rm p}_i = -\frac{n_{\rm n}}{n_{\rm p}}\xi^{\rm n}_i = -\frac{n_{\rm n}}{n}\xi^-_i \ . \tag{4.208}$$

By substituting the above expressions into equation 4.180 we get

$$E_c = \frac{1}{2}\int \rho_{\rm n}x_{\rm p}\left\{|\partial_t\xi^-_i|^2 + |v^j\nabla_j\xi^-_i|^2 + \xi^i_-\xi^{j*}_-\nabla_i\nabla_j(\Phi+\tilde{\mu})\right\}dV \tag{4.209}$$

where $x_p = n_{\rm p}/n$ is the proton fraction. Since the expression in the bracket has the same form as in the single fluid case, and the prefactor $\rho_{\rm n}x_{\rm p}$ is positive definite, it is easy to prove that $E_c < 0$ also for the counter-moving modes.

4.7 Lagrangian perturbation theory with entrainment

The next step in our Lagrangian perturbation analysis is to consider the situation where the entrainment parameter α is non-zero. In the entrainment free case our neutron and proton equations are coupled chemically through the equation of state and gravitationally since variations in the number densities of one fluid affects the gravitational potential and hence affect the other fluid. The function α describes how the internal energy of the system depends on the relative velocities of the two fluids and introduces a much stronger coupling of the equations. The Euler equation with entrainment, equation (2.20) is,

$$\left(\partial_t + v_X^j \nabla_j\right)\left(v_i^X + \varepsilon_X w_i^{YX}\right) + \nabla_i\left(\Phi + \widetilde{\mu}_X\right) + \varepsilon_X w_j^{YX} \nabla_i v_X^j = 0 \tag{4.210}$$

Where $\varepsilon_X = 2\alpha/n_X$. Since we can write,

$$v_X^j \nabla_j\left(\varepsilon_X w_i^{YX}\right) = \pounds_{v_X}\left(\varepsilon_X w_i^{YX}\right) - \varepsilon_X w_j^{YX} \nabla_i v_X^j \tag{4.211}$$

we can write the Euler equations as

$$\left(\partial_t + \pounds_{v_X}\right)\left(v_i^X + \varepsilon_X w_i^{YX}\right) + \nabla_i\left(\Phi + \widetilde{\mu}_X - \frac{v_X^2}{2}\right) = 0 \tag{4.212}$$

To investigate Lagrangian perturbations of this system we take the same approach as in the entrainment free case and introduce two distinct Lagrangian displacement vectors, ξ_X^i. The continuity equations and the Poisson equation are not affected by entrainment and thus we can simply use equations (4.147) and (4.148) to describe the perturbations of the gravitational potential and the densities. Perturbing the Euler equations gives,

$$\left(\partial_t + \pounds_{v_X}\right)\left[\Delta_X v_i^X + \Delta_X\left(\varepsilon_X w_i^{YX}\right)\right] + \nabla_i\left(\Delta_X\Phi + \Delta_X\widetilde{\mu}_X - \frac{\Delta_X v_X^2}{2}\right) = 0 \tag{4.213}$$

We recognise the terms $\left(\partial_t + \pounds_{v_X}\right)\Delta_X v_i^X$ and $\nabla_i\left(\Delta_X\Phi + \Delta_X\widetilde{\mu}_X - \Delta_X v_X^2/2\right)$ from the entrainment free problem and can hence immediately write,

$$\begin{aligned}\left(\partial_t + \pounds_{v_X}\right)\Delta_X v_i^X &= \partial_t^2 \xi_i^X + v_X^j \nabla_j \partial_t \xi_i^X + v_X^j \nabla_i \partial_t \xi_j^X \\ &+ v_X^k \nabla_k\left(\Delta_X v_i^X\right) + \left(\Delta_X v_k^X\right)\nabla_i v_X^k\end{aligned} \tag{4.214}$$

and

$$\begin{aligned}\nabla_i\left(\Delta_X\Phi+\Delta_X\tilde{\mu}_X-\frac{\Delta_X v_X^2}{2}\right) &= -\partial_t\xi_X^j\nabla_i v_j^X-v_X^j\nabla_i\partial_t\xi_j^X\\ &- v_X^k\left(\nabla_k\xi_j^X+\nabla_j\xi_k^X\right)\nabla_i v_X^j\\ &- \left(v_X^j\nabla_j v_k^X\right)\nabla_i\xi_X^k-v_X^j v_X^k\nabla_j\nabla_i\xi_k^X\\ &+ \nabla_i\delta\Phi+\xi_X^j\nabla_i\nabla_j\left(\Phi+\tilde{\mu}_X\right)+\nabla_i\delta\tilde{\mu}_X\end{aligned} \tag{4.215}$$

In this case $\delta\tilde{\mu}_X$ depends on the entrainment. This is obvious from Section 2.2 where we observe that the chemical potential, μ_X, is simply a partial derivative of the energy functional, E, with respect to the corresponding number density, n_X. Since E depends on the entrainment the Eulerian variation in the chemical potential also depends on the entrainment. We can write it as follows,

$$\delta\tilde{\mu}_X=-\left(\frac{\partial\tilde{\mu}_X}{\partial n_X}\right)_{n_Y,w^2}\nabla_j\left(n_X\xi_X^j\right)-\left(\frac{\partial\tilde{\mu}_X}{\partial n_Y}\right)_{n_X,w^2}\nabla_j\left(n_X\xi_X^j\right)+\left(\frac{\partial\tilde{\mu}_X}{\partial w^2}\right)_{n_X,n_Y}\delta w^2 \tag{4.216}$$

where

$$\left(\frac{\partial\tilde{\mu}_X}{\partial w^2}\right)_{n_X,n_Y}=\frac{1}{m_{\mathrm{B}}}\left(\frac{\partial\alpha}{\partial n_X}\right)_{n_Y,w^2} \tag{4.217}$$

and

$$\delta w^2=w_j^{YX}\delta w_{YX}^j+w_{YX}^j\delta w_j^{YX}=2w_j^{YX}\delta w_{YX}^j \tag{4.218}$$

giving

$$\delta\tilde{\mu}_X=-\left(\frac{\partial\tilde{\mu}_X}{\partial n_X}\right)_{n_Y,w^2}\nabla_j\left(n_X\xi_X^j\right)-\left(\frac{\partial\tilde{\mu}_X}{\partial n_Y}\right)_{n_X,w^2}\nabla_j\left(n_Y\xi_Y^j\right)+\frac{2}{m_{\mathrm{B}}}A_X w_j^{YX}\delta w_{YX}^j \tag{4.219}$$

Where we have introduced

$$A_X=\left(\frac{\partial\alpha}{\partial n_X}\right)_{n_Y,w^2} \tag{4.220}$$

and where we can write,

$$\begin{aligned}\delta w_{YX}^j &= \delta v_Y^j-\delta v_X^j\\ &= \partial_t\xi_Y^j+v_Y^i\nabla_i\xi_Y^j-\xi_Y^i\nabla_i v_Y^j-\partial_t\xi_X^j-v_X^i\nabla_i\xi_X^j+\xi_X^i\nabla_i v_X^j\end{aligned} \tag{4.221}$$

The remaining term in equation (4.213), which was not present in the entrainment free problem, we can write as,

$$\left(\partial_t+\pounds_{v_X}\right)\Delta_X\left(\varepsilon_X w_i^{YX}\right)=\varepsilon_X\left(\partial_t+\pounds_{v_X}\right)\Delta_X w_i^{YX}+w_i^{YX}\left(\partial_t+\pounds_{v_X}\right)\Delta_X\varepsilon_X \tag{4.222}$$

We begin by looking at $(\partial_t + \pounds_{v_X})\,\Delta_X w_i^{YX}$

$$(\partial_t + \pounds_{v_X})\,\Delta_X w_i^{YX} = (\partial_t + \pounds_{v_X})\,\Delta_X v_i^{Y} - (\partial_t + \pounds_{v_X})\,\Delta_X v_i^{X} \tag{4.223}$$

Where,

$$\begin{aligned}
(\partial_t + \pounds_{v_X})\,\Delta_X v_i^X &= \partial_t^2 \xi_i^X + v_X^j \nabla_j \partial_t \xi_i^X + v_X^j \nabla_i \partial_t \xi_j^X \\
&+ v_X^k \nabla_k \left(\Delta_X v_i^X\right) + \left(\Delta_X v_k^X\right) \nabla_i v_X^k \\
\\
&= \partial_t^2 \xi_i^X + v_X^j \nabla_j \partial_t \xi_i^X + v_X^j \nabla_i \partial_t \xi_j^X + v_X^k \nabla_k \partial_t \xi_i^X \\
&+ v_X^k \nabla_k (v_X^j \nabla_j \xi_i^X) + v_X^k \nabla_k (v_X^j \nabla_i \xi_j^X) + \partial_t \xi_k^X \nabla_i v_X^k \\
&+ (v_X^j \nabla_j \xi_k^X) \nabla_i v_X^k + \left(v_X^j \nabla_k \xi_j^X\right) \nabla_i v_X^k \\
\\
&= \partial_t^2 \xi_i^X + 2 v_X^j \nabla_j \partial_t \xi_i^X + v_X^j \nabla_i \partial_t \xi_j^X + (v_X^j \nabla_j)^2 \xi_i^X \\
&+ \partial_t \xi_k^X \nabla_i v_X^k + v_X^j \left(\nabla_j \xi_k^X + \nabla_k \xi_j^X\right) \nabla_i v_X^k + (v_X^k \nabla_k v_X^j) \nabla_i \xi_j^X \\
&+ v_X^k v_X^j \nabla_k \nabla_i \xi_j^X
\end{aligned} \tag{4.224}$$

and,

$$
\begin{aligned}
\left(\partial_t + \pounds_{v_X}\right)\Delta_X v_i^Y &= \partial_t^2\xi_i^Y + v_Y^j\nabla_j\partial_t\xi_i^Y - \partial_t\xi_j^Y\nabla_j v_i^Y + \partial_t\xi_j^X\nabla_j v_i^Y + v_Y^j\nabla_i\partial_t\xi_j^X \\
&+ v_X^k\nabla_k\left[\partial_t\xi_i^Y + v_Y^j\nabla_j\xi_i^Y + v_Y^j\nabla_i\xi_j^Y - \xi_Y^j\nabla_j v_i^Y + \xi_X^j\nabla_j v_i^Y\right] \\
&+ \left[\partial_t\xi_k^Y + v_Y^j\nabla_j\xi_k^Y + v_Y^j\nabla_k\xi_j^Y - \xi_Y^j\nabla_j v_k^Y + \xi_X^j\nabla_j v_k^Y\right]\nabla_i v_X^k \\
&= \partial_t^2\xi_i^Y + \left(v_Y^j + v_X^j\right)\nabla_j\partial_t\xi_i^Y + \partial_t\xi_Y^j\left[\nabla_i v_j^X - \nabla_j v_i^Y\right] \\
&+ \partial_t\xi_j^X\nabla_j v_i^Y + v_Y^j\nabla_i\partial_t\xi_j^X + v_X^k v_X^j\nabla_k\nabla_j\xi_i^Y \\
&+ \left(v_X^k\nabla_k v_Y^j\right)\nabla_j\xi_i^Y - v_X^k\xi_Y^j\nabla_k\nabla_j v_i^Y - \left(v_X^k\nabla_k\xi_Y^j\right)\nabla_j v_i^Y \\
&+ v_X^k\xi_X^j\nabla_k\nabla_j v_i^Y + \left(v_X^k\nabla_k\xi_X^j\right)\nabla_j v_i^Y + v_X^k v_Y^j\nabla_k\nabla_i\xi_j^X \\
&+ \left(v_X^k\nabla_k\xi_Y^j\right)\nabla_i\xi_j^X + \left(v_Y^j\nabla_j\xi_k^Y\right)\nabla_i v_X^k - \left(\xi_Y^j\nabla_j v_k^Y\right)\nabla_i v_X^k \\
&+ \left(\xi_X^j\nabla_j v_k^Y\right)\nabla_i v_X^k + \left(v_Y^j\nabla_k\xi_j^X\right)\nabla_i v_X^k \\
&= \partial_t^2\xi_i^Y + \left(v_Y^j + v_X^j\right)\nabla_j\partial_t\xi_i^Y + \partial_t\xi_Y^j\left[\nabla_i v_j^X - \nabla_j v_i^Y\right] \\
&+ \partial_t\xi_j^X\nabla_j v_i^Y + v_Y^j\nabla_i\partial_t\xi_j^X + \left(\xi_X^j - \xi_Y^j\right)v_X^k\nabla_k\nabla_j v_i^Y \\
&+ \left[v_X^k\nabla_k\left(\xi_X^j - \xi_Y^j\right)\right]\nabla_j v_i^Y + \left(v_X^k\nabla_k v_Y^j\right)\left[\nabla_j\xi_i^Y + \nabla_i\xi_j^X\right] \\
&+ v_X^k v_Y^j\nabla_k\nabla_j\xi_i^Y + v_X^k v_Y^j\nabla_k\nabla_i\xi_j^X + \left(v_Y^j\nabla_j\xi_k^Y\right)\nabla_i v_X^k \\
&+ \left(v_Y^j\nabla_i v_X^k\right)\nabla_k\xi_j^X + \left(\xi_X^j - \xi_Y^j\right)\left(\nabla_j v_k^Y\right)\left(\nabla_i v_X^k\right) \qquad (4.225)
\end{aligned}
$$

We can define $\psi_{XY}^j = \xi_X^j - \xi_Y^j$ giving

$$
\begin{aligned}
\left(\partial_t + \pounds_{v_X}\right)\Delta_X v_i^Y &= \partial_t^2\xi_i^Y + (v_Y^j + v_X^j)\nabla_j\partial_t\xi_i^Y + \partial_t\xi_Y^j\left[\nabla_i v_j^X - \nabla_j v_i^Y\right] \\
&+ \partial_t\xi_j^X\nabla_j v_i^Y + v_Y^j\nabla_i\partial_t\xi_j^X + \psi_{XY}^j v_X^k\nabla_k\nabla_j v_i^Y \\
&+ \left[v_X^k\nabla_k\left(\psi_{XY}^j\right)\right]\nabla_j v_i^Y + \left(v_X^k\nabla_k v_Y^j\right)\left[\nabla_j\xi_i^Y + \nabla_i\xi_j^X\right] \\
&+ v_X^k v_Y^j\nabla_k\nabla_j\xi_i^Y + v_X^k v_Y^j\nabla_k\nabla_i\xi_j^X + \left(v_Y^j\nabla_j\xi_k^Y\right)\nabla_i v_X^k \\
&+ \left(v_Y^j\nabla_i v_X^k\right)\nabla_k\xi_j^X + \psi_{XY}^j\left(\nabla_j v_k^Y\right)\left(\nabla_i v_X^k\right) \qquad (4.226)
\end{aligned}
$$

Combining equations (4.224) and (4.226) gives,

$$
\begin{aligned}
\left(\partial_t + \pounds_{v_X}\right)\Delta_X w_i^{YX} &= \left(\partial_t + \pounds_{v_X}\right)\Delta_X v_i^Y - \left(\partial_t + \pounds_{v_X}\right)\Delta_X v_i^X \\
&= -\left[\partial_t^2 \xi_i^X + 2v_X^j \nabla_j \partial_t \xi_i^X + \left(v_X^j \nabla_j\right)^2 \xi_i^X\right] \\
&+ \left[\partial_t^2 \xi_i^Y + 2v_Y^j \nabla_j \partial_t \xi_i^Y + (v_Y^j \nabla_j)^2 \xi_i^Y\right] \\
&+ \left(v_X^j - v_Y^j\right)\nabla_j \partial_t \xi_t^Y - \left[\partial_t \xi_k^X (\nabla_i v_X^k) + v_X^j \nabla_i \partial_t \xi_j^X\right. \\
&+ v_X^j \left(\nabla_j \xi_k^X + \nabla_k \xi_j^X\right)\nabla_i v_X^k + \left(v_X^k \nabla_k v_X^j\right)\nabla_i \xi_j^X \\
&+ \left.v_X^k v_X^j \nabla_k \nabla_i \xi_j^X\right] + \partial_t \xi_Y^j \left[\nabla_i v_j^X - \nabla_j v_i^Y\right] + \partial_t \xi_X^j \nabla_j v_i^Y \\
&+ v_Y^j \nabla_i \partial_t \xi_j^X + \psi_{XY}^j v_X^k \nabla_k \nabla_j v_i^Y + \left(v_X^k \nabla_k \psi_X Y^j\right)\nabla_j v_i^Y \\
&+ \left(v_X^k \nabla^k v_Y^j\right)\nabla_i \xi_j^X + v_X^k v_Y^j \nabla_k \nabla_i \xi_j^X + \left(v_Y^j \nabla_j \xi_k^Y\right)\nabla_i v_X^k \\
&+ \left(v_Y^j \nabla_i v_X^k\right)\nabla_k \xi_j^X + \left(\psi_{XY}^j \nabla_j v_k^Y\right)\nabla_i v_X^k \\
&= -\left[\partial_t^2 \xi_i^X + 2v_X^j \nabla_j \partial_t \xi_i^X + (v_X^j \nabla_j)^2 \xi_i^X\right] \\
&+ \left[\partial_t^2 \xi_i^Y + 2v_Y^j \nabla_j \partial_t \xi_i^Y + (v_Y^j \nabla_j)^2 \xi_i^Y\right] \\
&+ \left(\partial_t \xi_X^j - \partial_t \xi_Y^j\right)\left(\nabla_j v_i^Y - \nabla_i v_j^X\right) + w_{YX}^j \left[\nabla_i \partial_t \xi_j^X - \nabla_j \partial_t \xi_i^Y\right] \\
&+ \psi_{XY}^j v_X^k \nabla_k \nabla_j v_i^Y - \left(v_X^j \nabla_i v_X^k + v_X^k \nabla_i v_X^j\right)\nabla_j \xi_k^X \\
&+ \left(v_Y^j \nabla_i v_X^k\right)\left(\nabla_j \xi_k^Y + \nabla_k \xi_j^X\right) + \left(\psi_{XY}^j \nabla_j v_k^Y\right)\nabla_i v_X^k \\
&+ \left(v_X^k \nabla_k \psi_{XY}^j\right)\nabla_j v_i^Y + \left[v_X^k \nabla_k v_Y^j - v_X^k \nabla_k v_X^j\right]\nabla_i \xi_j^X \\
&+ v_X^k w_{YX}^j \nabla_k \nabla_i \xi_j^X - \nabla_k \left(v_Y^j \nabla_j \xi_i^Y\right) \qquad (4.227)
\end{aligned}
$$

Where we have used the fact that

$$
v_X^k \nabla_k \left(v_y^j \nabla_j \xi_i^Y\right) = \left(v_Y^j \nabla_j\right)^2 \xi_i^Y + \left(v_X^k - v_Y^k\right)\nabla_k \left(v_Y^j \nabla_j \xi_i^Y\right) \qquad (4.228)
$$

To investigate the second term in equation (4.222), $\left(\partial_t + \pounds_{v_X}\right)\Delta_X \varepsilon_X$, we begin by looking at $\Delta_X \varepsilon_X$.

$$
\Delta_X \varepsilon_X = \delta \varepsilon_X + \xi_X^j \nabla_j \varepsilon_X \qquad (4.229)
$$

Using the definition for ε_X, equation (2.18), we find,

$$
\begin{aligned}
\Delta_X \varepsilon_X &= \delta\left(\frac{2\alpha}{n_X}\right) + \xi_X^j \nabla_j \left(\frac{2\alpha}{n_X}\right) \\
&= \frac{2}{n_X}\delta\alpha - \frac{2\alpha}{n_X^2}\delta n_X + \frac{2}{n_X}\xi_X^j \nabla_j \alpha - \frac{2\alpha}{n_X^2}\xi_X^j \nabla_j n_X
\end{aligned}
$$

We can use the perturbed continuity equation, $\delta n_X = -\nabla_i \left(n_X \xi_X^i\right)$, to give,

$$\begin{aligned}
\Delta_X \varepsilon_X &= \frac{2}{n_X}\delta\alpha + \frac{2\alpha}{n_X^2}\nabla_i\left(n_X\xi_X^i\right) + \frac{2}{n_X}\xi_X^j\nabla_j\alpha - \frac{2\alpha}{n_X^2}\xi_X^j\nabla_j n_X \\
&= \frac{2}{n_X}\delta\alpha + \frac{2\alpha}{n_X^2}\left[n_X\nabla_i\xi_X^i + \xi_X^i\nabla_i n_X - \xi_X^i\nabla_i n_X\right] + \frac{2}{n_X}\xi_X^j\nabla_j\alpha \\
&= \frac{2}{n_X}\delta\alpha + \frac{2}{n_X}\left[\alpha\nabla_i\xi_X^i + \xi_X^i\nabla_i\alpha\right] \\
&= \frac{2}{n_X}\delta\alpha + \frac{2}{n_X}\nabla_i\left(\alpha\xi_X^i\right) \qquad (4.230)
\end{aligned}$$

The entrainment function, α is a function of n_X, n_Y, and w^2 i.e $\alpha = \alpha(n_X, n_Y, w^2)$ and hence,

$$\delta\alpha = A_X\delta n_X + A_Y\delta n_Y + 2A_w w_j^{YX}\delta w_{YX}^j \qquad (4.231)$$

where once again A_X is given by equation (4.220) and we define

$$A_w = \left(\frac{\partial\alpha}{\partial w^2}\right)_{n_X,n_Y} \qquad (4.232)$$

Since

$$\delta w_{YX}^j = \delta v_Y^j - \delta v_X^j \qquad (4.233)$$

where

$$\delta v_X^j = \partial_i\xi_X^j + v_X^i\nabla_i\xi_X^j - \xi_X^i\nabla_i v_X^j \qquad (4.234)$$

we can write $\delta\alpha$ as,

$$\begin{aligned}
\delta\alpha &= -A_X\nabla_i\left(n_X\xi_X^i\right) - A_Y\nabla_i\left(n_Y\xi_Y^i\right) \\
&+ 2A_w w_j^{YX}\left[\partial_i\xi_Y^j - \partial_i\xi_X^j + v_Y^i\nabla_i\xi_Y^j - v_X^i\nabla_i\xi_X^j - \xi_Y^i\nabla_i v_Y^j + \xi_X^i\nabla_i v_X^j\right] \qquad (4.235)
\end{aligned}$$

and consequently

$$\begin{aligned}
\Delta_X\varepsilon_X &= \frac{2}{n_X}[-A_X\nabla_i\left(n_X\xi_X^i\right) - A_Y\nabla_i\left(n_Y\xi_Y^i\right) + \nabla_i\left(\alpha\xi_X^i\right) \\
&+ 2A_w w_j^{YX}\left(\partial_i\psi_{YX}^j - \partial_i\xi_X^j + v_Y^i\nabla_i\xi_Y^j - v_X^i\nabla_i\xi_X^j + \psi_{XY}^i\nabla_i v_Y^j + \xi_X^i\nabla_i v_X^j\right)] \\
&= \frac{2}{n_X}\Big\{\left(\alpha - A_X n_X\right)\nabla_i\xi_X^i + \xi_X^i\nabla_i\alpha - A_X\xi_X^i\nabla_i n_X \\
&- A_Y\left[n_Y\nabla_i\xi_Y^i + \xi_Y^i\nabla_i n_Y\right] + 2A_w w_j^{YX}\xi_X^i\nabla_i w_{YX}^j \\
&+ 2A_w w_j^{YX}\left[\psi_{XY}^i\nabla_i v_Y^j - \partial_i\psi_{XY}^j + v_Y^i\nabla_i\xi_Y^j - v_X^i\nabla_i\xi_X^j\right]\Big\} \qquad (4.236)
\end{aligned}$$

Using the substitution

$$\nabla_i \alpha = A_X \nabla_i n_X + A_Y \nabla_i n_Y + 2A_w w_j^{YX} \nabla_i w_{YX}^j \tag{4.237}$$

gives,

$$\begin{aligned} \Delta_X \varepsilon_X &= \frac{2}{n_X}\Big\{ A_Y \left[\psi_{XY}^i \nabla_i n_Y - n_Y \nabla_i \xi_Y^i\right] + (\alpha - A_X n_X)\nabla_i \xi_X^i \\ &+ 2A_w w_j^{YX}\left[\psi_{XY}^i \nabla_i v_Y^j - \partial_t \psi_{XY}^j + v_Y^i \nabla_i \xi_Y^j - v_X^i \nabla_i \xi_X^j\right]\Big\} \end{aligned} \tag{4.238}$$

Finally,

$$\begin{aligned} (\partial_t + \pounds_{v_X})\Delta_X \varepsilon_X &= \frac{2}{n_X}\Big\{ A_Y \left[\partial_t \psi_{XY}^i \nabla_i n_Y - n_Y \nabla_i \partial_t \xi_Y^i\right] + (\alpha - A_X n_X)\nabla_i \partial_t \xi_X^i \\ &+ 2A_w w_j^{YX}\left[\partial_t \psi_{XY}^i \nabla_i v_Y^j - \partial_t^2 \psi_{XY}^j + v_Y^i \nabla_i \partial_t \xi_Y^j - v_X^i \nabla_i \partial_t \xi_X^j\right]\Big\} \\ &+ v_X^k \nabla_k \left[-\frac{4}{n_X} A_w w_j^{YX} \partial_t \psi_{XY}^j\right] \\ &+ v_X^k \nabla_k \left[\frac{2}{n_X}\Big\{ A_Y \left[\psi_{XY}^i \nabla_i n_Y - n_Y \nabla_i \xi_Y^i\right] + (\alpha - A_X n_X)\nabla_i \xi_X^i \right. \\ &+ \left. 2A_w w_j^{YX}\left(\psi_{XY}^i \nabla_i v_Y^j \partial_t \psi_{XY}^j + v_Y^i \nabla_i \xi_Y^j - v_X^i \nabla_i \xi_X^j\right)\Big\}\right] \end{aligned} \tag{4.240}$$

Consider for a moment simply the term $v_x^k \nabla_k \left[-4A_w w_j^{YX} \partial_t \psi_{XY}^j / n_X\right]$. We can write this as,

$$\begin{aligned} v_x^k \nabla_k \left[-\frac{4}{n_X} A_w w_j^{YX} \partial_t \psi_{XY}^j\right] &= -\frac{2}{n_X}\Big\{ 2A_w w_j^{YX} v_X^k \nabla_k \partial_t \psi_{XY}^j \\ &+ 2A_w \partial_t \psi_{XY}^j v_X^k \nabla_k w_j^{YX}\Big\} \\ &- w_j^{YX} \partial_t \psi_{XY}^j v_X^k \nabla_k \left(\frac{4A_w}{n_X}\right) \end{aligned} \tag{4.241}$$

If we assume the system is axisymmetric the final term in the above equation vanishes. Giving,

$$v_x^k \nabla_k \left[-\frac{4}{n_X} A_w w_j^{YX} \partial_t \psi_{XY}^j\right] = -\frac{2}{n_X}\left\{ 2A_w w_j^{YX} v_X^k \nabla_k \partial_t \psi_{XY}^j + 2A_w \partial_t \psi_{XY}^j v_X^k \nabla_k w_j^{YX}\right\} \tag{4.242}$$

Similarly

$$v_X^k \nabla_k \Big\{ \frac{2}{n_X} \left(\alpha - A_X n_X \right) \nabla_i \xi_X^i \Big\} \;=\; \frac{2}{n_X} \left(\alpha - n_X A_X \right) v_X^k \nabla_k \nabla_i \xi_X^i \quad (4.243)$$

where we have used the fact that in an axisymmetric system,

$$\begin{aligned} v_X^k \nabla_k \alpha &= A_X v_X^k \nabla_k n_X + A_Y v_X^k \nabla_k + 2 A_w w_j^{YX} v_X^k \nabla_k w_{YX}^j \\ &= 0 \end{aligned} \quad (4.244)$$

We can also write

$$\begin{aligned} v_X^k \nabla_k \Big\{ \frac{2}{n_X} A_Y \left[\psi_{XY}^i \nabla_i n_Y - n_Y \nabla_i \xi_Y^i \right] \Big\} = \frac{2}{n_X} \Big\{ A_Y \big\{ \psi_{XY}^i v_X^k \nabla_k \nabla_i n_Y \\ + \left(\nabla_i n_Y \right) v_X^k \nabla_k \psi_{XY}^i - n_Y v_X^k \nabla_k \nabla_i \xi_Y^i \big\} \Big\} \end{aligned} \quad (4.245)$$

The final term in equation (4.239) becomes,

$$\begin{aligned} & v_X^k \nabla_k \Big\{ \frac{2}{n_X} \left[2 A_w w_j^{YX} \left(\psi_{XY}^i \nabla_i v_Y^j \partial_t \psi_{XY}^j + v_Y^i \nabla_i \xi_Y^j - v_X^i \nabla_i \xi_X^j \right) \right] \Big\} \\ = \; & 2 A_w \big\{ \psi_{XY}^i v_X^k \nabla_k \left(w_j^{YX} \nabla_i v_Y^j \right) + \left(w_j^{YX} \nabla_i v_Y^j \right) v_X^k \nabla_k \psi_{XY}^i \\ + \; & \left(v_X^k \nabla_k w_j^{YX} \right) \left(v_Y^i \nabla_i \xi_Y^j - v_X^i \nabla_i \xi_X^j \right) + w_j^{YX} w_j^{YX} v_X^k \nabla_k \left(v_Y^i \nabla_i \xi_Y^j - v_X^i \nabla_i \xi_X^j \right) \\ = \; & 2 A_w \big\{ \psi_{XY}^i v_X^k \nabla_k \left(w_j^{YX} \nabla_i v_Y^j \right) - \left(v_Y^j \nabla_j w_i^{YX} \right) v_X^k \nabla_k \psi_{XY}^i \\ + \; & \left(v_X^k \nabla_k w_j^{YX} \right) \left(v_Y^i \nabla_i \xi_Y^j - v_X^i \nabla_i \xi_X^j \right) + w_j^{YX} w_j^{YX} v_X^k \nabla_k \left(v_Y^i \nabla_i \xi_Y^j - v_X^i \nabla_i \xi_X^j \right) \end{aligned} \quad (4.246)$$

In our system we are assuming the background is axisymmetric and hence we can write,

$$v_X^i = \Omega_X \varphi^i \quad (4.247)$$

and

$$w_{YX}^i = \left(\Omega_Y - \Omega_X \right) \varphi^i \quad (4.248)$$

with φ^i given by

$$\varphi^i \partial_i = \partial_\varphi \quad (4.249)$$

Therefore we find,

$$w_j^{YX} \nabla_i v_Y^j = \Omega_Y \left(\Omega_Y - \Omega_X \right) \varphi^j \nabla_i \varphi_j = -\Omega_Y \left(\Omega_Y - \Omega_X \right) \varphi^j \nabla_j \varphi_i = -v_Y^j \nabla_j w_i^{YX} \quad (4.250)$$

Thus,

$$
\begin{aligned}
\left(\partial_t + \pounds_{v_X}\right)\Delta_X\varepsilon_X &= -\frac{4}{n_X}A_w w_j^{YX}\partial_t^2\psi_{XY}^j + \frac{2}{n_X}\Big\{\left(\alpha - n_X A_X\right)\nabla_i\partial_t\xi_X^i \\
&- n_Y A_Y\nabla_i\partial_t\xi_Y^i + 2A_w w_j^{YX}\left(v_X^i + v_Y^i\right)\nabla_i\partial_t\xi_Y^j \\
&- 4A_w w_j^{YX}v_X^i\nabla_i\partial_t\xi_X^j \\
&+ \left[A_Y\nabla_k n_Y + 2A_w\left(w_j^{YX}\nabla_k v_Y^j - v_X^i\nabla_i\right)\right]\partial_t\psi_{XY}^k \\
&+ \left(\alpha - n_X A_X\right)v_X^k\nabla_k\nabla_i\xi_X^i \\
&+ A_Y\left\{\psi_{XY}^i v_X^k\nabla_k\nabla_i n_Y + \left(\nabla_i n_Y\right)v_X^k\nabla_k\psi_{XY}^i - n_Y v_X^k\nabla_k\nabla_i\xi_Y^i\right\} \\
&+ 2A_w\left\{\psi_{XY}^i v_X^k\nabla_k\left(w_j^{YX}\nabla_i v_Y^j\right) - \left(v_Y^j\nabla_j w_i^{YX}\right)v_X^k\nabla_k\psi_{XY}^i\right. \\
&+ \left(v_X^k\nabla_k w_j^{YX}\right)\left(v_Y^i\nabla_i\xi_Y^j - v_X^i\nabla_i\xi_X^j\right) \\
&+ \left.w_j^{YX}v_X^k\nabla_k\left(v_Y^i\nabla_i\xi_Y^j - v_X^i\nabla_i\xi_X^j\right)\right\}\Big\} \qquad (4.251)
\end{aligned}
$$

We can combine everything in a schematic way to give us

$$\mathcal{A}_X\partial_t^2\xi_i^X + B_X\partial_t\xi_i^X + C_X\xi_i^X + D_X\xi_i^Y + E_X(\xi_i^X, \xi_i^Y) = 0 \qquad (4.252)$$

It is important to note that $\mathcal{A}_X$ is an operator and should not be confused with A_X. The Operators $\mathcal{A}$, B, C and D are identical to those in the entrainment free problem where D couples the neutron and proton systems through the equation of state. The operator E is highly complicated, consisting of a combination of equations (4.219), (4.227), and (4.251). It depends explicitly on both α and w_j^{YX} and acts on both the neutron and proton displacement vectors as well as their first and second time derivatives.

It is clear that introducing an entrainment term substantially complicates the resulting perturbation equations. It would be highly constructive to continue from this point to derive a canonical energy equation for this general two-fluid system. In doing so we can hope to develop stability criteria for superfluid neutron stars. This analysis will hopefully be the focus of future work.

In this work we will study oscillations of a simple test problem with $\alpha = constant$. This simplifies the Lagrangian perturbation equations greatly since, as we see from equations 4.220 and 4.232,

$$A_X = A_w = 0 \qquad (4.253)$$

In this simplified case the perturbation equations can be written as,

$$
\begin{aligned}
& \partial_t^2 \xi_i^X + v_X^j \nabla_j \partial_t \xi_i^X + v_X^j \nabla_i \partial_t \xi_j^X + v_X^k \nabla_k \left(\Delta_X v_i^X \right) + \left(\Delta_X v_k^X \right) \nabla_i v_X^k \\
+ \; & \frac{2\alpha}{n_X} \Big\{ - \left[\partial_t^2 \xi_i^X + 2 v_X^j \nabla_j \partial_t \xi_i^X + (v_X^j \nabla_j)^2 \xi_i^X \right] + \left[\partial_t^2 \xi_i^Y + 2 v_Y^j \nabla_j \partial_t \xi_i^Y \right. \\
+ \; & \left. (v_Y^j \nabla_j)^2 \xi_i^Y \right] + \left(\partial_t \xi_X^j - \partial_t \xi_Y^j \right) \left(\nabla_j v_i^Y - \nabla_i v_j^X \right) w_{YX}^j \left[\nabla_i \partial_t \xi_j^X - \nabla_j \partial_t \xi_i^Y \right] \\
+ \; & \psi_{XY}^j v_X^k \nabla_k \nabla_j v_i^Y - \left(v_X^j \nabla_i v_X^k + v_X^k \nabla_i v_X^j \right) \nabla_j \xi_k^X + \left(v_Y^j \nabla_i v_X^k \right) \left(\nabla_j \xi_k^Y + \nabla_k \xi_j^X \right) \\
+ \; & \left(\psi_{XY}^j \nabla_j v_k^Y \right) \nabla_i v_X^k + \left(v_X^k \nabla_k \psi_{XY}^j \right) \nabla_j v_i^Y + \left[v_X^k \nabla_k v_Y^j - v_X^k \nabla_k v_X^j \right] \nabla_i \xi_j^X \\
+ \; & v_X^k w_{YX}^j \nabla_k \nabla_i \xi_j^X - \nabla_k \left(v_Y^j \nabla_j \xi_i^Y \right) \Big\} + w_i^{YX} \left\{ \frac{2\alpha}{n_X} \left(\nabla_i \partial_t \xi_X^i + v_X^k \nabla_k \nabla_i \xi_X^i \right) \right\} \\
- \; & \partial_t \xi_X^j \nabla_i v_j^X - v_X^j \nabla_i \partial_t \xi_j^X - v_X^k \left(\nabla_k \xi_j^X + \nabla_j \xi_k^X \right) \nabla_i v_X^j - \left(v_X^j \nabla_j v_k^X \right) \nabla_i \xi_X^k \\
- \; & v_X^j v_X^k \nabla_j \nabla_i \xi_k^X + \nabla_i \delta\Phi + \xi_X^j \nabla_i \nabla_j \left(\Phi + \tilde{\mu}_X \right) + \nabla_i \delta\tilde{\mu}_X = 0
\end{aligned}
\tag{4.254}
$$

where

$$
\delta\tilde{\mu}_X = - \left(\frac{\partial \tilde{\mu}_X}{\partial n_X} \right)_{n_Y, w^2} \nabla_j \left(n_X \xi_X^j \right) - \left(\frac{\partial \tilde{\mu}_X}{\partial n_Y} \right)_{n_X, w^2} \nabla_j \left(n_Y \xi_Y^j \right) \tag{4.255}
$$

Chapter 5

The oscillations and stability of superfluid cylinders: the entrainment free case

Having constructed Lagrangian perturbation equations in Chapter 4 we have reached a point where we can use this framework to study the modes of oscillation for a cylinder of superfluid. We begin with the case of vanishing entrainment, i.e. $\alpha = 0$. This involves expressing equation (4.156) in cylindrical coordinates, establishing appropriate boundary conditions and subsequently solving the equations numerically.

5.1 The equations

We proceed by assuming; (i) the time and azimuthal dependence of the perturbation is given by $\exp(i\omega t + im\phi)$, where ω is the oscillation frequency and m is the integer wave-number; (ii) both fluids exhibit uniform rotation about the z-axis such that, $v_X^i = \Omega_X \varphi^i$; (iii) the fluids obey an energy functional of the form equation (3.28); and finally assuming (iv) the Cowling approximation can be taken, i.e. $\delta\Phi = 0$. Using Table 3.2 and the substitution, $\xi_\phi = -ir_0 m\bar{\xi}_\phi$, the variables in these equations are scaled giving the following four equations (the bars have been dropped to avoid the equations becoming cluttered),

$$\frac{\partial \xi_r^X}{\partial r}\left[\left(\frac{\partial \mu_X}{\partial n_X}\right)_{n_Y,w^2} m\rho_X r^2\right] + \xi_r^X\left[\left(\frac{\partial \mu_X}{\partial n_X}\right)_{n_Y,w^2} mr\left(\rho_X + r\frac{\partial \rho_X}{\partial r}\right) - 2\Omega_X\sigma_X r^3\right]$$
$$+ \quad \xi_\phi^X\left[\left(\frac{\partial \mu_X}{\partial n_X}\right)_{n_Y,w^2} m^3\rho_X - m\sigma_X^2 r^2\right] = 0 \tag{5.1}$$

and

$$\frac{\partial^2 \xi_r^X}{\partial r^2}\left[\left(\frac{\partial \mu_X}{\partial n_X}\right)_{n_Y,w^2} r^3 \rho_X\right] + \frac{\partial \xi_r^X}{\partial r}\left[\left(\frac{\partial \mu_X}{\partial n_X}\right)_{n_Y,w^2} r^2\left(\rho_X + 2r\frac{\partial \rho_X}{\partial r}\right)\right]$$
$$+ \frac{\partial \xi_\phi^X}{\partial r}\left[\left(\frac{\partial \mu_X}{\partial n_X}\right)_{n_Y,w^2} m^2 \rho_X r\right]$$
$$+ \xi_r^X\left[\left(\frac{\partial \mu_X}{\partial n_X}\right)_{n_Y,w^2} r\left(r^2\frac{\partial^2 \rho_X}{\partial r^2} + r\frac{\partial \rho_X}{\partial r} - \rho_X\right) + \sigma_X^2 r^3\right]$$
$$+ \xi_\phi^X\left[\left(\frac{\partial \mu_X}{\partial n_X}\right)_{n_Y,w^2} m^2\left(r\frac{\partial \rho_X}{\partial r} - 2\rho_X\right) + 2m\Omega_X\sigma_X\, r^2\right] = 0 \qquad (5.2)$$

Where $\sigma_X = \omega + m\Omega_X$ and once again X and Y are the constituent indices which can represent either the neutrons or the protons. When X represents the neutrons, Y represents the protons and vice versa.

To find solutions to these equations numerically we express them as four first order equations. Equation (5.1) is already first order and to make equation (5.2) first order involves solving Equation (5.1) for $\partial\xi_r/\partial r$, differentiating to obtain an expression for $\partial^2\xi_r/\partial r^2$ and finally substituting these into equation (5.2). This results in,

$$\frac{\partial \xi_\phi^X}{\partial r}\left[m^2\left(\frac{\partial \mu_X}{\partial n_X}\right)_{n_Y,w^2}\sigma_X\rho_X r\right] + \xi_\phi^X\left[2m\Omega_X\sigma_X^2 r\right]$$
$$+ \xi_r^X\left[m\left(\frac{\partial \mu_X}{\partial n_X}\right)_{n_Y,w^2}\left(m\sigma_X\rho_X - 2\Omega_X r\frac{\partial \rho_X}{\partial r}\right) + 4\Omega_X^2\sigma_X r^2\right] = 0 \qquad (5.3)$$

Where we have used the fact that the background gravitational potential can be written as,

$$\Phi = \frac{1}{2}r^2\Omega_X^2 - \tilde{\mu}_X + \text{Constant} \qquad (5.4)$$

Equations (5.1) and (5.3) give us four first order differential equations representing the perturbations to our two fluid system. In analogy with the entrainment free Eulerian perturbation case we find that the neutron and proton systems are coupled only through the background gravitational potential. There will be an independent set of normal modes for the neutron superfluid and a second set for the proton fluid. Only in the co-rotating case will the mode frequencies be the same. If we introduce a relative rotation, modes will be either purely neutron or purely proton. One fluid will oscillate while the other remains stationary. If we considered non-zero perturbations to the gravitational potential, e.g. $\delta\Phi \neq 0$, we would find that a coupling exists between the equations in this entrainment free case.

5.2 A local analysis

Our objective is to study the influence of different relative rotation rates of the two fluids and varying K on the normal modes of superfluid cylinders. As a starting point we classify the modes by using a local analysis to construct propagation diagrams. We assume the modes take the following form,

$$\xi_r = \frac{1}{r}\xi_{rk}\exp(ikr) \tag{5.5}$$

$$\xi_\phi = \xi_{\phi k}\exp(ikr) \tag{5.6}$$

Substituting these into equations (5.1) and (5.3) leads to the following dispersion relation,

$$\begin{aligned}&\left(\frac{\partial\mu_X}{\partial n_X}\right)\sigma_X\rho_X r^2k^2 - i\left(\frac{\partial\mu_X}{\partial n_X}\right)\sigma_X\rho_X' r^2k + m^2\left(\frac{\partial\mu_X}{\partial n_X}\right)\sigma_X\rho_X - \sigma_X^3 r^2 \\ -\ &2m\left(\frac{\partial\mu_X}{\partial n_X}\right)\Omega_X\rho_X' r + 4\Omega_X^2\sigma_X r^2 = 0\end{aligned} \tag{5.7}$$

For propagating waves to exist k must have a real part and hence the condition for propagation is

$$\begin{aligned}&4\rho_X r^2\sigma_X^4 - \left[\left(\frac{\partial\mu_X}{\partial n_X}\right)(\rho_X')^2 r^2 + 16\Omega_X^2\rho_X r^2 + 4m^2\left(\frac{\partial\mu_X}{\partial n_X}\right)\rho_X^2\right]\sigma_X^2 \\ +\ &8m\left(\frac{\partial\mu_X}{\partial n_X}\right)\Omega_X\rho_X\rho_X' r\sigma_X > 0\end{aligned} \tag{5.8}$$

This is equivalent to equation (4.44), the condition for propagation in the single fluid, isentropic case. In this two fluid example we find distinct regions of propagation for the neutron modes and separate regions for the proton modes. The effect of one fluid on the propagation regions of the other occurs only through the coupling of the background densities through the gravitational potential. Only in the co-rotating case, where the neutrons and protons are rotating at the same velocity do these regions coincide. When both the fluids are stationary two regions of acoustic wave propagation are found, see Figure 5.1. These regions are symmetric with respect to $\omega = 0$. The direction of propagation depends on the sign of ω, waves with opposite signs propagate in opposite directions. When $\omega < 0$ the waves move forward and are consequently designated the label (f) in the Figure. Those for which $\omega > 0$ are labelled (b) as they move in the backward direction with respect to the pattern speed of the mode. In addition to the p modes which propagate in the acoustic regions we find, for both positive and negative frequencies, an f mode lying just outside. These modes do not originate from propagating body waves which is why they are situated outside the propagation areas.

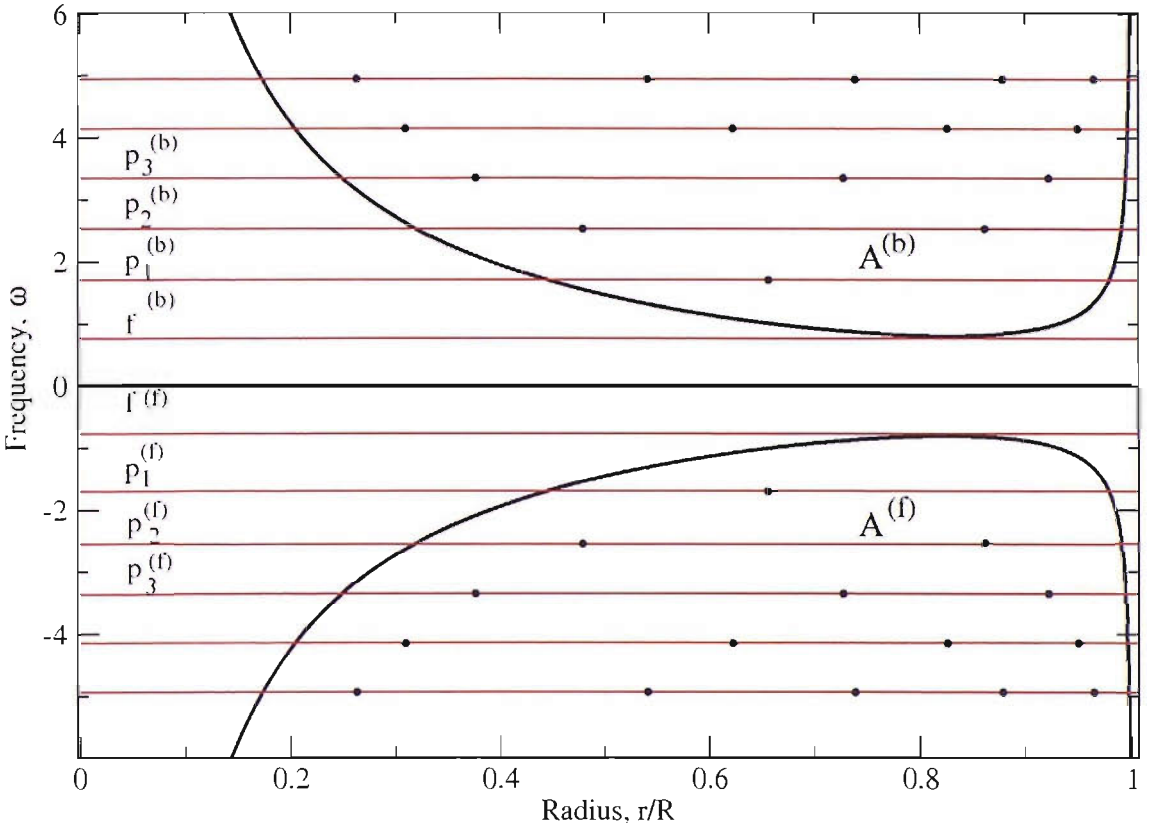

Figure 5.1: *The graph shows the regions of propagation for two non-rotating fluids in a cylinder. We observe two regions of acoustic wave propagation which are symmetric with respect to* $\omega = 0$. *The direction of propagation depends on the sign of* ω, *waves with opposite frequencies propagate in opposite directions. When* $\omega < 0$ *the waves move forward and are consequently designated the label (f). Those for which* $\omega > 0$ *are labelled (b) as they move in the backward direction. In addition to the p modes which propagate in the acoustic regions we find, for both positive and negative frequencies, an f mode lying just outside. Also shown in the graph are the mode eigenfrequencies and the zeros of the associated radial displacement. In this example* $m = 2$, $\Omega_n = 0$, $\Omega_p = 0$, $K = 1$.

We now look at the effect of a relative rotation of the fluid components on the modes. In Figure 5.2, where $\Omega_n = 0.3$ and $\Omega_p = 0$, we observe an additional region of propagation known as the R-region for the neutron superfluid modes. The forward and backward modes are now divided by the line $\omega = -m\Omega_n$. Waves with a frequency less than this are moving forward with respect to the background rotation, whereas for $\omega > -m\Omega_n$ the waves move backward with respect to the background rotation. Since the protons remain stationary we do not observe a presence of proton r-modes. The propagation regions for the protons are almost identical to those in the case where both fluids are stationary. Minimal modifications emerge due to the effect of the motion of the neutrons on the background density of the protons.

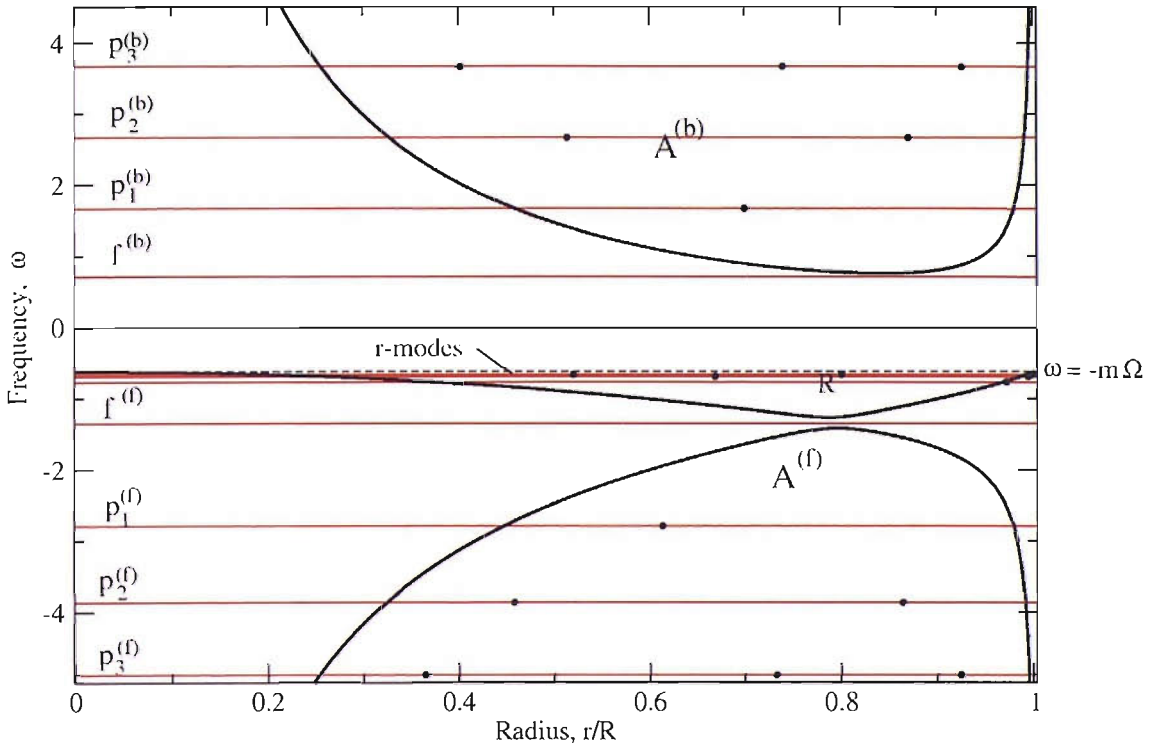

Figure 5.2: *The graph shows the regions of propagation for the neutron fluid in a cylinder containing two fluids, where the neutrons rotate while the protons remains at rest. In addition to the acoustic regions we observe an additional region of propagation known as the R-region for the neutron superfluid modes. The forward and backward modes are now divided by the line* $\omega = -m\Omega_n$. *Waves with a frequency less than this are moving forward with respect to the background rotation, whereas for* $\omega > -m\Omega_n$ *the waves move backward with respect to the background rotation. Also shown in the graph are the mode eigenfrequencies and the zeros of the associated radial displacement. In this example* $m = 2$, $\Omega_n = 0.3$, $\Omega_p = 0$, $K = 1$.

We investigate the effect of varying K on the allowed regions of propagation. Figure 5.3 shows the results for the case where $K = 0.1$. Since the coupling between the two fluids is weak the effect of this alteration is minimal. Table 5.1 summarises the frequencies of the various modes illustrated in the propagation diagrams. The Table highlights the effect of increasing the rotation rate on the mode frequency. A key observation is that the frequency of the forward moving modes is significantly altered whereas that of the backward moving modes changes only slightly. The Table also illustrates the effect of changing the value of K. While the r mode frequencies remain fairly unaltered the magnitude of the frequency of the p modes and f modes is decreased.

5.3 Normal mode solutions

We now investigate the oscillation modes of the system by integrating equations (5.1) and (5.3) numerically. If the term multiplying the derivative vanishes the

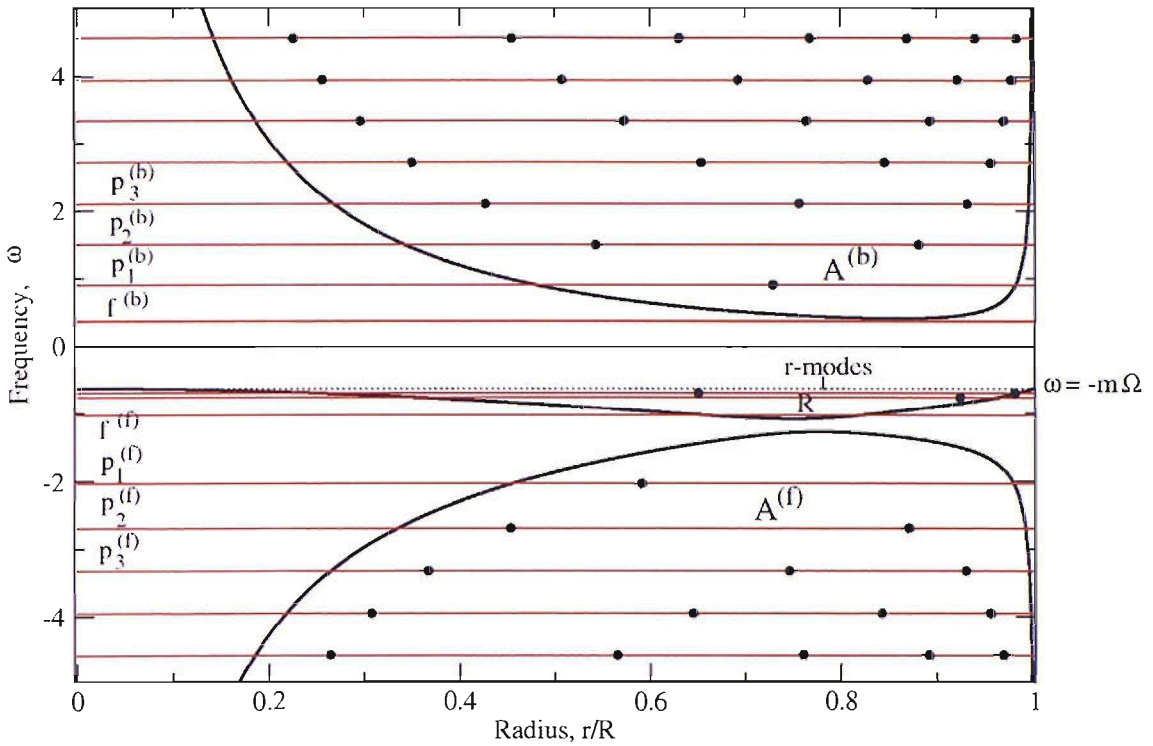

Figure 5.3: *We investigate the effect of varying the proton fraction on the propagation diagrams by considering an example containing* 90% *neutrons, similar to what one would expect for a neutron star. The graph shows the regions of propagation for the neutron fluid in a cylinder containing two fluids, where the neutrons rotate while the protons remains at rest. By comparison with Figure 5.2 we find that in this entrainment free case altering the proton fraction has very little effect on the propagation diagram. In this example* $m = 2$, $\Omega_n = 0.3$, $\Omega_p = 0$, $K = 0.1$.

respective equation will be singular and numerically we will encounter difficulties obtaining a solution. Clearly this will arise when either $r = 0$ or $\rho_X = 0$ corresponding to the centre and the surface of our cylinder. Consequently Frobenius expansions of the perturbations around these points were performed in order to obtain appropriate starting points for numerical integration. Integration of these equations is performed in exactly the same way as for the Lane-Emden equation using a FORTRAN fourth-order Runge-Kutta routine. The program integrates equations (5.1) and (5.3) along side the Lane-Emden equation; initially forward from $r = 0$ to $r = R/2$ and subsequently backward from $r = R$ to $r = R/2$. At the mid point the program evaluates $D = \xi_r^{in}\xi_\phi^{out} - \xi_r^{out}\xi_\phi^{in}$, where ξ^{in} represents the value of the radial part of displacement vector, ξ_r, obtained from the forward integration and ξ^{out} the value from the backward integration. If the eigenfunctions match D will equal zero. For most values of ω a match is not found, however, for the normal modes a match will be found and hence we can obtain the eigenfrequencies. The modes considered are those with an azimuthal wave-number, $m = 2$. The reason for this is they are the most significant for the gravitational wave driven

Mode	Frequency		
	$\Omega_n = 0,\ K = 1$	$\Omega_n = 0.3,\ K = 1$	$\Omega_n = 0.3,\ K = 0.1$
$p_3^{(f)}$	-3.35	-4.89	-3.32
$p_2^{(f)}$	-2.54	-3.86	-2.69
$p_1^{(f)}$	-1.70	-2.79	-2.04
$f^{(f)}$	-0.78	-1.35	-1.02
$r_1^{(f)}$		-0.77	-0.76
$r_2^{(f)}$		-0.70	-0.70
$r_3^{(f)}$		-0.67	-0.67
$f^{(b)}$	0.78	0.71	0.37
$p_3^{(b)}$	1.70	1.67	0.91
$p_2^{(b)}$	2.54	2.67	1.50
$p_1^{(b)}$	3.35	3.66	2.11

Table 5.1: *The frequency spectrum of the various modes which are plotted in the propagation diagrams 5.1-5.3. The Table highlights the effect of varying the neutron rotation rate and the proton fraction. In all the examples the frequency is in natural units* $\Omega_n/4\pi G\rho_{n0}$ *and* $\Omega_p = 0$.

instability in a real star.

5.3.1 Boundary and regularity conditions

When solving the background Lane-Emden equation, equation (3.49) was obtained as an expression for ρ_n around the origin. Performing a power series expansion of the solution around the centre we find that to first order ξ_r and ξ_ϕ take the following form

$$\begin{aligned} \xi_r^X &= A_X r^{aX} \\ \xi_\phi^X &= B_X r^{bX} \end{aligned} \tag{5.9}$$

By substituting these into equations (5.1) and (5.3) and we find near the centre the Lagrangian displacements can be approximated by,

$$\begin{aligned} \xi_r^X &= A_X r^{m-1} \\ \xi_\phi^X &= -\frac{A_X}{m} r^m \end{aligned} \tag{5.10}$$

At the surface of the cylinder ($r = R$) equations (5.1) and (5.3) contain singularities due to the fact that the densities vanish at this point. The value of the densities and their derivatives at the surface can be evaluated numerically from integration

of the Lane-Emden equation. By insisting that the perturbed Euler equation are regular at the surface we find,

$$\begin{aligned} \xi_r^X &= C_X \\ \xi_\phi^X &= -C_X \left[\frac{2\Omega_X R}{m\sigma_X} - \frac{\rho_X'(R)}{\sigma_X^2} \left(\frac{\partial \mu_X}{\partial n_X} \right)_{n_Y, w^2} \right] \end{aligned} \tag{5.11}$$

Where C_X is a constant. This corresponds to the Lagrangian perturbation of the pressure vanishing at the surface.

5.3.2 Numerical results

Since entrainment has been ignored the equations are coupled only through the background gravitational potential and the modes of each fluid are calculated independently. Initially the proton fluid was considered to be rotating at $\Omega_{\rm p} = 0.15$ and the neutron superfluid to be rotating at $\Omega_n = 0.2$. For this situation there was found to be f, p and r modes for both the neutrons and the protons. The f mode and p modes for the neutron fluid are plotted in Figure 5.4 and in Figure 5.5 we plot the r modes. Figures 5.6 and 5.7 show how the frequencies of particular modes vary as Ω_n changes. They also show how the modes of the normal fluid are affected by varying Ω_n. We can see from Figures 5.6 and 5.7 that as Ω_n increases the frequency of the superfluid modes decreases. For the normal fluid however the frequency of the backward moving p modes (those with positive frequency) is observed to increase slightly while the frequency of the forward moving $p$modes decrease slightly. However since the modes are essentially uncoupled the effect of the superfluid rotation on the proton modes is reasonably insignificant. Another key feature to note is that when the normal fluid and superfluid rotate with the same angular velocity the frequency of their modes are identical as one would expect.

5.3.3 Canonical energy

The motivation for investigating the oscillations of our system in a Lagrangian perturbation framework is that it gives us the opportunity to assess the mode stability through the canonical energy. A positive canonical energy suggests a stable mode while a negative canonical energy signifies a secular instability. Finally a dynamically unstable mode corresponds to zero canonical energy. In Section 4.6.4 the canonical energy for the normal modes of an entrainment free two fluid system was constructed in the form of equation (4.186). We now use this result to investigate the stability of the oscillations of our cylindrical system. Since the modes consist of one of the fluids oscillating while the other remains stationary we construct the

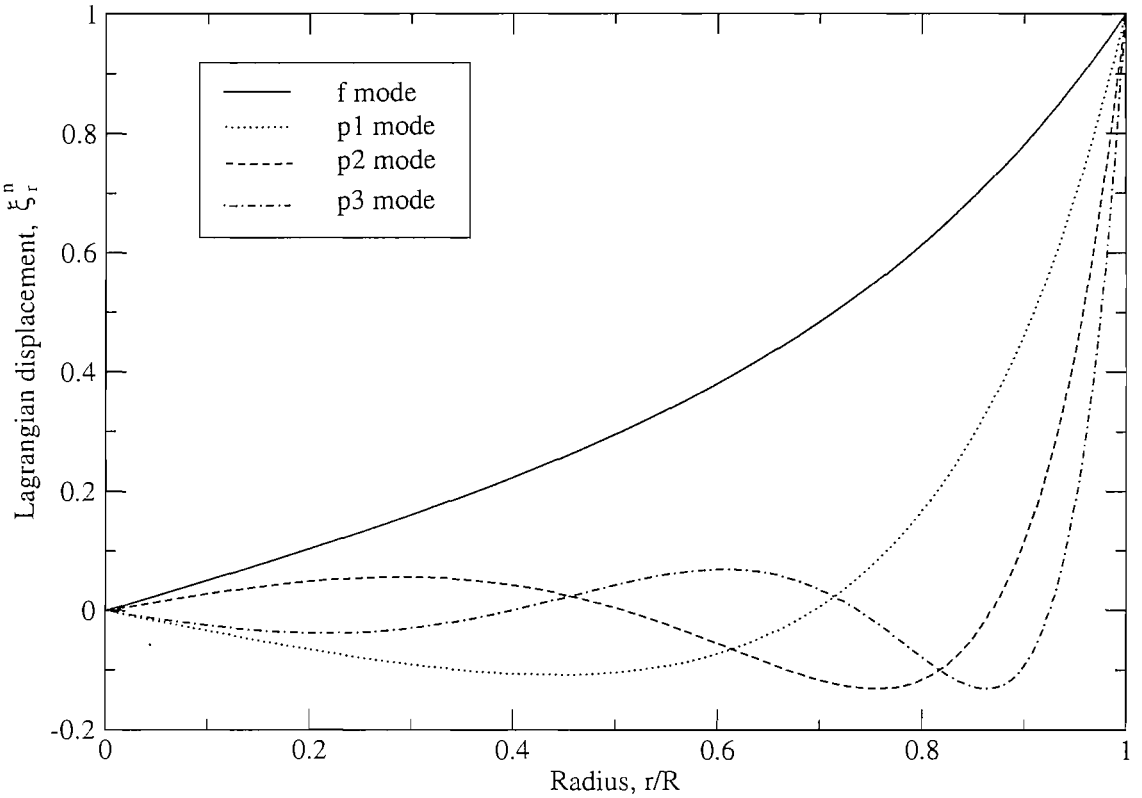

Figure 5.4: *The figure shows the fundamental mode and the lowest three p modes for the neutrons in a rotating superfluid cylinder. The configuration is such that the two fluids are rotating uniformly around the same axis at different angular velocities. We consider a cylinder with 90% neutrons, similar to what one would expect in a neutron star. We observe that the modes are all most influential in the outer layers. The parameters used in this example are* $m = 2$, $\Omega_n = 0.2$, $\Omega_p = 0.15$, $K = 0.1$. *The normalisation is such that* $\xi_r^{\rm n}(R) = 1$.

canonical energy for the neutron modes and set $\xi_p = 0$. After some manipulations the equation in our cylindrical system becomes,

$$\begin{aligned} E_c &= C\int_0^R \left\{-m^2\rho_{\rm n} r^2 \xi_\phi^{\rm n}\xi_r^{\rm n\prime} + (\xi_r^{\rm n})^2[-2m^2 r^4\Omega_{\rm n}^2 - 4mr^4\sigma_{\rm n}\Omega_{\rm n} + 4r^4\sigma_{\rm n}^2]\right. \\ &+ \xi_r^{\rm n}\xi_\phi^{\rm n}[-2m^2 r\rho_{\rm n} - 2m^2 r^2\rho_n{}' + 4m\Omega_n\sigma_{\rm n} r^3] \\ &+ \left.(\xi_\phi^{\rm n})^2[-2m^4\rho_{\rm n} + 4m^3\sigma_{\rm n}\Omega_{\rm n} r^2 - 2mr^2\sigma_{\rm n}^2]\right\}\frac{\rho_{\rm n}}{r^3}dr \end{aligned} \tag{5.12}$$

Where C is a normalisation constant. The canonical energy was calculated for the various modes of the two fluid system, see Table 5.2. It was found that for the configuration chosen the f and p modes had positive canonical energy while the canonical energy of the r modes was negative. This leads to the conclusion that the r modes are unstable to gravitational waves. This agrees with the conclusions reached in Andersson, Comer & Grosart [12] where we use the canonical energy to

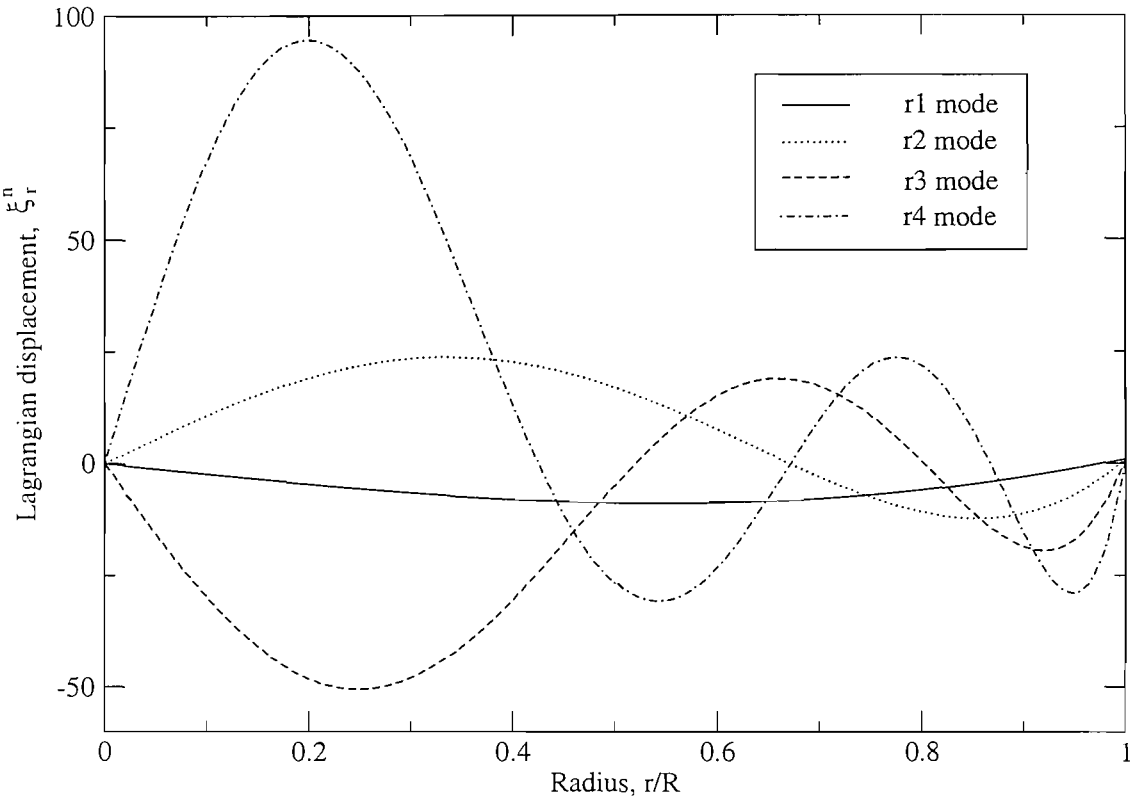

Figure 5.5: *The figure shows the lowest four r modes for the neutrons in a rotating superfluid cylinder. The configuration is such that the two fluids are rotating uniformly around the same axis at different angular velocities. We consider a cylinder with 90% neutrons, similar to what one would expect in a neutron star. In contrast with the f and p modes it appears that the r modes are more influential in the inner regions than the outer regions. The parameters used in this example are* $m = 2$, $\Omega_n = 0.2$, $\Omega_p = 0.15$, $K = 0.1$. *The normalisation is such that* $\xi^n_r(R) = 1$.

show that all r modes are secularly unstable to gravitational radiation.

In Section 4.6.7 we discussed the onset of a gravitational-wave driven CFS instability at the point where the (inertial frame) pattern speed of an originally backward moving mode changes sign. We investigate this for our two fluid system. By setting $\Omega_p = 0$ we expect the instability to appear as the mode frequency changes from $\omega > m\Omega_n$ to $\omega < m\Omega_n$. Figure 5.8 illustrates the effect of varying the neutron rotation rate, Ω_n, on the canonical energy of the originally backward moving f mode. Also plotted is the inertial frame pattern speed. We observe that the canonical energy becomes negative, signifying the onset of an instability, at the point where the mode becomes co-rotating confirming our analytical results.

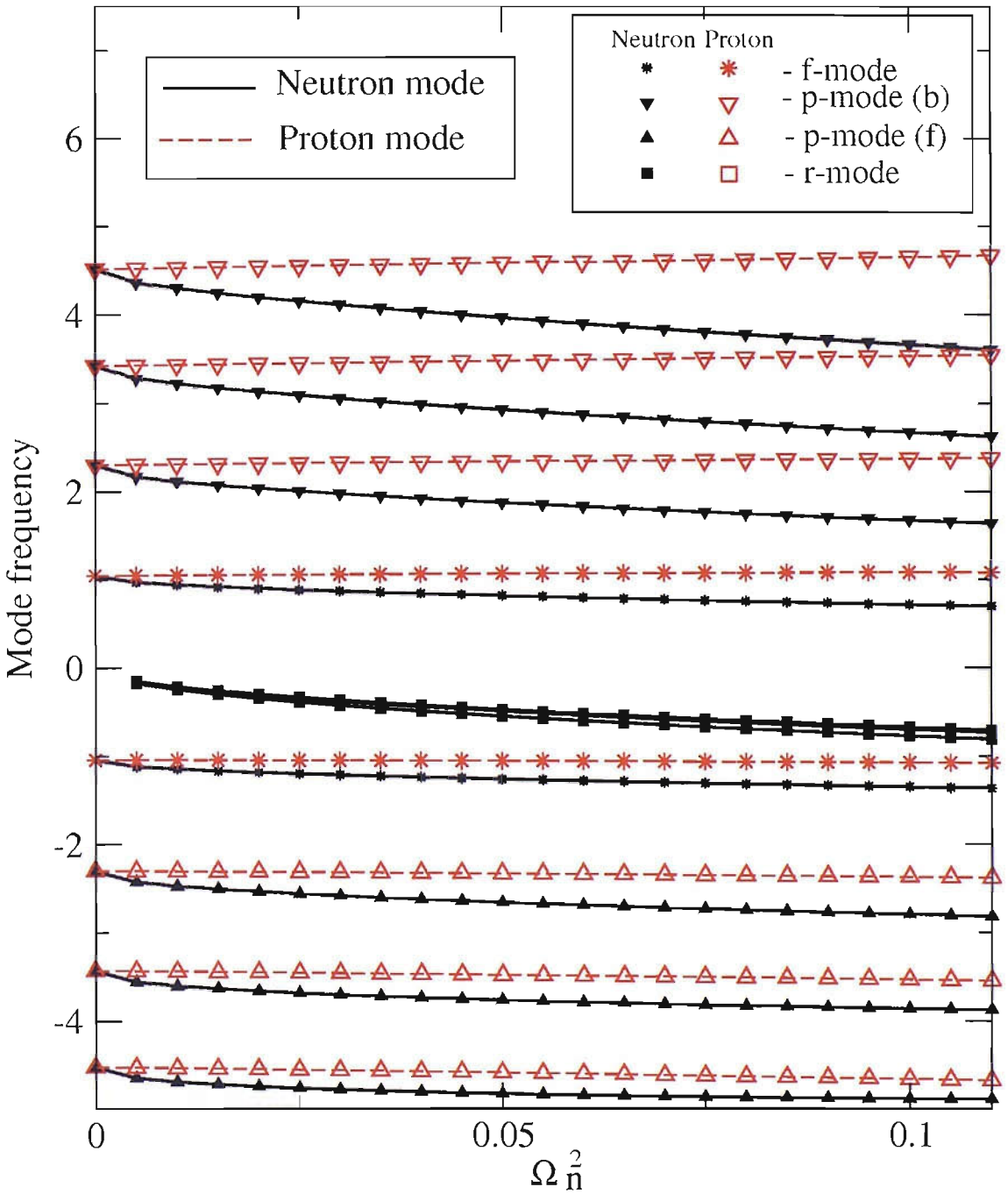

Figure 5.6: *The graph shows how the eigenfrequencies of the f, p and r modes change as Ω_n is increased whilst $\Omega_p = 0$. The graph shows the eigenfrequencies for the modes of both the neutron fluid and the proton fluid. As Ω_n increases the frequency of the neutron modes decrease. However since the modes are coupled only through the background gravitational potential the effect of the neutron fluid rotation on the proton modes is minimal. Another key feature to note is that when the proton fluid and neutron fluid rotate with the same angular velocity the frequency of their modes are identical as one would expect. An important observation is the absence of proton r modes (since $\Omega_p = 0$). The parameters in this example are $m = 2$, $\Omega_p = 0$.*

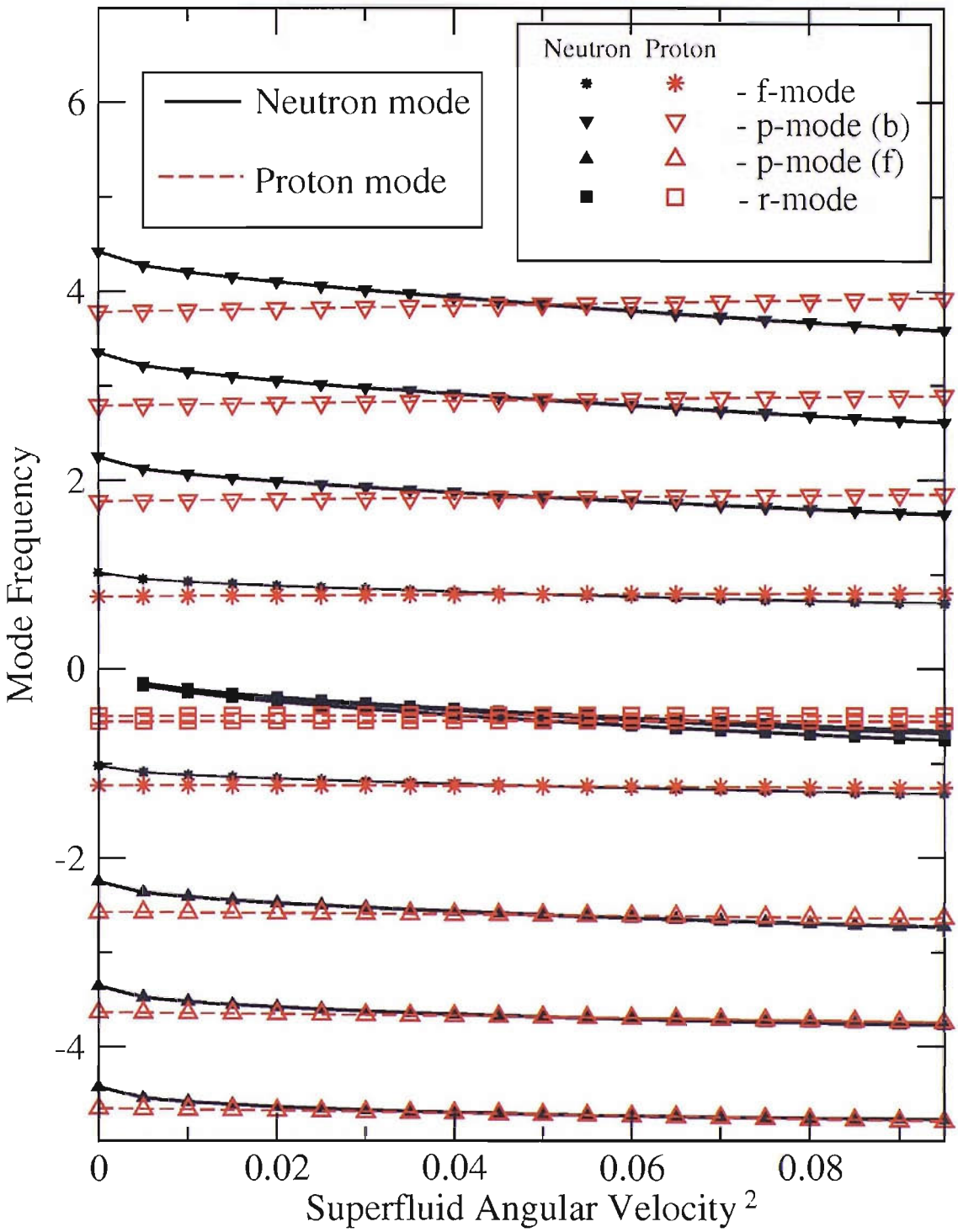

Figure 5.7: *The graph shows how the eigenfrequencies of the f, p and r modes change as Ω_n is increased whilst $\Omega_p^2 = 0.05$. The graph shows the eigenfrequencies for the modes of both the neutron fluid and the proton fluid. As Ω_n increases the frequency of the neutron modes decrease. However since the modes are essentially uncoupled the effect of the neutron fluid rotation on the proton modes is reasonably insignificant. Another key feature to note is that when the proton fluid and neutron fluid rotate with the same angular velocity the frequency of their modes are identical as one would expect. The parameters in this example are $m = 2$, $\Omega_p^2 = 0.05$.*

Frequency	Mode	Canonical Energy
-3.49749994	p3	22.7622039
-2.74945307	p2	25.9618476
-1.96757817	p1	26.3387658
-0.946015716	f	0.207443564
-0.491015702	r1	-0.917476246
-0.443750083	r2	-0.443750083
-0.425859451	r3	-0.323072024
-0.417031318	r4	-0.22729282
-0.412187576	r5	-0.169533188
-0.40906259	r6	-0.163646528
0.541328013	fb	0.498597932
1.25929677	p1b	7.74693899
1.99390614	p2b	10.4634301
2.72390604	p3b	11.0756489
3.44914055	p4b	10.8534123

Table 5.2: *The canonical energies for the various modes of a two fluid system, in which the neutrons and protons are rotating at different velocities around the same axis. We consider a configuration with* 90% *neutrons similar to what one would expect in a neutron star. For the configuration chosen the* f *and* p *modes had positive canonical energy while the canonical energy of the* r *modes was negative. This leads to the conclusion that the* r *modes are unstable to gravitational wave emission. The parameters used in this example are* $K = 0.1$, $\Omega_{\rm n} = 0.2$, $\Omega_{\rm p} = 0.15$.

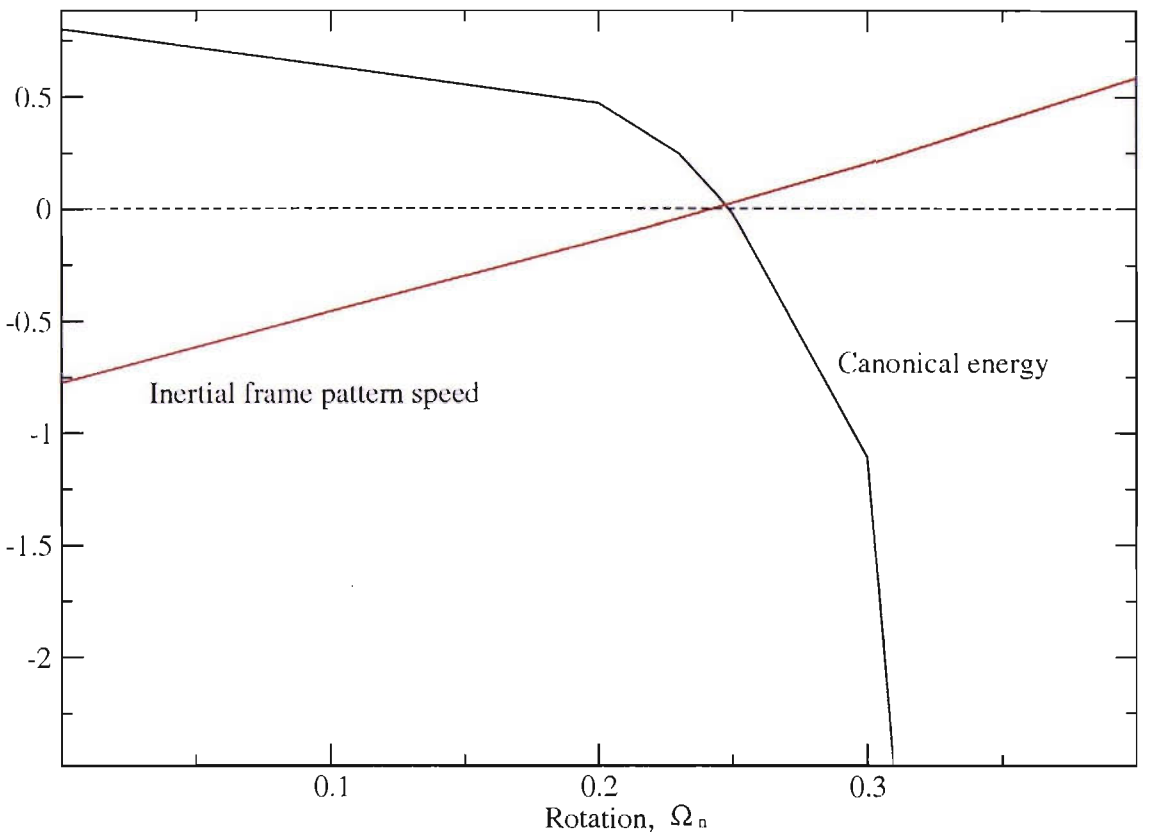

Figure 5.8: *The graph illustrates the effect of varying the neutron rotation rate,* Ω_n*, on the canonical energy of the originally backward moving f mode. Also plotted is the inertial frame pattern speed. We observe that the canonical energy becomes negative, signifying the onset of an instability, at the point where the mode becomes co-rotating confirming our analytical results. We consider an example in which* $\Omega_p = 0$ *and* $m = 2$*.*

Chapter 6

The oscillations and stability of superfluid cylinders: the case with non-vanishing entrainment

In the previous chapter we investigated the oscillations in superfluid cylinders for the situation where the entrainment is zero. In order to model more realistic configurations we must take into account entrainment. In Chapter 4 we observe that the inclusion of non vanishing entrainment in our calculation drastically complicates the corresponding perturbation equations. To simplify matters we will consider the case of constant entrainment, more specifically we will assume α to be a constant. An alternative would be to choose ε_{p} constant, as was done by Prix and Rieutord [71] and by Prix, Comer and Andersson [69]. Then ε_{n} is constrained by equation (6.1), and we have

$$\varepsilon_{\mathrm{p}} = \frac{2\alpha}{\rho_{\mathrm{p}}} = \frac{\rho_{\mathrm{n}}}{\rho_{\mathrm{p}}}\varepsilon_{\mathrm{n}} \tag{6.1}$$

The justification for simplifying the equations in this way is that there are such great uncertainties in any realistic models which nuclear physics has provided for the entrainment that we may as well begin with the most straightforward case. In doing so we hope to gain insight into what we can expect in more realistic cases. Incorporating constant entrainment is already a big technical step and allowing it to vary will not change anything conceptually.

The first step is to write the Lagrangian perturbation equations with entrainment in cylindrical coordinates. Scaling the variables as in Section 3.2, see Table 3.2, we obtain the following four equations,

$$
\begin{aligned}
&\frac{\partial \xi_r^X}{\partial r}\left[\left(\frac{\partial \mu_X}{\partial n_X}\right)_{n_Y,w^2} m\rho_X^2 r^2 - 2\alpha\sigma_X w_{YX} r^4\right] \\
+\ &\xi_r^X\left[\left(\frac{\partial \mu_X}{\partial n_X}\right)_{n_Y,w^2} m\rho_X r\left(\rho_X + r\frac{\partial \rho_X}{\partial r}\right) - 6\alpha\sigma_X w_{YX} r^3 - 2\Omega_X\sigma_X\rho_X r^3\right] \\
+\ &\xi_\phi^X\left[\left(\frac{\partial \mu_X}{\partial n_X}\right)_{n_Y,w^2} m^3\rho_X^2 + 2\alpha m r^2\sigma_X(\sigma_X - 2m w_{YX}) - m\sigma_X^2\rho_X r^2\right] \\
+\ &\xi_\phi^Y\left[-2m^2\alpha\sigma_X\sigma_Y r^2\right] = 0
\end{aligned}
\tag{6.2}
$$

and

$$
\begin{aligned}
&\frac{\partial^2 \xi_r^X}{\partial r^2}\left[\left(\frac{\partial \mu_X}{\partial n_X}\right)_{n_Y,w^2} r^3\rho_X^2\right] \\
+\ &\frac{\partial \xi_r^X}{\partial r}\left[\left(\frac{\partial \mu_X}{\partial n_X}\right)_{n_Y,w^2} r^2\rho_X\left(\rho_X + 2r\frac{\partial \rho_X}{\partial r}\right)\right] \\
+\ &\frac{\partial \xi_\phi^X}{\partial r}\left[\left(\frac{\partial \mu_X}{\partial n_X}\right)_{n_Y,w^2} m^2\rho_X^2 r - 2m\alpha\sigma_X w_{YX} r^3\right] \\
+\ &\xi_r^X\left[\left(\frac{\partial \mu_X}{\partial n_X}\right)_{n_Y,w^2} r\rho_X\left(r^2\frac{\partial^2 \rho_X}{\partial r^2} + r\frac{\partial \rho_X}{\partial r} - \rho_X\right) - 2\alpha\sigma_X^2 r^3 + \sigma_X^2\rho_X r^3\right] \\
+\ &\xi_r^Y\left[2\alpha\sigma_X r^3\sigma_Y\right] \\
+\ &\xi_\phi^X\left[\left(\frac{\partial \mu_X}{\partial n_X}\right)_{n_Y,w^2} m^2\rho_X(r\frac{\partial \rho_X}{\partial r} - 2\rho_X) + 4m\alpha\sigma_X w_{YX} r^2 + 2m\Omega_X\sigma_X\rho_X r^2\right] = 0
\end{aligned}
\tag{6.3}
$$

Once again X and Y are the constituent indices which can represent either the neutrons or the protons. When X represents the neutrons, Y represents the protons and vice versa.

In the entrainment free problem we reduced the analogous system to four first order differential equations which we subsequently solved numerically in FORTRAN. In that simpler case the approach taken was to solve the first order differential equations in ξ_r^X for $\partial\xi_r^X/\partial r$, differentiate with respect to r, and substitute $\partial\xi_r^X/\partial r$ and $\partial^2\xi_r^X/\partial r^2$ into the remaining equations. This gave first order differential equations in ξ_ϕ^X. The coupling of the equations that has arisen as a result of non-zero entrainment introduces slight complications. Performing an identical procedure gives us, instead of two uncoupled differential equations in ξ_ϕ^X and ξ_ϕ^Y as in the entrainment free case, two coupled equations which can be combined to give the following matrix

equation,

$$A \begin{pmatrix} \frac{\partial \xi_\phi^X}{\partial r} \\ \frac{\partial \xi_\phi^Y}{\partial r} \end{pmatrix} = B \begin{pmatrix} \xi_r^X \\ \xi_r^Y \\ \xi_\phi^X \\ \xi_\phi^Y \end{pmatrix} \tag{6.4}$$

Where A is a 2×2 matrix and B a 4×2 matrix. If A is invertible we can write,

$$\frac{\partial}{\partial r} \begin{pmatrix} \xi_\phi^X \\ \xi_\phi^Y \end{pmatrix} = C \begin{pmatrix} \xi_r^X \\ \xi_r^Y \\ \xi_\phi^X \\ \xi_\phi^Y \end{pmatrix} \tag{6.5}$$

Where C is a 4×2 matrix. However, if $detA = 0$ we observe the equations are singular.

We write our equations schematically as a system of four first order differential equations. Equation (6.2) can be written as,

$$f_1^X \frac{\partial \xi_r^X}{\partial r} + f_2^X \xi_r^X + f_3^X \xi_\phi^X + f_4 \xi_\phi^Y = 0 \tag{6.6}$$

and we express equation (6.4) in the following form,

$$g_1^X \frac{\partial \xi_\phi^X}{\partial r} + g_2^X \xi_r^X + g_3^X \xi_\phi^X + g_4^X \xi_r^Y + g_5^X \xi_\phi^Y = 0 \tag{6.7}$$

Where the coefficients are regular functions of r.

6.1 Singularities

It is clear that problems may be encountered at points where the coefficients f_1^X and g_1^X vanish. At such points our equations are singular and numerically we should expect difficulties. The location and nature of these singularities will be investigated throughout this section.

For the first two equations the singularities arise when

$$f_1^X = 0 \tag{6.8}$$

From equation (6.2) we see that this corresponds to,

$$\left(\frac{\rho_{\rm n}^2}{r^2} \right) = 2\alpha w_{\rm pn} \sigma_{\rm n} / m \left(\frac{\partial \mu_{\rm n}}{\partial n_{\rm n}} \right) \tag{6.9}$$

and,

$$\left(\frac{\rho_{\rm p}^2}{r^2}\right) = -2\alpha w_{\rm pn}\sigma_{\rm p}/m\left(\frac{\partial\mu_{\rm p}}{\partial n_{\rm p}}\right) \tag{6.10}$$

The position of these singular points vary with frequency. The quantities ρ_X^2/r^2 vary with r going from infinity at the centre to zero at the surface. Since $m\,(\partial\mu_X/\partial n_X)$ is always greater than zero the first singular point will be encountered at some point within our cylinder if $\alpha w_{\rm pn}\sigma_n > 0$, which I will refer to as condition (a), and the second encountered if $\alpha w_{\rm pn}\sigma_p < 0$, condition (b). Figure 6.1 illustrates when we expect these singular points to arise.

For the equations involving derivatives of ξ_ϕ^X we expect singular points when the determinant of matrix A vanishes. Let us look more closely at this matrix to see where the singularities occur. We have

$$A = \vec{a}\begin{pmatrix} -\sigma_{\rm n}m[4\alpha^2 w_{\rm pn}^2 r^2 + \rho_{\rm n}^2\rho_{\rm p}^2 Y_{\rm n}] & -2\alpha m\rho_{\rm n}^2\left(\frac{\partial\mu_{\rm n}}{\partial n_{\rm n}}\right)_{n_{\rm p},w^2}\sigma_{\rm p} \\ -2\alpha m\rho_{\rm p}^2\left(\frac{\partial\mu_{\rm p}}{\partial n_{\rm p}}\right)_{n_{\rm n},w^2}\sigma_{\rm n} & -\sigma_p m[4\alpha^2 w_{\rm pn}^2 r^2 + \rho_{\rm n}^2\rho_{\rm p}^2 Y_{\rm p}] \end{pmatrix} \tag{6.11}$$

where

$$\vec{a} = (f_1^{\rm n}, f_1^{\rm p}) \tag{6.12}$$

and

$$Y_X = \frac{(\rho_X - 2\alpha)}{\rho_Y^2}\left(\frac{\partial\mu_X}{\partial n_X}\right)_{n_Y,w^2} \tag{6.13}$$

The determinant of matrix A is therefore

$$\begin{aligned} detA &= f_1^{\rm n}f_1^{\rm p}\sigma_n\sigma_p m^2\Big\{[4\alpha^2 w_{\rm pn}^2 r^2 + \rho_{\rm n}^2\rho_{\rm p}^2 Y_{\rm n}][4\alpha^2 w_{\rm pn}^2 r^2 + \rho_{\rm n}^2\rho_{\rm p}^2 Y_{\rm p}] \\ &- 4\alpha^2\rho_{\rm n}^2\rho_{\rm p}^2\left(\frac{\partial\mu_{\rm n}}{\partial n_{\rm n}}\right)_{n_{\rm p},w^2}\left(\frac{\partial\mu_{\rm p}}{\partial n_{\rm p}}\right)_{n_{\rm n},w^2}\Big\} \end{aligned} \tag{6.14}$$

Which by substituting

$$T = \left(\frac{\partial\mu_{\rm n}}{\partial n_{\rm n}}\right)_{n_{\rm p},w^2}\left(\frac{\partial\mu_{\rm p}}{\partial n_{\rm p}}\right)_{n_{\rm n},w^2}/\rho_{\rm n}^2\rho_{\rm p}^2 \tag{6.15}$$

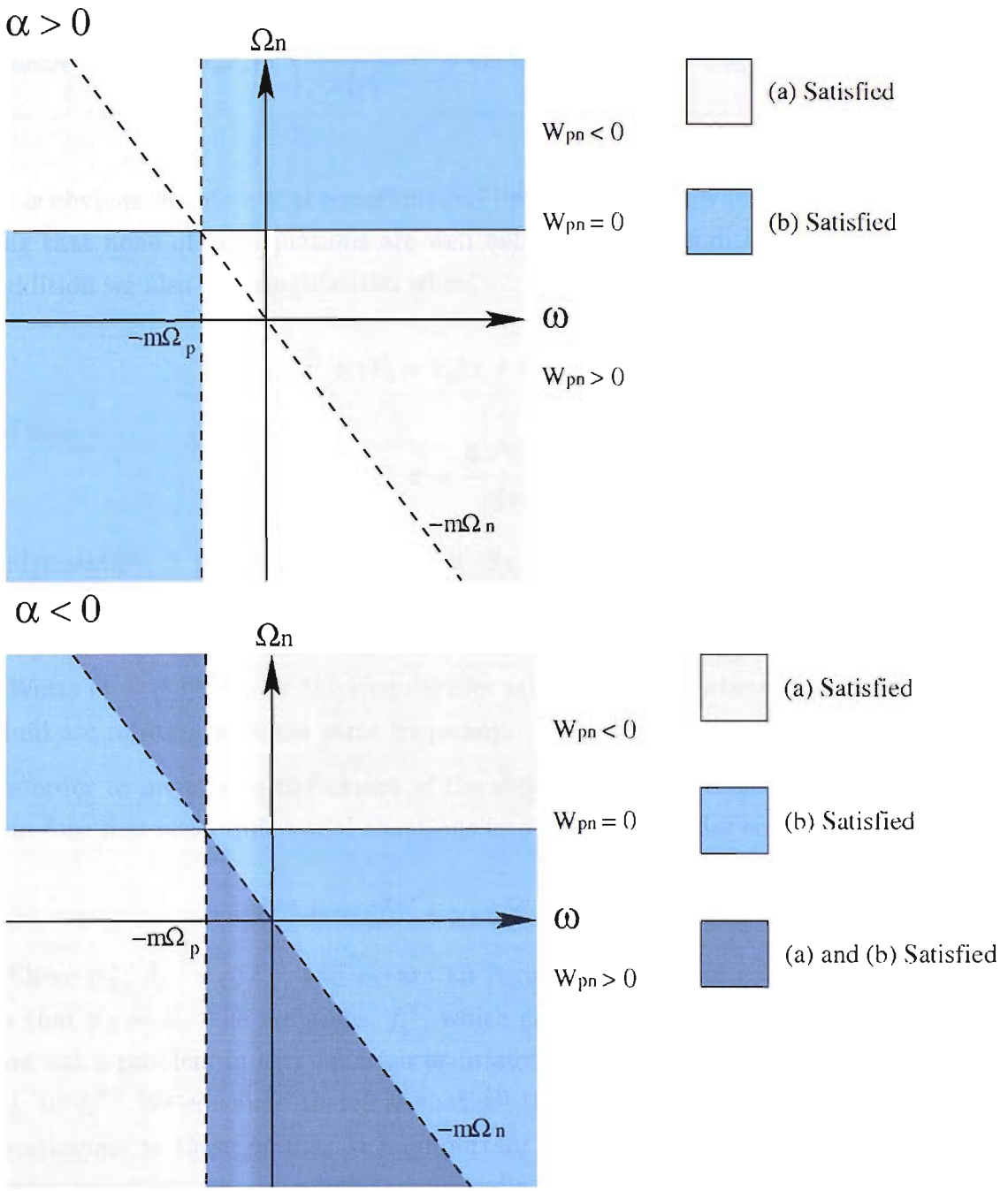

Figure 6.1: *The figures illustrate for which values of Ω_n and Ω_p we expect to encounter singularities in equations (6.6) for various values of ω. In the top figure we consider $\alpha > 0$ and in the bottom figure we consider $\alpha < 0$. In this example Ω_p is kept fixed as we vary Ω_n. For $\alpha > 0$ we observe that if both fluids are moving in the same direction with respect to the pattern speed of the mode one singularity will be present. However, in the mixed region where one fluid is moving forward with respect to the mode, while the other moves backward no singularities are observed. In the $\alpha < 0$ case we once again notice the existence of one singularity if both fluids are moving in the same direction with respect to the pattern speed of the mode but in the mixed region two singularities will be present.*

can be written as,

$$detA = f_1^{\rm n} f_1^{\rm p} \sigma_{\rm n} \sigma_{\rm p} m^2 \Big\{ \frac{16\alpha^4 w_{\rm pn}^4}{\rho_{\rm n}^2 \rho_{\rm p}^2} r^4 + 4\alpha^2 w_{\rm pn}^2 (Y_{\rm n} + Y_{\rm p}) r^2 + \rho_{\rm n}^2 \rho_{\rm p}^2 (Y_n Y_p - 4\alpha^2 T) \Big\} \tag{6.16}$$

It is obvious therefore that equations (6.7) will be singular when f_1^X vanish indicating that none of our equations are well behaved when condition (6.8) applies. In addition we also find singularities when,

$$S = x^2 + (Y_{\rm n} + Y_{\rm p})x + (Y_{\rm n} Y_{\rm p} - 4\alpha^2 T) = 0 \tag{6.17}$$

Where

$$x = \frac{4\alpha^2 w_{\rm pn}^2}{\rho_{\rm n}^2 \rho_{\rm p}^2} r^2 \tag{6.18}$$

Interestingly, S is dependent solely on the background quantities and completely independent of the frequency, ω. These are therefore different from co-rotation singularities, such as those observed in a differentially rotating single fluid problem, (Watts et al [86]), where the singularities arise at a point where the mode and the fluid are rotating with the same frequency.

In order to investigate the nature of the singularities it is constructive to combine our four first order differential equations into one fourth order equation of the form,

$$\pi_X \xi_r^{X\prime\prime\prime\prime} + \beta_X \xi_r^{X\prime\prime\prime} + \chi_X \xi_r^{X\prime\prime} + \delta_X \xi_r^{X\prime} + \epsilon_X \xi_r^X = 0 \tag{6.19}$$

Where π_X, β_X, χ_X, δ_X, and ϵ_X are all regular functions of r. What we discover is that $\pi_X = S$. The functions, f_1^X, which cause concern in our first order system are not a problem in this equation or in any of the equations relating ξ_r^Y, ξ_ϕ^X, and ξ_ϕ^Y to ξ_r^X. We conclude therefore that all the functions and their derivatives are continuous at these points. It is important to remember, however, that the first order equations we are solving numerically are singular when f_1^X vanish and so care must be taken when integrating through these points. We deal with these singularities by performing a second order extrapolation across the singular points.

The singularities that occur when $S = 0$ require greater consideration. Since they do not depend on the frequency, an appropriate choice of parameters may allow them to be avoided. In this way we can check our numerics without the complication of the singularities. In general, however, we need to worry about this problem since these singular points may be present in a realistic configuration. For a fixed value of the relative rotation and constant entrainment Y_X and T vary with x. We proceed

by writing equation (6.17) in the following way,

$$S = x^2 + 2B(x)x + C(x) = 0 \tag{6.20}$$

If we assume there is a solution to this equation at $r = r_s$, such that,

$$x = \frac{4\alpha^2 w_{\rm pn}^2}{\rho_{\rm n}^2 \rho_{\rm p}^2} r_s^2 = x_s \tag{6.21}$$

we can deduce that,

$$x_s = -B(x_s) \pm \sqrt{B(x_s)^2 - C(x_s)} \tag{6.22}$$

If the only possible solution to this equation is such that x_s is either negative or complex we can say that the singularity will not be present in our system. Equation (6.20) has real roots if $B(x_s)^2 > C(x_s)$. If $C(x_s) > 0$ we notice that both the roots will be negative. Hence there will be no singularities if either,

1. $C(x_s) > 0$ and $B(x_s) > 0$ or
2. $B(x_s)^2 < C(x_s)$

The first case results in two real negative roots, if there are any solutions at all, and the second leads to two complex roots. However,

$$\begin{aligned} B^2 - C &= \frac{1}{4}(Y_{\rm n} + Y_{\rm p})^2 - (Y_{\rm n}Y_{\rm p} - 4\alpha^2 T) \\ &= \frac{1}{4}[(Y_{\rm n} - Y_{\rm p})^2 + 16\alpha^2 T] \not< 0 \end{aligned}$$

Thus case two never arises. Therefore we find there will be no singularities present if $B(x_s) > 0$ and $C(x_s) > 0$. The first of these two conditions will apply if,

$$\frac{1}{2}\left[Y_{\rm n}(x_s) + Y_{\rm p}(x_s)\right] > 0 \tag{6.24}$$

$$\left[\rho_{\rm n}^2(\rho_{\rm n} - 2\alpha)\left(\frac{\partial \mu_{\rm n}}{\partial n_{\rm n}}\right) + \rho_{\rm p}^2(\rho_{\rm p} - 2\alpha)\left(\frac{\partial \mu_{\rm p}}{\partial n_{\rm p}}\right)\right] > 0 \tag{6.25}$$

giving,

$$\alpha < \frac{\rho_{\rm n}^3\left(\frac{\partial \mu_{\rm n}}{\partial n_{\rm n}}\right) + \rho_{\rm p}^3\left(\frac{\partial \mu_{\rm p}}{\partial n_{\rm p}}\right)}{2\left[\rho_{\rm n}^2\left(\frac{\partial \mu_{\rm n}}{\partial n_{\rm n}}\right) + \rho_{\rm p}^2\left(\frac{\partial \mu_{\rm p}}{\partial n_{\rm p}}\right)\right]} \tag{6.26}$$

In addition $C(x_s) > 0$ if,

$$Y_{\rm n} Y_{\rm p} > 4\alpha^2 T \tag{6.27}$$

$$(\rho_{\rm n} - 2\alpha)(\rho_{\rm p} - 2\alpha) > 4\alpha^2 \tag{6.28}$$

giving finally

$$\alpha < \frac{\rho_{\rm n}\rho_{\rm p}}{4(\rho_{\rm n} + \rho_{\rm p})} \tag{6.29}$$

Using the relationship between the entrainment and the effective mass, equation (2.24), we discover condition (6.29) corresponds to,

$$m^*_{\rm p} + m^*_{\rm n} > m_{\rm B} \tag{6.30}$$

By writing the effective mass of one constituent in terms of the other this can be written as,

$$\frac{\rho}{m_{\rm B}} > \frac{\rho_X}{m^*_X} \tag{6.31}$$

If we define the effective number density as,

$$n^*_X = \frac{\rho_X}{m^*_X} \tag{6.32}$$

the condition for singularity avoidance becomes

$$n > n^*_X \tag{6.33}$$

Provided condition (6.33) holds it is straightforward to show that the condition (6.26) is always satisfied. Thus the singularity will not be present if the total number density of the baryons is greater than the effective number densities of both the neutrons and the protons. Predicted values of the effective masses for neutron stars give typically $m_X > \frac{2}{3}m_{\rm B}$ which suggests that for any real system these singularities will not be a problem.

Figure 6.2 illustrates the regions $C(x_s) > 0$ and $B(x_s) > 0$. Values of α that lie below both lines will satisfy the necessary condition for singularity avoidance. Since $\rho_{\rm n}$ and $\rho_{\rm p}$ tend to zero at the surface a negative value of the entrainment parameter α will ensure these singularities are never encountered. However, this does not necessarily mean that there will always exist a singular point for $\alpha > 0$. In fact if we look at S numerically we find that there is a small range of positive α where these singularities are not present, see Figure 6.3.

Ideally we would like to solve the problem in both the situation where the singularities are not present and the case where they are present. The latter involves investigating the behaviour of the functions at the singular points using a power

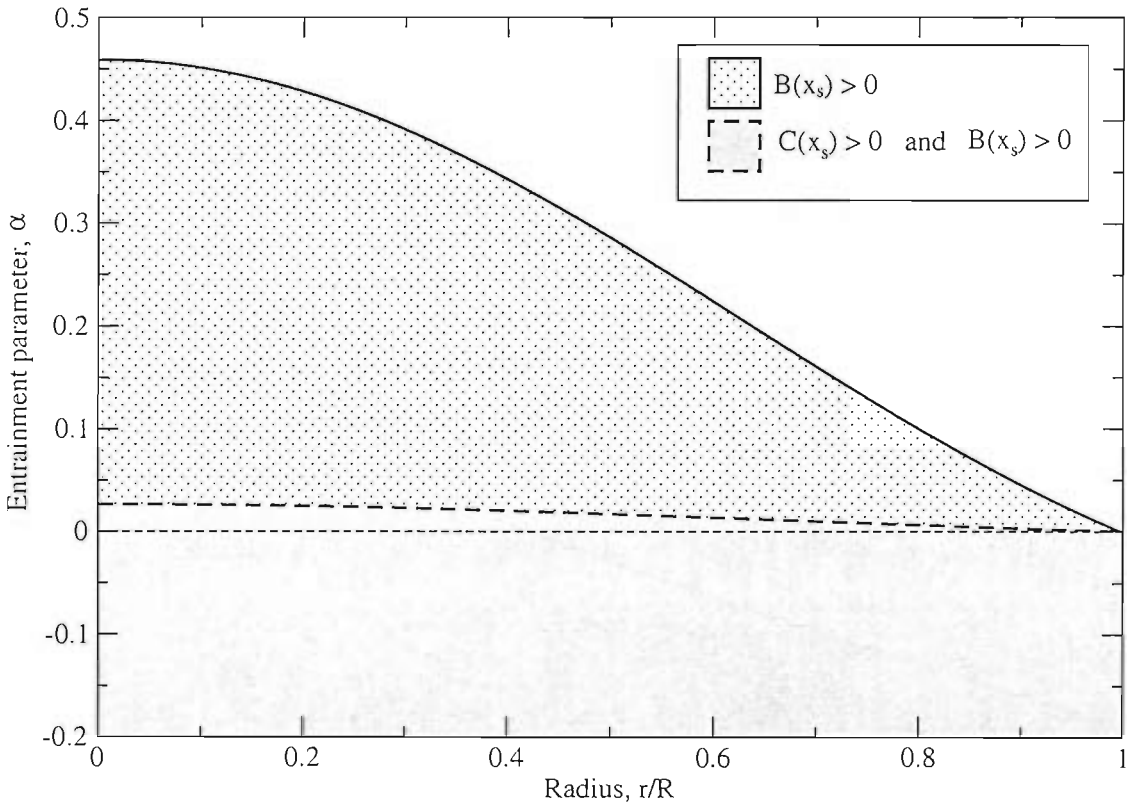

Figure 6.2: *The graph shows the regions $C(x_s) > 0$ and $B(x_s) > 0$. The area shaded grey represents points where the singularities that appear when $\det A = 0$ will definitely not be present. These singularities occur in equations (6.7), two of the four first order differential equations that describe our superfluid cylinder with entrainment. The configuration considered is $K = 0.1$, $\Omega_{\rm n} = \Omega_{\rm p} = 0.1$.*

series expansion. The complexity of our equations makes this unfeasible in the time available and so we chose to investigate in detail the former problem while for the second case we will simply outline the process that would be involved and discuss the complications.

6.2 Boundary conditions

6.2.1 At the centre

In order to characterise the behaviour of the solutions at the centre we approximate the background densities, as in Section 3.2, as power series of the form,

$$\begin{aligned} \rho_{\rm n} &= 1 + a_2 r^2 \\ \rho_{\rm p} &= b_0 + b_2 r^2 \end{aligned} \tag{6.34}$$

In order to satisfy our system of equations the solutions, ξ_r^X and ξ_ϕ^X, must vanish at $r = 0$. A power series expansion around the centre gives (to leading order),

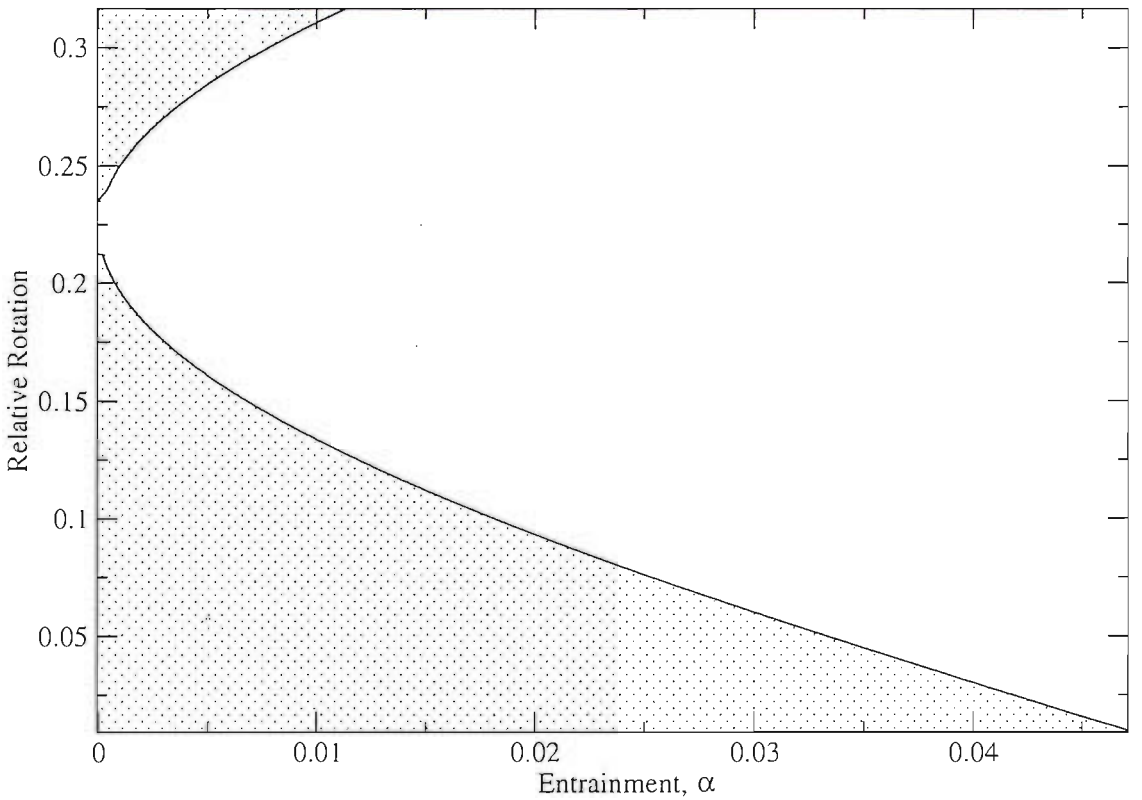

Figure 6.3: *If $\alpha < 0$ we have shown that the g_1 singularities will not appear in our cylinder. However, there is also a small range of positive α in which they will not be present. We perform a numerical analysis to investigate the regions in which condition (6.20) is not satisfied for all $0 < r < R$. The shaded area is a region in which the singularities will not be present. The configuration considered is $K = 0.1$, $\Omega_{\rm n} = \Omega_{\rm p} = 0.1$.*

$$\begin{aligned} \xi_r^X &= A_X r^{a_X} \\ \xi_\phi^X &= B_X r^{b_X} \end{aligned} \tag{6.35}$$

We observe that, to first order, the two sets of equations (the one with $X = n$ and the one with $X = p$) decouple at the centre. The resulting constraint is identical to that found in the entrainment free case.

$$\begin{aligned} \xi_r^X &= A_X r^{m-1} \\ \xi_\phi^X &= -\frac{A_X}{m} r^m \end{aligned} \tag{6.36}$$

We obtain two linearly independent solutions by considering different values of $A_{\rm n}$ and $A_{\rm p}$. For simplicity we initially consider $A_{\rm n} = 1$ and $A_{\rm p} = 0$ followed by $A_{\rm n} = 0$ and $A_{\rm p} = 1$. The true solution is a linear combination of the two results.

6.2.2 *At the surface*

In the entrainment free problem we imposed a condition on the eigenfunctions at the surface to ensure regularity of the solutions. This corresponded to the Lagrangian perturbation of the pressure vanishing at this point. Ideally in this more complicated problem we would construct a similar constraint. However, the assumption that $\alpha = constant$ leads to a highly unphysical surface. It is unlikely that as the fluid densities vanish the entrainment remains constant and in this sense the behaviour near the surface is *artificial*. We find that there is no longer a singularity at the surface. The densities of the two fluids vanish, yet the entrainment remains finite and hence the terms involving the entrainment dominate the system. Therefore, in order to guarantee that the solution is regular as the entrainment vanishes we impose an identical constraint as that imposed in the entrainment free problem.

$$\xi_r^X = B_X \sigma_X^2 \tag{6.37}$$

$$\xi_\phi^X = B_X \left[\left(\frac{\partial \mu_X}{\partial n_X} \right)_{n_Y, w^2} \rho_X'(R) - 2\Omega_X \sigma_X R/m \right] \tag{6.38}$$

With this condition imposed we are left with the following four equations which must be satisfied at the surface,

$$\begin{aligned} & -\frac{\partial \xi_r^X}{\partial r}[2\alpha\sigma_X w_{YX} r^4] - \xi_r^X[6\alpha\sigma_X W_{YX} r^3] + \xi_\phi^X[2\alpha m r^2 \sigma_X(\sigma_X - 2m w_{YX})] \\ - \; & \xi_\phi^Y[2m^2\alpha\sigma_X\sigma_Y r^2] = 0 \end{aligned} \tag{6.39}$$

and

$$-\frac{\partial \xi_\phi^X}{\partial r}[2m\alpha\sigma_X w_{YX} r^3] - \xi_r^X[2\alpha\sigma_X^2 r^3] + \xi_r^Y[2\alpha\sigma_X r^3\sigma_Y] + \xi_\phi^X[4m\alpha\sigma_X w_{YX} r^2] = 0 \tag{6.40}$$

Initially it was assumed that these equations would automatically be satisfied by the numerical Runge-Kutta routine when integrating from the surface. Subsequently a more detailed approach which involved solving the above system analytically at the surface resulted in almost identical results, see Table 6.1. The main discrepancy between the two methods arises as a consequence of the fact that in the initial method our two independent solutions were such that one of the two fluid displacement vectors vanished at the surface. In the more detailed calculation a combination of the two fluid displacement vectors was required to satisfy the analytic solution. We are confident that these solutions are precise enough to illustrate the general behaviour of our toy problem. Thus in this work we present the results from the first case.

Mode	Frequency using first approach	Frequency using second approach
p_9 mode	-4.271	-4.275
p_8 mode	-3.825	-3.825
p_7 mode	-3.795	-3.795
p_6 mode	-3.350	-3.351
p_5 mode	-2.890	-2.900
p_4 mode	-2.622	-2.600
p_3 mode	-2.422	-2.400
p_2 mode	-1.951	-1.912
p_1 mode	-1.463	-1.444
f mode	-1.212	-1.239

Table 6.1: *In order to guarantee that the solution at the surface is regular as the entrainment vanishes we impose an identical constraint as that imposed in the entrainment free problem. We consider two different methods of initiating our numerical integration, one which relies on the Runge-Kutta routine automatically satisfying any additional constraints and a second in which we insist these constraints are satisfied by analytically solving the equations at the surface. The results indicate that the two approaches give almost identical results. In the table all the modes are moving forward with respect to the fluid.*

6.3 Eigenvalues and matching

As was mentioned earlier there exists two independent solutions initiating at the centre and two initiating at the surface. The desired solution will be a linear combination of the two independent solutions from the centre matched to a linear combination of the two independent solutions from the surface. We can construct an equation at the matching point,

$$d_1 \begin{pmatrix} \xi_r^{\mathrm{n}}(c1) \\ \xi_\phi^{\mathrm{n}}(c1) \\ \xi_r^{\mathrm{p}}(c1) \\ \xi_\phi^{\mathrm{p}}(c1) \end{pmatrix} + d_2 \begin{pmatrix} \xi_r^{\mathrm{n}}(c2) \\ \xi_\phi^{\mathrm{n}}(c2) \\ \xi_r^{\mathrm{p}}(c2) \\ \xi_\phi^{\mathrm{p}}(c2) \end{pmatrix} = d_3 \begin{pmatrix} \xi_r^{\mathrm{n}}(s1) \\ \xi_\phi^{\mathrm{n}}(s1) \\ \xi_r^{\mathrm{p}}(s1) \\ \xi_\phi^{\mathrm{p}}(s1) \end{pmatrix} + d_4 \begin{pmatrix} \xi_r^{\mathrm{n}}(s2) \\ \xi_\phi^{\mathrm{n}}(s2) \\ \xi_r^{\mathrm{p}}(s2) \\ \xi_\phi^{\mathrm{p}}(s2) \end{pmatrix} \tag{6.41}$$

Where c means from the centre and s from the surface. We can write this as a matrix equation,

$$\begin{pmatrix} \xi_r^{\mathrm{n}}(c1) & \xi_r^{\mathrm{n}}(c2) & -\xi_r^{\mathrm{n}}(s1) & -\xi_r^{\mathrm{n}}(s2) \\ \xi_\phi^{\mathrm{n}}(c1) & \xi_\phi^{\mathrm{n}}(c2) & -\xi_\phi^{\mathrm{n}}(s1) & -\xi_\phi^{\mathrm{n}}(s2) \\ \xi_r^{\mathrm{p}}(c1) & \xi_r^{\mathrm{p}}(c2) & -\xi_r^{\mathrm{p}}(s1) & -\xi_r^{\mathrm{p}}(s2) \\ \xi_\phi^{\mathrm{p}}(c1) & \xi_\phi^{\mathrm{p}}(c2) & -\xi_\phi^{\mathrm{p}}(s1) & -\xi_\phi^{\mathrm{p}}(s2) \end{pmatrix} \begin{pmatrix} d_1 \\ d_2 \\ d_3 \\ d_4 \end{pmatrix} = 0 \tag{6.42}$$

For the existence of non-trivial solutions for $\vec{d}$ we require the determinant of the above matrix to vanish. We shall call this matrix $\mathbf{Y}$. By finding where $det\mathbf{Y}$ vanishes we are able to obtain the eigenvalues and corresponding eigenvectors of the system.

6.4 *Ordinary* and *superfluid* modes

In many previous studies of superfluid neutron star oscillations [54], [55], [76], [10], alternative variables were introduced in an attempt to distinguish between modes in which the neutrons and protons were co-moving, sometimes referred to as *ordinary* modes, and those in which the two constituents were counter-moving, *superfluid* modes. Namely,

$$\psi_{sf} = \xi_{\mathrm{p}} - \xi_{\mathrm{n}} \tag{6.43}$$

and

$$\psi_{o} = x_{\mathrm{p}}\xi_{\mathrm{p}} + x_{\mathrm{n}}\xi_{\mathrm{n}} \tag{6.44}$$

Where x_{p} is the proton fraction and x_{n} the neutron fraction. Prix [71] showed that it is only in the non-stratified case, i.e. when there is no composition gradient, that the two types of mode decouple. In general the modes will not be purely co-moving or counter-moving. However, using the above variables does allow us to determine if modes are predominantly of one or the other type. During analysis of the results it is often constructive to make the separation into *ordinary* and *superfluid* modes.

6.5 Negative entrainment

We consider two specific background configurations; one in which $K = 1$ and the neutron and proton central densities are similar and another in which $K = 0.1$ and we have central neutron fraction close to what we would expect for a typical neutron star. The density profiles for these configurations are illustrated in Figures 3.3 to 3.7.

Following the same strategy as in the entrainment free case we begin with a local analysis of the equations to investigate the qualitative nature of the solution using propagation diagrams. Subsequently we investigate how the frequency of the modes change firstly as we vary the relative rotation for fixed entrainment and secondly as we vary the entrainment for a fixed relative velocity.

6.5.1 A local analysis

We investigate the local behaviour of our equations by assuming the modes take the following form,

$$\xi_{r} = \frac{1}{r}\xi_{rk}\exp\left(ikr\right) \tag{6.45}$$

$$\xi_{\phi} = \xi_{\phi r}\exp\left(ikr\right) \tag{6.46}$$

Substituting these into equations (6.6) and (6.7) leads to a dispersion relation between k and ω. Regions in which waves can propagate are regions in which k has a real part for real ω. Figures 6.5 to 6.6 illustrate the effect of decreasing the entrainment function, α slowly from 0 to -1 and Figure 6.7 illustrates the effect of varying the relative rotation, $\mathcal{R}$. The blue areas represent regions where we find four solutions to the dispersion relation in which k has a real part and hence there exists the possibility of four propagating waves. The grey regions highlight where two waves can propagate and the white regions are where we find only evanescent solutions. Figure 6.5 is the propagation diagram for the situation where $\alpha = 0$. It is identical to a superposition of the two independent propagation diagrams that exist in this case, one for the neutron fluid and a second for the proton fluid. This result is identical to that found in Section 5.2. As we introduce entrainment to the problem we notice that the propagation diagrams very rapidly become exceptionally complicated. The Figures not only illustrate the emergence of additional regions of propagation but also highlight the complexities introduced by the f_1^X singularities. It appears the singular points, represented in the Figures by a red line, split the propagation regions. Since the solutions are regular at this point I expect that this splitting is a consequence only of the way in which we have chosen to express our equations and in no way represents a physical effect. However, the general shape of the diagrams should give an approximation of where we can expect to observe oscillatory modes.

A key observation concerns the regions of propagation of the r modes. In the entrainment free case, Figure 6.5, we observe two distinct R-regions corresponding to the oscillations of the individual fluids. The location of these regions is directly beneath the line $\omega = m\Omega_X$ such that the r modes will all be moving forward with respect to the corresponding fluid. In the *mixed* region $m\Omega_{\rm p} < \omega < m\Omega_{\rm n}$ the proton r modes will move forward with respect to the protons but backward with respect to the neutrons. As we introduce entrainment the location of the proton R-region changes until it appears on the opposite side of the line $\omega = m\Omega_{\rm p}$, see Figure 6.6. The neutron r modes still move forward with respect to both fluids but the proton r modes now move backward with respect to both fluids. The *mixed* region in between seems almost free of modes. Another interesting observation is the extension of the acoustic regions toward $\omega = 0$ as the magnitude of the entrainment is increased, particularly close to the surface. The same effects are observed as we increase the relative rotation for a fixed value of the entrainment, see Figure 6.7.

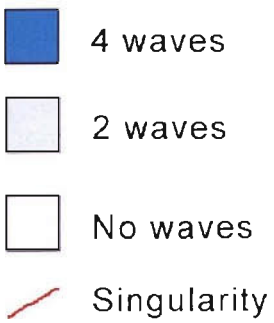

Figure 6.4: *Key for propagation diagrams: Shaded areas represent regions where either* 4, 2 *or no waves can propagate.*

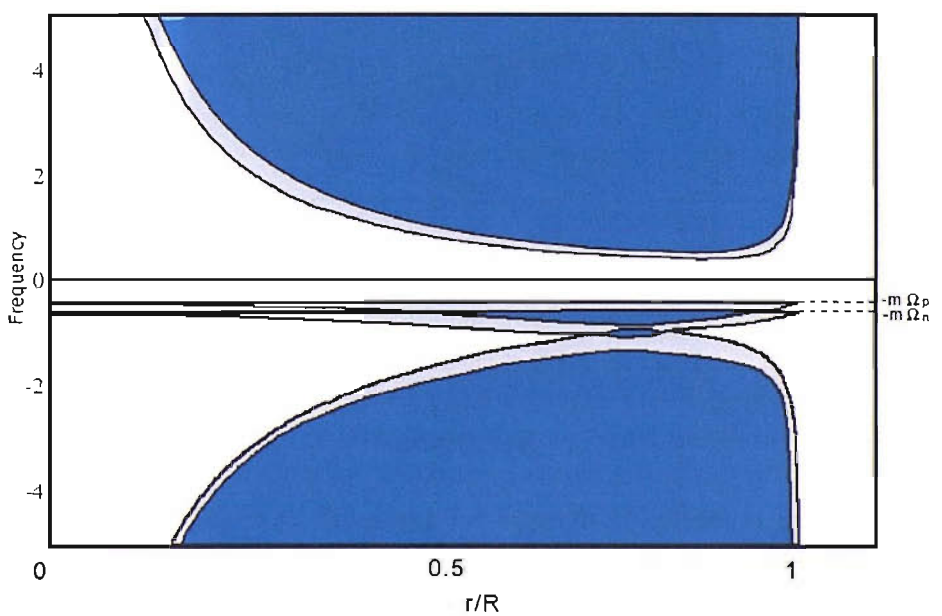

Figure 6.5: *The propagation diagram for an entrainment free superfluid cylinder in which the two fluids are rotating at different angular velocities around the same axis. In this case the regions of propagation correspond to a superposition of the two independent propagation diagrams that exist in this entrainment free case, one for the neutron fluid and a second for the proton fluid. The parameters we are considering are* $\alpha = 0$, $K = 1$, *and* $\mathcal{R} = 0.2$.

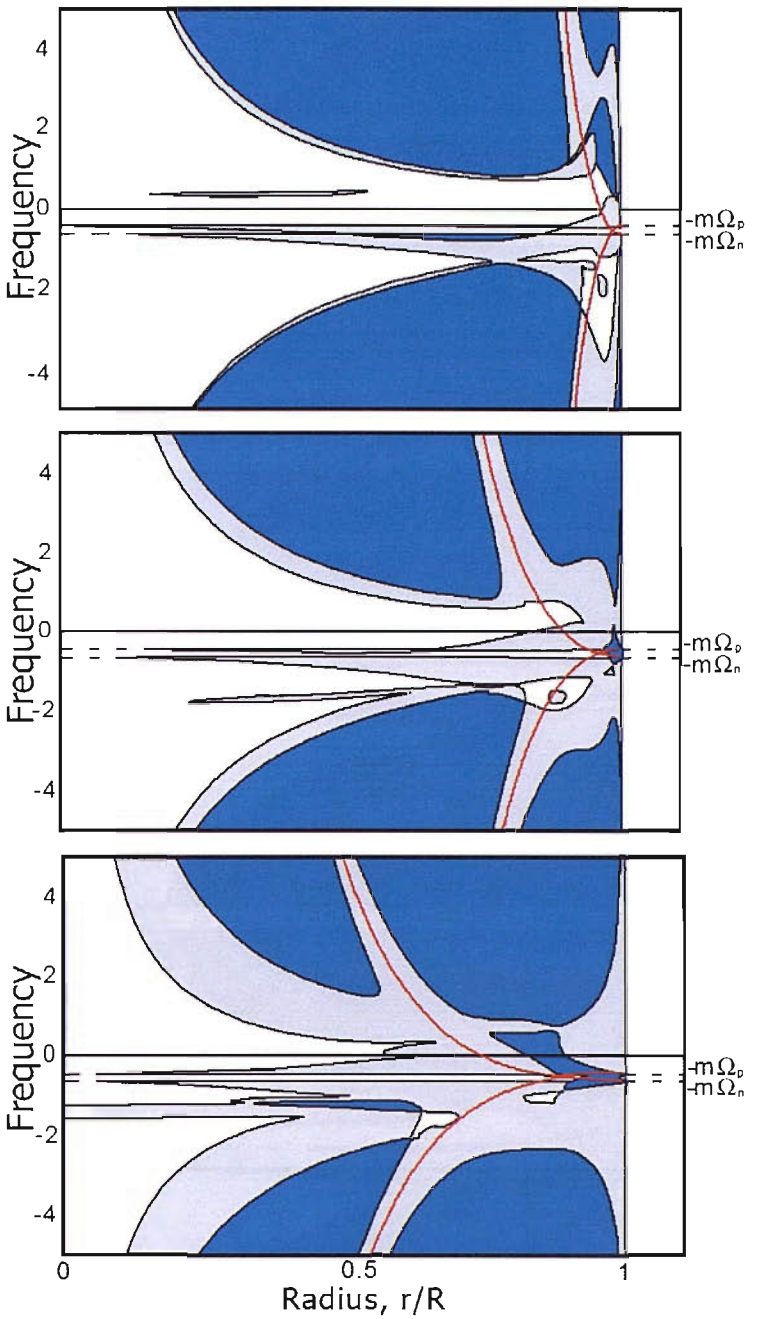

Figure 6.6: *The propagation diagrams for superfluid cylinders with non-vanishing entrainment in which the two fluids are rotating at different angular velocities around the same axis. The diagrams illustrate the effect of decreasing the entrainment function, α. It appears the singular points, represented by a red line, split the propagation regions. As we increase the magnitude of the entrainment the location of the proton R-region changes until it appears on the opposite side of the line $\omega = m\Omega_{\rm p}$. The neutron r modes continue to move forward with respect to both fluids but the proton r modes move backward with respect to both fluids. The mixed region in between seems almost free of any modes. Another interesting observation is the extension of the acoustic regions toward $\omega = 0$ as the magnitude of the entrainment is increased, particularly close to the surface. The parameters we are considering are $K = 1$, $\mathcal{R} = 0.2$, and from the top to the bottom $\alpha = -0.01$, $\alpha = -0.1$, and $\alpha = -1$.*

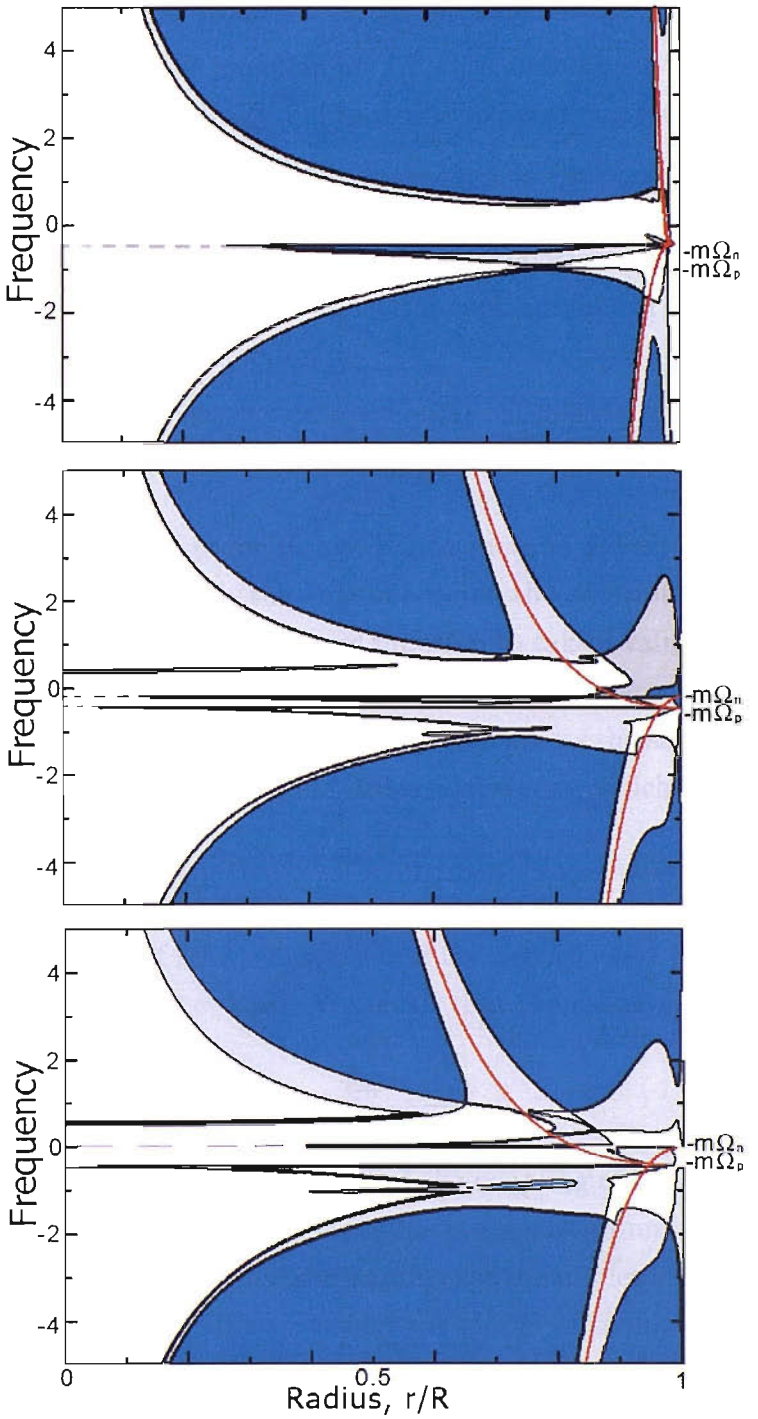

Figure 6.7: *The propagation diagrams for superfluid cylinders with non-vanishing entrainment in which the two fluids are rotating at different angular velocities around the same axis. The diagrams illustrate the effect of increasing the relative rotation. Again the singular points, represented by a red line, split the propagation regions. As we increase the relative rotation the location of the neutron R-region changes until it appears on the opposite side of the line* $\omega = m\Omega_n$. *The proton r modes continue to move forward with respect to both fluids but the neutron r modes move backward with respect to both fluids. The mixed region in between becomes almost free of any modes. Another interesting observation is the extension of the acoustic regions toward* $\omega = 0$ *as the size of the relative rotation is increased, particularly close to the surface. The parameters we are considering are* $K = 0.1$, $\alpha = -0.01$, *and from the top to the bottom* $\mathcal{R} = -0.01$, $\mathcal{R} = -0.5$, *and* $\mathcal{R} = -1$.

6.5.2 *Convergence and extrapolation across the singularity*

Although the solution is not singular at $f_1^X = 0$ numerically we will encounter problems at these points. Ideally a Frobenius expansion around the singularity could be done, however, due to the complexity of the equations we instead chose to use a second-order extrapolation to obtain the solution across the singularity. It is important to test if this technique is accurate so we performed a convergence test. This involved finding a solution with three different number of steps say k, $2k$ and $4k$. In Figure 6.8 we plot the function

$$C_k = \frac{(\xi^{2k} - \xi^k)^2}{(\xi^{4k} - \xi^{2k})^2} \tag{6.47}$$

Since we are using a fourth-order Runge-Kutta method for numerical integration we expect that before we reach the singular point the solution should be fourth-order convergent and we expect the above function to take a value of approximately 16. However, after extrapolation we can no longer expect the solution to have this property. Since we use a second-order extrapolation across the singularity we expect the solution to be approximately second-order convergent, which is what we observe in Figure 6.8.

6.5.3 *The effect of relative rotation*

We investigate the effect of relative rotation of the neutron and proton components by varying $\mathcal{R}$ whilst holding α fixed. We recall that the relative rotation is defined as,

$$\mathcal{R} \equiv \frac{\Omega_{\rm n} - \Omega_{\rm p}}{\Omega_{\rm p}}$$

In the co-rotating case, where $\mathcal{R} = 0$, we find the coupling of the equations through the entrainment vanishes. The equations reduce to the entrainment free system and we recall from Section 5 that in this co-rotating case the modes are identical for both the neutrons and the protons. If we consider the modes in terms of the *ordinary* and *superfluid* variables introduced in Section 6.4, $\psi_{sf} = \xi_{\rm p} - \xi_{\rm n}$ and $\psi_o = x_{\rm p}\xi_{\rm p} + x_{\rm n}\xi_{\rm n}$, it is obvious that $\psi_{sf} = 0$ and hence we describe the modes as being *ordinary*.

Relative rotation initiates a coupling between the neutron and proton equations. We begin by considering a configuration typical for a neutron star, where the densities are such that the cylinder is composed of approximately 90% neutrons. There are great uncertainties concerning appropriate values for the entrainment. It is predicted that in the neutron star core the entrainment is positive. Nuclear physics calculations put constraints on *realistic* values for this entrainment [18], [23]. In Prix & Rieutord [71] they state that these calculations give *realistic* values which lie between $0.3 \leq \varepsilon_{\rm p} \leq 0.7$. Although to demonstrate the qualitative behaviour

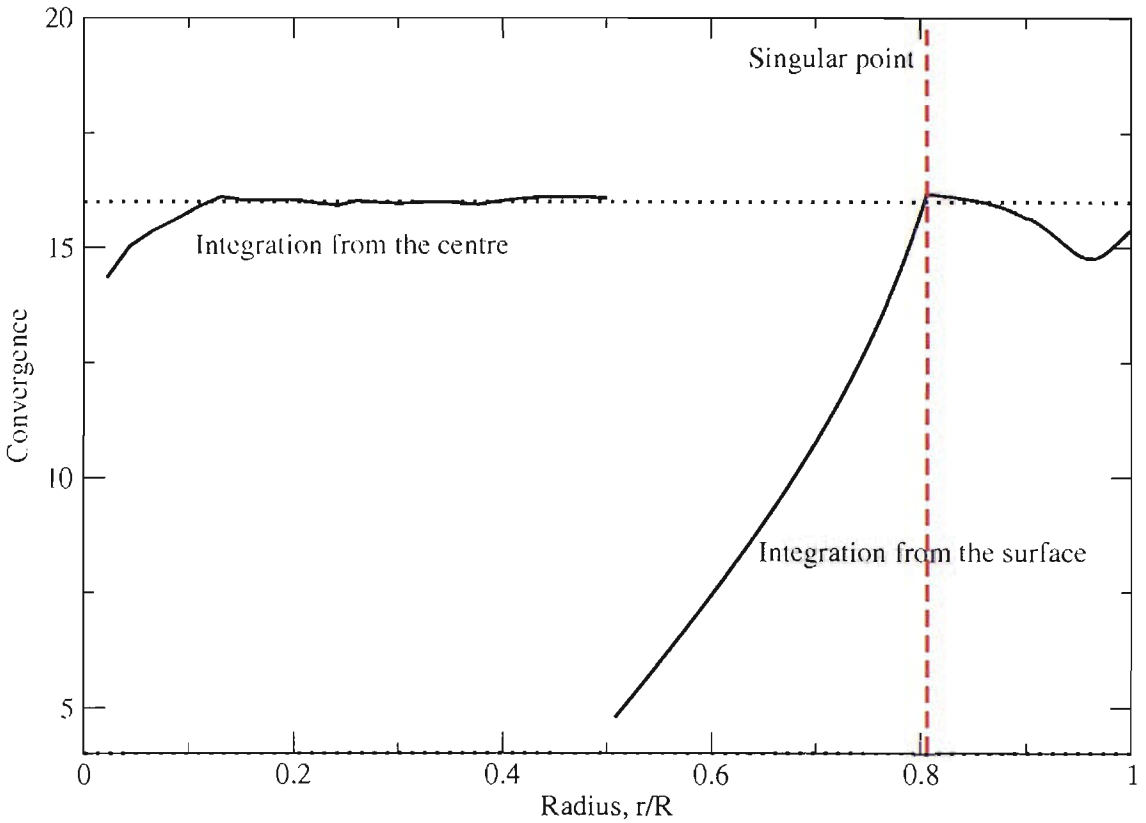

Figure 6.8: *The graph illustrates the convergence of our numerical solution. Since we are using a fourth-order Runge-Kutta integration method we expect the solution to be fourth-order convergent. This would result in a value of* 16 *for* C_k *which is what we observe before we reach the singular point. Here we observe a decrease in* C_k *to a value of approximately* 4 *which tells us the solution at this point is approximately second-order convergent. Since we perform a second-order extrapolation across the singularity this is what we would expect.*

more clearly they consider the broader range $-0.8 \leq \varepsilon_{\mathrm{p}} \leq 0.8$. Furthermore, recent work by Carter et al [27], [28] predicts negative entrainment for neutron star crusts. In the constant α case we are considering, since $\varepsilon_{\mathrm{p}} = 2\alpha/\rho_{\mathrm{p}}$, regardless of the value of α, the entrainment parameter ε_{p} will approach infinity at the surface. Although this is unphysical we already expect the behaviour near the surface to be artificial as a result of insisting a common surface for both the neutrons and the protons.

To investigate the effect of relative rotation we consider the entrainment function, $\alpha = -0.01$. Figure 6.9 illustrates how the frequency of the f modes and p modes vary with $\mathcal{R}$. Subsequently the individual modes are focused on in more detail beginning in Figure 6.10 with the f modes, followed by the p_1 modes in Figure 6.11 and finally the p_2 modes in Figure 6.12. Although the modes are not strictly co-moving or counter-moving, we define *ordinary*-type modes, represented graphically by a solid line, as those which continue from $\mathcal{R} = 0$. Since in the co-rotating case we observe only modes of the *ordinary*-type the *superfluid*-type modes, represented

by a dashed line, appear to emerge from $\omega = 0$. For this reason we find it difficult to resolve our solutions close to $\mathcal{R} = 0$, and hence the shaded area in the figures represents the undetermined region. By looking at the eigenfunctions it is clear that ψ_{sf} dominates over ψ_o for the *superfluid*-type modes whereas for the *ordinary*-type modes the dominance lies with ψ_o.

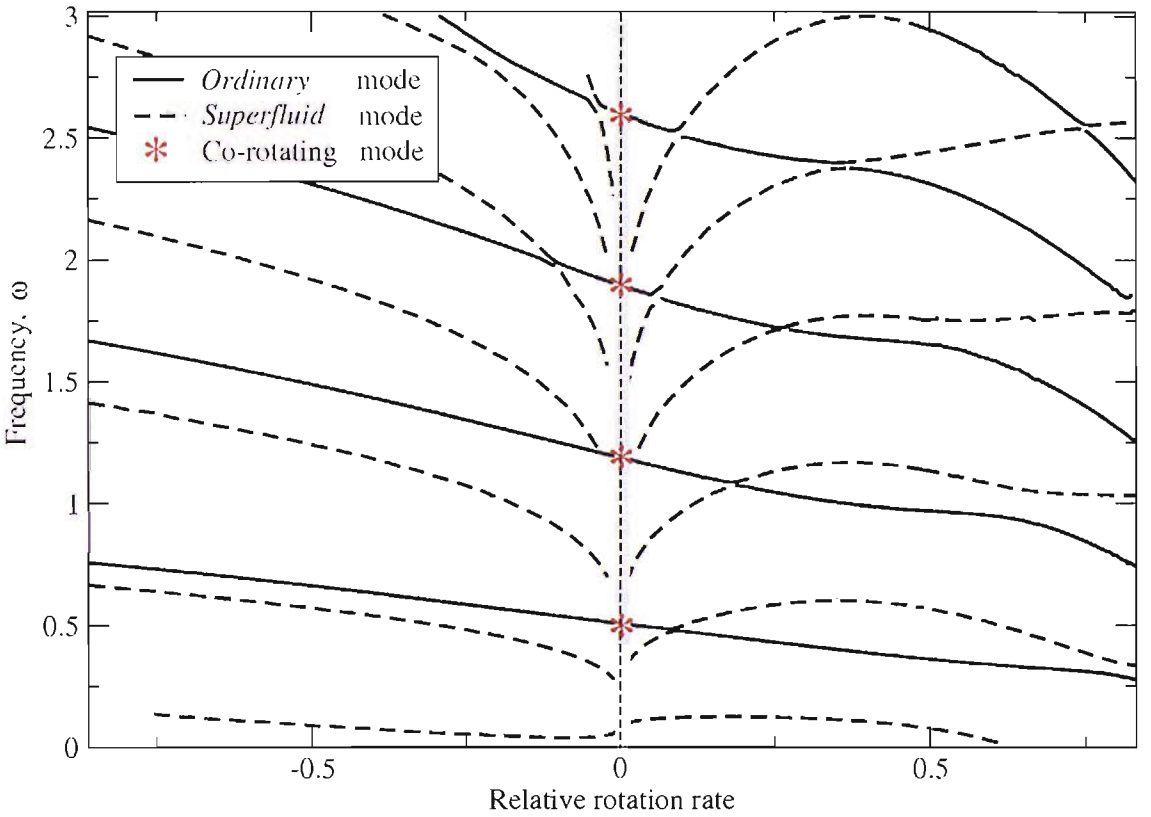

Figure 6.9: *The graph illustrate how the frequency of the f modes and p modes vary with $\mathcal{R}$. Although the modes are not strictly co-moving or counter-moving, we define ordinary-type modes as those which continue from $\mathcal{R} = 0$. While there are no avoided crossings between any two modes of the same type, we do observe avoided crossings between the ordinary-type modes and the superfluid-type modes. We find it difficult to resolve our solutions close to $\mathcal{R} = 0$, and hence the shaded area in the Figures represents the undetermined region. The parameters in this example are $\alpha = -0.01$ and $K = 0.1$.*

While there are no avoided crossings between any two modes of the same type, we do observe avoided crossings between the *ordinary*-type modes and the *superfluid*-type modes. As in Prix et al [68] the crossings coincide with an exchange in mode properties. After such a crossing the *ordinary*-type mode will become a *superfluid*-type mode and vice-versa. Consider for example the avoided crossing between the *ordinary*-type f mode and the *superfluid*-type p_1 mode. Figure 6.13 illustrates this crossing. We consider two particular points on either side of the crossing, labelled points $A \rightarrow D$, and investigate the change in the mode behaviour. Figure 6.14 shows

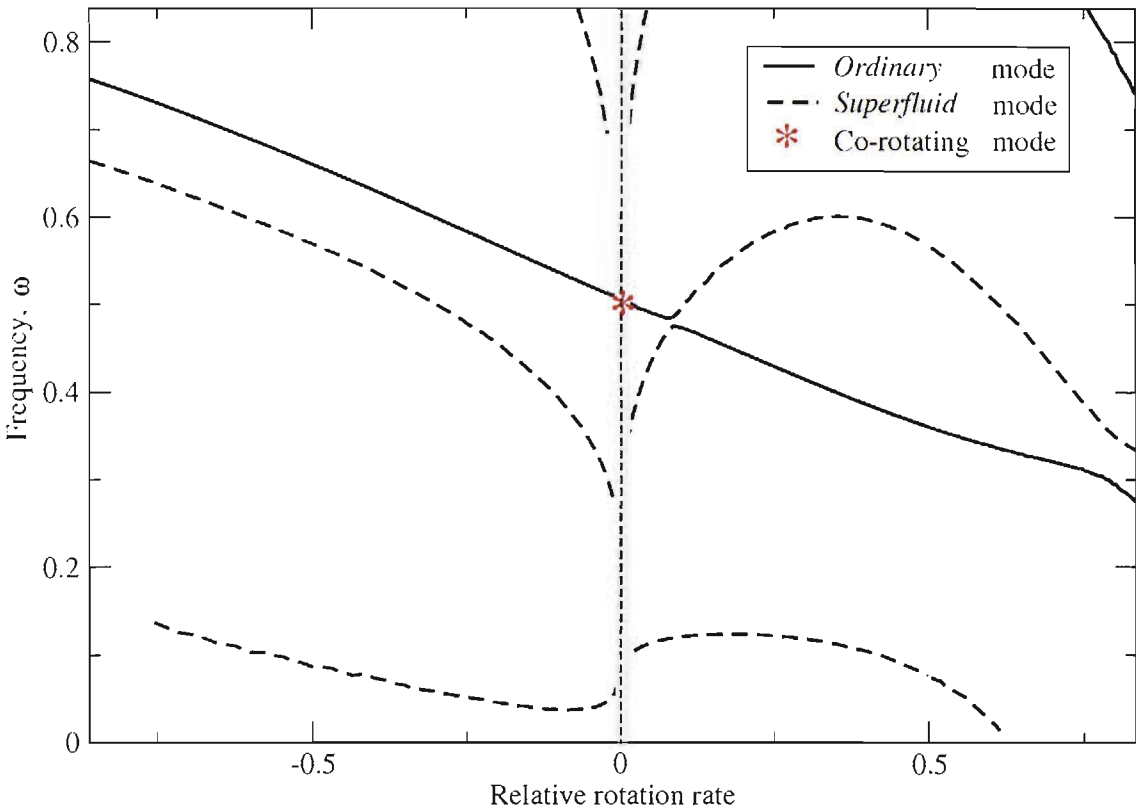

Figure 6.10: *The graph illustrates in detail how the frequency of the f modes, from Figure 6.9, vary with $\mathcal{R}$. We observe an avoided crossing between the ordinary-type mode and the superfluid-type mode. The crossing coincides with an exchange in mode properties. After such a crossing the ordinary-type mode will become a superfluid-type mode and vice-versa. We find it difficult to resolve our solutions close to $\mathcal{R} = 0$, and hence the shaded area in the figures represents the undetermined region. The parameters in this example are $\alpha = -0.01$ and $K = 0.1$.*

the ordinary and superfluid eigenfunctions, ψ_o and ψ_{sf}, of each of these four modes. At point A we observe that the eigenfunction is dominated by the ψ_o part which resembles an f mode. This is coupled to an ψ_{sf} part which is significantly smaller in magnitude and resembles a p_1 mode. Consequently the mode at point A is labelled an *ordinary*-type f mode. The eigenfunctions at point B on the other hand, also shown in Figure 6.14, are dominated by the ψ_{sf} part which we observe looks like a p_1 mode. Therefore, we classify this mode as a *superfluid*-type p_1 mode. After the crossing the lower mode, at point D, is dominated by the ψ_o part, resembling an f mode. We thus label this mode an *ordinary*-type f mode. The upper mode at point C, however, appears to have switched to a *superfluid*-type mode. The superfluid part of the solution, ψ_{sf}, looks like a p_1 mode but the ordinary part of the solution, ψ_o now also resembles a p_1 type mode. Prior to the avoided crossing the ψ_o part of *superfluid*-type mode looked like an f mode. However, if we investigate closer to the crossing there is a very small region after the switch takes place where ψ_o resembles an f mode. It is clear that the avoided crossing has resulted in an exchange in mode

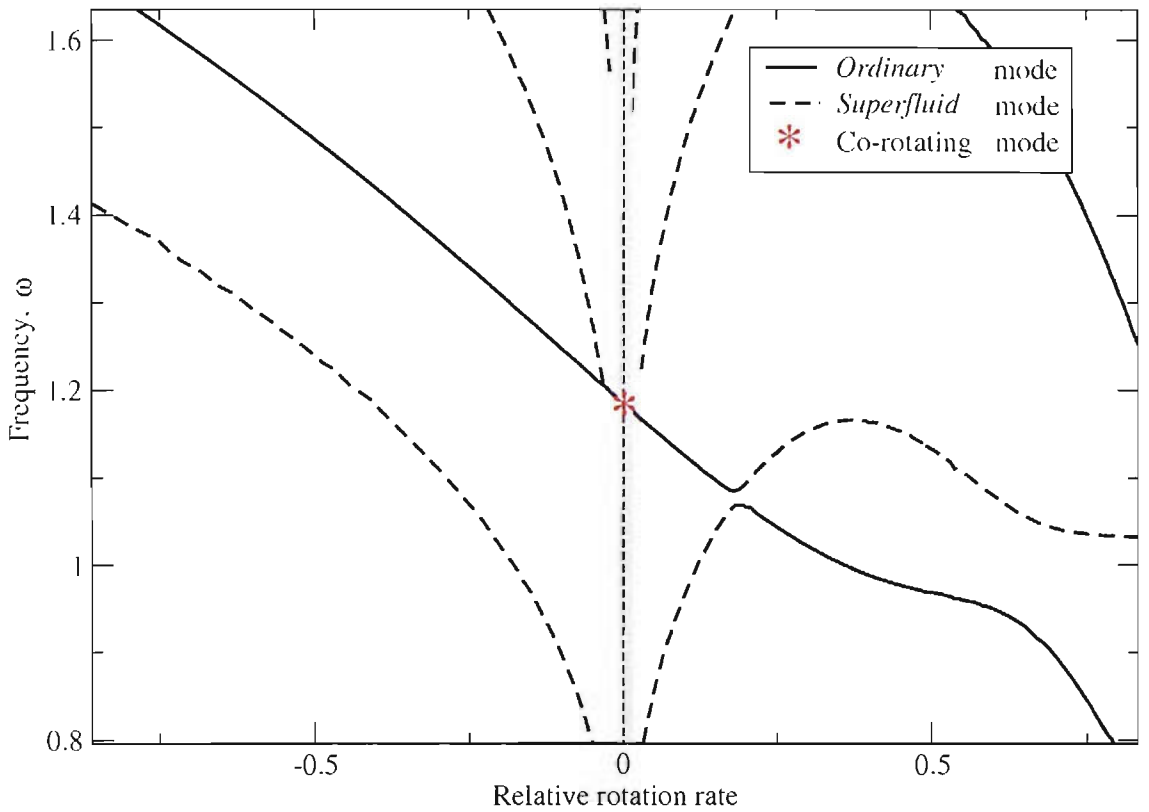

Figure 6.11: *The graph illustrates in detail how the frequency of the p_1 modes, from Figure 6.9, vary with $\mathcal{R}$. We observe an avoided crossing between the ordinary-type mode and the superfluid-type mode. The crossing coincides with an exchange in mode properties. The parameters in this example are $\alpha = -0.01$ and $K = 0.1$.*

properties. Similar exchanges in mode character resulting from avoided crossings have been observed in many neutron star mode investigations, [68], [13], [90].

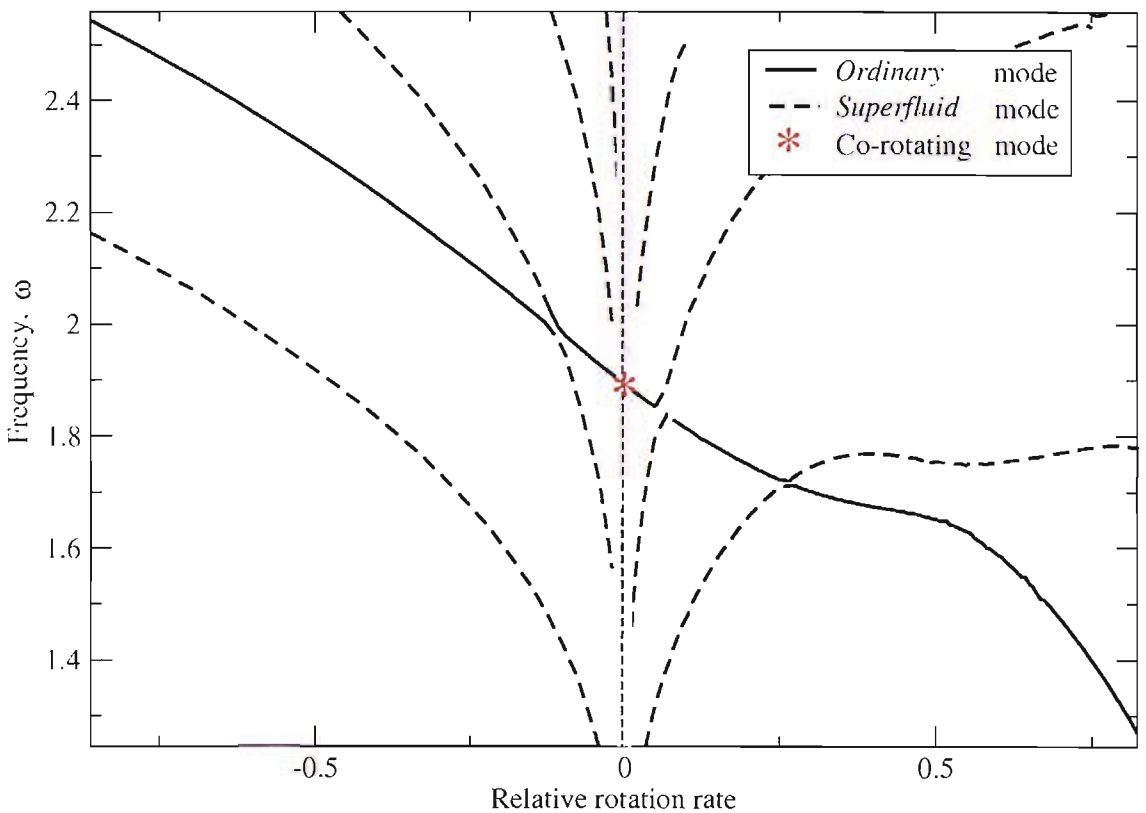

Figure 6.12: *The graph illustrate in detail how the frequency of the p_2 modes, from Figure 6.9, vary with $\mathcal{R}$. We observe avoided crossings between the ordinary-type modes and the superfluid-type modes. The crossing coincides with an exchange in mode properties. The parameters in this example are $\alpha = -0.01$ and $K = 0.1$.*

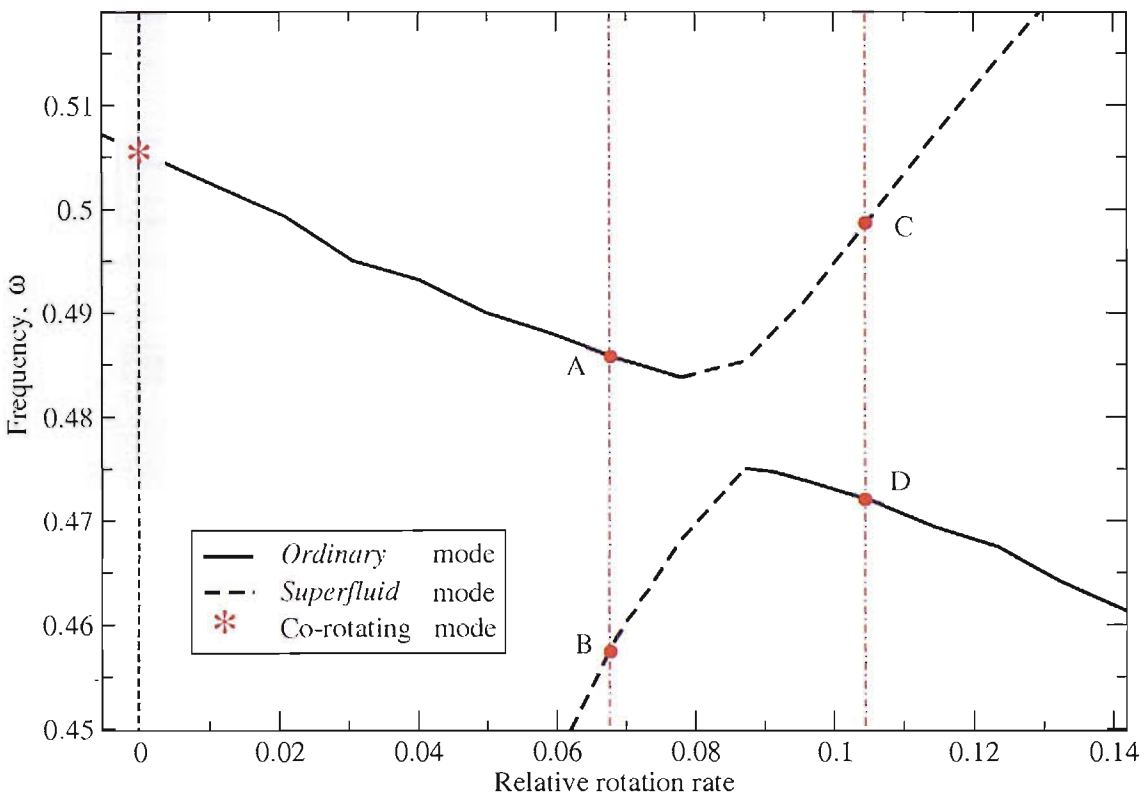

Figure 6.13: *We magnify the avoided crossing between the ordinary f mode and the superfluid p_1 mode to investigate the exchange of mode properties in more detail. Highlighted in the Figure are two particular points on either side of the crossing. Figure 6.14 shows the eigenfunctions at these different points illustrating the exchange in mode properties which results from avoided crossings.*

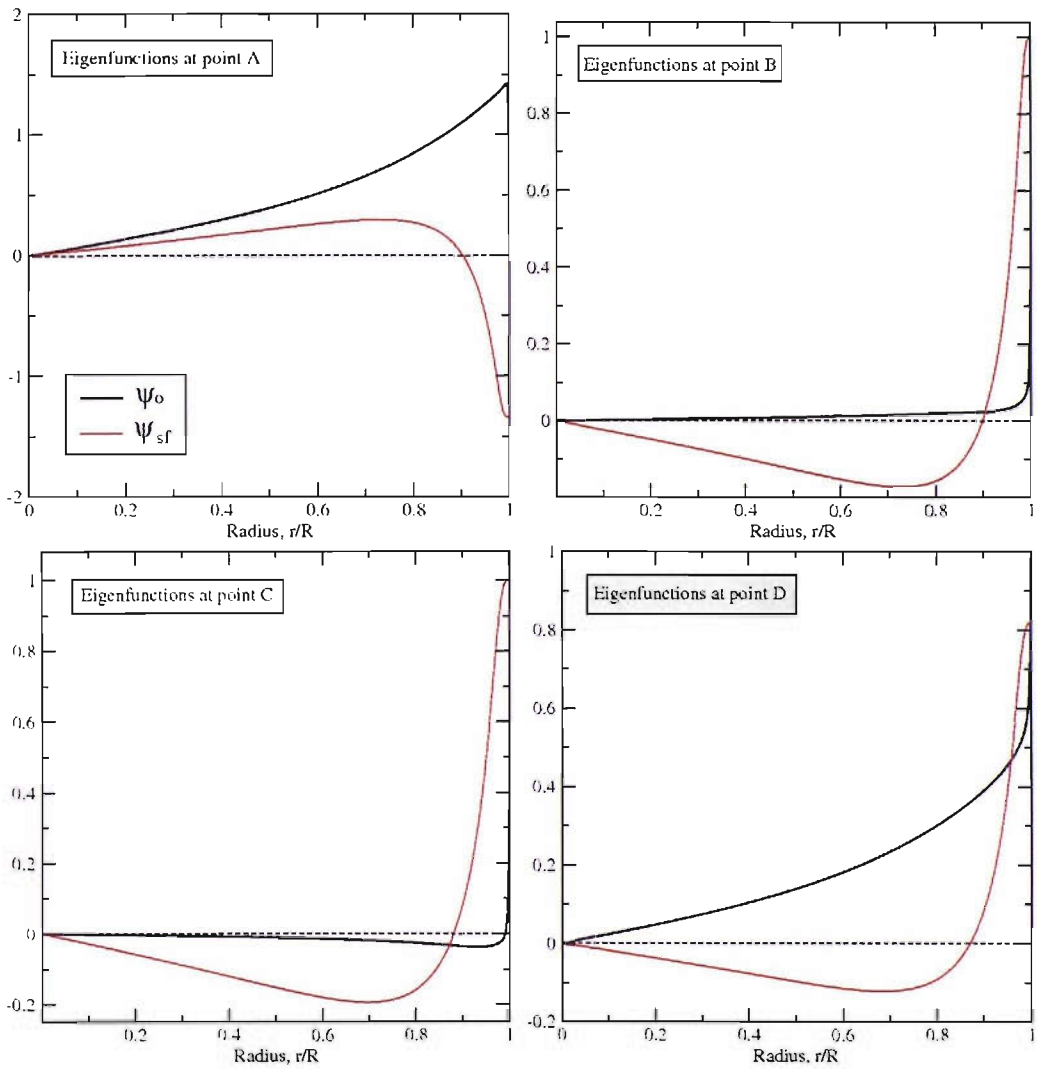

Figure 6.14: *The Figure shows the eigenfunctions at various points before and after an avoided crossing. On the top left are the eigenfunctions found at point A where we observe that the mode is dominated by the ψ_o part which resembles an f mode. This part is coupled to the superfluid part, ψ_{sf}. The eigenfunctions at point B on the other hand, which appear on the top right, are dominated by the ψ_{sf} part, resembling a p_1 mode. After the crossing at point D, seen on the bottom right, the dominant part of the mode is the ψ_o part, which looks like an f mode. However, the mode at point C, shown on the bottom left, appears to have switched to a superfluid-type mode dominated by the ψ_{sf} part, which resembles a p_1 mode. What we observe is that the avoided crossing coincides with an exchange of mode properties.*

In the single fluid case we found an infinite number of r modes, moving backward with respect to the fluid, lying closer together as they approached the line $\omega = -m\Omega$. In the two fluid case we introduce the possibility of two distinct rotation rates. There will therefore exist regions where modes can be moving forward with respect to one constituent and yet backward with respect to the other. These *mixed* regions are highlighted in Figure 6.15. In Prix et al (2004) [68] it was discov-

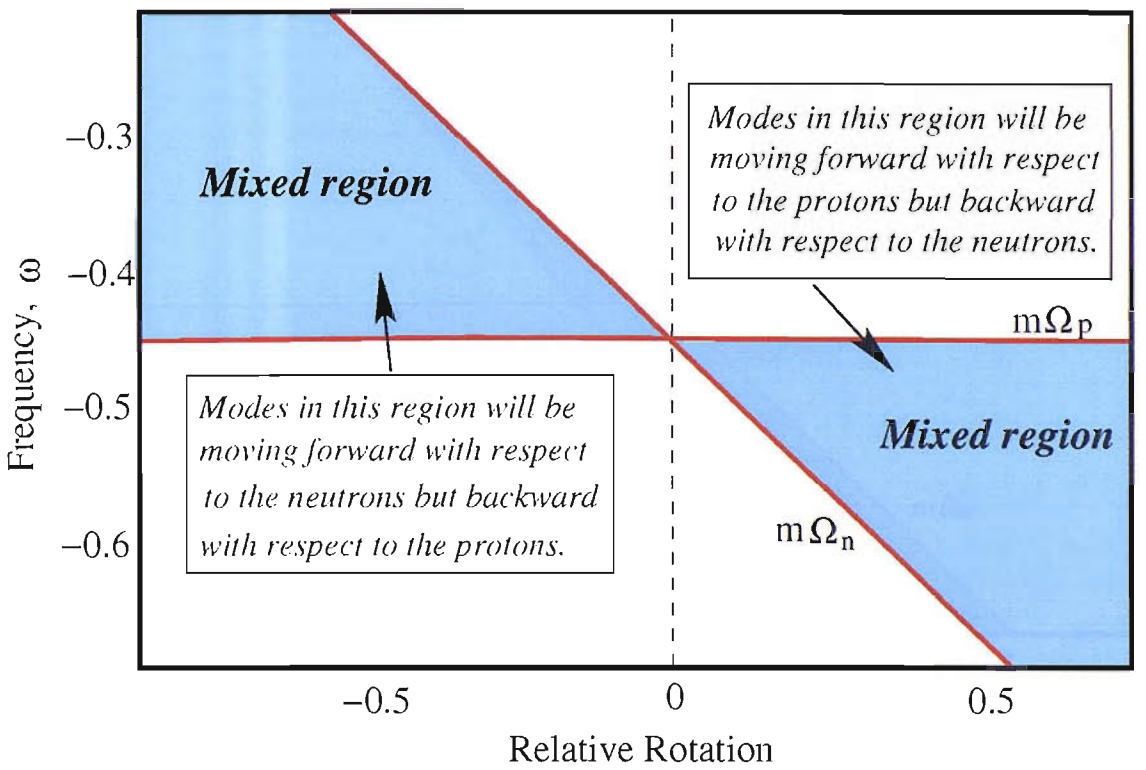

Figure 6.15: *Illustration of regions in which the modes are moving in opposite directions with respect to the two different fluids.*

ered that the onset of the two-stream instability in the inertial modes occurred in or close to these so-called *mixed* regions. This serves as a strong motivation to investigate closely the superfluid r modes in our cylindrical problem. Due to the vast number of modes arising in this area we choose to represent our results schematically, see Figure 6.16. What we discover is that rather than finding modes which are predominantly either *ordinary* or *superfluid*, we find modes which predominantly involve motion in either the proton fluid or the neutron fluid. The amplitude of oscillation of one fluid remains small while the other fluid dominates. What we notice from Figure 6.16 is that the r modes corresponding to the fluid which is rotating faster predominantly move forward with respect to both fluids, where as the modes corresponding to the slower fluid tend to exist either in the *mixed* region or in a region where they are moving backward with respect to both fluids. The greater the relative rotation the fewer the number of modes we observe moving in different

directions with respect to the two fluids. This confirms the results concerning the allowed regions of propagation in Section 6.5.1.

There are a number of particularly interesting features apparent in Figure 6.16 such as avoided crossings and the merger of two modes at a critical value of the relative rotation. We consider these details individually beginning by concentrating

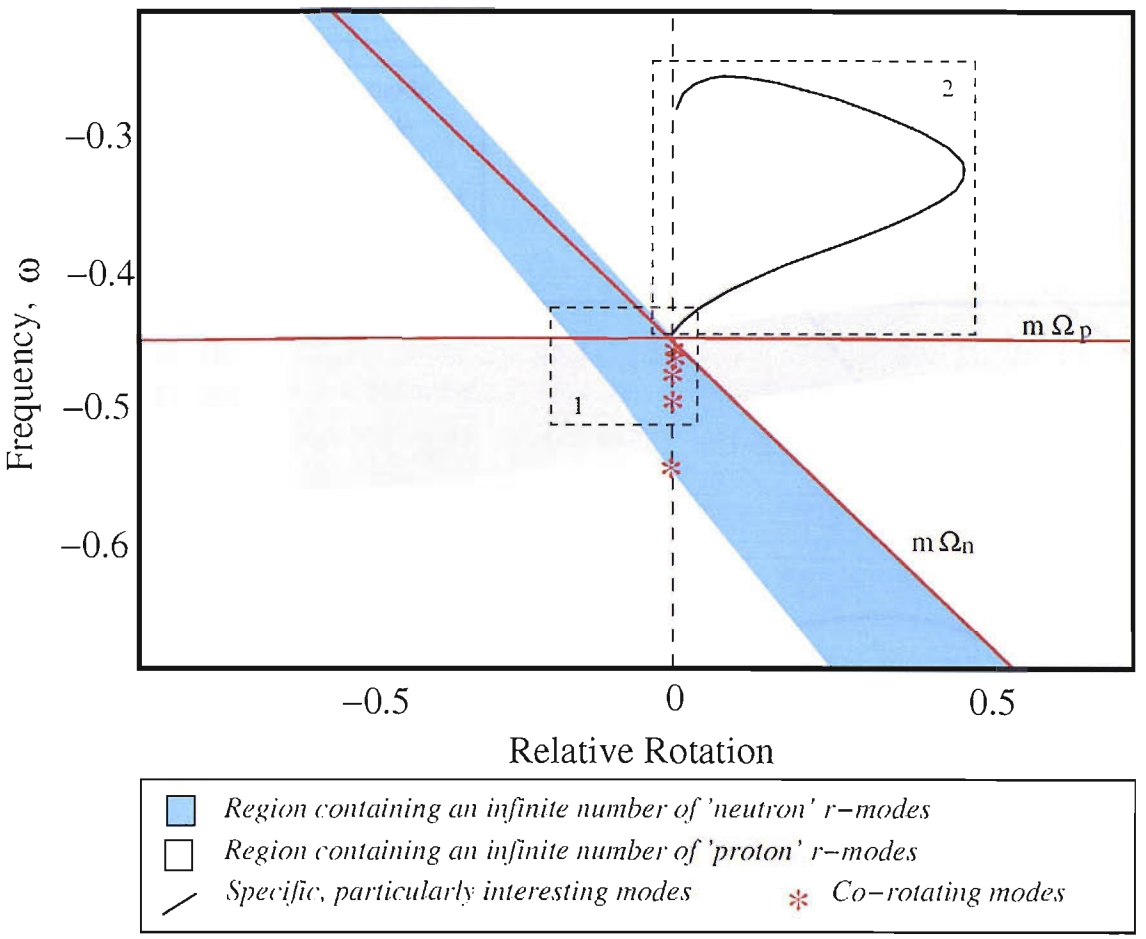

Figure 6.16: *A schematic representation of the r modes for the superfluid cylinder with entrainment, highlighting key features. For $\mathcal{R} < 0$, the proton r modes are observed to be moving forward with respect to both fluids. However the neutron r modes tend to exist either in the mixed region or in a region where they are moving backward with respect to both fluids. For $\mathcal{R} > 0$ the reverse is observed. This confirms the results concerning the allowed regions of propagation in Section 6.5.1. There are a number of particularly interesting features apparent in this Figure such as avoided crossings and the merger of two modes at a critical value of the relative rotation. These features are focused on in Figures 6.17 and 6.19. The parameters in this example are $K = 0.1$, $\alpha = -0.01$.*

on a single mode in the region close to co-rotation, highlighted as region 1. We observe avoided crossings between *proton*-type modes, see Figure 6.17. Since at co-rotation the frequencies of the *neutron*-type mode and the *proton*-type mode should be identical we hypothesise that the frequency of the *neutron*-type mode follows a

path from point (a) to point (b). We are unfortunately unable to resolve the modes in this region due to the fact that we have an infinite number of modes crossing each other. Figure 6.18 illustrates the modes at points 1 and 2 and emphasises why we label them as being either of *neutron*-type or *proton*-type. At point 1 the amplitude of the proton oscillation remains small while that of the neutron oscillation is large. At point 2 the reverse is observed.

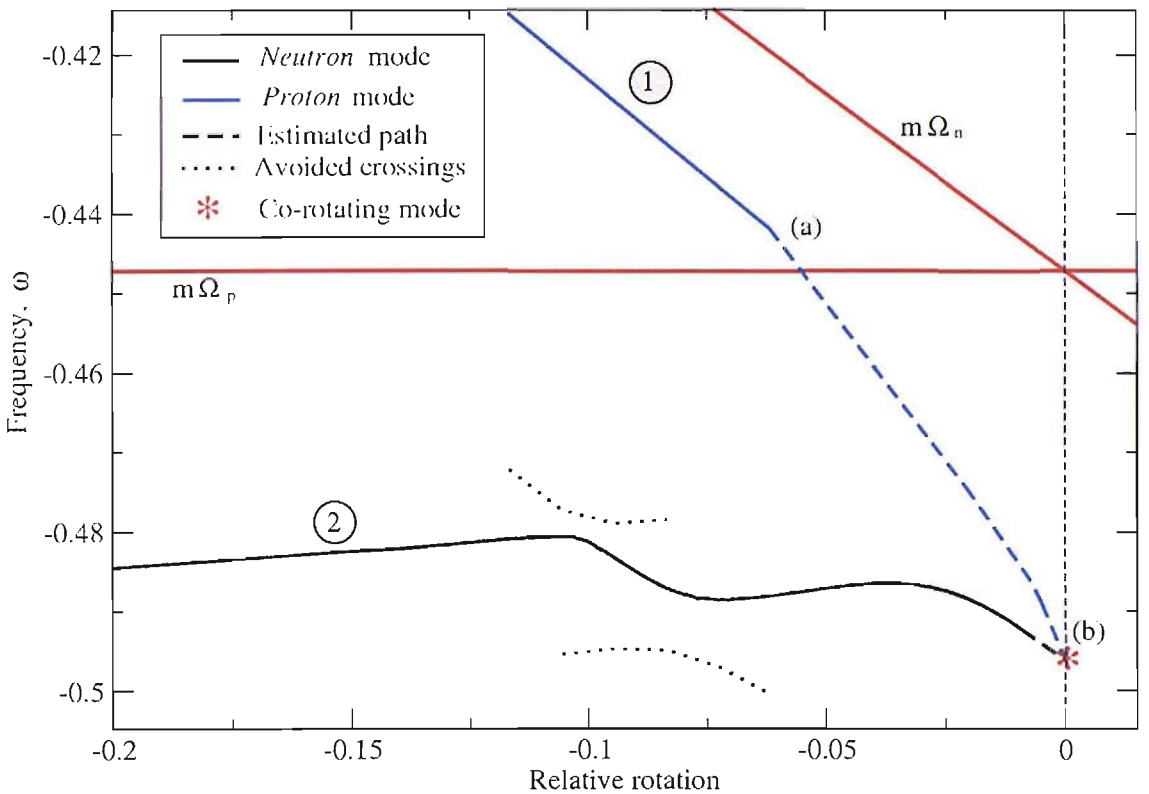

Figure 6.17: *This Figure is a magnification of region 1 from Figure 6.16 and highlights one particular r mode and its associated properties. We observe avoided crossings between proton-type modes. We are unable to resolve the modes in certain regions but since at co-rotation the frequencies of the neutron-type mode and the proton-type mode should be identical we hypothesise that the frequency of the neutron-type mode follows a path from point (a) to point (b). The parameters in this example are* $K = 0.1$, $\alpha = -0.01$.

We now investigate the modes in region two. What we observe is two modes merging at a critical value of the relative rotation. Further analysis shows that at this point the mode frequencies become complex signifying the onset of a dynamical instability. Figure 6.19 shows the real and the corresponding imaginary part of this unstable mode in detail. After the modes merge the mode frequencies are complex conjugates, and the real part of the mode appears to be approximately linear in $\mathcal{R}$. This agrees with results of Prix et al [68] where it was observed that when inertial modes merged, becoming unstable, the real part of the frequency was linear

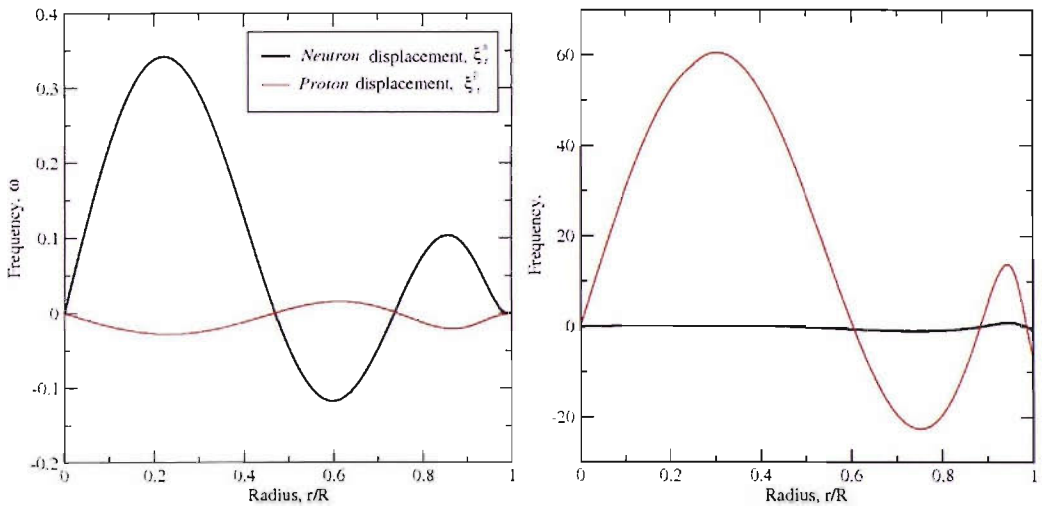

Figure 6.18: *This Figure illustrates the modes at points 1 and 2, from Figure 6.17 and emphasises why we label them as being either of neutron-type or proton-type. The graph on the left shows the modes at point 1 and we observe that the amplitude of the proton oscillation remains small while that of the neutron oscillation is large. At point 2, the graph on the right, the reverse is observed. The parameters in this example are* $K = 0.1$, $\alpha = -0.01$.

in $\mathcal{R}$. Figure 6.20 illustrates the modes before they merge. It appears that these are an f mode and a p_1 mode. Not only are these modes interesting due to their instability they are also unusual in that it is not clear how they should be classified. The *ordinary*-type and *superfluid*-type f and p_1 mode both occur at frequencies higher than this. The modes are also neither predominantly of one type or the other. However, what we observe is modes which become dynamically unstable at a critical value of the relative rotation signifying a *two-stream instability*.

6.5.4 The effect of entrainment

We investigate the effect of entrainment on the modes of our superfluid cylinder. Since we are ignoring perturbations to the gravitational potential, i.e. $\delta\Phi = 0$, when $\alpha = 0$ we observe two independent sets of modes; one in which the neutrons move while the protons remain stationary and another where the neutrons remain stationary and the protons oscillate. Introducing entrainment eliminates this independence and introduces a coupling between the modes. Figure 6.21 illustrates that as mode frequencies approach each other instead of crossing they tend to avoid each other. These avoided crossings are only observed between *ordinary*-type modes and *superfluid*-type modes and never between modes of the same type. During this process the *superfluid*-type modes which are predominantly counter-moving become predominantly co-moving and the *ordinary*-type modes become predominantly counter-moving. As we move toward the entrainment free case the frequency

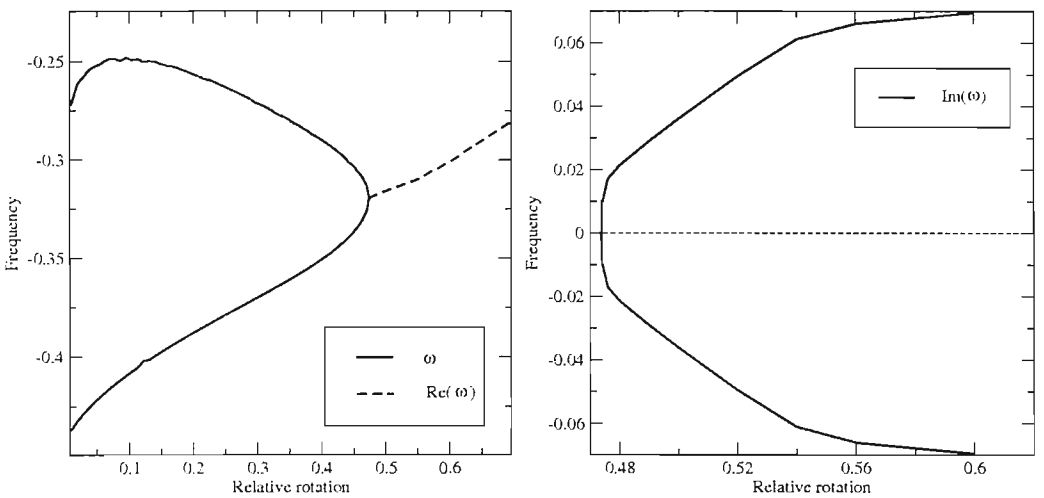

Figure 6.19: *This Figure shows the modes in region 2 of Figure 6.16. What we observe is two modes merging at a critical value of the relative rotation and becoming complex signifying the onset of a dynamical instability. On the left we see the real part of this unstable mode and on the right the corresponding imaginary part. After the modes merge the mode frequencies are complex conjugates, and the real part of the mode appears to be approximately linear in $\mathcal{R}$. The parameters in this example are $K = 0.1$, $\alpha = -0.01$.*

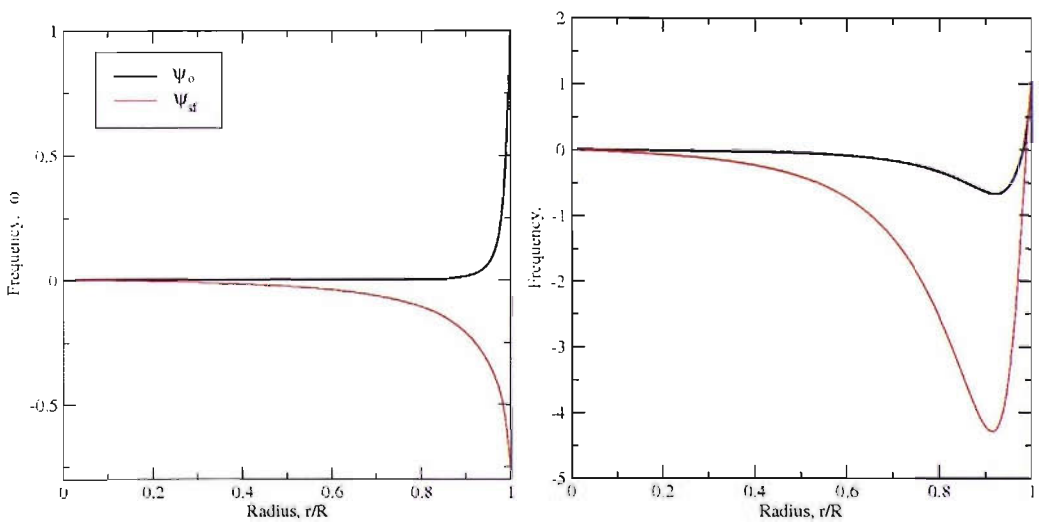

Figure 6.20: *This Figure illustrates the eigenfunctions of the modes before they merge. It appears that these are an f mode and a p_1 mode. The parameters in this example are $K = 0.1$, $\alpha = -0.01$.*

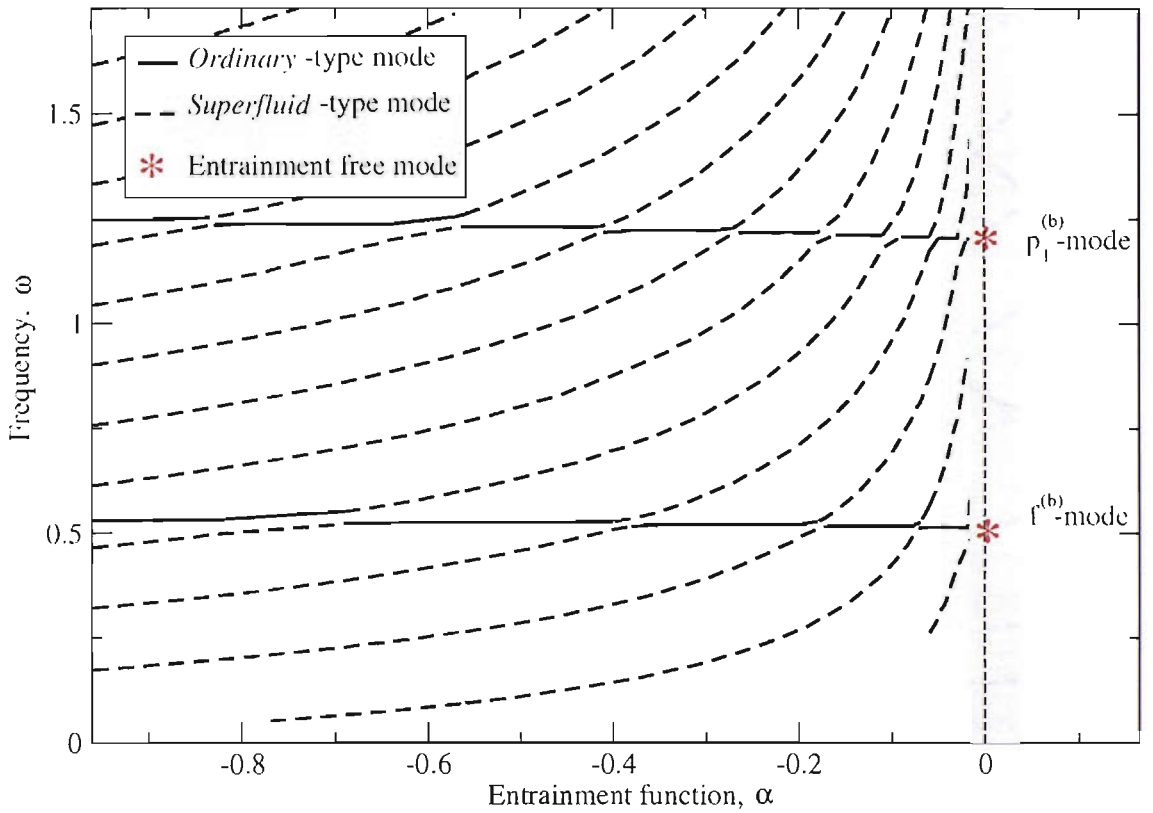

Figure 6.21: *This Figure illustrates the effect of varying the entrainment on the frequency of various modes. We observe many avoided crossings between ordinary-type modes and superfluid-type modes. During this process the superfluid-type modes which are predominantly counter-moving become predominantly co-moving and the ordinary-type modes become predominantly counter-moving. As we move toward the entrainment free case the frequency of the superfluid-type modes appear to approach infinity. Therefore close to $\alpha = 0$ the Figure becomes overcrowded and to prevent confusion we do not try to resolve it and shade this area in grey. Interestingly the frequency of both the ordinary-type f mode and p_1 mode are relatively unaltered by the introduction of entrainment. The parameters we consider in this example are $K = 0.1$ and $\mathcal{R} = 0.025$.*

of the *superfluid*-type modes approaches infinity. Therefore close to $\alpha = 0$ the Figure becomes overcrowded and to prevent confusion we do not try to resolve the region near $\alpha = 0$ and shade this area in grey. We have considered a case with approximately 90% neutrons and a small relative rotation, $\mathcal{R} = 0.025$, in order to relate the results to a neutron star. An interesting observation is that the frequency of both the *ordinary*-type f mode and p_1 mode are relatively unaltered by the introduction of entrainment. What does occur is the emergence of a vast number of *superfluid*-type modes. However, if we consider a much larger relative rotation, see Figure 6.22, the frequency of the *ordinary*-type modes are greatly affected. In this case distinguishing the mode type from the eigenfunctions becomes difficult as they no longer appear to be predominantly of one type or the other. The split which

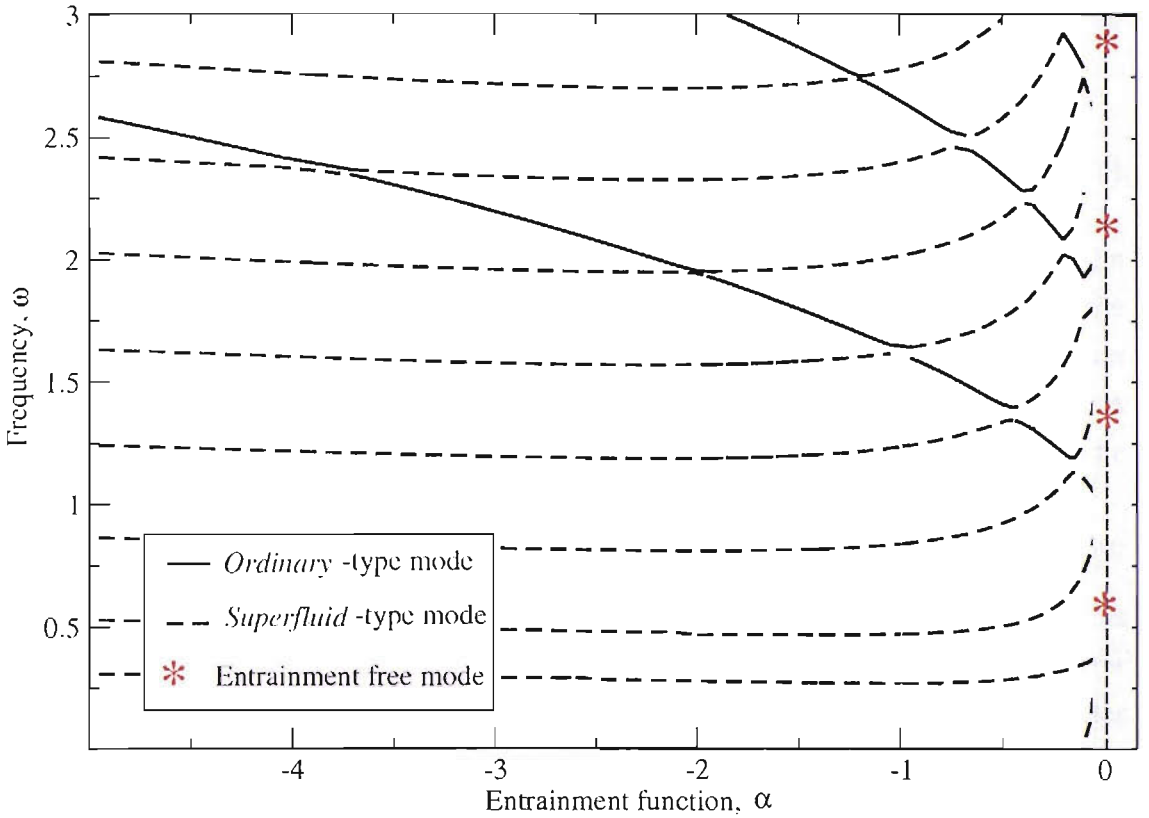

Figure 6.22: *This Figure illustrates the effect of varying the entrainment on the frequency of various modes. The relative rotation in this case is much larger than that in Figure 6.21 and we observe that in contrast to that case the frequency of the ordinary-type modes are greatly affected by α. The parameters we consider in this example are $K = 0.1$ and $\mathcal{R} = 0.4$.*

was so apparent when the relative rotation was low is now much less obvious. We classify the *ordinary*-type modes as those which extend from the entrainment free results and the *superfluid*-type modes as those which appear from infinity. What is clear is that there are two coupled families of modes which instead of crossing will avoid each other and exchange mode properties.

6.6 Frobenius expansions around the singular points

The singularities that are independent of the mode frequency and are present in the fourth order equation can be avoided if we consider negative entrainment. However, in neutron star cores the entrainment is generally expected to be positive so it is important to consider this case. We recall that these singularities arise when,

$$\pi_X = S = 0 \tag{6.48}$$

Where π_X is defined such that

$$\pi_X \xi_r^{X\prime\prime\prime\prime} + \beta_X \xi_r^{X\prime\prime\prime} + \chi_X \xi_r^{X\prime\prime} + \delta_X \xi_r^{X\prime} + \epsilon_X \xi_r^{X} = 0$$

If we consider a point $r = r_0$ where such a singularity exists, we can hypothesise that there is nevertheless a solution of the form,

$$\xi_r^X = x^\nu \sum_{n=0}^{\infty} a_n x^n \tag{6.49}$$

where $x = r - r_0$. We investigate the existence of such a solution by substituting the power series solution into the fourth order equation and equating coefficients of the dominant term (namely the term of lowest degree in x). If the resulting equation is independent of ν there is no solution of this form. Otherwise the equation is a polynomial in ν and we have an equation, known as the *indicial equation*, of the form

$$P(\nu) = 0 \tag{6.50}$$

Since we have a fourth order differential equation there will be four roots of this indicial equation. If the roots are distinct and no two of them differ by an integer there will be four linearly-distinct solutions of the type considered. If, on the other hand, two or more of the roots are equal or differ by an integer we require solutions of a less simple character.

We find that for our fourth order equation there are points where π_X vanishes but all the other coefficients remain non-zero. Since the coefficients depend on r we can power series expand them around the singularity, such that

$$\pi = \pi_1 x + \pi_2 x^2 + ... \tag{6.51}$$

$$\beta = \beta_0 + \beta_1 x + \beta_2 x^2 + ... \tag{6.52}$$

and the other coefficients take the same form as β. We have dropped the X subscript to avoid our equations becoming cluttered. What we find is an indicial equation of the form

$$\nu(\nu-1)(\nu-2)(\nu-3)\pi_1 + \nu(\nu-1)(\nu-2)\beta_0 = 0 \tag{6.53}$$

$$\nu(\nu-1)(\nu-2)[(\nu-3)\pi_1 + \beta_0] = 0 \tag{6.54}$$

giving

$$\nu_1 = 2 \tag{6.55}$$

$$\nu_2 = 1 \tag{6.56}$$

$$\nu_3 = 0 \tag{6.57}$$

$$\nu_4 = 3 - \frac{\beta_0}{\pi_1} \tag{6.58}$$

Assuming that β_0/π_1 is not an integer, we see that we have 3 roots which differ from each other by integer values. Since $\nu_1 > \nu_2 > \nu_3$ we have one solution of the form

$$w_1 = x^{\nu_1} u_1(x) = x^2 u_1(x) \tag{6.59}$$

where

$$u_1 = \sum_{n=0}^{\infty} a_n x^n \tag{6.60}$$

At this stage we introduce a function v such that there will also exist a solution w_2 where,

$$w_2 = w_1 \int v dx \tag{6.61}$$

Substituting this into equation (6.19) gives the following third order equation in v,

$$\pi w_1 v''' + (4\pi w_1' + \beta w_1)v'' + (6\pi w_1'' + 3\beta w_1' + \gamma w_1)v' + (4\pi w_1''' + 3\beta w_1'' + 2\gamma w_1' + \delta w_1)v = 0 \tag{6.62}$$

Assuming v takes the form

$$v = x^t \mu(x) = x^t \sum_{n=0}^{\infty} b_n x^n \tag{6.63}$$

we find the following roots,

$$t_1 = \nu_2 - \nu_1 - 1 = -2 \tag{6.64}$$

$$t_2 = \nu_3 - \nu_1 - 1 = -3 \tag{6.65}$$

$$t_3 = \nu_4 - \nu_1 - 1 = -\frac{\beta_0}{\pi_1} \tag{6.66}$$

Consequently there exists a solution,

$$\begin{aligned} w_2 &= w_1 \int x^{(\nu_2 - \nu_1 - 1)} \mu(x) dx \\ &= w_1 \int x^{-2} \mu(x) dx \\ &= w_1 \int (b_0 x^{-2} + b_1 x^{-1} + b_2 + b_3 x + ...) dx \\ &= w_1 [-b_0 x^{-1} + b_1 \log x + b_2 x + \frac{1}{2} b_3 x^2 + ...] \\ &= x^{\nu_1} [u_1(x) \log x + u_{22}(x)] \end{aligned} \tag{6.67}$$

where

$$u_{22}(x) = \sum_{n=0}^{\infty} c_n x^n \tag{6.68}$$

The third solution is dealt with in an identical fashion. Again we begin by assuming we can introduce a function y such that there is a third solution,

$$w_3 = w_2 \int y dx \tag{6.69}$$

Following an identical procedure we find,

$$\begin{aligned} w_3 &= w_2 \int x^{(\nu_3-\nu_1-1)}\psi(x)dx \\ &= w_2[\log x + u_{33}(x)] \\ &= x^{\nu_1}[u_1(x)(\log x)^2 + u_{32}(x)\log x + u_{33}(x)] \end{aligned} \tag{6.70}$$

where the functions $u(x)$ are all power series expansions which are analytic in the neighbourhood of $x = 0$. Therefore at the singular points we find solutions of the form

$$\xi_r^X = x^2 u_1(x) + x^2 [u_1(x)\log(x) + u_{22}(x)] + x^2\{u_1(x)[\log(x)]^2 + u_{32}(x)\log(x) + u_{33}(x)\} \tag{6.71}$$

Since $x\log(x)$ and $x[\log(x)]^2$ are regular at $x = 0$ we observe that ξ_r^X and its derivative at this point are in fact finite and continuous. However, the second derivative of ξ_r^X is singular. ξ_r^Y can be inferred from ξ_r^X using the following relation,

$$\xi_r^Y = a_1\xi_r^{X\prime\prime\prime} + a_2\xi_r^{X\prime\prime} + a_3\xi_r^{X\prime} + a_4\xi_r^X \tag{6.72}$$

where the coefficients are all regular functions of r. We deduce that since ξ_r^Y depend on the second and third derivatives of ξ_r^X it must be singular. Similarly we note that since we can write,

$$\xi_\phi^X = b_1\xi_r^{X\prime} + b_2\xi_r^X + b_3\xi_r^{Y\prime} + b_4\xi_r^Y \tag{6.73}$$

both ξ_ϕ^X and ξ_ϕ^Y are also singular at this point. We therefore conclude that at the singularity we have one function that is regular and three that are singular.

It may seem unphysical that there exists a singular solution at any point within our system. However, such complications arise in numerous mode calculations, [86] [68]. In Watts et al [86] the singularities resulted in a finite step in the first derivative which meant that there were two solutions that met the boundary conditions for any frequency; a continuous spectrum. Removing the step and looking simply at zero step solutions resulted in normal modes which could merge and become dynamically unstable. A major difference in their problem was that the singularity depended on the mode frequency. In this case the solution can be regularised by solving the

initial value problem. The resulting integral solution will not be singular and the continuous spectrum will have physical relevance.

Since our singularities do not depend on the mode frequency we can not take this approach to overcome our problem. In principle we could use the Frobenius analysis to find an approximation to the solution close to the singular point. We could obtain one solution either side of the singularity and subsequently integrate in both directions and match with solutions from the centre and surface. In practise we expect the equations to be regularised by physics, [58]. For example, introducing terms such as superfluid dissipation or viscosity may eliminate the singularities we have encountered. The singular nature of our equations is almost certainly a result of assumptions or approximations we have made in constructing our system and is unlikely to be a genuine physical phenomenon.

6.7 Constant $\varepsilon_{\rm n}$

In the previous section we took constant entrainment to mean that the entrainment function α is constant. The entrainment can also be characterised by the two dimensionless entrainment functions $\varepsilon_{\rm n}$ and $\varepsilon_{\rm p}$ such that,

$$\varepsilon_{\rm n} = \frac{2\alpha}{\rho_{\rm n}}$$

and

$$\varepsilon_{\rm p} = \frac{2\alpha}{\rho_{\rm p}} = \frac{\rho_{\rm n}}{\rho_{\rm p}}\varepsilon_{\rm n} \tag{6.74}$$

An alternative to choosing constant α is to choose $\varepsilon_{\rm n}$ to be constant. This is the approach taken by Prix et al [68] and Yoshida & Lee [89]. The explicit difference between the two possibilities is that in the first case we find that at the surface $\varepsilon_{\rm n} \to \infty$ and the entrainment terms dominate the perturbed Euler equations. However, in the second case we observe that α vanishes at the surface. The entrainment terms are no more influential at the surface than throughout the rest of the cylinder. It is interesting to investigate the effect this has on the system in a hope to determine whether or not the difficulties involving the singular points and the *artificial* surface condition are in any way connected to our decision to assume α constant. We begin with the Lagrangian perturbation equations for $\varepsilon_{\rm n}$ constant. In this case the equations are no longer symmetric with respect to n and p and in cylindrical coordinates may be written as,

$$\begin{aligned} &\frac{\partial \xi^{\rm n}_r}{\partial r} m\left(\frac{\partial \mu_{\rm n}}{\partial n_{\rm n}}\right)\rho_{\rm n} r^2 + \xi^{\rm n}_r\left[m\left(\frac{\partial \mu_{\rm n}}{\partial n_{\rm n}}\right) r(\rho_{\rm n} + r\frac{\partial \rho_{\rm n}}{\partial r}) - 2\Omega_{\rm n}\sigma_{\rm n} r^3 - 2\varepsilon_{\rm n} w_{\rm pn}\sigma_{\rm n} r^3\right] \\ + \;& \xi^{\rm n}_\phi\left[m^3\left(\frac{\partial \mu_{\rm n}}{\partial n_{\rm n}}\right)\rho_{\rm n} + m\sigma_{\rm n}^2 r^2(\varepsilon_{\rm n} - 1)\right] - \xi^{\rm p}_\phi\left[m\varepsilon_{\rm n}\sigma_{\rm p}^2 r^2\right] = 0 \end{aligned} \tag{6.75}$$

$$
\begin{aligned}
&\frac{\partial \xi_r^{\rm p}}{\partial r} r^2 \left[m \left(\frac{\partial \mu_{\rm p}}{\partial n_{\rm p}} \right) \rho_{\rm p}^2 + \varepsilon_{\rm n} w_{\rm pn} \sigma_{\rm p} r^2 (\rho_{\rm n} - \rho_{\rm p}) \right] \\
+ \;& \xi_r^{\rm p} \left[m \left(\frac{\partial \mu_{\rm p}}{\partial n_{\rm p}} \right) r \rho_{\rm p} (\rho_{\rm p} + r \frac{\partial \rho_{\rm n}}{\partial r}) - 2 \Omega_{\rm p} \sigma_{\rm p} \rho_{\rm p} r^3 + \varepsilon_{\rm n} w_{\rm pn} \sigma_{\rm p} r^3 (3\rho_{\rm n} - \rho_{\rm p}) \right] \\
&\xi_\phi^{\rm p} \left[m^3 \left(\frac{\partial \mu_{\rm p}}{\partial n_{\rm p}} \right) \rho_{\rm p}^2 - m \sigma_{\rm p}^2 \rho_{\rm p} r^2 + m \varepsilon_{\rm n} \sigma_{\rm p}^2 \rho_{\rm n} r^2 + 2 m^2 \varepsilon_{\rm n} w_{\rm pn} \sigma_{\rm p} r^2 (\rho_{\rm n} - \rho_{\rm p}) \right] \\
+ \;& \xi_\phi^{\rm n} \left[m \varepsilon_{\rm n} \sigma_{\rm n} r^2 (m w_{\rm pn} \rho_{\rm p} - \sigma_{\rm p} \rho_{\rm n}) \right] = 0
\end{aligned} \tag{6.76}
$$

$$
\begin{aligned}
&\frac{\partial^2 \xi_r^{\rm n}}{\partial r'^2} \left(\frac{\partial \mu_{\rm n}}{\partial n_{\rm n}} \right) \rho_{\rm n} r^3 + \frac{\partial \xi_r^{\rm n}}{\partial r} \left[\left(\frac{\partial \mu_{\rm n}}{\partial n_{\rm n}} \right) r^2 (\rho_{\rm n} + 2r \frac{\partial \rho_{\rm n}}{\partial r}) \right] \\
+ \;& \xi_r^{\rm n} \left[\left(\frac{\partial \mu_{\rm p}}{\partial n_{\rm p}} \right) r (r^2 \frac{\partial^2 \rho_{\rm n}}{\partial r^2} + r \frac{\partial \rho_{\rm n}}{\partial r} - \rho_{\rm n}) + r^3 \sigma_{\rm n}^2 (1 - \varepsilon_{\rm n}) \right] \\
+ \;& \frac{\partial \xi_\phi^{\rm n}}{\partial r} \left[m^2 \left(\frac{\partial \mu_{\rm n}}{\partial n_{\rm n}} \right) \rho_{\rm n} r \right] + \xi_\phi^{\rm n} \left[m^2 \left(\frac{\partial \mu_{\rm n}}{\partial n_{\rm n}} \right) (r \frac{\partial \rho_{\rm n}}{\partial r} - 2\rho_{\rm n}) + 2 m \sigma_{\rm n} r^2 (\Omega_{\rm n} + \varepsilon_{\rm n} w_{\rm pn}) \right] \\
- \;& \frac{\partial \xi_\phi^{\rm p}}{\partial r} \left[m \varepsilon_{\rm n} w_{\rm pn} \sigma_{\rm p} r^3 \right] + \xi_r^{\rm p} \left[\varepsilon_{\rm n} \sigma_{\rm n} \sigma_{\rm p} r^3 \right] = 0
\end{aligned} \tag{6.77}
$$

$$
\begin{aligned}
&\frac{\partial^2 \xi_r^{\rm p}}{\partial r'^2} \left(\frac{\partial \mu_{\rm p}}{\partial n_{\rm p}} \right) \rho_{\rm p}^2 r^3 + \frac{\partial \xi_r^{\rm p}}{\partial r} \left[\left(\frac{\partial \mu_{\rm p}}{\partial n_{\rm p}} \right) \rho_{\rm p} r^2 (2r \frac{\partial \rho_{\rm p}}{\partial r} + \rho_{\rm p}) \right] \\
+ \;& \xi_r^{\rm p} \left[\left(\frac{\partial \mu_{\rm p}}{\partial n_{\rm p}} \right) r \rho_{\rm p} (r^2 \frac{\partial^2 \rho_{\rm p}}{\partial r^2} + r \frac{\partial \rho_{\rm p}}{\partial r} - r \rho_{\rm p}) + \sigma_{\rm p}^2 r^3 (\rho_{\rm p} - \varepsilon_{\rm n} \rho_{\rm n}) \right] \\
+ \;& \frac{\partial \xi_\phi^{\rm p}}{\partial r} \left[m^2 \left(\frac{\partial \mu_{\rm p}}{\partial n_{\rm p}} \right) \rho_{\rm p}^2 r + m \varepsilon_{\rm n} w_{\rm pn} \sigma_{\rm n} r^3 (\rho_{\rm n} - \rho_{\rm p}) \right] \\
+ \;& \xi_\phi^{\rm p} \left[m^2 \left(\frac{\partial \mu_{\rm p}}{\partial n_{\rm p}} \right) \rho_{\rm p} (r \frac{\partial \rho_{\rm p}}{\partial r} - 2\rho_{\rm p}) + 2 m \Omega_{\rm p} \sigma_{\rm n} \rho_{\rm p} r^2 - 2 m \varepsilon_{\rm n} w_{\rm pn} \sigma_{\rm n} \rho_{\rm n} r^2 \right] \\
+ \;& \frac{\partial \xi_\phi^{\rm n}}{\partial r} \left[m \varepsilon_{\rm n} w_{\rm pn} \rho_{\rm p} r^3 (\sigma_{\rm n} - m w_{\rm pn}) \right] + \xi_r^{\rm n} \left[\varepsilon_{\rm n} \sigma_{\rm n} \rho_{\rm p} r^3 (\sigma_{\rm n} - m w_{\rm pn}) \right]
\end{aligned} \tag{6.78}
$$

Once again we have two first order equations and two second order equations. Following an identical procedure as in the α constant case we can make use of equations (6.75) and (6.76) to write equations (6.77) and (6.78) as,

$$
A \begin{pmatrix} \frac{\partial \xi_\phi^X}{\partial r} \\ \frac{\partial \xi_\phi^Y}{\partial r} \end{pmatrix} = B \begin{pmatrix} \xi_r^X \\ \xi_r^Y \\ \xi_\phi^X \\ \xi_\phi^Y \end{pmatrix}
$$

and thus write our system schematically as,

$$f_1^X \frac{\partial \xi_r^X}{\partial r} + f_2^X \xi_r^X + f_3^X \xi_\phi^X + f_4 \xi_\phi^Y = 0$$

and

$$g_1^X \frac{\partial \xi_\phi^X}{\partial r} + g_2^X \xi_r^X + g_3^X \xi_\phi^X + g_4^X \xi_r^Y + g_5^X \xi_\phi^Y = 0$$

We will again encounter singularities when f_1^X and g_1^X vanish. We can see immediately that,

$$f_1^{\rm n} = m \left(\frac{\partial \mu_{\rm n}}{\partial n_{\rm n}} \right) \rho_{\rm n} r^2 \tag{6.79}$$

and

$$f_1^{\rm p} = r^2 [m \left(\frac{\partial \mu_{\rm p}}{\partial n_{\rm p}} \right) \rho_{\rm p}^2 + \varepsilon_{\rm n} w_{\rm pn} \sigma_{\rm p} r^2 (\rho_{\rm n} - \rho_{\rm p})] \tag{6.80}$$

Clearly $f_1^{\rm n}$ will vanish at the centre and at the surface whereas $f_1^{\rm p}$ will vanish at the centre and at,

$$r = \sqrt{\frac{m \left(\frac{\partial \mu_{\rm p}}{\partial n_{\rm p}} \right) \rho_{\rm p}^2}{\varepsilon_{\rm n} w_{\rm pn} \sigma_{\rm p} (\rho_{\rm n} - \rho_{\rm p})}} \tag{6.81}$$

This singular point is similar to the f_1^X singularities we discovered in the constant α analysis, however, in that case both $f_1^{\rm n}$ and $f_1^{\rm p}$ vanished at such points. We recall that the g_1 singularities appear when the determinant of matrix A vanishes, i.e when

$$f_1^n f_1^p \sigma_{\rm n} \sigma_{\rm p} [r^2 (\varepsilon_{\rm n}^2 w_{\rm pn}^2 (\rho_{\rm p} - \rho_{\rm n})(\rho_{\rm p} - \rho_{\rm n} + \varepsilon_{\rm n} \rho_{\rm n})) + \left(\frac{\partial \mu_{\rm p}}{\partial n_{\rm p}} \right) \rho_{\rm p}^2 (\varepsilon_{\rm n} (\rho_{\rm p} + \rho_{\rm n}) - \rho_{\rm p})] = 0 \tag{6.82}$$

Once again we have both singular points which depend on the frequency and ones which depend solely on the background quantities. It is possible to chose a configuration where the frequency independent singularities do not exist, however, it is clear that we can also find parameter values where they are present. In this sense the problem is identical to that of the α constant problem. We can conclude that the singularities are not an artifact of the assumption that $\alpha = constant$.

In the α constant problem difficulties arose concerning how to define an appropriate condition at the surface. In the entrainment free case by insisting the equations were regular we were able to impose a suitable constraint. The aim, as we introduced a non-vanishing entrainment, was to identify a condition which satisfied the necessary equations but which also reduced to the regularity constraint as α became zero. The resulting procedure was to simply apply the entrainment free condition for all α and allow the numerical routine to insist that the equations were satisfied. This appeared to be effective, see Section 6.2.2, although it remains slightly *artificial*. It is thus

interesting to investigate whether a more suitable surface condition is apparent in the $\varepsilon_{\rm n}$ constant case. Demanding equation (6.75) is regular at the surface we find,

$$\xi_r^{\rm n}(R)\left[m\left(\frac{\partial\mu_{\rm n}}{\partial n_{\rm n}}\right)\frac{\partial\rho_{\rm n}(R)}{\partial r}-2\Omega_{\rm n}\sigma_{\rm n}R-2\varepsilon_{\rm n}w_{\rm pn}\sigma_{\rm n}R\right]+\xi_\phi^{\rm n}(R)\left[m\sigma_{\rm n}^2(\varepsilon_{\rm n}-1)\right]$$
$$-\ \xi_\phi^{\rm p}(R)\left[m\varepsilon_{\rm n}\sigma_{\rm p}^2\right]=0 \tag{6.83}$$

Equation (6.76) is regular at the surface. Close to the surface we can approximate the densities as $\rho_X = c_X(R-r)$. Keeping only leading order terms in $R-r$ and noting that at the surface $\rho_{\rm p} = K\rho_{\rm n}$ we obtain,

$$\frac{\partial\xi_r^{\rm p}}{\partial r}\left[\varepsilon_{\rm n}w_{\rm pn}\sigma_{\rm p}R^2(\frac{1}{K}-1)\right]+\xi_r^{\rm p}\left[m\left(\frac{\partial\mu_{\rm p}}{\partial n_{\rm p}}\right)\frac{\partial\rho_{\rm n}}{\partial r}-2\Omega_{\rm p}\sigma_{\rm p}R+\varepsilon_{\rm n}w_{\rm pn}\sigma_{\rm p}R(\frac{3}{K}-1)\right]$$
$$+\ \xi_\phi^{\rm p}\left[-m\sigma_{\rm p}^2+\frac{m\varepsilon_{\rm n}\sigma_{\rm p}^2}{K}+2m^2\varepsilon_{\rm n}w_{\rm pn}\sigma_{\rm p}(\frac{1}{K}-1)\right]+\xi_\phi^{\rm n}\left[m\varepsilon_{\rm n}\sigma_{\rm n}(mw_{\rm pn}-\frac{\sigma_{\rm p}}{K})\right]=0 \tag{6.84}$$

For the case where $K=1$ this leads to,

$$\xi_r^{\rm p}(R)[m\left(\frac{\partial\mu_{\rm p}}{\partial n_{\rm p}}\right)\frac{\partial\rho_{\rm n}(R)}{\partial r}-2\Omega_{\rm p}\sigma_{\rm p}R+\varepsilon_{\rm n}w_{\rm pn}2\sigma_{\rm p}R]+\xi_\phi^{\rm p}(R)[-m\sigma_{\rm p}^2+m\varepsilon_{\rm n}\sigma_{\rm p}^2]$$
$$+\ \xi_\phi^{\rm n}(R)[m\varepsilon_{\rm n}\sigma_{\rm n}(mw_{\rm pn}-\sigma_{\rm p})]=0 \tag{6.85}$$

In this case we have two equations, (6.83) and (6.85), and four unknowns. Eliminating two of the variables leaves us with two free parameters which we can assign appropriately to give us two independent solutions at the surface, as required. It is clear to see that equations (6.83) and (6.85) also reduce to the necessary constraint as $\varepsilon_{\rm n}\to 0$. However, if $K\neq 1$ the equations are once again not singular at the surface and we have an identical problem to that found in the α constant case.

It is apparent that the decision to choose α constant as opposed to $\varepsilon_{\rm n}$ constant did not result in complications that were otherwise not present. The singular points and the problems at the surface seem to be generic of the problem and were not a result of our decision to use a constant entrainment.

6.8 Comparison with the Eulerian case

Finally we look at Eulerian perturbations in the two-fluid case with non-vanishing entrainment. Our motivation is to investigate whether or not a similar analysis in an Eulerian framework would free us of the complications involving the singular points and the surface problems encountered in the Lagrangian example. The system is described by equations (2.19), (2.20) and (2.21). A perturbation can be applied

to this system such that, $v_X^i \to v_X^i + \delta v_X^i$, $\Phi \to \Phi + \delta\Phi$, $\mu_X \to \mu_X + \delta\mu_X$, and $n_X \to n_X + \delta n_X$ giving the following linearised Euler equations,

$$\begin{aligned}
& \partial_t \delta v_X^i + v_X^j \nabla_j \delta v_X^i + \delta v_X^j \nabla_j v_X^i + g^{ij} \nabla_j (\delta\Phi + \delta\tilde{\mu}_X) \\
+ \; & \partial_t \left(\frac{2\alpha}{n_X} \delta w_i^{YX} \right) + \partial_t \left(-\frac{2\alpha}{n_X^2} w_i^{YX} \delta n_X \right) \\
+ \; & \delta v_X^j \nabla_j \left(\frac{2\alpha}{n_X} \delta w_i^{YX} \right) + \delta v_X^j \nabla_j \left(-\frac{2\alpha}{n_X^2} w_i^{YX} \delta n_X \right) + \delta v_X^j \nabla_j \left(\frac{2\alpha}{n_X} w_i^{YX} \right) \\
+ \; & \frac{2\alpha}{n_X} w_j^{YX} \nabla_i \delta v_X^j + \frac{2\alpha}{n_X} \delta w_j^{YX} \nabla_i v_X^j - \frac{2\alpha}{n_X^2} \delta n_X w_j^{YX} \nabla_i v_X^j = 0
\end{aligned} \tag{6.86}$$

the following perturbed continuity equations,

$$\frac{\partial \delta n_X}{\partial t} + \nabla_i (n_X \delta v_X^i) + \nabla_i (\delta n_X v_X^i) = 0 \tag{6.87}$$

and the perturbed Poisson equation,

$$\partial_i \partial^i \delta\Phi = 4\pi G m_{\mathrm{B}} (\delta n_X + \delta n_Y) \tag{6.88}$$

Our intentions in this Eulerian analysis are to compare the perturbed equations to the Lagrangian perturbation equations. We thus consider an identical configuration. That is we consider two fluids in a cylinder, which are free to rotate at different uniform velocities around the z-axis. We take the Cowling approximation, i.e. assume $\delta\Phi = 0$, and assume the entrainment function, α, is constant. We also note that in principle $\delta\tilde{\mu}_X$ depends on the entrainment. We can write it as follows,

$$\delta\tilde{\mu}_X = \left(\frac{\partial \tilde{\mu}_X}{\partial n_X} \right)_{n_Y, w^2} \delta n_X + \left(\frac{\partial \tilde{\mu}_X}{\partial n_Y} \right)_{n_X, w^2} \delta n_Y + \left(\frac{\partial \tilde{\mu}_X}{\partial w^2} \right)_{n_X, n_Y} \delta w^2 \tag{6.89}$$

where

$$\left(\frac{\partial \tilde{\mu}_X}{\partial w^2} \right)_{n_X, n_Y} = \frac{1}{m_{\mathrm{B}}} \left(\frac{\partial \alpha}{\partial n_X} \right)_{n_Y, w^2} \tag{6.90}$$

Since we are assuming α constant and since our equation of state is such that $\left(\frac{\partial \tilde{\mu}_X}{\partial n_Y} \right)_{n_X, w^2} = 0$ we find,

$$\delta\tilde{\mu}_X = \left(\frac{\partial \tilde{\mu}_X}{\partial n_X} \right)_{n_Y, w^2} \delta n_X \tag{6.91}$$

The result is six equations; two continuity equations and four equations obtained by taking components of each of the two Euler equations. The continuity equations become

$$\frac{\partial \delta v_r^X}{\partial r} (n_X r^2) + \delta v_r^X (n_X + n_X' r) r + \delta v_\phi^X (imn_X) + \delta n_X (i\sigma_X r^2) = 0 \tag{6.92}$$

Taking the ϕ component of the Perturbed Euler equations gives us,

$$\begin{aligned} & \delta v_r^X [2\Omega_X n_X^2 r + 2\alpha w_{YX} r(2n_X - n_X' r)] + \delta v_\phi^X \left[\sigma_X n_X^2 - 2\alpha\sigma_X n_X + 2m\alpha w_{YX} n_X\right] i \\ + \quad & \delta v_\phi^Y [\alpha\sigma_X n_X] i + \delta n_X \left[m \left(\frac{\partial \tilde{\mu}_X}{\partial n_X} \right) n_X^2 - 2\alpha\sigma_X w_{YX} r^2 \right] i = 0 \end{aligned} \tag{6.93}$$

and taking the r component

$$\begin{aligned} & \frac{\partial \delta v_\phi^X}{\partial r} [2\alpha w_{YX} r] - \delta v_\phi^X [2\Omega_X n_X + 4\alpha w_{YX}] + \delta v_r^X [\sigma_X r(n_X - 2\alpha)] i + \delta v_r^Y [2\alpha\sigma_X r] i \\ + \quad & \frac{\partial \delta n_X}{\partial r} \left[\left(\frac{\partial \tilde{\mu}_X}{\partial n_X} \right) n_X r \right] = 0 \end{aligned} \tag{6.94}$$

In the Lagrangian case our system consists of four first order equations in ξ_r^X and ξ_ϕ^X. In order to compare the Eulerian equations we eliminate δn_X from the above system by substituting from equation (6.93) into equations (6.92) and (6.94). In solving equation (6.93) for δn_X we observe that there is a singular point when,

$$\left[m \left(\frac{\partial \tilde{\mu}_X}{\partial n_X} \right) n_X^2 - 2\alpha\sigma_X w_{YX} r^2 \right] = 0 \tag{6.95}$$

This is identical to the f_1^X singularities in the Lagrangian case. What results from these substitutions is four equations which can be written schematically as,

$$a_1^X \frac{\delta v_r^X}{\partial r} + a_2^X \delta v_r^X + a_3^X \delta v_\phi^X + a_4^X \delta v_\phi^Y = 0 \tag{6.96}$$

and

$$b_1^X \frac{\partial \delta v_\phi^X}{\partial r} + b_2^X \frac{\partial \delta v_\phi^Y}{\partial r} + b_3^x \frac{\partial \delta v_r^X}{\partial r} + b_4^X \delta v_\phi^X + b_5^X \delta v_\phi^Y + b_6^X \delta v_r^X + b_7^X \delta v_r^Y = 0 \tag{6.97}$$

An important observation is that $a_1^X = f_1^X$. By substituting for $\partial \delta v_r^X / \partial r$ from equation (6.96) equation (6.97) becomes,

$$c_1^X \frac{\partial \delta v_\phi^X}{\partial r} + c_2^X \frac{\partial \delta v_\phi^Y}{\partial r} + c_3^X \delta v_\phi^X + c_4^X \delta v_\phi^Y + c_5^X \delta v_r^X + c_6^X \delta v_r^Y = 0 \tag{6.98}$$

Since X and Y are constituent indices we note that we now have one first order differential equation in δv_r^{n}, one in δv_r^{p}, and two coupled first order equations in $\delta v_\phi^{\mathrm{n}}$ and $\delta v_\phi^{\mathrm{p}}$. The differential equations in δv_r^X are singular at $a_1^x = f_1^X = 0$. This is identical to the situation in the Lagrangian analysis where the ξ_r^X differential equations are singular when $f_1^X = 0$. We can investigate the singularities of the δv_ϕ^X equations by writing the two equations which result from equation (6.98), one

with $X = \mathrm{n}$, $Y = \mathrm{p}$ and another with $X = \mathrm{p}$, $Y = \mathrm{n}$, as

$$A \begin{pmatrix} \frac{\partial \delta v_\phi^X}{\partial r} \\ \frac{\partial \delta v_\phi^Y}{\partial r} \end{pmatrix} = B \begin{pmatrix} \delta v_r^X \\ \delta v_r^Y \\ \delta v_\phi^X \\ \delta v_\phi^Y \end{pmatrix} \tag{6.99}$$

We recall that the singularities correspond to $det(A) = 0$. This gives the following condition for a singularity

$$\left(\frac{\partial \tilde{\mu}_\mathrm{n}}{\partial n_\mathrm{n}}\right)\left(\frac{\partial \tilde{\mu}_\mathrm{p}}{\partial n_\mathrm{p}}\right) n_\mathrm{n}^2 n_\mathrm{p}^2 (n_\mathrm{n} - n_\mathrm{p}) - 4\alpha^2 r^2 w_\mathrm{np}^2 \left[\left(\frac{\partial \tilde{\mu}_\mathrm{n}}{\partial n_\mathrm{n}}\right) n_\mathrm{n}^2 - \left(\frac{\partial \tilde{\mu}_\mathrm{p}}{\partial n_\mathrm{p}}\right) n_\mathrm{p}^2\right] = 0 \tag{6.100}$$

Once again these are singularities that depend solely on the background system and are independent of the frequency. We can choose parameter values where these singularities do not occur, however we can equally choose values where they are present. We conclude therefore that a Eulerian framework is no less problematic concerning singular points than the corresponding Lagrangian framework. It is also clear that since equations (6.96) are singular at $f_1^X = 0$ and not at the surface identical difficulties will be encountered defining an appropriate surface condition.

These results confirm that our choice to analyse oscillations and stability in a Lagrangian framework and defining constant entrainment as $\alpha = constant$ does not introduce unnecessary difficulties. The singularities and surface complications appear to be generic of the superfluid cylinder problem.

Chapter 7

Conclusions and future work

Various different secular and dynamical instabilities can in principle exist in rotating, superfluid systems. Throughout this thesis the oscillations and stability of such a system have been investigated in detail. By developing a Lagrangian perturbation framework, an initial step has been taken in constructing stability criteria for superfluids analogous to the single fluid results obtained by Friedman and Schutz [39]. It was shown that in the entrainment free, two-fluid case the onset of a radiation driven instability at a critical rate of rotation remains unchanged from the single fluid case. At present we have yet to fully develop the problem with non-vanishing entrainment. Since the inclusion of this effect introduces a much greater coupling between the two fluids constructing analogous stability criteria is an exciting yet highly challenging prospect. However, normal mode calculations show that the inclusion of entrainment gives rise to numerous interesting modes. Not only do we observe a new family of *superfluid* modes we also observe avoided crossings of modes and the presence of instabilities at critical values of the relative rotation. This provides motivation to continue the Lagrangian investigations with the hope of obtaining stability criteria in this complex, non-vanishing entrainment case.

Neutron stars are extremely complicated astrophysical objects, which to model fully requires an understanding of a vast range of physical extremes. General relativity, magnetic fields, supranuclear physics, particle physics and superfluidity are a few of the areas which must be considered in order to accurately describe these stars. Encompassing such an extensive range of physics into a single model is exceptionally challenging, and due to numerous uncertainties in each individual field unlikely to provide an accurate description of a real neutron star. Thus any analysis will have limitations and approximations which must be considered when making any conclusions about the astrophysical relevance of results obtained. Our investigations focused on the effect of superfluidity using a simple two-fluid model. Not only did we ignore general relativistic effects, magnetic fields and the presence of exotic

particles in the core we also neglected the presence of superfluid dissipative effects such as shear viscosity due to electron-electron scattering and mutual friction. For our instabilities to be important for real neutron stars the unstable modes must grow faster than the timescales related to this superfluid dissipation. The inclusion of these dissipative effects in our equations is highly nontrivial [61]. The approach to investigating their effect on damping times is to solve the simpler non-dissipative equations and calculate the damping time via the introduction of a real energy functional, E, such that,

$$\frac{1}{\tau} = -\frac{1}{2E}\frac{dE}{dt} \tag{7.1}$$

The appropriate energy functional can be found in Lindblom & Mendell (1995) [54]. They showed that mutual friction tends to stabilise the f mode CFS gravitational wave driven instability in a rotating Newtonian star. However, in a subsequent paper [55] they proved that the CFS r mode instability can be suppressed by mutual friction only for a small fraction of the presently accepted models. They conclude that it seems unlikely that mutual friction is acting to suppress this instability in neutron stars. It would be interesting to investigate this damping time for the secularly unstable r modes and f mode shown to exist within our entrainment free superfluid cylinder. From the results of Lindblom & Mendell we can hypothesise that while mutual friction will most likely suppress the f mode instability the unstable r modes remain and thus could occur in real neutron stars.

One reason unstable modes of oscillation are exciting is the prospect of the resulting gravitational wave emission reaching a detectable level. If this is achieved the information obtained could allow us to put constraints on the interior structure of the star. It is interesting therefore to investigate how efficient unstable oscillations of neutron stars are as a source of gravitational waves. To accurately model the gravitational waves from neutron stars we must use a relativistic description. This is incredibly demanding and we are often forced to work with Newtonian models and subsequently estimate the gravitational waves using a post-Newtonian approach. An estimate of the total energy radiated and the frequency of the signal may be enough to assess the relevance of an event as a gravitational wave source. We compare the effective gravitational wave strain h_c to the sensitivity of the various gravitational wave interferometers to investigate whether or not particular modes produce detectable signals. h_c can be evaluated using the following formula taken from Andersson (2003) [7].

$$h_c \approx 5 \times 10^{-22} \left(\frac{E}{10^{-3} M_\odot c^2}\right)^{1/2} \left(\frac{f}{1kHz}\right)^{-1/2} \left(\frac{D}{15Mpc}\right)^{-1} \tag{7.2}$$

where E is the energy radiated, f the frequency and D the distance to the source. In

Andersson, Comer & Grosart (2004) [12] we discuss the gravitational wave emission from the oscillations of superfluid neutron stars. We calculate the current multipoles for a superfluid star which could be used to analyse the rate at which the motion generates gravitational radiation and hence the relevance of instabilities. These results are for a spherical configuration. Since our cylindrical system is not a very accurate representation of the shape of a real star it is not constructive to investigate the gravitational wave emission associated with our instabilities. However, the presence of the instabilities in the cylinder do give hope that the same modes will exist in a sphere. If we can investigate the corresponding oscillations in this system it will then make sense to investigate the amplitude of the gravitational wave emission.

In principle a *two-stream instability* can operate in any system where there exists relative motion between two interpenetrating fluids. The onset of the instability occurs at a critical relative rotation [9]. It is unclear to what extent this instability may effect true physical neutron stars, it is however interesting to consider the possibilities. It has been suggested that it may be a trigger mechanism for neutron star glitches. It is generally believed that glitches occur as a rotation difference builds up between the normal fluid, which slows down due to magnetic braking, and the superfluid neutrons which are unable to slow down due to vortex pinning. Since both the *two-stream instability* and glitches are predicted to occur at a critical relative rotation it is intriguing to hypothesise as to whether the first can be the cause of the latter. The question we must consider is whether or not realistic data can instigate the onset of this instability. The difficulty with this lies in the fact that there are great uncertainties in the values of the true parameters. Neutron stars are such complicated objects that so far no firm conclusions have been drawn on typical values of the entrainment function and on how big a rotational lag can be built up in various regions of the star. Much further theoretical work in this area is an essential requirement if we hope to understand the true astrophysical relevance of our instabilities. At present, the estimated critical point for the occurrence of a glitch event is at a relative rotation of $\mathcal{R} = 5 \times 10^{-4}$, [59]. In our calculation, since the *superfluid*-type modes all originated from the origin, close to $\mathcal{R} = 0$ distinguishing between modes was exceptionally challenging. Unfortunately this physically realistic region occurred outside of the area we were able to resolve. Inclusion of the perturbation to the gravitational potential, $\delta\Phi$, would mean that even in the co-rotating case we should find both *ordinary* and *superfluid* modes and would not expect the sudden emergence of a vast number of modes as we move away from co-rotation. Therefore including $\delta\Phi$ is a possible way to clarify the uncertainties close to co-rotation. Another limitation lies in our inability to investigate the modes when the parameters were such that the g_1^X singularities appeared. This is disappointing as the conditions in a neutron star core lead to parameters whereby

this singularity exists. It is possible that an alternative numerical approach could allow investigations in this region. We used a FORTRAN numerical integration routine. However, Prix et al [68] worked with a spectral method code which by expanding the solution in terms of Chebyshev polynomials insists that the solution is regular. In fact they used the same linear eigenvalue solver package, LSB, that we made use of in Section 4.3. An identical approach in the superfluid problem is an appealing prospect. Provided the solution is in fact regular this approach will allow us to avoid the numerous difficulties introduced by the singularities in our system.

The Lagrangian perturbation framework developed for our two-fluid system is in no way limited to superfluid neutron stars. The equations developed could equally describe any system involving two interpenetrating fluids. Primarily they may be of significance in laboratory situations involving rotating superfluid helium. Thus stability criteria developed could be use to investigate instabilities, such as the *two-stream instability*, in laboratory experiments. What is particularly appealing is the possibility of testing the calculations and detecting these instabilities in a true physical system. Confirmation of the presence of the superfluid *two-stream instability* in a real system would give considerable confidence in the prediction of their existence in superfluid neutron stars. The primary consideration we must take to investigate this analogous system is to determine an appropriate equation of state. Investigating the relevant superfluid helium literature is therefore the first step we must take in order to move forward with this research.

As well as extending the Lagrangian stability analysis to develop criteria for the onset of instabilities in superfluid systems with entrainment there are also many improvements that should be made to our mode analysis. In particular investigations into the singularities, their physical relevance and how to deal with them in a numerical investigation is a key step which should be the focus of more work. Another question our mode analysis raised concerned an appropriate choice of surface condition. Since the situation where each species extends from the centre of the star all the way to the surface is not a physically realistic model we believe that any condition at this point would be in some sense artificial. While we therefore believe our boundary constraint is justified developing a more physically realistic condition would be desirable. Establishing a more realistic scenario would involve extending the protons and electrons further than the neutrons to mimic the configuration in the neutron star crust. A physically realistic model would also account for the elasticity of this crust. It is clear that there is still tremendous scope for improvements and extensions to our work to enhance our knowledge of the effects of superfluidity in neutron stars. It is also undeniably an area of research full of exciting prospects

for interesting astrophysical effects. Thus while investigations may be challenging it is evident that if we hope to understand the dynamics of these stars we must continue this work.

Appendix A

Numerical techniques

Various numerical techniques are employed throughout this work to obtain solutions to systems of differential equations. In this appendix the main two methods used will be outlined. These are spectral methods and numerical integration.

A.1 Solving eigenvalue problems with spectral methods

Solving boundary value, eigenvalue and time-dependent problems with spectral methods is a highly effective numerical technique. Using the harmonic oscillator as a simple illustration the general principles involved in solving ordinary differential equations with spectral methods are outlined in this chapter. For a more in depth introduction see [24], [45] & [30] while for a demonstration on how to use spectral methods to overcome some of the difficulties involved in solving equations which arise from astrophysical problems in the framework of general relativity see Bonazzola, Gourgoulhon,and Marck [22].

Solving differential equations with spectral methods involves expanding the solution to the equation in terms of some finite basis of polynomials or trigonometric functions. By minimising the residual function, which is obtained by substituting the approximate solution into the differential equation, the coefficients of the expansion can be found. The method uses test functions to ensure that the differential equation is satisfied as closely as possible by the truncated series expansion. There are three different methods classified according to the choice of test function. In the Galerkin method the test functions are identical to the trial functions and each function satisfies the boundary conditions. The Tau method also has the test functions equal to the trial functions but in this case they do not satisfy the boundary conditions, instead they are enforced by an additional set of equations. The third method is the pseudospectral method in which the test functions are delta functions located at certain grid points known as the collocation points. This introduction to spectral methods will focus on the final case.

Consider a differential equation defined by the operator $\mathbf{L}$ subject to certain boundary conditions,

$$\mathbf{L}u(x) = s(x) \tag{A.1}$$

The approximate solution, $\bar{u}$, can be written as,

$$\bar{u}_N(x) = \sum_{k=0}^{N} \tilde{u}_k \phi_k(x) \tag{A.2}$$

where $\tilde{u}_k$ are the coefficients of the expansion, $\phi_k(x)$ are the basis functions, and N is the number of basis functions considered. The residual function is defined as,

$$R = \mathbf{L}\bar{u} - s \tag{A.3}$$

By requiring R to vanish at certain collocation points, x_n, we arrive at the following equation,

$$\mathbf{L}\bar{u}(x_n) = s(x_n) \tag{A.4}$$

Solving this equation with appropriately chosen basis functions and collocation points is found to give accurate numerical approximations to the solution.

A.1.1 Choice of basis functions and collocation points

In most cases in spectral methods Chebyshev polynomials are taken as the basis set. They not only form a complete basis but are easy to compute and converge rapidly. The Chebyshev polynomials are defined by,

$$T_k(x) = \cos(k \cos^{-1} x) \tag{A.5}$$

A suitable choice of collocation points is the roots of the first neglected basis functions. For the Chebyshev polynomials this turns out to be,

$$x_n = \cos\left(\frac{\pi n}{N}\right) \tag{A.6}$$

A.1.2 Boundary conditions

There are two methods of imposing the boundary conditions in spectral method problems. The first involves adding additional explicit constraints,

$$\sum_{k=0}^{N} \tilde{u}_k \phi_k(y) = \alpha, \quad y \epsilon B \tag{A.7}$$

Where B is the boundary. The second involves selecting basis functions that independently satisfy the boundary conditions.

A.1.3 Eigenvalue problems

The pseudo-spectral collocation method can be used to approximate eigenvalues and eigenvectors of boundary value problems. Consider the eigenvalue problem,

$$\mathbf{L}u(x) = \lambda u(x) \tag{A.8}$$

If we represent the operator $\mathbf{L}$ in terms of a matrix, the eigenvalues an eigenvectors of the system are simply the eigenvalues and vectors of the matrix.

A.1.4 A simple example

Consider the harmonic oscillator equation,

$$\frac{d^2u}{dx^2} = -\lambda u \tag{A.9}$$

with the boundary condition being that $u(\pm 1) = 0$. For eigenvalue problems it is particularly useful to choose basis functions that independently satisfy the boundary conditions. This is because the explicit constraints which must be imposed if the basis functions do not satisfy the boundary conditions do not depend on λ and as such the matrix equation is not a standard eigenvalue problem. This introduces complications in the eigenvalue calculation which do not exist otherwise. Therefore we define the basis functions,

$$\phi_{2n}(x) = T_{2n}(x) - 1 \quad n = 1, 2, ... \tag{A.10}$$

$$\phi_{2n+1}(x) = T_{2n+1}(x) - x \quad n = 1, 2, ... \tag{A.11}$$

By rewriting this problem as a generalised eigenvalue problem, such that,

$$\mathbf{H}\underline{\mathbf{b}} = -\lambda \mathbf{B}\underline{\mathbf{b}} \tag{A.12}$$

we find the matrix representing the operator $\mathbf{H}$ is simply,

$$H_{ij} = \phi_{j+1,xx}(x_i) \tag{A.13}$$

The double x in the index represents the second derivative and the collocation points are,

$$x_i = -\cos\left(\frac{(2i-1)\pi}{2(N-2)}\right) \quad i = 1, 2, .., (N-2) \tag{A.14}$$

In this basis set

$$B_{ij} = \phi_{j+1}(x_i) \tag{A.15}$$

If we consider the case where $N = 4$ then this equation becomes

$$\begin{bmatrix} 4 & -16.97056274 \\ 4 & 16.97056274 \end{bmatrix} \underline{b} = -\lambda \begin{bmatrix} -1.000000001 & 1.414213563 \\ -1.000000001 & -1.414213563 \end{bmatrix} \underline{b} \tag{A.16}$$

This give $\lambda_1 = 12$, $\lambda_2 = 4$ and the corresponding eigenvectors,

$$\underline{b}_1 = \begin{bmatrix} 0 \\ 1.0 \end{bmatrix} \qquad \text{and} \qquad \underline{b}_2 = \begin{bmatrix} 1.0 \\ 0 \end{bmatrix} \tag{A.17}$$

It is now trivial to convert these eigenvectors back into an ordinary Chebyshev basis by noting that,

$$a_n = b_n \quad n \geq 2 \tag{A.18}$$

$$a_0 = -\sum_{n=1}^{2n \leq (N-1)} b_{2n} \tag{A.19}$$

$$a_1 = -\sum_{n=1}^{(2n+1) \leq (N+1)} b_{2n+1} \tag{A.20}$$

Where a_n is the coefficient in the Chebyshev series expansion, such that,

$$u(x) = \sum_{n=0}^{N-1} a_n T_n(x) \tag{A.21}$$

Therefore the solutions in the ordinary Chebyshev basis are,

$$\underline{a}_1 = \begin{bmatrix} 0 \\ -1 \\ 0 \\ 1 \end{bmatrix} \qquad \text{and} \qquad \underline{a}_2 = \begin{bmatrix} -1 \\ 0 \\ 1 \\ 0 \end{bmatrix} \tag{A.22}$$

Since it is straightforward to evaluate solutions to the harmonic oscillator problem analytically we investigate the accuracy of our spectral analysis. Figure A.1 shows the first two solutions to the harmonic oscillator equation for the $N = 4$ case and the corresponding exact solutions. While the solutions are obviously similar to the exact results it is clear that there are significant discrepancies. To obtain a greater degree of precision we increase the number of basis functions considered.

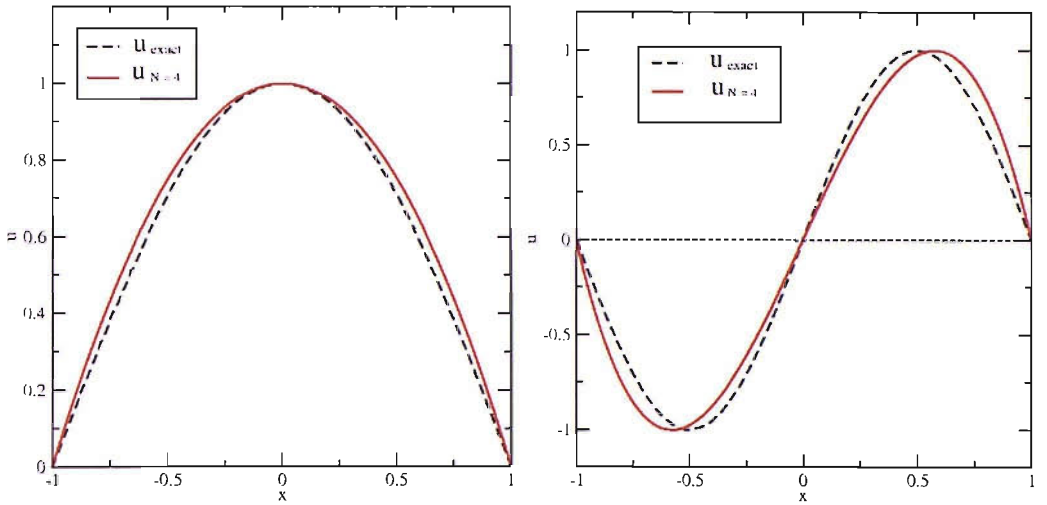

Figure A.1: *The first two exact eigenvectors for the harmonic oscillator problem, alongside our approximate solutions obtained using a pseudo-spectral method. In this example we consider only 4 basis functions, $N = 4$, and the exact solution is normalised such that $u_{max} = 1$. While the solutions are obviously similar to the exact results it is clear that there are significant discrepancies.*

Figure A.2 illustrates the effect of increasing N on the accuracy of the resulting eigenvalue solutions. As N increases the eigenvalues rapidly become within a few percent of the true solution. Since the y-axis is logarithmic and the graphs are roughly linear we conclude that the accuracy improves exponentially. However, for a particular value of N not all the calculated eigenvalues have a similar precision. With $N = 25$ for example we obtain 23 eigenvalues, 12 of which are accurate to within 0.2 percent and the rest of which are reasonably inaccurate. It appears that this is always the case, [24]. When applying a spectral method with $(N + 1)$ terms typically the lowest $N/2$ terms are accurate to within a few percent while the larger $N/2$ numerical eigenvalues differ from those of the differential equation by such large amounts as to be useless. The only reliable test is to repeat the calculation with different N and compare the results.

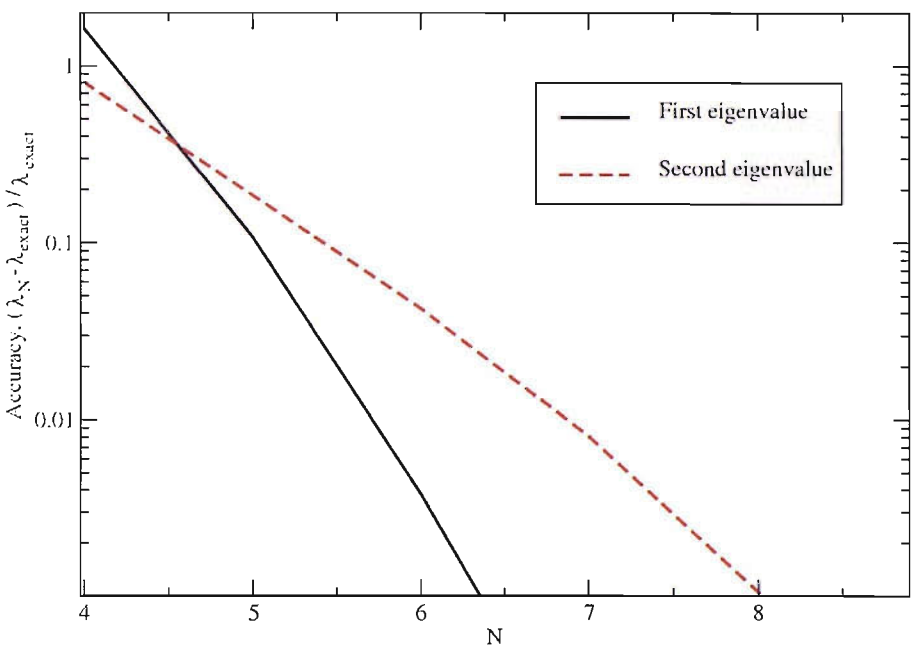

Figure A.2: *Illustration of the effect of increasing the number of basis functions considered on the accuracy of the solution. As N increases the eigenvalues rapidly become within a few percent of the true solution. Since the y-axis is logarithmic and the graphs are roughly linear we conclude that the accuracy improves exponentially.*

A.2 Numerical integration

Solutions to ordinary differential equations can be approximated numerically using numerical integration. A fourth order Runge-Kutta FORTRAN scheme is used to solve equations throughout this work. This is an extension of the Euler method using a trial step at the mid-point of an interval to cancel out lower order terms. Consider the curve in Figure A.3.

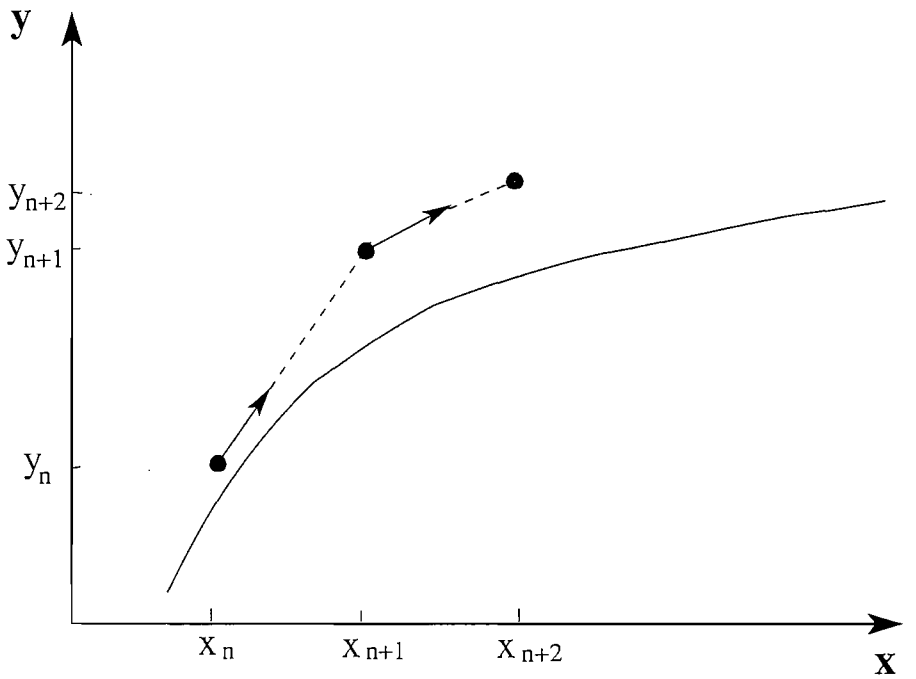

Figure A.3: *The Euler Method: Euler's method makes an approximation to the solutions at x_{n+1} by extrapolating along the derivative as shown by the dotted line.*

If we define the gradient at a particular point as $dy/dx = f(x, y)$, Euler's method makes an approximation to the solutions at x_{n+1} by extrapolating along the derivative as shown by the dotted line. Thus,

$$k_1 = hf(x_n, y_n) \tag{A.23}$$

$$y_{n+1} = y_n + k_1 + O(h^2) \tag{A.24}$$

Where h is the step size. The second order Runge-Kutta method adds one extra step, as we can see in Figure A.4. The second order formula is

$$k_2 = hf(x_n + \frac{1}{2}h, y_n + \frac{1}{2}k_1) \tag{A.25}$$

$$y_{n+1} = y_n + k_2 + O(h^3) \tag{A.26}$$

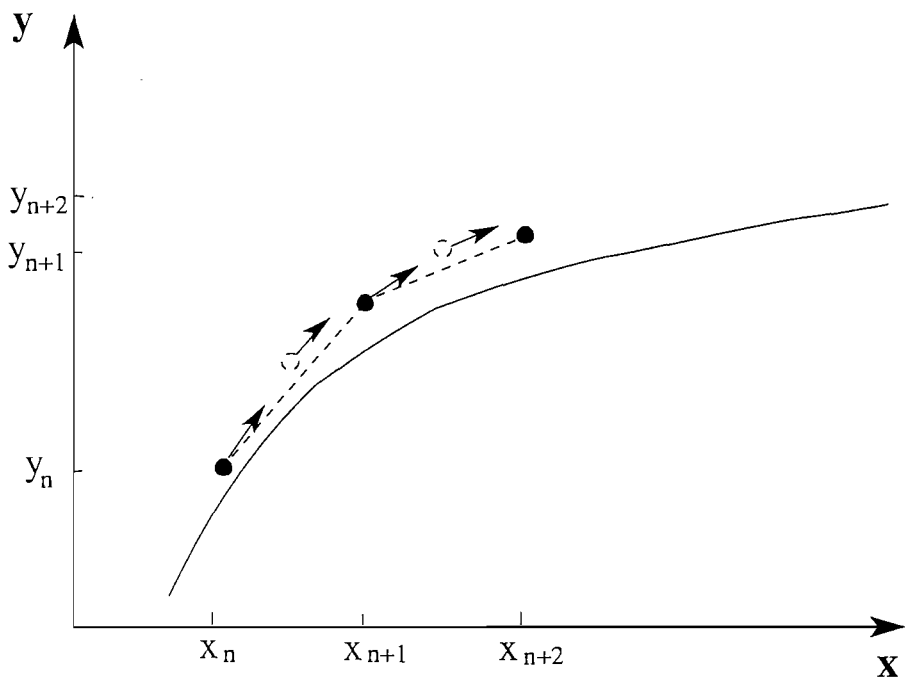

Figure A.4: *Second Order Runge-Kutta Method: This is an extension of the Euler method using a trial step at the mid-point of an interval to cancel out lower order terms.*

Extending this to the fourth order formula gives,

$$k_3 = hf(x_n + \frac{1}{2}h, y_n + \frac{1}{2}k_2) \tag{A.27}$$

$$k_4 = hf(x_n + \frac{1}{2}h, y_n + \frac{1}{2}k_3) \tag{A.28}$$

$$y_{n+1} = y_n + \frac{1}{6}k_1 + \frac{1}{3}k_2 + \frac{1}{3}k_3 + \frac{1}{6}k_4 + O(h^5) \tag{A.29}$$

This system is reasonably simple, robust and good for numerical solutions of differential equations.

Appendix B

Cylindrical coordinates

Many operators have a particularly simply form in Cartesian coordinates. However, in situations where a problem has a specific symmetry it is useful to use a coordinate system which exploits this symmetry. Much of the work in this PhD focuses on cylindrical systems and consequently we use cylindrical coordinates. This Appendix summarises the properties of such a coordinate system and explains how one can express operators using this framework.

Cylindrical coordinates are an extension of the two-dimensional polar coordinates to three-dimensions by superimposing a height, z, axis. The coordinates (r, ϕ, z) can be related to the Cartesian coordinates (x, y, z) through equations (B.1) to (B.3).

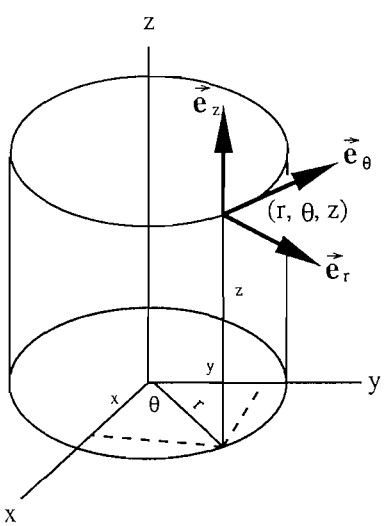

$$r = \sqrt{x^2 + y^2} \tag{B.1}$$

$$\tan\phi = \frac{y}{x} \tag{B.2}$$

$$z = z \tag{B.3}$$

Figure B.1: *Cylindrical Coordinates*

The basis vectors in this coordinate system are defined as a set of orthonormal vectors pointing in the direction of increasing coordinate values. In contrast with Cartesian basis vectors, the cylindrical basis vectors depend on position; $\vec{e}_r(\vec{x})$ points in different directions for points with coordinates $(x, y, z) = (1, 0, 0)$ and $(x, y, z) = (0, 1, 0)$. As a result we observe that in cylindrical coordinates the partial derivatives

of the basis vectors with respect to the coordinates do not necessarily vanish, i.e $\partial_i \vec{e}_j \neq 0$ for all i and j. The non-zero cases are,

$$\frac{\partial \vec{e}_r}{\partial \phi} = \vec{e}_\phi \quad \text{and} \quad \frac{\partial \vec{e}_\phi}{\partial \phi} = \vec{e}_r \tag{B.4}$$

We introduce the metric tensor, g_{ij} and the connection coefficients Γ^k_{ij} for cylindrical systems. These will be needed for various calculations throughout this thesis.

$$g_{ij} = \begin{bmatrix} 1 & 0 & 0 \\ 0 & r^2 & 0 \\ 0 & 0 & 1 \end{bmatrix} \tag{B.5}$$

and

$$\Gamma^r_{ij} = \begin{bmatrix} 0 & 0 & 0 \\ 0 & -r & 0 \\ 0 & 0 & 0 \end{bmatrix}, \Gamma^\phi_{ij} = \begin{bmatrix} 0 & \frac{1}{r} & 0 \\ \frac{1}{r} & 0 & 0 \\ 0 & 0 & 0 \end{bmatrix}, \Gamma^z_{ij} = \begin{bmatrix} 0 & 0 & 0 \\ 0 & 0 & 0 \\ 0 & 0 & 0 \end{bmatrix} \tag{B.6}$$

For cylindrical coordinates, the physical components are denoted $\{v_r, v_\phi, v_z\}$. Whenever a formula is derived in terms of the general covariant and contravariant vector components it is a good idea to convert the final result to physical coordinates and the physical basis. For cylindrical coordinates these conversion formulae are,

$$v_1 = v_r, \qquad v^1 = v_r, \tag{B.7}$$

$$v_2 = r v_\phi, \qquad v^2 = \frac{v_\phi}{r}, \tag{B.8}$$

$$v_3 = v_z, \qquad v^3 = v_z \tag{B.9}$$

B.1 Vector calculus in cylindrical coordinates

The vector operator ∇ can be expressed explicitly in cylindrical coordinates. We begin with the gradient,

$$\nabla f = \vec{e}_r \frac{\partial f}{\partial r} + \vec{e}_\phi \frac{1}{r} \frac{\partial f}{\partial \phi} + \vec{e}_z \frac{\partial f}{\partial z} \tag{B.10}$$

The divergence can be written as

$$\nabla \cdot \vec{F} = \frac{1}{r} \frac{\partial}{\partial r}(r F_r) + \frac{1}{r} \frac{\partial F_\phi}{\partial \phi} + \frac{\partial F_z}{\partial z} \tag{B.11}$$

The concept of divergence can be generalised to tensor fields where it is known as the covariant derivative, written

$$\nabla \cdot A = A^{\alpha}_{;\alpha} \tag{B.12}$$

The curl of a vector $\vec{F}$ is,

$$\nabla \times \vec{F} = \left(\vec{e}_r \frac{1}{r} \frac{\partial F_z}{\partial \phi} - \frac{\partial F_\phi}{\partial z} \right) + \vec{e}_\phi \left(\frac{\partial F_r}{\partial z} - \frac{\partial F_z}{\partial r} \right) + \vec{e}_z \frac{1}{r} \left(\frac{\partial}{\partial r} (r F_\phi) - \frac{\partial F_r}{\partial \phi} \right) \tag{B.13}$$

And finally we can write the scalar Laplacian as,

$$\nabla^2 f = \frac{1}{r} \frac{\partial}{\partial r} \left(r \frac{\partial f}{\partial r} \right) + \frac{1}{r^2} \frac{\partial^2 f}{\partial \phi^2} + \frac{\partial^2 f}{\partial z^2} \tag{B.14}$$

Appendix C

Solving the two-fluid Lane-Emden equation with Green's functions

A Green's function is an integral kernel that can be used to solve an inhomogeneous differential equation with boundary conditions.
We can rewrite the Lane-Emden equation for two fluids in a cylinder, equation (3.44) as

$$\bar{\theta}'' + \frac{1}{s}\bar{\theta}' + \bar{\theta} = f(s) \tag{C.1}$$

Where,

$$\bar{\theta} = (1 + K_{\rm n})\theta_{\rm n} \tag{C.2}$$

$$s = \sqrt{1 + K_{\rm n}}r \tag{C.3}$$

$$f(s) = 2\Omega_n^2 + R^2 Q_{\rm n} - \frac{Q_{\rm n}}{1 + K_{\rm n}}s^2 \tag{C.4}$$

and a prime represents a derivative with respect to s. The Green's function is a function $G(s, s_0)$ of the two variables s and s_0 that satisfies,

$$G'' + \frac{1}{s}G' + G = \delta(s - s_0) \tag{C.5}$$

If we can solve for this equation for $G(s, s_0)$, the Green's function, we can then obtain $\bar{\theta}(s)$ as follows. Equations (C.1) and (C.5) can be rewritten as,

$$\frac{1}{s}\frac{d}{ds}(s\bar{\theta}') + \bar{\theta} = f(s) \tag{C.6}$$

$$\frac{1}{s}\frac{d}{ds}(sG') + G = \delta(s - s_0) \tag{C.7}$$

(C.6) $\times G-$ (C.7) $\times\bar{\theta}$

$$G\frac{d}{ds}(s\bar{\theta}') - \bar{\theta}\frac{d}{ds}(sG') = sf(s)G - s\delta(s-s_0)\bar{\theta} \tag{C.8}$$

$$\frac{d}{ds}[Gs\bar{\theta}' - \bar{\theta}sG'] = sf(s)G - s\delta(s-s_0)\bar{\theta} \tag{C.9}$$

If we now integrate this equation from $0 \rightarrow S$, , where $S = \sqrt{1+K}R$,

$$[Gs\bar{\theta}' - \bar{\theta}sG']_0^S = \int_0^S sf(s)Gds - s_0\bar{\theta}(s_0) \tag{C.10}$$

We can chose the term in the square bracket to equal zero leaving,

$$s_0\bar{\theta}(s_0) = \int_0^S sf(s)Gds \tag{C.11}$$

Rearranging and relabelling gives

$$\bar{\theta}(s) = \frac{1}{s}\int_0^s s_0 f(s_0)G(s,s_0)ds_0 \tag{C.12}$$

Thus once we know G we can obtain $\bar{\theta}$. To solve for G we note that for $s \neq s_0$ we have

$$G'' + \frac{1}{s}G' + G = 0 \tag{C.13}$$

and therefore

$$G(s,s_0) = AJ_0(s) + BY_0(s) \tag{C.14}$$

Where $J_0(s)$ and $Y_0(s)$ are Bessel functions.

$$s < s_0 \qquad G^-(s,s_0) = \alpha J_0(s) \tag{C.15}$$

$$s > s_0 \qquad G^+(s,s_0) = AJ_0(s) + BY_0(s) \tag{C.16}$$

Where the first result is achieved by noting that $Y_0(s)$ is singular at $r = 0$. These two results must be consistent with each other and since $G(s,s_0)$ is continuous they must equate at $s = s_0$,

$$\alpha J_0(s_0) = AJ_0(s_0) + BY_0(s_0) \tag{C.17}$$

Another condition we can impose on $G(s,s_0)$ is that $G(S,s_0) = 0$, i.e the Green's function goes to zero at the edge of the star.

$$A = -B\frac{Y_0(S)}{J_0(S)} \tag{C.18}$$

The final condition involves matching the derivatives of $G(r, r_0)$ at r_0. At this point the differential equation is

$$\frac{d}{ds}(sG') + sG = s\delta(s - s_0) \tag{C.19}$$

We can integrate this equation over the range $s_0 - \epsilon \rightarrow s_0 + \epsilon$, and then take the limit as $\epsilon \rightarrow 0$.

$$\int_{s_0-\epsilon}^{s_0+\epsilon} \left[\frac{d}{ds}(sG')\right] ds = s_0 \tag{C.20}$$

$$[sG']^{s=s_0+\epsilon} - [sG']^{s=r_0-\epsilon} = s_0 \tag{C.21}$$

$$[G']^{s=s_0+\epsilon} - [G']^{s=s_0-\epsilon} = 1 \tag{C.22}$$

$$G^{+'}(s, s_0) - G^{-'}(s, s_0) = 1 \tag{C.23}$$

$$\alpha J_1(s_0) - AJ_1(s_0) - BY_1(s_0) = 1 \tag{C.24}$$

Equations (C.17), (C.18), and (C.24) can be solved to give A,B, and α

$$A = -\frac{Y_0(s_0)J_0(s_0)}{J_0(S)[Y_0(s_0)J_1(s_0) - Y_1(s_0)J_0(s_0)]} \tag{C.25}$$

$$B = \frac{J_0(s_0)}{Y_0(s_0)J_1(s_0) - Y_1(s_0)J_0(s_0)} \tag{C.26}$$

$$\alpha = \frac{J_0(S)Y_0(s_0) - Y_0(S)J_0(s_0)}{J_0(S)[Y_0(s_0)J_1(s_0) - Y_1(s_0)J_0(s_0)]} \tag{C.27}$$

Equation (C.12) can then be applied giving,

$$\begin{aligned}\bar{\theta}(s) &= 2\Omega_n^2 + \frac{Q_{\rm n}S^2}{1+K_{\rm n}} + \left(1 + K_{\rm n} - 2\Omega_n^2 - \frac{Q_{\rm n}S^2}{1+K_{\rm n}}\right) J_0(s) \\ &- \frac{Q_{\rm n}\pi}{2(1+K_{\rm n})}[J_0(s)Y_0(s)(2ss_{2,-1}(s) - 2s^2) \\ &+ Y_0(s)J_1(s)(4s - s^3) + sJ_0(s)Y_1(s)s_{3,0}(s)]\end{aligned} \tag{C.28}$$

Where $s_{2,-1}(s)$ and $s_{3,0}(s)$ are the Lommel functions.

This exact solution can be compared to our numerical solution illustrating that our numerical results are accurate.

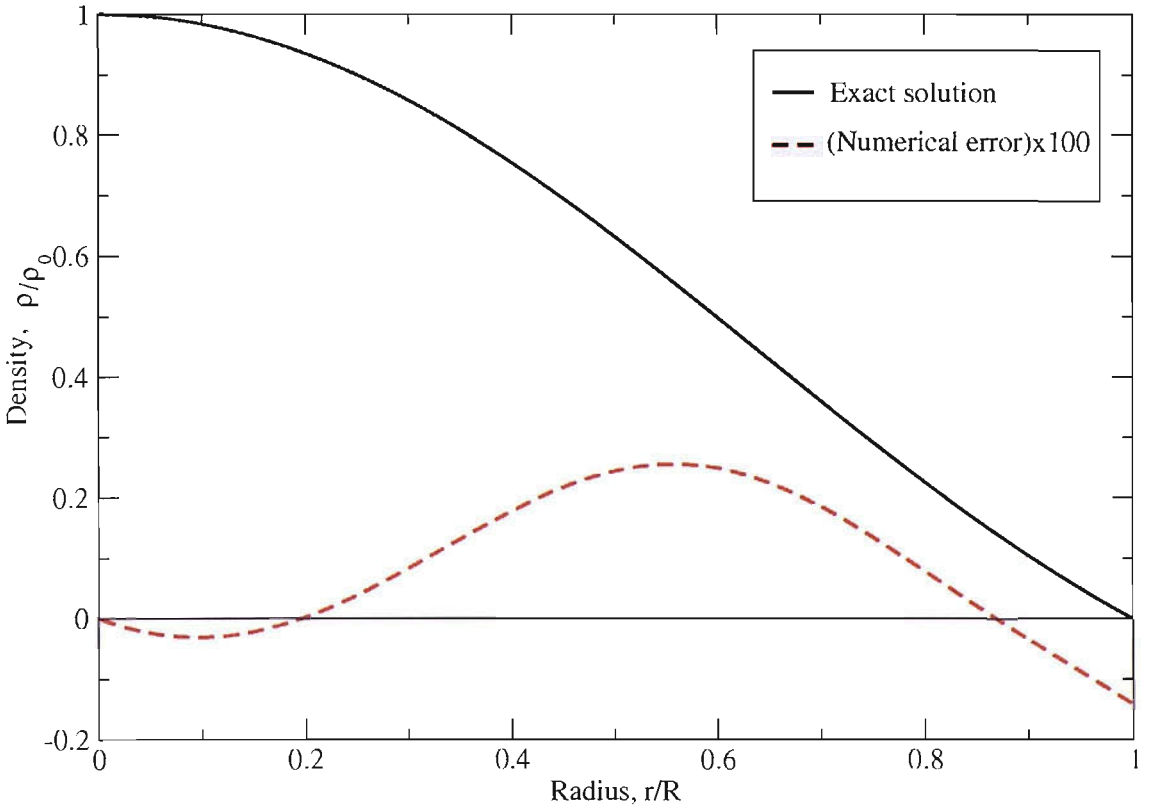

Figure C.1: *The Figure illustrates the exact solution to the two-fluid Lane-Emden equation and also the error in our numerical integration. The error is defined as difference between the exact solution and the numerical solution,* $\rho_{exact} - \rho_{numerical}$, *and in the Figure has been multiplied by* 100.

Bibliography

[1] Alpar, M. A.; Langer, S.A.; Sauls, J.A. *Rapid postglitch spin-up of the superfluid core in pulsars.* ApJ, **282**, 533-541, 1984.

[2] Alpar, M. A.; Cheng, K. S.; Pines, D. *Vortex creep and the internal temperature of neutron stars - Linear and nonlinear response to a glitch.* ApJ, **346,** 823-832, 1989.

[3] Alpar, M. A.; Chau, H. F.; Cheng, K. S.; Pines, David. *Postglitch relaxation of the VELA pulsar after its first eight large glitches - A reevaluation with the vortex creep model.* ApJ, **409,** 345-359, 1993.

[4] Ambartsumyan, V. A.; Saakyan, G. S. *The Degenerate Superdense Gas of Elementary Particles.* Astronomicheskii Zhurnal, **37,** 193, 1960.

[5] Anderson, D.; Fedele, R.; Lisak, M., *A tutorial presentation of the two stream instability and Landau damping.* American Journal of Physics, **69,** 1262-1266, 2001.

[6] Andersson N., *A New Class of Unstable Modes of Rotating Relativistic Stars.* ApJ, **502,** 708, 1998.

[7] Andersson, N., *TOPICAL REVIEW: Gravitational waves from instabilities in relativistic stars.* CQG, **20**, R105, 2003.

[8] Andersson, N.;Comer, G.L.; Prix, R., *Are Pulsar Glitches Triggered by a Superfluid Two-Stream Instability?* Phys. Rev. Lett., **90**., 091101, 2003.

[9] Andersson, N.,Comer, G.L. and Prix, R., *The superfluid two-stream instability.* MNRAS, **354,** 101-110, 2004.

[10] Andersson, N.; Comer, G.L., *On the dynamics of superfluid neutron star cores.* MNRAS, **328,** 1129-1143, 2001.

[11] Andersson, N.; Comer, G.L., *Probing Neutron-Star Superfluidity with Gravitational-Wave Data.* Phys. Rev. Lett., **87**, 24, 241101, 2001.

[12] Andersson, N.; Comer, G. L.; Grosart, K. *Lagrangian perturbation theory of non-relativistic rotating superfluid stars.* MNRAS, **355** 918-928, 2004.

[13] Andersson, N.; Comer, G. L.; Langlois, D. *Oscillations of general relativistic superfluid neutron stars.* Phys. Rev. D, **66,** 104002, 2002.

[14] Andersson N.; Kokkotas K.D., *The R-Mode Instability in Rotating Neutron Stars.* International Journal of Modern Physics D, 10, 381, 2001.

[15] Andersson N.; Kokkotas K.D. *Towards gravitational wave asteroseismology.* MNRAS, **299**, 1059-1068, 1998.

[16] Arnett, W.D.; Bowers, R.L., *A Microscopic Interpretation of Neutron Star Structure.* Astrophysical Journal Supplement, **33**, 415, 1977.

[17] Baade, W.; Zwicky, F. *Cosmic rays from super-novae.* Proceedings of the national academy of sciences of the United States of America, **20**, 259-236, 1934.

[18] Baldo, M.; Cugnon, J.; Lejeune, A.; Lombardo, U. *Proton and neutron superfluidity in neutron star matter.* Nucl. Phys. A, **536**, 349, 1992.

[19] Baym, G.; Pethick, C.; Pines, D.; Ruderman, M. *Spin up in neutron stars: The future of the Vela pulsar.* Nature, **224**, 872, 1969.

[20] Benhar, O.; Ferrari, V.; Gualtieri, L. *Gravitational wave asteroseismology reexamined.* Phys. Rev. D., **70**, 12, 124015, 2004.

[21] Bildsten L.; Ushomirsky G., *Viscous Boundary-Layer Damping of R-Modes in Neutron Stars.* ApJ, **529**, L33, 2000.

[22] Bonazzola, S.; Gourgoulhon, E.; Marck, J.A., *Spectral methods in general relativistic astrophysics.* arXiv:gr-qc/981109 v1, 1998.

[23] Borumand, M.; Joynt, R.; Kluzniak. *Superfluid densities in neutron star matter.* Phys. Rev. C., **54**, 2745, 1996.

[24] Boyd, J.P., *Chebyshev and Fourier Spectral Methods.* Dover Publications, Mineola, New York, 1999.

[25] Bradley, D.I., *Matter at low temperatures.* Lecture notes.

[26] Carter, B. *Relativistic Superfluid Models for Rotating Neutron Stars.* Lecture Notes in Physics, **578,** 54, 2001.

[27] Carter, B.; Chamel, N.; Haensel, P., *Entrainment coefficient and effective mass for conduction neutrons in neutron star crust: simple microscopic models.* Nuclear Physics A, **748,**, 675-697, 2005.

[28] Carter, B.; Chamel, N.; Haensel, P., *Entrainment coefficient and effective mass for conduction neutrons in neutron star crust: II Macroscopic treatment.* astro-ph/0408083, 2004.

[29] Carter, B.; Langlois, D.; Sedrakian, D.M., *Centrifugal buoyancy as a mechanism for neutron star glitches.* A&A, **361**, 795-802, 2000.

[30] Caunto, C.; Hussaini, M.Y.; Quarteroni, A.; Zang, T.A., *Spectral Methods in Fluid Dynamics.* Springer-Verlag, Berlin, 1998.

[31] Comer, G.L.; Langlois, D.; Lin, L.M.; *Quasi-normal modes of general relativistic superfluid neutron stars.* Phys. Rev. D., **60**, 10, 104025, 1999.

[32] Cowling T.G., *The non-radial oscillations of polytropic stars.* MNRAS, **101**, 367, 1941.

[33] Easson, I., *Postglitch behavior of the plasma inside neutron stars.* ApJ, **228**: 257-267, 1979.

[34] Epstein, R.I.; Baym, G., *Vortex pinning in neutron stars.* ApJ, **328**: 680-690, 1988.

[35] Epstein, R.I., *Acoustic properties of neutron stars.* ApJ, **333**, 880-894, 1988.

[36] Drazin, P.G.; Reid, W.H., *Hydrodynamic Stability.* Cambridge university press, 1991.

[37] Farley, D. T., *Two-Stream Plasma Instability as a Source of Irregularities in the Ionosphere.* Phys. Rev. Lett., **10,** 279-282, 1963.

[38] Feynman, R.P in *Progress in Low Temperature Physics.* ed. by C.J. Gorter, Vol. 1, p17, North Holland, Amsterdam.

[39] Friedman, J.L.; Schutz, B.F., *Lagrangian perturbation theory of non-relativistic fluids.* ApJ, **221**: 937-957, 1978.

[40] Friedman, J.L.; Schutz, B.F., *Secular instabilities of rotating Newtonian stars.* ApJ, **222**: 281-296, 1978.

[41] Fryer, C.L., *Stellar Collapse.* Book. Volume 302 Kluwer publishers, 2004.

[42] Glendenning, N.K, *Compact Stars.* Springer-Verlag, 1996.

[43] Goodstein, D.L., *States of Matter.*

[44] Gotthelf, E.V.; Zhang, W.; Marshall, F.E.; Middleditch, J.; Wang, Q.D., *Hiccups in the night: X-ray monitoring of the two Crab-like LMC pulsars.* Neutron stars in supernova remnants. ASP conference series, **9999**, 2002.

[45] Gourgoulhon, E., *Introduction to Spectral Methods* lecture notes, http://www.luth.obspm.fr.

[46] Hewish, A.; Bell, S.J.; Pilkington, J.D.; Scott, P.F.; Collins, R.A. *Observations of a rapidly pulsating radio source.* Nature, **217**, 709, 1968.

[47] Keesom, W.H., *Helium.* elsevier, Amsterdam, 1942.

[48] Khalanikov, I.M., *An Introduction to the Theory of Superfluidity.* Advanced Book Classics, 1965.

[49] Landau, L.D. and Lifshitz, E.M. *Fluid Mechanics 2nd edition*, Butterworth Heinemann, 1987.

[50] Langlois, D.; Sedrakian, D.M.; Carter, B., *Differential rotation of relativistic superfluid in neutron stars.* MNRAS, **297**, 1189-1201, 1998.

[51] Lee, U. *Nonradial oscillations of neutron stars with the superfluid core.* A & A, **303**, 515, 1995.

[52] Lee, U.; Yoshida, S., *r-Modes of Neutron Stars with Superfluid Cores.* ApJ, **586**, 403-418, 2003.

[53] Lindblom, L.; Mendell, G., *The oscillations of superfluid neutron stars.* ApJ, **421**, 689-704, 1994.

[54] Lindblom, L.; Mendell, G., *Does gravitational radiation limit the angular velocities of superfluid neutron stars?* ApJ, **444**, 804-809, 1995.

[55] Lindblom, L.; Mendell, G., *r-modes in superfluid neutron stars.* Phys. Rev. D., **61**, 104003, 2000.

[56] Lindblom L.; Owen B.J., *Effect of hyperon bulk viscosity on neutron-star r-modes* Phys.Rev.D., **65**, 063006, 2002.

[57] Lockitch K.L.; Andersson N.; Friedman J.L., *Rotational modes of relativistic stars: Analytic results.* Phys. Rev. D., **3**, 024019, 2001.

[58] Lockitch K.L.; Andersson N.; Watts, A.L., *Regularizing the r-mode problem for nonbarotropic relativistic stars.* CQG, **21**, 19, 4661-4675, 2004.

[59] Lyne, A.G.; Shemar, S.L.; Graham Smith, F., *Statistical studies of pulsar glitches.* MNRAS, **315**, 534, 2000.

[60] Ma, Z.X.; Dai, Z.G.; Lu, T., *Properties of neutron stars with hyperons in the relativistic mean field theory.* A&A, **366**, 532-537, 2001.

[61] Mendell, G., *Superfluid hydrodynamics in rotating neutron stars. I - Nondissipative equations. II - Dissipative effects.* ApJ, **380**, 515-540, 1991.

[62] Miller, M.C., *Twinkle, twinkle, neutron star.* Nature, **420**, 31-33, 2002.

[63] Miller, M.C.; Lamb, F.K.; Psaltis, D. *Constraints on the equation of state of neutron star matter from observations of kilohertz QPOs.* In The Active X-ray Sky, p. 123, 1998.

[64] Onsager, L., *Statistical hydrodynamics.* Nuovo Cimento Suppl., **6**, 279, 1949.

[65] Ostriker, J. *Cylindrical Emden and Associated Functions.* Astrophysical Journal Supplement, **11**, 167, 1965.

[66] Ostriker, J. *The Equilibrium of Polytropic and Isothermal Cylinders.* ApJ, **140**, 1056, 1964.

[67] Packard, R.E., *Pulsar Speedups Related to Metastability of the Superfluid Neutron-Star Core.* Phys.Rev.Lett. **28**, 1080, 1972.

[68] Prix, R.; Comer, G. L.; Andersson, N., *Inertial modes of non-stratified superfluid neutron stars.* MNRAS, **348**, 625-637, 2004.

[69] Prix, R.; Comer, G.L.; Andersson, N., *Slowly rotating superfluid Newtonian neutron star model with entrainment.* A&A **381**, 178-196, 2002.

[70] Prix, R., *Variational description of multifluid hydrodynamics: Uncharged fluids.* Phys. Rev. D., **69**, Issue 4, id. 043001, 2004.

[71] Prix, R.; Rieutord, M., *Adiabatic oscillations of non-rotating superfluid neutron stars.* A&A, **393**, 949-963, 2002.

[72] Robe, H., *Les oscillations non radiales des polytropes.* Annales d'Astrophysique. **31**, 549, 1968.

[73] Ruderman, M., *Neutron Star Crustal Plate Tectonics. III. Cracking, Glitches, and Gamma-Ray Bursts.* ApJ, **382**, 587, 1991.

[74] Ruderman, M.; Zhu, T.; Chen, K., *Neutron Star Magnetic Field Evolution, Crust Movement, and Glitches.* ApJ,**492**, 267., 1998.

[75] Sauls, J.A., in *Superfluidity in the interior of neutron stars.* Timing Neutron Stars, edited by Ögelman, H. and van den Heuvel, E.P.J., pp. 457-490, 1989.

[76] Sedrakian, A.; Wasserman, I., *Perturbations of self-gravitating, ellipsoidal superfluid-normal fluid mixtures.* Phys. Rev. D., **63**, 2, 024016, 2001.

[77] Sonin, E.B., *Magnus force in superfluids and superconductors.* Phys. Rev. B., **55**, 485-501, 1996

[78] Thompson, M.J. *Solar interior: Helioseismology and the Sun's interior.* Astronomy & Geophysics, **45**, 4.21-4.25, 2004.

[79] Tilley and Tilley, *Superfluidity and Superconductivity.*

[80] Unno, W., *non-radial oscillations of stars.* Tokyo Univ. Press, 1989.

[81] Veugelen, P. *Linear oscillations of differentially rotating self-gravitating cylinders.* A&A, **143**, 256-266, 1985.

[82] Veugelen, P. *Classification of normal modes of rotating cylindrical systems.* A&A, **143**, 458-460, 1985.

[83] Veugelen, P. *Equilibrium models of differentially-rotating polytropic cylinders.* Astrophysics and space science, **109**, 45-55, 1984.

[84] Viandana, I.; Tolos, L. *Superfluidity of σ hyperons in β stable neutron star matter.* Phys. Rev. C., **70**, 2, 028802, 2004.

[85] Wang, N.; Manchester, R.N.; Pace, R.T.; Bailes, M.; Kaspi, V.M.; Stappers, B.W.; Lyne, A.G., *Glitches in southern pulsars.* MNRAS, **317**, 843W, 2000.

[86] Watts A.L.; Andersson N.; Beyer H.; Schutz B.F., *The oscillation and stability of differentially rotating spherical shells: the normal-mode problem.* MNRAS, **342**, 1156, 2003.

[87] Yakovler, D.G.; Levenfish, K.P.; Shibanov, Y.A., *Cooling neutron stars and superfluidity in their interiors.* Physics-Uspekhi, **42**, 737-778, 1998.

[88] Yoshida, S.; Lee, U., *r-modes in relativistic superfluid stars.* Phys. Rev. D., **67**, 12, 2003.

[89] Yoshida, S.; Lee, U., *Inertial modes of neutron stars with a superfluid core.* MNRAS, **344**, 207-222, 2003.

[90] Yoshida, S.; Lee, U., *Nonradial oscillations of neutron stars with a solid crust. Analysis in the relativistic Cowling approximation* A & A, **395**, 201-208, 2002.

[91] Zdunik, J.L.; Haensel, P.; Gourgoulhon, E.; Bejger, M. *Hyperon softening of the EOS of dense matter and the spin evolution of isolated neutron stars.* A&A, **416**, 1013-1022, 2004.

[92] Ziman, J.M., *Principle of the theory of solids.* Cambridge, 1965.

A&A: Astronomy & Astrophysics
AJ: Astronomical Journal
ApJ: Astrophysical Journal
ApJSS: Astrophysical Journal Supplement Series
CQG: Classical & Quantum Gravity
MNRAS: Monthly Notices of the Royal Astronomical Society
Nucl. Phys. A.: Nuclear Physics A
Phys. Rev. B.: Physical Review B
Phys. Rev. C.: Physical Review C
Phys. Rev. D.: Physical Review D
Phys. Rev. Lett.: Physical Review Letters